UNIVERSITY OF SOUTHAMPTON

FACULTY OF PHYSICAL AND APPLIED SCIENCES

Electronics and Computer Science

Investigating Phase Synchronisation in EEG signals for Brain Connectivity Analysis

by

Wasifa Jamal

Thesis for the degree of Doctor of Philosophy

February 2015

Declaration of Authorship

I, Wasifa Jamal , declare that the thesis entitled *Investigating Phase Synchronisation in EEG signals for Brain Connectivity Analysis* and the work presented in the thesis are both my own, and have been generated by me as the result of my own original research. I confirm that:

- this work was done wholly or mainly while in candidature for a research degree at this University;
- where any part of this thesis has previously been submitted for a degree or any other qualification at this University or any other institution, this has been clearly stated;
- where I have consulted the published work of others, this is always clearly attributed;
- where I have quoted from the work of others, the source is always given. With the exception of such quotations, this thesis is entirely my own work;
- I have acknowledged all main sources of help;
- where the thesis is based on work done by myself jointly with others, I have made clear exactly what was done by others and what I have contributed myself;
- parts of this work have been published as: (Jamal et al., 2013a), (Jamal et al., 2013b), (Jamal et al., 2014) and (Jamal et al., 2015)

Signed:.....

Date:.....

UNIVERSITY OF SOUTHAMPTON

ABSTRACT

FACULTY OF PHYSICAL AND APPLIED SCIENCES
Electronics and Computer Science

Doctor of Philosophy

INVESTIGATING PHASE SYNCHRONISATION IN EEG SIGNALS FOR BRAIN CONNECTIVITY ANALYSIS

by Wasifa Jamal

The brain holds key information regarding the information processing capability of individuals and recent advances in sensor devices and technology have attracted researchers to question the working of this complex organ. It is not only the elusiveness of the brain that has drawn recent research attention but also the claim of doctors that brain function is key in neurological disorders. Disorders like Autism and Attention Deficit Hyperactivity Disorder (ADHD) not to mention other forms of neurobiological diseases have been attributed to disproportionate and disrupted connectivity in the brain. It is envisaged that more accurate and thorough understanding such connectivity can pave the way for medical research of diseases such as these which are deeply rooted to neural level information exchange deficits.

The main objective of this work is to develop an effective means to quantitatively characterise functional connectivity in the brain. Phase synchronisation is reported as the key manifestation of the underlying mechanism of information coupling between different brain regions. This work, therefore first the phase relationships between Electroencephalogram (EEG) signals have been investigated to understand the synchronisation pattern underlying them during the execution of a task. The pursuit to characterise time evolving phase synchrony leads to the identification of the existence of discrete states with quasi-stable phase topography call synchrostates in EEG datasets from range of subjects. These states exhibited switching patterns which were characteristic to the stimuli provided during a cognitive task, specifically in this case face perception tasks. The switching of these states were modelled in a probabilistic framework using a finite Markov model and the stability of the states are represented by the self-transition probabilities.

The degree of phase synchronisation during the existence of each state is then translated into functional connectivity maps and complex network graph measures were applied on it to obtain a set of metrics that quantify the characteristics of such connections formed within the brain. These quantitative brain connectivity measures were used as features to solve a classification problem between autistic and typical children which resulted in an accuracy of 94.7%. The connectivity parameters were then used to characterise behavioural trait scores of anxious children by developing a regression model correlating these to the standardised behavioural scores calculated from questionnaires. Traits like sadness, state anxiety and anger could be modelled effectively using the metrics reported in this study.

This work lays the foundation for further exploration of these quantitative measures for characterising a variety of neurodegenerative diseases and hence may result in a new type of diagnostic process to aid the existing tools available to the clinicians.

Contents

List of Figures

List of Tables

Acknowledgements

All praise be to Almighty Allah (SWT) who gave me the strength, patience and wisdom to struggle through during the last few years of my degree. It is because of His blessing that it has been possible for me to come so far.

Being a Ph.D student at the University of Southampton has been a challenging yet great experience for me. The help of many individuals have been instrumental in my research work. The academics, my colleagues and peers at the University of Southampton have inspired me to continue doing research and pursue a career in academia.

I would like to take this opportunity to thank Dr. Kouhsik Maharatna for his continuous support and for his technical help during the last three years. His enthusiasm, encouragement and faith in me always motivated me to do better. I am grateful to Dr. Srinandan Dasmahapatra for his technical advice and friendly suggestions.

I am thankful to Dr Saptarshi Das for his continuous support and insight on the work done. I would also like to take the opportunity to acknowledge all my colleagues in the research group Dwaipayan, Sanmitra, Valentina, Evangelos, Shre and Taihai for their co-operation and great company.

Next I would like to thank the people who have contributed to my thesis in their own special ways. I thank my special friends, Zunaira, Tayyaba, Sehla and Sana, who without knowing much about EEG signal processing motivated me as well as supported me throughout my time here in Southampton. Thank you for always being there for me!

And finally my dearest parents and my family, without their love, support and efforts I would not have come so far. They have been the driving force behind my work and they never cease to encourage me.

To my parents, family, friends and mentors ...

Chapter 1

Introduction

1.1 Motivation

The prevalence rates for neurobiological disorders like Autism, Aspergers Syndrome (AS), Attention Deficit Hyperactivity Disorder (ADHD), anxiety etc. is increasing throughout the world (Kramer (1980)). There is a rising pandemic of people suffering from such polygenetic developmental and neurological disorders and the chronic symptoms associated with them. Due to the absence of effective techniques to reduce incidence, the prevalence of such diseases will continue to increase (Landa (2008)). Typically although the symptoms of these illnesses are present at the age of 2-4 years they are only diagnosed an average of 10 years after the advent of the first symptom (of the Surgeon General (US et al.(2001)). It is well accepted in the scientific community that early diagnosis can greatly improve the prognosis of a child with disorders such as autism (Morrison et al. (2002)). Researchers like Dawson, Oberman and others (Dawson (2008), Oberman and Pascual-Leone (2008)) consider early treatment of children with Autism Spectrum Disorder (ASD) as a crucial step by intervention during a critical period when the brain's plasticity is maximal. Others have reported that intensive and specialised treatment in a timely manner can have an encouraging impact on the development of language, cognitive and social functions of an autistic patient (Dawson et al. (2010), National Research Council (2001)).

Initiation of early intervention in children with neurobiological disorders is pivotal for attaining an eminent outcome through treatment (Altemeier and Altemeier (2009)) and timely, intensive treatments have been known to have a favourable impact on the behaviour of children (Rogers and Vismara (2008)). Undetected disorders lead to a delay in the initiation of appropriate treatment, which can mute the effects of the syndrome if not prevent the onset of a full-blown disorder all together (Reichow and Wolery (2009), Stone and Yoder (2001)). Hence, early detection is essential in controlling the onset of such traits and critical for early intervention (Szatmari et al. (2003)).

There are a myriad of treatment protocols that have been demonstrated to be efficacious with children with behaviour disorders (Taylor (2014), Lang et al. (2012), Hakamata et al. (2010)). However, since most of these neurobiological disorders, including autism and ADHD, are by nature heterogeneous and evolutionary, it is not likely that a specific treatment will work for all children (Doyle (2005), Amaral et al. (2008)). The disarrayed attributes of such diseases and the irregular manifestation of symptoms among those afflicted, calls for more individualised intervention schemes based on the individual characteristics of children (White (2000)). Such personalised patient centric therapies could have substantial benefits for individuals as well as the society, however they call for task specific, subjective evaluation of the individuals (Morrison et al. (2002)).

Current methods of assessing children and adolescents with disorders encompass a wide range of interview formats and behavioural screening scales. The conventional approach to screen for developmental disorders in children is through behavioural assessments or from self-reported tests and interviews (Dietz et al. (2006)). This method of scoring a child is influenced by many factors, such as difference in opinion of the clinicians, environmental impact, as well as uncertain or doubtful answers to interview questions. The conventional screening method is only effective in children who externalise their problems through atypical behaviour. Many of them rely on parent-rated symptoms of a child's behaviour and researchers have questioned the extent to which adults are able to detect and accurately report internalising symptoms in children and adolescents (Choudhury et al. (2003)). Some symptoms are too mild to be noticed by the parents and teachers, hence the child's problems are neglected until a full blown set of symptoms emerge. Diagnostic accuracy and reliability of self-report measures is also questioned and clinician administered formats are limited by difference in opinion and potential bias (Antony (2001)).

The subjective nature of the behavioural evaluation technique stipulates the need for more qualitative and objective psychophysiological measures, that have the potential to supplement the existing conventional methods in providing a more accurate evaluation of symptoms in children in the general population. This approach, if further developed in clinical samples, can aid diagnostic accuracy of such disorders in the future. As the conventional behavioural methods are not very conclusive and do not generally facilitate the early diagnosis and patient centric treatment protocol, we look into physiological signatures for the quantification of the disease. The aim is to use physiological signals for the identification of variables that support the doctors in the diagnosis as well as to characterise the patients so as to give *apriori* indication on the most suitable therapeutic program that will benefit the individual children.

Research like that of (Rippon et al. (2007b)) proposing that, disorders such as autism could be a manifestation of disproportionate connections between brain regions, motivates researchers to look into the brain to find answers to clinical questions. With the advent of technology and the development of sophisticated techniques to study brain

function, research can take a different turn and brain dynamics can be used to better understand these disorders.

Researchers have looked into many techniques to understand the information exchange in the brain in order to decrypt the signal propagation pathways (Friston (2011)). Although there has been progressive research, the mystery of the brain remains elusive till date. Most of the knowledge of how the brain operates and its localised functional areas is known from studies of the brain done over many years (Schoenemann (2006), Cohen et al. (2008)). Modern technology provides a window into the human brain using an array of techniques. Most commonly used methods by researchers to carry out studies in the field of cognitive neuroscience are given below:

- Analysing electroencephalograms (EEG): electrical activity of the brain recorded at the scalp
- Other modern techniques used are Positron Emission Tomography (PET), functional Magnetic Resonance Imaging (fMRI), Single Photon Emission Computed Tomography (SPECT), Magnetoencephalopham (MEG), Magnetic Resonance Spectroscopy (MRS), Diffusion Tensor Imaging (DTI) etc.
- Synthesized data

In case of studying the brain of children and pathological patients, the ideal modality is the one that is non-invasive. More detailed spatial information can be achieved by using invasive tools, however it is difficult to attain the same level of detail using other non-invasive modalities. Spatial information gathered using BOLD (Blood-oxygen-level dependent) signals allows one to gain millimetre-resolution information about the physical areas of the brain and there relative activation during a task (Logothetis and Wandell (2004)). However the steep cost of PET scanners and the low time and temporal precision of fMRI has made EEG a very popular choice among researchers. Currently there is no existing non-invasive recording tool that trace neural activity at both high temporal and spacial resolution. Temporal information is crucial in understanding the dynamics of patients as it allow the investigation of time-sensitive integration of information from discrete brain areas (Cold et al. (2007)). EEG signals have a high temporal resolution which makes them ideal for estimating functional and effective connectivity which depend largely on calculating the correspondence of neural signals over time (Sakkalis (2011)).

Signal analysis plays an important role in the mapping of brain dynamics as it throws some light into the understanding of electrophysiological signals recorded from the brain and brings us a step closer to discovering the underlying mechanics of the brain. Neurobiological disorders, like the ones mentioned above can prevail due to under functioning integrative circuitry leading to deficits in neural level information integration (Just et al.

(2004)), (Rippon et al. (2007b)). With more and more advances in the field of cognitive neuroscience for measuring and modelling connectivity, it sets an ideal platform for studying the complexity of the brain network. The comparison of brain network topologies between subject populations can reveal presumed abnormalities and may also lead to the identification of distinguishable measures for the classification of such populations (Rubinov and Sporns (2010)) hence leading to early detection. Various techniques have been proposed for mapping brain connectivity, but developing an effective and accurate method has always been a challenge.

Deeper insight into the mechanics of the brain will allow the use of technology to guide the clinicians in diagnosis as well as early detection and allow more tailored therapy, like neurofeedback, to the patients. Quantitative results acquired from connectivity analysis and a comprehensive understanding of the disrupted connections in the brain will pave the way for future neurofeedback to patients. The efficacy and effectiveness of neurofeedback weighs heavily on the computer generated metric that the system tries to regulate in the feedback loop (Coben et al. (2010)). The current neurofeedback protocols call for enhancing poorly regulated brainwave (delta, theta, alpha and beta) patterns. However these do not take into account the temporal dynamics of the brain waves and also the underlying connectivity patterns of the patient undergoing the therapy (Koush et al. (2013)). Since many of the neurobiological disorders stem from disruptions in the neural connectivity (Just et al. (2004), Rippon et al. (2007b)), connectivity data when considered during neurofeedback has remediating effects (Coben (2007)). Thus connectivity analysis is essential in therapy and also in any form of neurofeedback to achieve reduced symptomatology of these disorders.

1.2 Objective

Motivated by the fact that early detection and therapy can reduce some of the numerous impacts of neurobiological diseases like Autism, ADHD, AS, etc., research in these fields have taken a turn towards being more proactive than reactive. Since many of these disorders are constellations of disrupted connectivity (Hazlett et al. (2005), Lainhart et al. (2006)) in the brain, the focus of this research is to find quantitative metrics from brain connectivity, which can then be applied for biomedical applications like the diagnosis and prognosis of neurodevelopmental disorders such as autism, ADHD, AS etc.

In order for the therapy or treatment method to be applicable in the clinical environment, it needs to be capable of carrying out the task specific characterisation of subjects. Furthermore, intensive neurofeedback treatment systems, like Deep brain stimulation and transcranial magnetic stimulation or any form of bio feedback that is to be provided to the patients, require knowledge of the transients of the brain dynamics during cognition

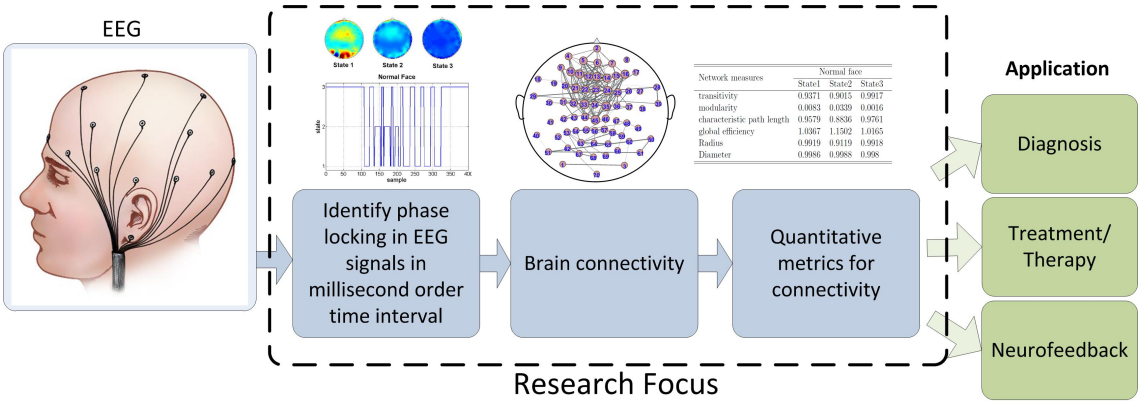

Figure 1.1: Flowchart showing the core issues to be investigated to accomplish the research objective.

(Koush et al. (2013)). Hence stimulus specific and dynamic quantification of connectivity is a prerequisite for an effective connectivity guided therapy and feedback. This sort of temporal information is crucial in understanding of the dynamics of patients as it allow the investigation of time-sensitive integration of information from discrete brain areas (Terry and Mahadik (2007)).

The objective here is to utilise a set of advanced, sophisticated signal processing algorithms that facilitate accurate characterisation of stimulation-specific brainwave anomalies and connectivity between different regions of the brain; thus giving definite insight into the process of information integration ability of the brain in a stimulus-specific way.

The Figure 1.1 highlights the research focus and the flowchart with the blocks required to achieve our objectives.

1.3 Challenges

High complexity of the mammalian brain in conjunction with the limited understanding of its physiology is one of the major reasons why it is difficult to model its connectivity. Another major bottleneck is that the human brain reaction time to any stimuli is around 150ms (Thorpe et al. (1996)). Modelling connectivity at such granular time intervals is not an easy task. The current research trend is steered towards tackling these issues.

Given the above challenges, advances in the neuroimaging techniques allow brain researchers to non-invasively monitor brain at millisecond order time resolution with EEG; however one has to compromise on the spatial accuracy of this modality. EEG signals also come with its trail of problems, like contamination from artifacts (Romo Vázquez et al. (2012)), corruption from volume conduction (Vinck et al. (2011)), etc. Any conclusions made from these signals need to be validated and carefully interpreted to be free from such problems.

EEG connectivity can also be rendered at sensor or source level. These two paradigms have their own set of advantages and disadvantages. In connectivity estimates, artificial synchrony may occur due to linear mixing between nearby sources (Palva and Palva (2012)). Nevertheless, this artificial component may be attenuated or removed by using precautionary methods. When conducting analysis on stimulus evoked responses in humans, one must also consider the latency of the evoked responses. Latency should be factored into the experimental design so that the time window of interest is long enough for the response to be acquired and not contaminated by other irrelavent evoked responses (Truccolo et al. (2002)).

1.4 Contribution

The contributions of this research are:

- Reports the existence of a new phenomenon called *synchrostates*. These are a set of distinct states, where the relative phase between EEG electrodes are quasi-stable of the order of milliseconds and they switch amongst themselves during the execution period of a task.
- Establishes the presence of the synchrostates and their consistency during face perception tasks by showing their existence over a large number of different simulations and studies.
- Shows that these states when coupled with their stability time periods may be used to derive the functional connectivity in brain following the principles of phase synchronisation.
- Reports the theoretical foundation to model the synchrostates and their transition to predict future state sequences with high performance results and models the stability of each state in probabilistic framework.
- Proposes the use of graph theory measures on connectivity networks derived from synchrostates as quantitative metrics for information integration (global connectivity) and segregation (local connectivity) in the brain.
- Proves that the quantifiable network measures when used as features for classification of typical and autistic children achieves state of the art classification performance with low complexity classifiers and hence has a potential to be used as a diagnostic tool for early detection of ASD from physiological signals, in future.
- Shows that network measures can be used to construct a set of simple parametric models to characterise negative affectivity in children based on brain connectivity measures derived from EEG synchrostates. This study can lay the foundation

for the application of such models to assist in the screening process of behaviour problems in children as well as in applications of emotion recognition in healthcare, rehabilitation as well as brain computer interface (BCI).

1.5 Organisation

The rest of thesis is organised as follows:

Chapter 2 includes detailed background and literature review of EEG, EEG phase locking and its relevance in this research, brain connectivity and graph theory. It also reviews the current state of the art in EEG signal processing techniques and then discusses the caveats of those tools, which motivated the formulation of the new method described in this work. It also goes on to list some of the technical concerns revolving around EEG signal processing, such as the issues related to the volume conduction and artifacts embedded in EEG signals. Chapter 3 describes the technique proposed to investigate the phase locking in EEG signals which lead to the observation of the new phenomenon called *synchrostates* and their transition. They were first shown to exist in single adult EEG during face perception. Later the similar states were observed in multiple adult subjects. Chapter 4 reports the synchrostate analysis results on EEG from pathological populations with neurological disorders from two different datasets with different experimental paradigms. Chapter 5 explains how the synchrostates can be modelled and validated in probabilistic framework using Markov properties for comparison between groups in a study. Chapter 6 explains how connectivity can be derived from synchrostates and their transition using a synchronisation index and how graph theory can be applied to obtain quantitative measures for segregation and integration in the brain functional network. Chapter 7 explains the details of the experimental results, which were carried out for classifying typical and autistic children using synchrostates and there subsequent network measures as well as reports evidence for a model to evaluate scores of negative affectivity (sadness) in children as a function of brain connectivity measures. The conclusions along with the highlights of the possible future work that can follow this research is detailed in Chapter 8.

1.6 Accepted papers for publication

1. Wasifa Jamal, Saptarshi Das, and Koushik Maharatna, "Existence of Millisecond-order Stable States in Time-Varying Phase Synchronization Measure in EEG Signals", *35th Annual International Conference of the IEEE Engineering in Medicine and Biology Society, IEEE EMBC*, July 2013, Osaka, Japan, pp. 2539-2542.

2. Wasifa Jamal, Saptarshi Das, Koushik Maharatna, Doga Kuyucu, Federico Sicca, Lucia Billeci, Fabio Apicella, and Filippo Muratori, "Using brain connectivity

measure of EEG synchrostates for discriminating typical and autism spectrum disorder", *6th International IEEE EMBS Conference on Neural Engineering*, Nov. 2013, San Diego, CA, pp. 1402-1405.

3. Valentina Bono, Wasifa Jamal, Saptarshi Das, and Koushik Maharatna, "Artifact reduction in multichannel pervasive EEG using hybrid WPT-ICA and WPT-EMD signal decomposition techniques", *Acoustics, Speech and Signal Processing (ICASSP), 2014 IEEE International Conference on*, May. 2014, Florence,pp. 5864-5868.

4. Wasifa Jamal, Saptarshi Das, Ioana-Anastasia Oprescu, Koushik Maharatna, Fabio Apicella, Federico Sicca, "Classification of autism spectrum disorder using supervised learning of brain connectivity measures extracted from synchrostates", *Journal of Neural Engineering*, vol. 11, no. 4, pp. 046019 Aug. 2014.

5. Wasifa Jamal, Saptarshi Das, Ioana-Anastasia Oprescu, and Koushik Maharatna, "Prediction of Synchrostate Transitions in EEG Signals Using Markov Chain Models", *IEEE Signal Processing Letters*, vol. 22, no. 2, pp. 149-152, Feb. 2015.

1.7 Papers submitted and under review

1. Wasifa Jamal, Saptarshi Das, Koushik Maharatna, Indranil Pan, and Doga Kuyucu, "Brain Connectivity Analysis from EEG Signals Using Stable Phase-synchronized States during Face Perception Task", *Physica A: Statistical Mechanics and its Applications*. (Revised)

2. Wasifa Jamal, Saptarshi Das, Georgia Chronaki, Koushik Maharatna, Edmund Sonuga-Barke and Ioana-Anastasia Oprescu, "Using brain connectivity measures from synchrostates to characterise negative affectivity in children". (To be submitted)

3. Valentina Bono, Antonio Narzisi, Anne-Lise Jouen, Elodie Tilmont, Wasifa Jamal, Mike Wald, Mohamed Chetouani, Jean Xavier, David Cohen, Filippo Muratori and Koushik Maharatna, "Principles underlying the design of "michelangelo", a gaming platform for delivering ASD children intensive intervention in nomadic settings", *Molecular Autism (BioMed Central)*, (Under Review).

Chapter 2

Literature Review

This chapter discusses the necessary theoretical background and reviews the current state of the art techniques in the field of brain dynamics. It goes into details about the various methods currently used to study the brain. The different types of brain connectivity that is popular in the field are also discussed. Studying EEG can take two directions, time or frequency. Common methods used in both domains are briefly discussed. The chapter highlights how phase synchrony is attributed to interactions in the brain and goes on to reporting the popular methods currently available in literature to study synchrony in brain. The reported facts justify the aim to study phase synchrony in EEG. The detailed review of the current state of the art methods to study synchrony reveals that these methods are unable to perverse the time information about the temporal evolution of phase locking hence fueling the objective of investigating time varying phase locking in EEG. The challenges faced in phase synchrony studies due to the effect of volume conduction are reported in Section 2.2.2. The chapter also includes information regrading the implications of carrying out source level connectivity over sensor level and justifies the approach to carry out sensor level connectivity analysis. Sections 2.3 and 2.4 briefly accounts on the characteristics of autism and behaviour disorder and also recounts the finding of brain connectivity and other related research conducted on them. There is also a discussion about microstates in this chapter which is a time domain phenomenon observed in EEG potential maps.

2.1 The Human Brain

Neurons or brain cells are the basic working units of the brain that generate the electrical activity. Large assemblies of neurons behave as electrical generators producing EEG signals measured on the scalp. Neurons need both electrical and chemical stimulation for excitation. Neurons, when triggered by a stimulus, which can be any activity inside or outside the body that evokes a physical or psychological response, produce electrical

impulse. After being triggered, the electrical impulse travels along the neuron's axon until it meets the dendrite (incoming branch) of the next neuron at a synapse. Neurotransmitters are specialised chemicals that are released from the tip of the dendrites that assist nerve signals jump the synaptic gap, and hence carrying messages from neuron to neuron.

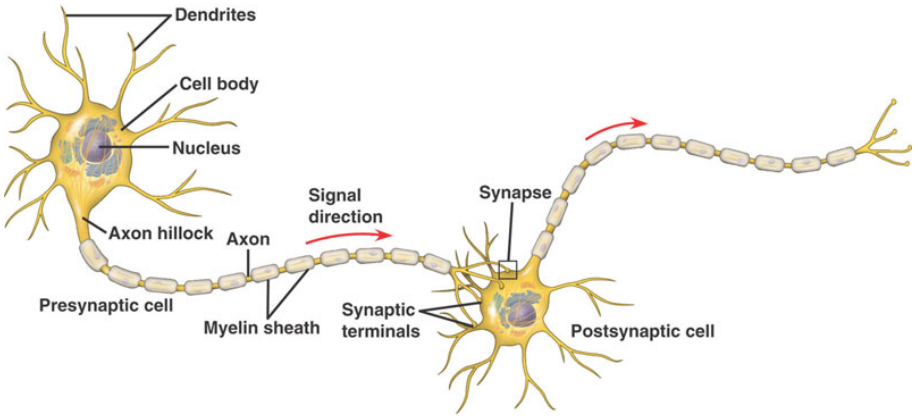

Figure 2.1: Figure showing the structure of a neuron and how a neuronal signal passes along two neuron cells. Image taken from (http://www.kvhs.nbed.nb.ca/gallant/biology/neuron_structure.jpg)

The electroencephalogram is the time series data of the electrical signals generated in the brain recorded by scalp electrodes. These signals are scalp potentials produced by the synchronised cortical pyramidal neurons during excitation. Postsynaptic graded potentials from the pyramidal cells form dipoles between the cell body, soma and dendrites (Sanei and Chambers (2007)). The array of electrodes placed on the scalp measure the potential difference of these dipoles between the electrode itself and a reference, which is then amplified and then recorded. These electrical currents are caused mostly by the movement of ions through the neuron membrane in a direction governed by the membrane potential (Attwood and MacKay (1989)). However due to the different layers inside the human head, like the brain, skull and scalp, with different electrical properties, the signal is attenuated. Please refer to Appendix B for details. As a result only a large population of neurons which are active can generate enough potential that is measurable by the electrodes on the scalp (Sanei and Chambers (2007)) and is thus useful as it gives a coarse view of neural activity and thus can be used to unobtrusively study brain activities. Modern techniques allow researchers to work with up to 256 electrodes giving them excellent temporal resolution.

EEG Clinical bands:

The recorded electrical activity from the brain occur at different frequencies. They are known as brain waves and are classified into EEG bands called delta, theta, alpha, beta and gamma and are identified according to their frequency measured in Hertz (Hz). There are difference of opinion as to the best way to group brain waves into clinical

bands, but generally, it is agreed that the waves should be grouped as shown in Table 2.1.

Table 2.1: Table detailing the clinical EEG frequency bands, and their typical properties and the typical distribution of these rhythms

Frequency (Hz)	Band	Distribution	Characteristics
0.5-4	Delta (δ)	Generally broad, frontally in adults and posterior distribution in children	Slow, high Amplitude waves. Usually related to deep sleep. Has been detected in continuous attention tasks (Kirmizi-Alsan et al. (2006)).
4-8	Theta (θ)	Found in many lobes and is regional	Associated with drowsiness in older children and adults and inhibition of elicited responses (Kirmizi-Alsan et al. (2006))
8-13	Alpha (α)	Found in posterior regions of the head and at central sites during rest	Indicates relaxed and mediated level of consciousness. Predominant when eyes closed.
13- 30	Beta (β)	Symmetrical distribution predominant in frontal and occipital lobes.	Indicates a level of alertness with active focus and readiness for action. Low amplitude waves.
> 30	Gamma (γ)	Localised around the somatosensory cortex	Associated with high level information processing, memory matching tasks and cross modal sensory processing (Kisley and Cornwell (2006)).

2.2 Connectivity in the Brain: Background and Literature review

The brain has areas of specialised neurons which are responsible for distinct functions (Brett et al. (2002)). These clusters of specialised neurons in turn form a part of a big coherent organisation of segregated cortical areas which dynamically interact to steer the brain into specific cognitive states. These assemblies influence each other through excitatory and inhibitory synaptic connections (Fell and Axmacher (2011a)). The phenomenon of integration and co-ordination of interacting cortical regions is known as synchronisation in time scale (P. R. Roelfsema and Singer (1997)). The temporal evolution of these synchronised cortical areas is instrumental in understanding how the human brain performs certain tasks given a particular stimulus. Research has established phase synchronisation as a key feature for communication between the brain regions (Quiroga et al. (2002a), Makarenko and Llins (1998), Gray et al. (1989)) serving as the

manifestation of underpinning mechanism of information exchange in the brain during cognition (Engel et al. (2001a)). There is evidence of short range synchrony and long range synchrony in several studies and these have been most commonly interpreted as biological mechanism of integration (Varela et al. (2001a)). There is also evidence of synchronisation in the visual cortex and the role it plays in binding features, through experiments carried out on animals (Gray et al. (1989)). One of the objectives of this research is to characterise the patterns of phase synchronisation and to translate them into functional connectivity network giving an insight into how the segregated brain areas interact during a task.

Connectivity within the brain mediates the process of functional segregation and functional integration (Wass (2011)). Various techniques have been proposed for formulating brain connectivity but developing an effective and accurate method has always been a challenge. This section details the different types of connectivity measures and the most widely used methods.

Structural connectivity

The structural connectivity of the brain highlights the anatomical connections which link the neural elements (Sporns (2011)). These can vary in scale from large scale connections between hemispheres or small networks of single cells.

Functional connectivity

Karl Friston defined function connectivity as the time based temporal correlations between distributed neuronal units or the synchronisation of activation of brain areas when performing a task (Horwitz (2003), Rippon et al. (2007a)). It reflects the patterns derived from statistical dependence between spatially remote neurophysiological events (Friston et al. (1993a)). Functional connectivity is defined to be highly time dependent and changes on the scale of a milliseconds and is prone to change depending on the task and stimuli (Sporns (2011)).

Effective connectivity

This type of connectivity models the network of interactions that are casual in nature. It accounts for both direct and indirect influences that one neural unit has over another which can be local or distant (Friston et al. (1993b)).

The importance of studying the temporal dynamics of the communication system of the brain have been highlighted in Chapter 1, hence tracking functional connectivity is

the focus of this work. Tracing time dependent functional connections will allow us to quantify the quality and stability of connections made in a stimulus specific way for it to be useful in the understanding of implications of neurobiological disorders in the brain.

Typically synchronisation can be studied from EEG signals in two domains i.e. time and frequency. The work reported in (Lehmann et al. (1987), Koenig et al. (2014)) considered brain electric states with consistent scalp electric field topography and their sequence which lead to what is commonly known as EEG microstates. Since the scalp electric field topography is the sum of all momentarily active sources in the brain irrespective of frequency, this method allows one to obtain a global measure of momentary brain activity in a temporal resolution of that of the EEG. It has been shown that such EEG microstates can effectively characterise qualitative aspects of spontaneous thoughts and play an instrumental role for gaining deeper insights into the cognitive and perceptual processes (Lehmann et al. (1998)). The idea of microstates was first established by Lehmann et al. (Lehmann et al. (1987)) where he found stable map configurations when he viewed momentary EEG field across the scalp. It has been proposed that the microstates reflect the "contents" of information processing and are claimed to be the "atoms of thoughts" (Lehmann et al. (1998), Michel and Murray (2012)). Later on this concept was applied to EEG, acquired in awake and sleep states, during deep hypnosis and from schizophrenic patients (J.L. Cantero and Salas (2002), H. Katayama and Lehmann (2007), S. Irisawa and Kinoshita (2006)). The most important characteristic of the EEG microstates is that the topography does not change randomly or continuously over time but exhibit quasi-stable behaviour in the order of 80 - 120 ms; and abruptly switches from one topography to another - the number of unique topographies being small (typically 3 - 10) (Koenig et al. (2002)). Researchers have investigated microstates in healthy adults to classify the dominant microstates in spontaneous EEG when they were awake (Britz et al. (2010)). Microstates have also been found to be independent of frequency and have been reported to have correlations with fMRI resting state networks (Britz et al. (2010)). The microstate transitions have also been shown to follow the Markovian property in (Schack et al. (2001)).

Granger causality is another time domain method used to infer functional connectivity that measures the temporal dependency of the data itself (Roebroeck et al. (2005)). Granger Causal Modelling (GCM) is in essence a vector autoregressive model in discrete time (Friston (2009)) hence it assumes that EEG signals are stationary and does not take the phase coupling information into account. Generalised Synchronisation (GS) hinges on the concept of chaotic oscillators and represents how well an oscillator maps onto the other, which again reports on non-linear interdependencies rather than phase synchronisation (Arnhold et al. (1999)).

Another way, other than time domain, to study the synchronisation phenomenon is in the frequency domain. This is led by the assumption that if two points (i.e. two EEG electrode sites) are in coherence (i.e. maintaining constant phase relationship over time),

they can be considered as functionally synchronised or connected (Fries et al. (2001)). Therefore computation of phase coherence is fundamental in this approach. Recent research has established phase coherence as a biological mechanism for communication between different brain regions. Evidence has been found of short- and long-range phase synchrony as a key manifestation of information integration process in brain during cognition providing an independent dimension of understanding the information processing in brain ((Mulert et al. (2011), Fell and Axmacher (2011b), Fries et al. (2001)). Phase coupling has been studied in patients with mental disorders (Razavi et al. (2013)) and the merits of synchrony analysis have been found in the understanding of neurodevelopmental disorders (Uhlhaas et al. (2008)).

Covariance and coherence is classically used to model synchronisation and has been applied extensively for multichannel EEG signal analysis (Koenig et al. (2005)). The frequency coherence is typically computed by first taking Fourier Transform (FT) of the EEG signals recorded at two arbitrary EEG electrode sites and then considering the imaginary parts of the transformed signals. Leocani et al. (Leocani et al. (1997)), Weiss and Rappelsberger (Weiss and Rappelsberger (2000)) and Nolte et al. (Nolte et al. (2004)) studied the Fourier Transform coherency to formulate synchronisation in EEG. Since the method for coherence analysis use Fourier transform (Kottlow et al. (2012)), it does not preserve the temporal information of phase evolution and therefore gives an average measure of synchronisation over a time window at each of the bands. Also the methods mentioned, measure frequency coherence which mixes the effect of phase and amplitude when computing the synchrony between two signals (Varela et al. (2001b)) whereas it is vital to investigate the phase synchrony independently, as phase interactions are independent of the neural firing rates in different regions. This provides an independent dimension to the study of neural information processing (Fell and Axmacher (2011b), Fries et al. (2001)).

FT coherence methodology was later modified by several researchers by using Continuous Wavelet Transform (CWT) and Hilbert Transform (HT) to compute phase in transformed domains and for deriving associated synchronisation indices from the coherence values thus obtained. Rosenblum et al. (Rosenblum et al. (1996)) studied phase synchronisation of chaotic oscillators using HT to decompose signals and inspected only the phase component by taking the argument of the complex result. Lachaux et al. (Lachaux et al. (1999)) also did phase analysis by convolving with a Gabor wavelet to transform the signal. The methods mentioned above have been applied to EEG and MEG signals; from epileptic patients for both analysis (Gupta et al. (2006), Mormann et al. (2000)) and seizure prediction (Lehnertz et al. (2003)), for modeling correlations between synaptic strength and cortical synchronisation (Esser et al. (2007)), for studying stability of synchronisation in the auditory cortex of schizophrenic patients (Maharajh et al. (2010)) and measuring synchrony in EEG of elderly people participating in a visual search task (Phillips and Takeda (2010)). The Hilbert and wavelet coherence

approaches have the advantage of allowing phase extraction over non-stationary signals than the FT which can be applied to stationary signals- which EEG is not (Lee et al. (2003)). The mean phase coherence is a measure (Mormann et al. (2000)) that computes the Hilbert coherence synchronisation over the whole time series and therefore gives an average measure of synchronisation for the whole signal span and hence does not provide us with the means to investigate phase at fine temporal scale. The Phase Locking Value (PLV) uses wavelet coherence to quantify phase locking in EEG signals. The signals are transformed using a Gabor wavelet to measures the inter-trial variability of phase difference (Rodriguez et al. (1999)). Although PLV varies with time, it measures phase locking across trials rather than the temporal variability of phase over the period when the subject is engaged in a task. Partial Directed Coherence (PDC) extends from the concept of partial coherence and measures the causal influences in the time series using the multivariate autoregressive (MVAR) models (Baccalá and Sameshima (2001)) which is not stationary independent. Additionally, various other measures of phase synchronisation have been reported in (Quiroga et al. (2002b)). In Mutlu et al. (Mutlu et al. (2012)) and Fallani et al. (Fallani et al. (2008)) time varying brain connectivity analyses have also been explored considering the whole time course, using measures like PLV and PDC for completing a specific cognitive task. Although useful, such approaches only give insight into the phase synchronisation in a time-averaged way over all the frequency bands, rather than capturing the true picture of the temporal or transient evolution of phase synchrony in a band-specific way. On the other hand, in principle, CWT and HT both being time-frequency transform methods, have potential to describe the temporal evolution of phase synchronisation at sub-second resolution level which could be more informative to understand the dynamics of the synchronisation phenomena from the onset of a given stimulus till the end of the corresponding cognitive action. Astolfi and Babiloni (Astolfi et al. (2008)) proposed an adaptive multivariate approach on directed transfer function and partial direct coherence to estimate time varying cortical connectivity. However these do not measure phase coupling which is the main focus of the present study.

Dynamic Casual Modelling (DCM) models a network of discretely located interacting neuronal sources whose dynamic system response can be explained by neural mass models. It employs a forward model to generate data in order to explain how the observed data was caused, however it relies on a biophysical model of neuronal dynamics (Sakkalis (2011)) and requires one to predefine a large set of parameters which is a drawback of such an approach (Kiebel et al. (2006)). Again this method does not measure phase coupling and also suffers from the generalisation error as there may be multiple models that are equally probable from the given data (Sakkalis (2011)).

Sakkalis (Sakkalis (2011)) recently conducted a thorough review of the all the modalities available at present to researchers for estimating brain connectivity. In his review he highlights the underlying assumptions, and important caveats of each technique with

the clinical applications suited to their use. He summarises the modalities as measures which can be linear, nonlinear, model-based or data driven, bivariate or multivariate etc. The scope of this work is not to study the underlying neuroanatomy of patients but to understand the underlying dynamics therefore this research only looks into the methods for modelling functional connectivity. His comparison is represented in the Table 2.2 listing the characteristic of the each technique he discusses:

Table 2.2: Table adapted from (Sakkalis (2011)) showing the different measures of connectivity and their characteristics

Case	Dynamic Causal Modelling(DCM)	Coherence	Short Term Fourier Coherence	Wavelet Coherence	Phase Locking Value(PLV)	Generalised Synchronisation	Granger Causality	Partial Direct Coherence
Linear	X	X	X	X				
Nonlinear					X	X		
Info-based							X	X
Model-based	X							
Data-driven		X	X	X	X	X	X	X
Causality assessing	X						X	X
Multivariate	X					X		X
Stationarity independent				X	X			
Functional Connectivity		X	X	X	X	X	X	X
Effective Connectivity	X						X	X

To understand the transient dynamics of the information integration process in the brain in a task-specific way it is necessary to estimate the evolution of phase relationships from the onset of a stimulus at different bands amongst different EEG electrodes and finally mapping them to the temporal evolution pattern of synchronisation over the entire scalp. Recently there has been a lot of interest and ongoing research in the field of dynamic connectivity analysis owing to the inherent dynamic nature of the human brain using EEG, MEG and fMRI data.

As evident from the foregoing discussion the existing frequency domain methods compute the phase synchronisation over the entire post stimulus segment of the signal and therefore are unable to retain the transient information at finer temporal granularity, whereas the method of microstate finds the unique electric potential patterns and their transients during the execution period of the task (Gianotti et al. (2008)). Research has

established and stressed on the idea that the phenomenon of phase synchrony over the scalp extends to dynamic brain mapping (Rodriguez et al. (1999)). Information processing between neural assemblies with similar dynamical functional state is facilitated by synchronised oscillatory activity of the neural groups. Deeper understanding of this integration process between such groups during cognitive tasks can be useful in describing brain organisation (Aviyente et al. (2011)). Therefore new measures are needed to estimate such transient dynamics of synchronisation to understand the interactions between different brain regions subject to a specific task. In this study both of these concepts are merged, i.e. the concept of temporal switching (transient behaviour) of stable states along with the band specific phase locking by considering a joint time-frequency representation of the EEG signal. The focus on transient phase synchronisation is not intended to imply that the other measures are not relevant. However, it provides more insight into understanding connectivity and dynamics of brain states.

2.2.1 Source level and sensor level connectivity

Modalities such as fMRI and DTI provides great spatial information as they can provide information about specific brain activation areas by tracking blood flow however the signals are slow and the cost related, is very high. The bulky nature of their acquisition system also prevents researchers from using them for tracking brain activity from subjects while performing day to day activities. EEG is cheaper, non-invasive, less bulky and has very good temporal resolution. EEG is acquired from sensors which are placed over the scalp. The sensors and the current sources within the brain are separated by the scalp, skull and by cerebrospinal fluid. Consequently EEG has a poor spatial resolution (Srinivasan (1999)). Because of the lack of spatial good resolution in EEG, popularly researchers do source level phase synchrony analysis, which gives more reliable physiological interpretations. The process of acquiring source level information from EEG involves solving the inverse problem. Although source level connectivity has more reliable physiological interpretations, reconstructing source activity from EEG is intrinsically an ill-posed problem and is known to have infinite solutions (Sanei and Chambers (2008), Pascual-Marqui (2007)) as many spatial patterns of EEG signals can be fit with a least-squares scheme by many equally plausible equivalent dipoles solutions. It suffers from the issue that using only EEG one cannot uniquely determine the spatial configuration of the underlying neural activity. Thus to resolve this issue with the inverse problem, one has to make a lot of assumptions about the problem to obtain an optimal and unique solution (Phillips et al. (2005)) and thus it only leads to approximate solutions (Phillips et al. (2005)). The use of *apriori* assumptions are not always justifiable in certain experiments.

One must also consider that each equivalent dipole only reflects the center of mass of the activity distributed throughout a region of the brain (He et al. (2011), Srinivasan

(1999)). The interpretation of dipole fitting must be restrained as there is little evidence from intracranial recordings that support the contention that only a few sites in the brain are active while generating evoked or spontaneous EEG (Towle et al. (1998)). It is more likely that there exist spatio-temporal patterns of neural activity that are distributed throughout the brain which are correlated at multiple spatial scales (Nunez (1995)).

The accuracy with which a source can be localised is affected by the approximate volume conduction model of the head which is influenced by conductivity values (refer to Appendix B for examples) of tissue compartments (i.e skull scalp, white matter etc.) and their distribution, head-modelling (geometric model of the head), co-registration (mapping of functional information into anatomical space in the brain) etc. (Whittingstall et al. (2003), Grech et al. (2008)). Correct modelling of head tissue conductivities, as well as the forward head model employed can be a source of error in such a problem (Acar and Makeig (2013)). Since the localised nodes within the brain are non-unique, connectivity analysis based on these nodes are still unreliable and based on some *apriori* assumptions that are made (Grech et al. (2008)). Research has established and stressed on the idea that the phenomenon of phase synchrony over the scalp extends to dynamic brain mapping (Rodriguez et al. (1999)). This encouraged us to analyse the EEG signals at sensor level as they do no suffer from the problems of source localisation mentioned above.

2.2.2 The effect of volume conduction on EEG phase analysis

The phase synchrony, derived from EEG signals recorded over the scalp has been doubted, as it is believed to be the result of spurious synchronisation that can occur due to volume conduction (Nunez et al. (1997)). Volume conduction is the undesired effect when an electric current passing through any biological matter from a source is recorded at the sensor. In the case of the brain there are action potentials from the neurons near the surface of the brain spreading to the EEG sensor scalp electrodes. Electrical events inside the human brain spread nearly instantaneously throughout any volume, like membranes, skin, tissues etc. The signal recorded at the electrodes are smaller in amplitude since the amplitude of the action potential are reduced as they travel along the various media to be detected by the sensors. The potential recorded at the scalp is inversely proportional to the distance from the source. Hence any small change in distance causes large changes in the recorded signal. The signals between nearby sensors may cause artificial synchrony due to linear mixing. Due to the problem of volume conduction, synchronisation reported from scalp EEG is deemed corrupted and masked.

When understanding synchrony of the brain the fundamental principle of the quasi-static approximation is assumed, i.e. the measured potential on the scalp surface by the electrodes have no time-lag to the underlying source activity (Nolte (2003)). Thus lagged correlations and out-of-phase components are said to be personalities or properties of

EEG resulting from connectivity. Volume conduction is known to occur at zero time delay and is hence defined by zero phase lag (Thatcher et al. (2008)). Phase delays measured from spontaneous EEG do not account for volume conduction owing to the quasi-static approximation (Nolte et al. (2004), Pascual-Marqui (2007). The zero phase lag property of volume conduction is used in pioneering works on phase synchronisation like that of (Gysels and Celka (2004), Kramer (1980), Urbano et al. (1998)), to mitigate the effects of volume conduction in their measure of phase synchronisation. On the premise of this assumption one can conclude that the synchrony derived from phase difference which does not report zero phase lag (phase difference of zero) is free from the affect of volume conduction and represents true brain interaction.

2.3 Autism Spectrum Disorder (ASD) and issues relating to brain connectivity

One of the aims of this study is to understand autism spectrum disorder and functional brain connectivity concerns related to it. Autism is a lifetime condition which Minshew and William defined as a polygenetic developmental and neurobiological disorder (Minshew and Williams (2007a)) that is characterised by atypical behaviour and lack of social reciprocity. ASD comprises of a complex group of behaviourally defined conditions with core deficits in social interaction, communication and stereotyped and restricted behaviours. Autistic patients have disorders which span over a broad spectrum and can range from moderate to severe. Although problems in perception and attention are not considered as primary diagnostic categories, individuals with ASD often present difficulties in these domains. It is believed these symptoms suggest generalised dysfunction in the association cortex (Minshew and Williams (2007b)). Researchers have suggested that autism is due to under functioning integrative circuitry leading to deficits in neural level information integration (Just et al. (2004), Rippon et al. (2007b)). Research has shown that a key feature in the neuro-anatomy of autism is the early brain overgrowth (Simmons et al. (2009)) subsequently leading to greater local connectivity and suppressed long-range connectivity. Findings from (Lainhart (2006), Hazlett et al. (2005), Kleinhans et al. (2008), Courchesne et al. (2001)) show evidence of overgrowth of shorter range cortico-cortical intra-hemispheric connections with little involvement of connections between hemispheres and cortex and subcortical structures. The behavioural symptoms of autism could be a manifestation of these disrupted neural circuits. The overgrowth is believed to be a cause of the disrupted development of normal function in autism, as the onset of brain overgrowth matches with the advent of the symptoms of autism (Minshew and Williams (2007b)). Evidence has been found for supporting the hypothesis of under-connectivity within large-distant networks and also under-connectivity within the local networks. This evidence comes from several studies done using functional Magnetic Resonance Imaging (fMRI), EEG and Magneto-encephalogram (MEG) recording.

Kleinhans et al. (Kleinhans et al. (2008)) found disrupted functional connectivity between the Fusiform face area and the left amygdala and between the posterior cingulate and thalamus in the social brain during face processing. An fMRI based study carried out by Just et al. reported evidence of overall functional under-connectivity in autistic subjects compared to controls (Just et al. (2004)). Horwitz et al. (Horwitz et al. (1988)) was the first to present data supporting such theories, where he found PET scans revealing lower level of activation between frontal, parietal and other regions in resting autistic adults. Power studies of EEG/MEG report decreased peri-stimulus induced gamma power. Elsabbagha et al. (Elsabbagha et al. (2009)) reported these findings in response to direct gaze, Wilson et al. (Wilson et al. (2007)) found them in 7-17 year old autistic subjects after onset of auditory presented clicks. Tommerdahl et al. (Tommerdahl et al. (2008)) detected local under-connectivity in autistic adults in their study of sensory perception. Coben et al. (Coben et al. (2008)) found reduced inter-hemispheric coherence across different frequency bands. Bosl et al. used the complexity of EEG signals recorded during resting state as a feature to distinguish typically developing children from children with the risk for ASD (Bosl et al. (2011)). Studies have found various disruptions while performing different task, some of these studies have been listed in the Table 2.3:

Table 2.3: Table detailing some studies carried out on autism listing the disruption area and the task that was being performed

Study	Area	Task
Welchew et al. (2005)	between medial temporal lobe and other cortical areas	emotion recognition task
Kana et al. (2007)	anterior cingulate gyrus, middle cingulate gyrus, insula, parietal and premotor regions	emotion recognition task
Villalobos et al. (2005)	V1 and inferior frontal cortex	visuomotor task
Solomon et al. (2009) and Just et al. (2007)	frontal and other areas	executive planning task
M. A. Just (2004)	Wernicke's area, Broca's area and the dorsolateral prefrontal cortex	sentence comprehension

The theory suggested by Johnson et al. (Johnson et al. (2002)) that the small development failures in early years may lead a cascading effect on behavioural diffculties can be more a conclusive explanation for conditions like autism. Models implicating anomalies in connectivity in autism have been deemed constructive and are supported by genetic, psychological and physiological theories. Genetic anomalies in neuroligin 3 and 4 which are known to control synaptic assembly and dendritic development are found in such patients (Polleux and Lauder (2004)). Autistic individuals are said to have abnormal

neuronal development in the cortical columns which is associated with biochemical deficiencies in serotonin activity (Chandana et al. (2005)). Belmonte et al. (Belmonte et al. (2004)) proposes a model of local over-connectivity and long-range under-connectivity. He suggests that the dysfunctions in the developing brain pilots the cognitive and behavioural symptoms one often sees in the autistic patients. Brock et al. (Brock et al. (2002)), suggested another model where there were deficits in the dynamics between specialised local neural networks and over-connectivity within the isolated individual neural assemblies (Brock et al. (2002)).

It is very important to understand how these finding translate into differences in the functional organisation of the brain between typical and high risk populations. Thus studying the functional connectivity patterns may be the key to understanding the differences between the typical and autistic brain. Therefore quantitative characterisation of the connectivity derived from phase synchronisation measures in ASD patients may lead to an diagnostic tool enabling intervention at appropriate stage.

2.4 Behaviour and Anxiety Disorder

Another pathological disorder in children that is quantitatively modeled is behaviour disorder. Behaviour disorder is heterogeneous disorder that has very high prevalence rates and is associated with a great deal of financial burden and stress to the families. Internalising behaviour problems (i.e. anxiety and depression) in children is a growing concern for parents, clinicians, and policy makers alike. The most common types of behaviour problems in children include hyperactivity, conduct problems and anxiety. Hyperactivity is a symptom dimension of ADHD which is a complex developmental disorder characterised by inappropriate levels of inattention and hyperactivity (Association et al. (2013), Chronaki (2011)). The symptoms of ADHD often overlap with other behavioural problems, such as conduct disorder, hyperactivity, oppositional defiant disorder, etc. (Brown (2009), Waschbusch et al. (2002)). Conduct disorder is a more extreme form of oppositional defiant disorder and is reported to have 6-16% and 2-9% lifetime prevalence rate for males and females respectively (Loeber et al. (2000), Maughan et al. (2004)). Anxiety in children is one of the most prevalent forms of child psychopathy and affects about 20% of children (Morris and March (2004), Verhulst et al. (1997)). External behaviour problems often co-exist with anxiety and depression in children (Jensen et al. (2001), Brown (2000)). Though anxiety is thought to be transient, studies have shown that anxiety disorders may exist all the way into adulthood (Pine et al. (1998)). Temperament factors of negative affectivity (i.e. sadness) are strongly associated with internalising symptoms in children and adolescents (Muris et al. (2007)). Research has shown that children with internalising behaviour problems are rated as more sad by parents and teachers compared to typically developing children (Eisenberg et al. (2001)). Recent research has supported strong links between negative affectivity

and anxiety and depressive dimensions consistently across ethnic groups (Austin and Chorpita (2004)). Longitudinal research has shown that temperamental traits in children at 3 years can predict anxiety symptoms four years later (Volbrecht and Goldsmith (2010)).

Developmentally inappropriate behaviours, such as persistent fears, alongside clinical levels of anxiety can have devastating effects on a child's daily functioning (Association et al. (2013)). They have adverse academic and social outcomes in the long run and can lead to depression (Pine et al. (1998)) hence it is imperative to study high risk children before the advent of any chronic form of mental illness. Hence it is important to define these disorders in children early with the hope of identifying the factors leading to the disorder and also to start early intervention where possible. An affective study would be one that integrates clinical psychology with the information about the neural circuitry. Given the debilitating effects of internalising behavioural problems on a child's daily life (Quilty et al. (2003)), early and accurate evaluation of traits of internalising disorders and their associated characteristics (i.e. negative affectivity) is essential for the design of effective intervention.

Biological correlates (i.e., frontal EEG activation) of inhibited behaviour have been proposed as endophenotypes for anxiety. In addition, earlier temperament and biological (i.e., basal cortisol) measures have been shown to have predictive value for internalising problems during the preschool years (Goldsmith and Lemery (2000)). Children with ADHD have been reported to have lower short and long range connectivity in the superior parietal cortex and in the default-mode networks compared to the control subjects (Tomasi and Volkow (2012)). Other studies state the prevalence of dysfunctional connectivity during resting and cognitive task in ADHD patients (Konrad and Eickhoff (2010)). Differential connectivity patterns have been reported in resting functional connectivity in major depression (Greicius et al. (2007)). Studies conducted on anxious cohorts revealed differences in large scale connectivity (Etkin et al. (2009)).

It is imperative to understand how these biological correlates are reflected in the functional connectivity networks of the behavioural disorder cohort. A quantitative measure that stems from physiological measurements to characterise such heterogenous disorders would have a pre-eminent effect on the diagnosis and therapeutic protocols used.

2.5 Face perception: a stimulus for characterising cognition in subjects

Humans have complex abilities that are essential to the recognition of facial emotion. Facial expressions give a lot of information and play a cardinal role in daily social communication (Ekman (1994)). Faces provide critical information about a subject's

social stand, such as the identity, intention, and emotional state (Sugita (2009)) and hence is a biologically significant visual stimulus for humans. Generally, faces are the most fundamental channel of communication with humans. The process of facial emotion recognition involves perception and the recognition of meaning (Adolphs (2002)). Perception involves the ability to discriminate key features of an expression (Chronaki (2011)). Research in the field of emotion processing highlights that the process of emotion perception involves perceptual skills (Gosselin and Simard (1999)) as well as conceptual abilities (Widen and Russell (2008)). Differences between emotion processing in individuals are closely related to social adjustment especially in children (Mostow et al. (2002)). A child's ability to gather information from face features is a pivotal skill in his/her development, and hence is a basic condition for social interaction (Apicella et al. (2012)). Over the last decade face processing and recognition have been studied in great detail. The face recognition system of humans is extremely fine and has the capacity to recognise and to discriminate between faces and different facial expressions and involves unique functional properties that are do not exist in the recognition of other visual stimuli (Sugita (2009)). A neuro-scientific approach to this issue lead to the identification of specific brain areas and circuits involved in face processing. The research conducted in Boiten et al. (Boiten et al. (1992)) established that different cognitive processes yield responses in different EEG bands indicating the association of a particular frequency band to a specific cognitive task. As an example, the β rhythms have been reported to be linked to cognitive processing, visual attention and perception related modulations (Wróbel (2000), Gross et al. (2004)). Previous research conducted in the domain of face perception has reported different responses in brain oscillation in processing varying emotional face expression (Güntekin and Basar (2007)). They found amplitude differences in the oscillations during processing of angry and happy faces. Basar et al. (Bacsar et al. (2008)) also found different responses in the frequency bands when subjects were exposed to pictures of a loved person as opposed to an unknown person.

Previous research has suggested that social dysfunctioning in school-aged children with behaviour problems may stem from difficulties in understanding others emotions from facial expressions. Recent studies have found correlations between emotion knowledge (recognition of facial and vocal emotion) and various internalised and externalised problems (Trentacosta and Fine (2010)). Highly anxious children were likely to mistake happy faces as angry (Richards et al. (2007)) and display an attentional bias toward angry faces when paired with happy and neutral expressions (Roy et al. (2008), Waters et al. (2010)), a finding consistent with visual search studies using self-reported anxiety measures (Hadwin et al. (2003)). Facial emotion-recognition difficulties have been reported in school-aged children with behaviour problems (Izard et al. (2001)). Recent studies have focused on associations between emotion processing and experiences of negative emotional states (i.e., symptoms of anxiety and depression) in children and adolescents. Facial emotional recognition constitutes one of the most reliable and

widely used methods to assess emotion processing in anxiety disorders (McClure et al. (2003)). Research with anxious adults has found increased C1 amplitudes (80ms post stimulus) in response to angry-neutral face pairs compared to non-anxious individuals in dot-probe tasks (Eldar et al. (2010)). Similar research has showed that increased processing of negative compared to neutral pictorial stimuli in 5-7-year olds (reflected by the posterior Late Positive Potential; LPP) was associated with parent-rated child anxiety (DeCicco et al. (2012)). These findings support models of increased allocation of attention to threat at early processing stages in anxiety.

The neural processing underpinning face processing allows us to understand social information and cues conveyed by faces, especially in subjects who have dysfunctions that have been postulated to underlie their behavioural impairments like those in ASD. Deficiencies in children with autism in understanding social information conveyed by emotional faces have been attributed to the inability in activation of brain circuitry involved in face processing (Apicella et al. (2012)). This impairment in social processing is said to be a core difficulty in autism (Carver and Dawson (2002)). Owing to all the information about face emotion processing and perception mentioned above one can presume that face stimuli may be useful for tracing the congition traits and anomalies in typical adults and children and in pathological subject groups.

2.6 Application of Complex network graph theory in brain connectivity analysis

The integrative nature of brain connectivity can be addressed from a complex network perspective (Sporns (2011)). Describing a complex system such as the brain in terms of graph theory allows one to meaningfully describe them as networks. The characterisation of the brain network as a complex system is a multidisciplinary approach which applies graph theory methods on connectivity matrices derived from neurophysiological data. In principle the adjacency matrix of a graph is representative of the brain connectivity matrix. The adjacency matrix, A of a graph with n vertices is a n x n matrix with the entries A_{ij} consisting of the weights of the edges between the nodes i and j. The networks constitute of nodes and edges i.e. the connections between the nodes. The structure of the adjacency matrix essentially describes the communication pattern of the brain network. The graphical measures are all derived from the adjacency matrix. Brain networks have common features with networks from other biological and physical systems and are also perpetually complex and hence can be characterised with the standard methods.

The use of graph theory provides a new dimension to the investigation of the brain network organisation in humans at different levels of granularity (Supekar et al. (2009)) and thus gives a holistic analysis. Complex network measures have been used to quantify

the underlying brain network from EEG signals (Rubinov and Sporns (2010), Sporns (2011)). These parameters have been useful to draw network topology comparisons between typical and patients with neurological injury or disorder (Watts and Strogatz (1998)). Complex network metrics have been used to model the organisation of the human brain in various studies conducted on fMRI and MEG recoding. Supekar et al. (Supekar et al. (2008)) applied graph theory on task-free Alzheimers disease fMRI. Liu et al. (Liu et al. (2008)) investigated the network properties of functional networks of schizophrenic patients from resting state fMRI data, Bassett et al. (Bassett et al. (2006)) used similar graph metrics for MEG analysis of healthy adults during resting state and fingertapping task. Studies in this field suggest that in complex networks more robust results are obtained by retaining weight information of the graphs as compared to the binary graphs (Newman (2004), Barrat et al. (2004)), since binary networks only provide an approximation of the original weighted network as the whole range of connection strengths are lost. It is also known that weighted characterisation is useful to filter out the influence of weak and potentially less-significant links (Rubinov and Sporns (2010)).

Here in this study complex network measures are used to represent the brain connectivity maps quantitatively which can encapsulate the network properties of the connections. These parameters allow one to utilise them as features for a myriad of problems, like classification, regression analysis etc. EEG classification is a popular research area and the scope of its application is endless. The simple linear classifier is a very popular algorithm for event related potential (ERP) analysis in Brain Computer Interface (BCI) applications (Lotte et al. (2007), Blankertz et al. (2011)) that have been applied for classification of motor imagination (Ramoser et al. (2000)). Garrett et al. (Garrett et al. (2003)) applied both linear discriminant analysis (LDA), conventional neural networks and support vector machine (SVM) on EEG recorded during mental tasks and concluded SVM to be the more sound and conclusive algorithm, although the other two did not perform much worse. Variants of the classical SVM learning algorithm have been applied to classification problems in EEG for application in BCI systems (Liyanage et al. (2013), Liao et al. (2007), Jrad et al. (2011)). ERP regression or correlation analysis is extensively used in neuroscience and psychology. ERP components like P300, N170 and their latencies are used to fit models and prove hypothesises about the brain information processing (Eldar et al. (2010)).

2.7 This Work

From the discussion in Chapter 1 one realises that EEG modality favours the motivations to study the brain dynamics of neurological disordered patients. The literature review conducted highlights how EEG has excellent temporal resolution as it provides the most direct access to neural signals (Sporns (2011)). Studying the signals in a band specific

way is essential as the neural activity manifest themselves differently across the different EEG bands. Functional connectivity is fundamental when trying to understand stimulus specific responses of the brain. As mentioned in Section 2.2 functional connectivity is highly time-dependent in nature and thus it is pivotal to retain the temporal evolution of such connections to assess the observations in a comprehensive manner. The review revealed that the phase synchronisation of neural activity is key for understandings patterns of connectivity that appear within the neural assemblies. The review exposes the limitations of the current EEG signal processing tools for investigating the dynamic attributes of phase locking. Focusing on the low spatial resolution of EEG, researchers attempt to reconstruct the electrical sources responsible for observed signals however this leads to ambiguous results (Sporns (2011)). Hence it is preferred to process signals in the EEG sensor space by applying a different range of frequency domain techniques. Since it is difficult to uniquely localise sources onto the anatomical space it was decided to investigate phase locking at EEG sensor (i.e scalp) level. However this track also comes with its own set of problems like contamination from artifact and volume conduction. Studies revealed that volume conduction is attributed by zero phase lag hence the method for investigating phase coupling should be insensitive to zero phase difference. The application of graph theory is a new approach for evaluating brain networks quantitatively, however it has been successfully used in studies on diseased patients. The aim is to use the existing principles of representing brain connectivity as complex networks and obtain graph measures for further analysis.

The thorough review on autism and behaviour disorder reveals that these disorders have been correlated to disrupted connectivity between brain regions. This is used as the basis for this analysis to use biological signals from the brain to gain insight into how these disruptions are reflected onto functional connectivity. The perception of face by humans has been deemed to be biologically significant and perceived to highlight conceptual abilities in children (Widen and Russell (2008)). Hence face perception data is used for the analysis of phase locking in adults and children with behaviour disorders.

2.8 Summary

In this chapter, a range of clinical and technical concepts that are related to the thesis are reviewed. The chapter started of by discussing the basic human brain, the source of the action potentials and how they are propagated through the volume of material to the scalp, where it is recorded as EEGs. The concept of synchrony as an attribute of brain interaction is highlighted and followed by a detailed review of the current state of the art signal processing techniques to measure synchrony in EEG. The review revealed that the current techniques lack the capability to preserve the temporal evolution of phase locking which is fundamental to this research as mentioned in Chapter 1. A brief background is reported on Autism and behaviour disorder along with some outline on

the significance of studying face perception on both healthy and pathological populations to discern their social and emotional state. In the next chapter, a new methodology is proposed to identify phase locking periods with temporal information which then leads us to the observation of the new phenomenon called synchrostates in EEG.

Chapter 3

Investigating Phase Topography in Multichannel EEG Signals during Face−perception Tasks

As discussed earlier in Chapter 1 and 2, in order to understand the communication system of the brain it is important to investigate the time varying phase relations during cognition. Here a discussion on the algorithms to derive time varying phase patterns using continuous wavelet transform is presented. In essence, in the method developed exploits the time-frequency preservation property of wavelet transform for studying the temporal dynamics or evolution of synchronisation amongst different areas of the brain. The main goal is to explore the possible existence of stimulus-specific characteristic phase synchronisation patterns and their temporal stability that may enable one to objectively measure the information integration or processing capability. Compared to the contemporary approaches, here the time course is subdivided by associating them with a finite number of phase-synchronised states (using clustering) to find out how their switching sequence describes the execution of the face-perception task involving different types of stimuli. This may in turn lay the foundation of a methodology that will allow one to reliably diagnose or characterise different atypical neuro-pathological conditions more accurately.

After applying the method it is found that there exists a small number of well-defined phase-stable states, each of which is stable of the order of milliseconds during the execution of a task. These quasi-stable states are termed as *synchrostates*. The chapter also includes a discussion two particular issues that are fundamental for developing an integrated methodology for analysing the temporal evolution of phase synchrony from the onset of a stimulus using EEG time-series data. These issues are: 1) the definition of an objective measure for capturing the effect of time-varying synchronisation amongst the

EEG electrodes, 2) clustering of characteristic phase difference patterns and translating those unique clusters into synchrostates.

The method is validated and the existence of the phenomenon is investigated across two datasets of adult EEG. All the EEG analysis was conducted on face perception tasks. The preliminary experiments were run on a single subject adult EEG. The phenomenon was then shown to be free of artifact and volume conduction effects. Then the existence of synchrostates were shown on a group of 10 normal adults.

3.1 Wavelet Phase Synchronisation

The concept of phase synchronisation was first introduced by Huygens into the field of physics of coupled oscillators. When in perfect phase synchronisation the two phases of the signals are locked i.e. $\phi_x(t) - \phi_x(t) =$ constant. If the relative phase varies little in time, the two sources are considered to be synchronised.

Wavelet phase synchronisation is computed by using the complex argument of the complex wavelet series, $W_x(a,t)$ of a signal $x(t)$. Instantaneous phase difference between two signals $x(t)$ and $y(t)$ can be calculated by taking the difference of the instantaneous phases of the signals which are essentially the complex argument of the wavelet series $W_x(a,t)$ and $W_y(a,t)$ respectively. Instantaneous phase difference, $\Delta\phi_{xy}(a,t) = \phi_x(a,t) - \phi_y(a,t)$; where ϕ_x and ϕ_y are the complex arguments of the continuous wavelet transform of the time series $x(t)$ and $y(t)$ respectively.

Continuous Wavelet Transform (CWT) improves on the resolution problem that short-time Fourier transform (STFT) suffers from as the width of the window changes when the transform is computed for each spectral component. Thus the time and frequency resolution varies along the plane and hence it obtains better time resolution at higher frequencies while frequency resolution improves at low frequencies. $CWT(a,t)$ is a function of wavelet scale a, and time t (Quyen et al. (2001)) is defined below:

$$CWT(a,t) = \frac{1}{\sqrt{|a|}} \int x(t) h(\frac{t-\tau}{a}) dt \tag{3.1}$$

where $h(t)$ is the mother wavelet. CWT gives the user the freedom to choose the mother wavelet which serves as a wavelet prototype for all the windows. The wavelet transform is then computed up to a certain value of a, as required. As the scale is increased the window widens, picking up the lower frequency components.

3.2 Method

Phase synchrony analysis in EEG signals acquired over the scalp has been projected as an effective tool for understanding co-operative interactions between different regions in brain. However the conventional synchrony analysis in EEG does not preserve the temporal information and therefore offers average characteristics of phase synchrony only. Here, a wavelet-based synchronisation measure is proposed which inherently preserves the temporal information and therefore may give an accurate picture of transient synchrony evolution from the onset of a stimulus.

3.2.1 Computation of time-dependent phase difference topography

For the estimation of time varying phase synchronisation between two signals the first step is to compute their instantaneous phase difference and then to estimate the degree of phase locking over a period of time (Varela et al. (2001a)). If the instantaneous phase difference between two signals $x(t)$ and $y(t)$ is constant over a certain time then these two signals can be considered in synchrony over that time period. Here propose a CWT based methodology is proposed for investigating the transient dynamics of phase synchronisation in EEG signals. The time-frequency localisation property of CWT can be used in this case for first computing the instantaneous phase differences between different EEG electrode sites over the scalp which may then be used for analysing the temporal stability of the phase difference topography to get an idea of the extent of synchronisation between different brain regions.

It has been observed by different researchers that the spectral power of different EEG bands significantly changes depending upon the stimulus given, i.e. different types of stimuli yield dominant responses in different EEG band (Boiten et al. (1992)). As a consequence it may be assumed that the temporal stability of instantaneous phase difference topographies and hence the overall synchronisation pattern may manifest differently in different EEG bands. Therefore it appears to be more logical to study the synchronisation phenomenon in a band-specific way. Since CWT decomposes a signal to different scales (equivalent frequencies) at each time instant, it is possible to study the temporal evolution pattern of phase difference topographies for an isolated frequency band of interest. Therefore CWT is used as the main analysis tool, more precisely, a complex Morlet basis function is used as shown in (3.2) for computing the CWT of the EEG data.

$$\Psi_M(t) = \frac{1}{\sqrt{\pi F_b}} e^{2j\pi F_c t} e^{-(t^2/F_b)} \tag{3.2}$$

where, $\{F_b, F_c\}$ denote the bandwidth parameter and the centre frequency respectively. As can be seen from (3.2) this wavelet is a simple complex exponential centered at F_c. The values of F_b are chosen according to how much bandwidth one wants in the wavelet

filter. For the present case F_b=1 and F_c=1.5 are considered, as it gives a good trade off between time and frequency bandwidth.

Although one can choose from a number of mother wavelets, for more effective modeling of biological signals like EEG waveforms, the wavelet has to give a biologically plausible fit to the signal that is being modelled (Roach and Mathalon (2008)). The Morlet wavelet is one common biologically plausible wavelet used extensively in EEG analysis (Adeli et al. (2003)).

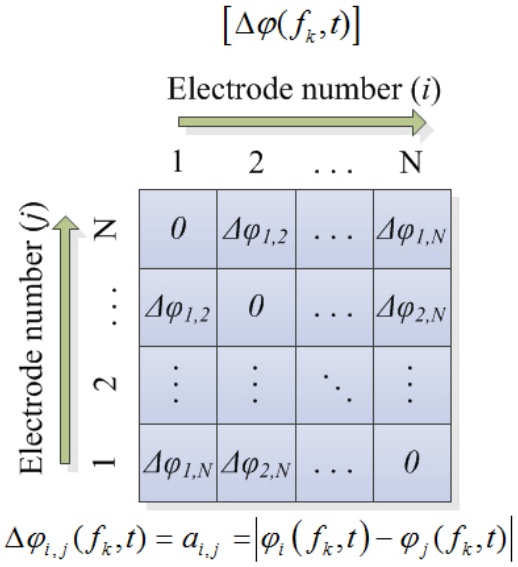

Figure 3.1: The structure of the phase difference matrix at frequency f_k at time t.

Considering N number of EEG channels placed over the scalp and $x_1(t), x_2(t), \cdots, x_N(t)$ be the EEG signals acquired at the respective channels, application of complex Morlet CWT on $x_i(t)\,; i \in \{1, 2, \ldots, N\}$ results in a complex time series $W_i(a,t)$ at the wavelet scale a at time t. $W_i(a,t)$ can be converted to a function of frequency and time $W_i(f,t)$ using the following relation (Addison (2010)) in (3.3).

$$f = F_c/(a \cdot \delta) \tag{3.3}$$

where, δ and f are the sampling period and the approximate pseudo-frequency, i.e. the frequencies corresponding to the scales, respectively. Subsequently, the instantaneous phase $\varphi_i(f,t)$ of $W_i(f,t)$ can be computed as (3.4).

$$\varphi_i(f,t) = \tan^{-1}\left(\frac{\mathrm{Im}\left[W_i(f,t)\right]}{\mathrm{Re}\left[W_i(f,t)\right]}\right) \tag{3.4}$$

$\mathrm{Im}[W_i(f,t)]$ and $\mathrm{Re}[W_i(f,t)]$ being the imaginary and the real part of $W_i(f,t)$ respectively. Consequently, the instantaneous phase difference $\Delta\varphi_{i,j}(f,t)$ between the channels

i and j can be given by (3.5).

$$\Delta\varphi_{i,j}(f,t) = |\varphi_i(f,t) - \varphi_j(f,t)| \tag{3.5}$$

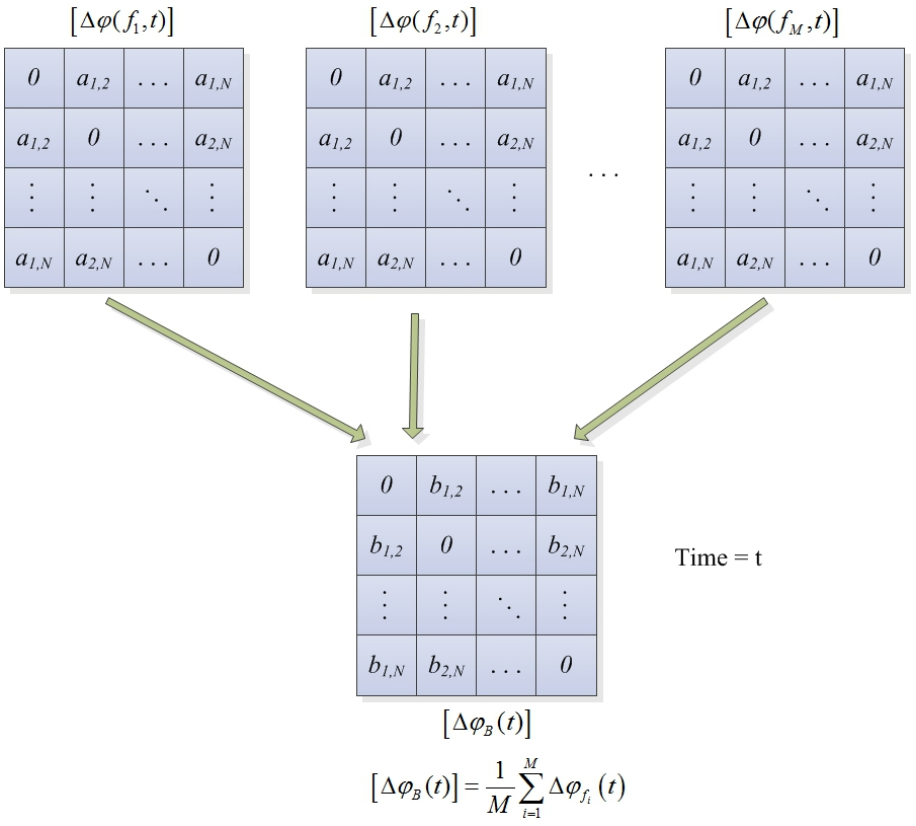

Figure 3.2: Computation principle of band-specific phase difference matrix construction

Computation of $\Delta\varphi_{i,j}(f,t)$ at a time instant t_1 and frequency f_1 for $i,j \in \{1,2,\ldots,N\}$ yields a symmetric square matrix $[\Delta\varphi(f_1,t_1)]$ that describes the pairwise relationship of phase difference at the frequency f_1 for all the EEG channels at t_1 time instant. Figure 3.1 shows an example of one such phase difference matrix at a frequency f_k at time t. For computing the average response within a subject group the individual $\Delta\varphi_{i,j}(f,t)$ are averaged over all the subjects to get the average wavelet response for the group in consideration. If an arbitrary frequency band of interest B is spanned over the frequencies $\{f_1, f_2, \cdots, f_M\}$ then the instantaneous phase difference matrix for B at time t can be formulated as (3.6)-(3.7). Figure 3.2 depicts the averaging step across all frequency matrices within a chosen band B to derive the band average $\Delta\varphi_B(t)$ as a function of time.

$$[\Delta\varphi_B(t)] = \frac{1}{M}\sum_{i=1}^{M}\Delta\varphi(f_i,t) \tag{3.6}$$

$$(b_{i,j})_{\Delta\varphi_B}(t) = \frac{1}{M}\sum_{k=1}^{M}(a_{i,j})_{\Delta\varphi_{f_k}}(t) \tag{3.7}$$

where, $(b_{i,j})_{\Delta\varphi_B}(t)$ is the $(i,\ j)^{th}$ element of the matrix $[\Delta\varphi_B(t)]$ and $(a_{i,j})_{\Delta\varphi_{f_k}}(t)$ is the $(i,\ j)^{th}$ element of $[\Delta\varphi_{f_k}(t)]$. Subsequently, $[\Delta\varphi_B(t)]$ can be computed at different time instants $\{t_1,\ t_2,...,\ t_n\}$ resulting in a set of such matrices $[\Delta\varphi_B(t_1)]$, $[\Delta\varphi_B(t_2)]$, ..., $[\Delta\varphi_B(t_n)]$ (a shown in Figure 3.3) that describes the complete picture of temporal evolution of the phase difference from the onset of a stimulus till the end of the corresponding action in the particular frequency band B over all the EEG channels on the scalp. The whole process is pictorially depicted in Figure 3.1- Figure 3.3.

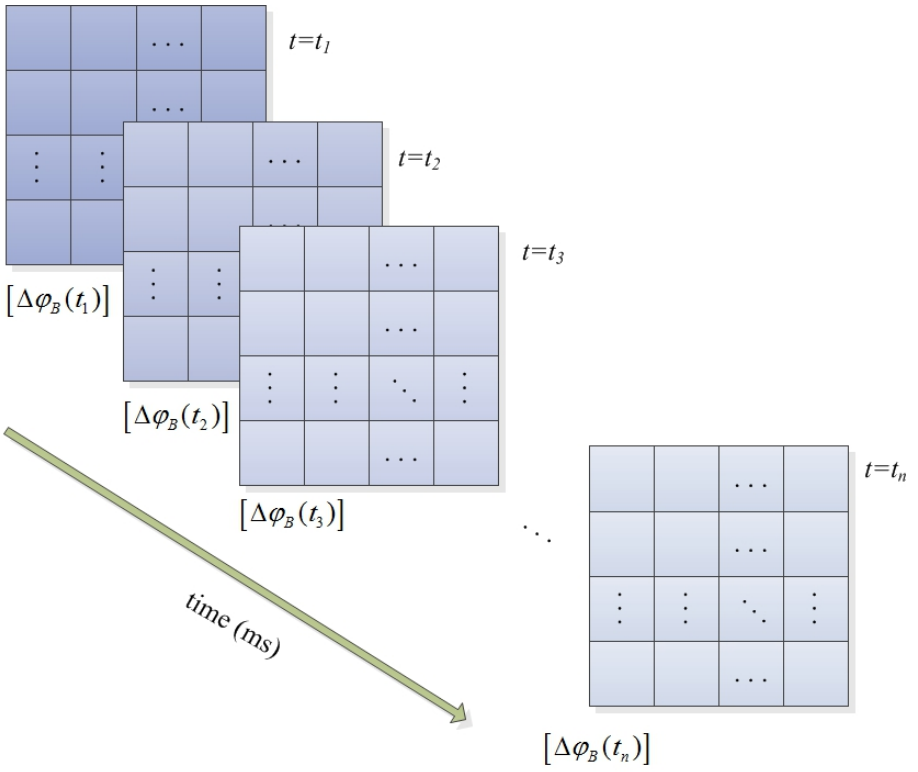

Figure 3.3: Computation of band-specific phase difference matrix from the onset of a stimulus till the end of the desired time window.

3.2.2 Clustering of phase difference matrices into unique set of states

Once all the cross-electrode phase difference matrices for a particular band are formulated over the entire duration of a specified time interval - in this case, it would be interesting to see the temporal evolution of these topographies at subsecond order time interval, the next pertinent question is whether there exists any unique spatio-temporal pattern of phase difference topographies during the execution of the cognitive task. The first step for that is to identify all possibly unique topographies over the entire time duration of interest. A certain class of pattern recognition techniques could be employed

for this purpose. The k-means clustering is one such unsupervised pattern recognition technique. Contemporary researchers have used various clustering and segregation tools to solve many biomedical problems. Clustering problems resolved using pattern recognition techniques include the segregation of densely connected brain regions (Rubinov and Sporns (2010)), estimating microstates (Pascual-Marqui et al. (1995)) and for localising interictal epileptic activity from functional Magnetic Resonance Imaging (fMRI) (V.L. Morgan and Abou-Khalil (2007)).

For a given dataset χ, $\chi = \{x_p\}, p \in [1, \cdots, P]$, assuming the number of underlying clusters is known, k-means algorithm iteratively minimises a cost function given below (3.8).

$$J(\theta, U) = \sum_{p=1}^{P} \sum_{q=1}^{m} u_{pq} \|x_p - \theta_p\|^2 \tag{3.8}$$

where, $\theta = [\theta_{T1} \ldots \theta_{Tm}]^T$, $\|\cdot\|$ is the Euclidean distance, θ_q is mean vectors of the q^{th} cluster and $u_{pq} = 1$ if x_p lies closest to θ_q; 0 otherwise (Theodoridis et al. (2010)). Here, $\chi = \{X_i\}, i \in [1, \cdots, P]$ is the dataset of all pairwise EEG instantaneous phase differences, as a function of time and frequency calculated using (3.5). The dataset χ was clustered along time, for a chosen frequency band, to find out unique phase synchronised patterns. Initially a range [m_{min}, m_{max}] is defined for possible clusters m for the dataset χ. The k-means clustering runs n (n random initialisations) times for each m within that range and for every n runs the minimum value of the cost function J_m (as shown in 3.8) is calculated and stored. The cost function J_m essentially indicates the sum of distances of the data-points from the nearest cluster mean when m clusters are considered. The value of J_m is dependent on the number of clusters and also the dataset under consideration where a high value of J_m represents a less compact cluster. Thus the knee in the plot of J_m against m is an indication of the number of optimal clusters underlying the data. If the plot of J_m against m shows a significant knee at m = $m1$ (say) then it signifies that the number of optimum clusters underlying the dataset χ is likely to be $m1$. To be noted that in the plot of J_m versus m it is typical to have multiple such knees as m varies within its selected range. In cases, where there is an increase in the J_m value, it indicates that the distance between all the data points with respect to the nearest mean of clusters has increased. This increase could be due to the splitting of large compact clusters into several smaller ones, caused by increasing the value of m. In such cases, as conventionally followed in machine learning, the earliest and the most prominent knee should be considered as the characteristic knee, as it explains the underlying dataset with minimum complexity. The main information lies in the fact how many compact clusters can be identified in the whole dataset and what are the average characteristics of the data-points associated with each cluster. Thus the absolute value of J_m in the plot of J_m against m is not important but the value of m at which J_m attains minimum value (the significant knee) is the important parameter indicating the number of underlying clusters.

In a higher dimensional feature space, the landscape of the cost function $J(\theta)$ may have multiple local minima and there is small probability of finding a higher value of the cost function if a local minima has been found by the optimisation process. Since the k-means clustering have the problem of getting trapped to local minima, it should be run multiple times with different initialisation of the cluster means and the best result with the minimum value of the cost function should be considered. Therefore in the proposed method, the best-results of the k-means algorithm for each choice of k is considered out of $n = 10$ different random initialisations of the cluster means. This way the incremental k-means plots the best cost function to obtain the J_m as also suggested in (Theodoridis et al. (2010)).

In order to determine possible unique clusters optimally, incremental k-means clustering is performed over the time series of all phase matrices, to associate similar patterns into a single class, following the method described above. It is well known that the phase and hence the phase difference data is circular in nature (circular data) therefore standard Euclidean distance based clustering should not be directly applied on such datasets (Mardia and Jupp (2009)). In order to circumvent this problem, it is first ensured that the phase of CWT based complex time-frequency decomposition is always bounded within $\varphi_x \in [-\pi, \pi], x \in [1, \cdots, N]$. Next the phase difference data for all electrode pairs are normalised using the minimum and maximum values of the phase difference $\Delta\varphi_{xy}^{\max} = 2\pi$ and $\Delta\varphi_{xy}^{\min} = 0$, so that the transformed data lies within $\Delta\varphi_{xy}^{normalised} \in [0, 1]$. This transformed phase difference data is fed to the clustering algorithm described in (3.8).

In this case, χ is the dataset of all pairwise EEG instantaneous phase differences $[\Delta\varphi_B(t_1)]$, $[\Delta\varphi_B(t_2)]$, ..., $[\Delta\varphi_B(t_n)]$, as a function of time. The dataset χ is clustered along time t, for a chosen frequency band B, to find out unique phase difference patterns. The algorithm yields k centroids, for each cluster or state and a vector of length n with the corresponding state or cluster labels for each and every time instance over which it was clustered. The centroids hold average information for each of the clustered states whereas the cluster labels signify when in time each state has occurred.

Once the phase-difference matrices are uniquely clustered over different time instances, the centroids are translated into corresponding colour-coded head-map topographies following arbitrary colour coding convention. This is done by first calculating the average phase difference seen at a particular electrode with respect to the rest of the electrodes, i.e. taking row-wise average and considering it as the average phase difference at that electrode index and assigning a particular colour corresponding to the numerical value of that phase difference and finally transforming it to a contour plot. Such head-map topographies give a visual representation of the distribution of average phase differences between different regions of brain over the scalp. Note that these plots should not be viewed or compared to the typical EEG potential plots or the power spectrum plots typically generated in quantitative EEG (qEEG) analysis. Here the plots show the

gross phase difference between different electrodes over the scalp over a particular time window. Higher numerical values represent greater gross phase difference of the electrode with all the other electrodes and low values indicate that the electrode has relatively less phase difference with all the other electrodes in that configuration. The set of topography clusters identified using k-means algorithm are termed as *synchrostates*. The state labels are used to construct a transition plot to illustrate the switching sequence of the synchrostates over the time of the EEG recording. This is simply done by plotting the cluster labels yielded by the clustering algorithm.

The unsupervised learning technique adopted here is based on the concept of hard clustering, i.e. a single data-point corresponding to each time instant should belong to one of the clusters. Since the phase coupling is measured in the temporal resolution of millisecond one can assume for practical reasons that the intrinsic brain dynamics is bound within one state at each time step over the non stationary time window of EEG.

3.3 Results

Once the critical steps for investigating transient phase coupling was identified the algorithm was run on multichannel EEG data using Matlab. The following experiments were carried out on a normal single-subject multiple-trial EEG dataset and normal adults multiple-subjects multiple-trials dataset. All data was baseline corrected and epochs over 200μV threshold were rejected as artifacts. Data was then band-pass filtered within 0.5-50 Hz using a 5^{th} order digital Butterworth filter to isolate the EEG bands of interest.

For each of the experiments, the instantaneous phase difference between all pairs of electrodes were computed following the procedure described in Section 3.2.1 by taking the argument of the continuous complex Morlet wavelet transform of the signals on each channel and subtracting it from the other electrodes. The cross-electrode relative phase at a particular time instant is represented as a symmetric square matrix with zero diagonal elements as they represent the phase difference of an electrode to itself (as shown in Figure 3.1). These matrices are then averaged across the number of trials considered during that run. Observation of this resultant multi-channel phase data in a sequence of intervals of the order of milliseconds reveals the existence of discrete and distinctive patterns that are stable over finite number of time-frames. This is an interesting observation, as it is similar to the concept of microstates in (Musso et al. (2010)) where the authors observed stable potential distribution maps over millisecond order time segments. Similarly, it is observed that the phase difference maps remain stable for certain time interval of the order of milliseconds i.e. they are phase synchronised and then suddenly change to a new configuration that also remains stable for finite time. The temporal stability of such synchrostates may be indicative of the time, required for

maintaining such a phase relationship between different regions of the brain in order to perform a certain task - in this case, a face perception task.

Incremental k-means clustering is performed over the time series of all phase matrices along time t, for a chosen frequency band (θ, α, β, γ), to quantitatively define the unique phase difference patterns. The k-means algorithm clusters similar states and yields k centroids for each cluster or state and a vector of length t, with the corresponding state or cluster labels for each phase difference matrix, for every time instance, along which it was clustered the data. All the data-points within a cluster are considered to have a generalised characteristic of that of the mean of the cluster (state), even though they can slightly differ from each other, as they possess EEG temporal information of the order of milliseconds. The state labels are used to construct a transition plot to illustrate the transients of the synchrostates over the time of the EEG recording. The consecutive occurrences of same labels (i.e. similar phase synchronised patterns) have been interpreted as the prevalence of the same state. On the other hand, sudden changes in the cluster label (i.e. different phase-difference pattern) from previous clusters are considered as switching of the state. The run time for each experiment varied depending on the number of electrodes and trials in each study. Each experiment took and average 20 mins to run.

3.3.1 Experimental results and analysis of single subject multiple trial EEG dataset

The first set of experiments were carried out on the SPM multimodal face-evoked dataset (SPM). This data was acquired from a single subject while the person was presented images of normal and scrambled faces. The stimulus dataset consisted of 86 normal and 86 scrambled face images. Each face stimulus went through 2D Fourier transformation, random phase permutation, inverse transformation and outline-masking to create the scrambled face (Ashburner et al. (2008)). Figure 3.4 show examples of the normal and scrambled face stimuli presentation protocol for the single subject analysis reported in this section. The EEG recording was done by randomly selecting stimuli from this set and presenting it to the subject, multiple times creating multiple trials for each type of stimulus. The data was sampled at 2048 Hz and was recorded with 128 EEG channels over several trials of which the first 100 trials were used for this analysis.

In order to compensate for the variability of the results and to investigate its consistency over different trials the whole data set was divided into two non-overlapping groups (trial 1-50 and trial 51-100) and taking all the trials (trial 1-100) as the third group. This is done from the point of view that the ensemble statistics of the pattern underlying the cross-electrode phase difference should be consistent over small subsets of multiple trials and the trials consisting of the entire dataset.

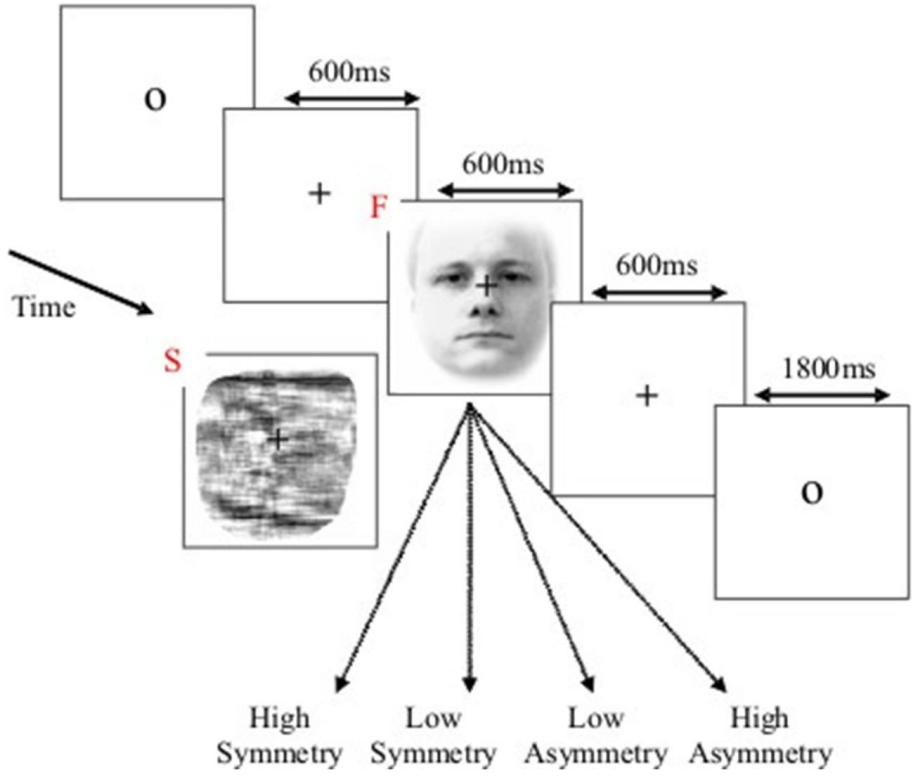

Figure 3.4: Stimulus presentation protocol for the single subject face perception experiment. Image taken from (SPM)

3.3.1.1 Analysis for normal face

Figure 3.5 shows the results from all the three runs of the incremental k-means optimisation routine for optimally clustering the synchrostates in the β band when applied on EEG data for normal face perception task. Here β rhythms are considered, as they have been reported to be linked to perception related modulations Wróbel (2000). In this case, over all the runs the k-means clustering consistently results into three unique states as there exists a knee in the cost function (J_m) at $k = 3$.

After obtaining three unique synchrostates, the cross-channel EEG phase differences are averaged for each electrode to get an average phase corresponding to that node. These are next used to generate a contour plot over a head-map by connecting nodes having the same average phase difference values. The topographical distributions or contour plots of each of these three synchrostates are shown in Figure 3.6. Note that the topographies should not be interpreted like standard quantitative EEG (qEEG) plots (which show the average spectral power over the scalp), as they are fundamentally different. Here, the plots show the gross phase difference between different electrodes over the scalp during the occurrence of the state. Such head-map topographies give a visual representation of the distribution of average phase differences between different regions of brain over the scalp. Higher numerical values (reddish hues) represent greater gross phase difference of the electrode with respect to all the other electrodes and low values (bluish hues) indicate

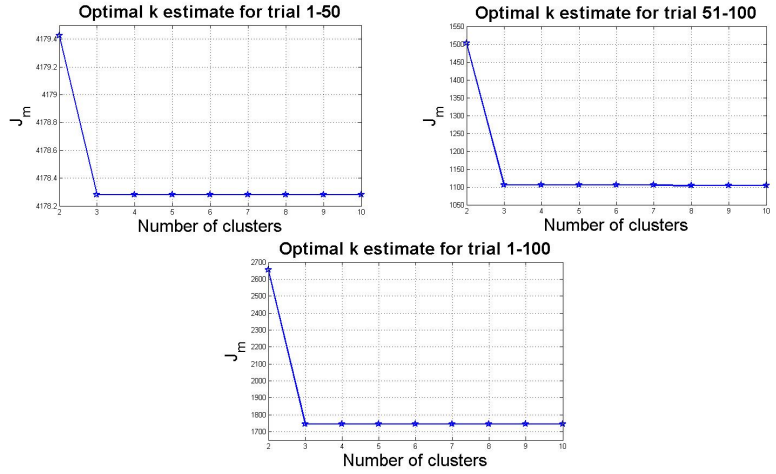

Figure 3.5: Determination of the optimum number of underlying clusters (k) for different group of EEG trials during normal face perception. All the plots show that the first significant knee is three, i.e. the optimal number of synchrostates is three.

that the electrode has relatively less phase difference relative to all other electrodes, in that configuration. It is interesting to note that the topographical maps of synchrostates are consistent across different sets of runs and are almost unique in the experiment. In Figure 3.6, there is slight difference in the first state topography, especially in the fronto-central electrodes. This much of difference is expected due to variability of the trials, mood or mental condition of the subject, attention level, particular characteristics of the face stimulus and various other subconscious random processes going on within the brain during the data-recording. In most literature on EEG studies, there is evidence of such inter-trial variability. Despite these incongruences, the main unifying theme among these plots is that almost similar phase synchronisation phenomenon can be observed in these states.

To explore the consistent repeatability of the synchrostates for the present task, the number of times each of these states occurs in the β band were computed. The results, as shown in Table 3.1, confirm that the number of occurrence of each of the synchrostates is consistent over separate trial groups with little difference. The little variation observed could be attributed to the fact that even during a focused task, there could be multiple cognitive processes that run in the background. These may not be directly related to that specific task but may influence the phase relationship between different brain regions in an indirect way.

The same technique was applied for extracting the synchrostates in the θ, α and γ bands and the cost function results of incremental k-means are shown in Figure 3.7. It was found that, in θ and α band, the optimal number of synchrostates varies between separate trials but within a small range (approximately 3-5) whereas, for γ band the optimal number of synchrostates is obtained at k=3 consistently. This small variation of

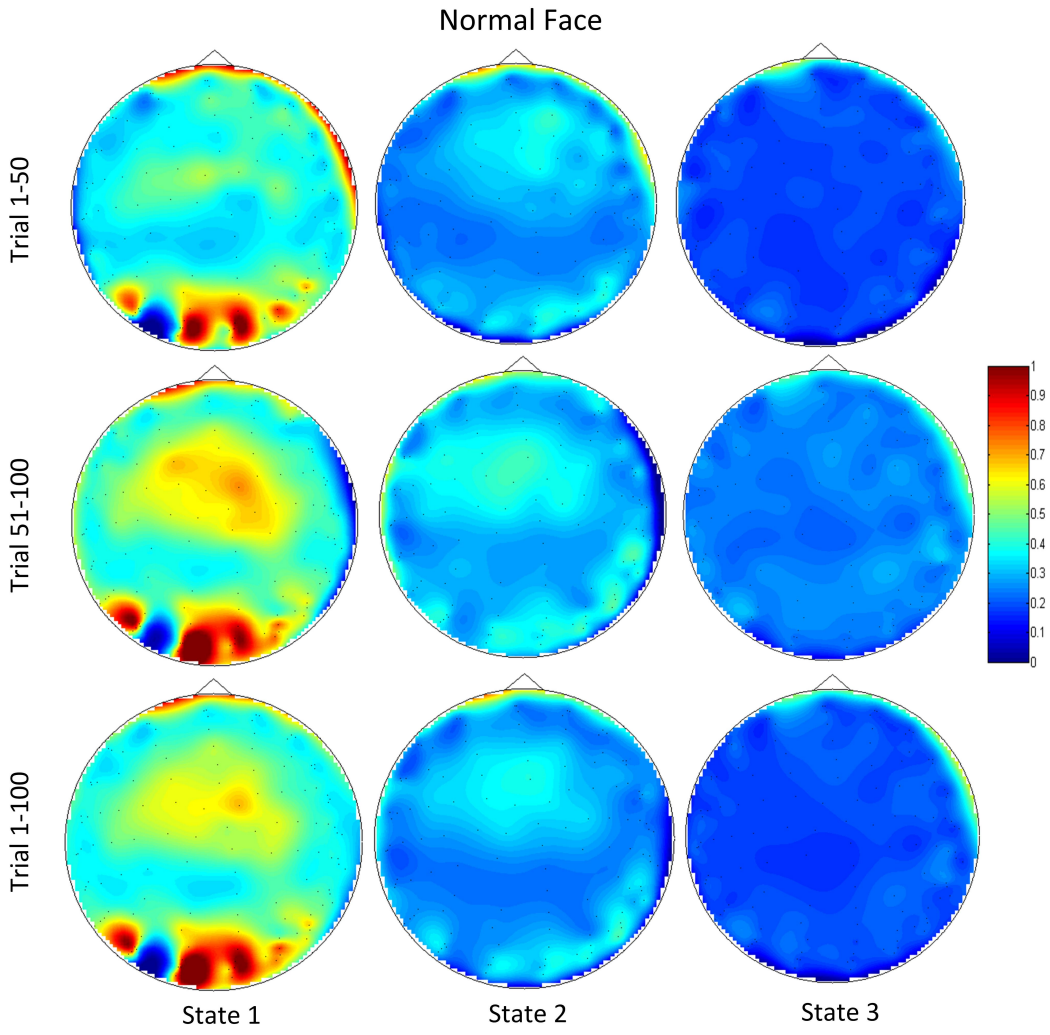

Figure 3.6: Clustered synchrostate headplots showing the gross phase difference between different electrodes over the scalp during the occurrence of the state for trials 1-50, 51-100 and 1-100 of normal face perception in the β band.

Table 3.1: Time of Occurrence (time instants) of three states for β band with normal face stimulus

EEG segments	State 1	State 2	State 3
trial 1-50	101	43	256
trial 51-100	105	31	264
trial 1-100	113	42	245
Mean	106.33	38.67	255

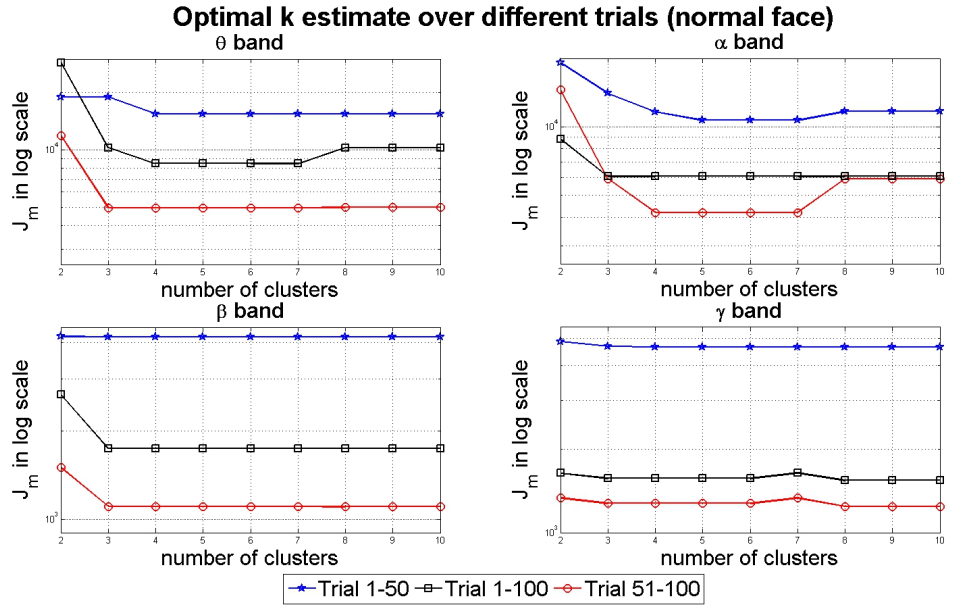

Figure 3.7: Cost functions for clustering in different EEG bands with increasing k during normal face perception. The first significant knee of the plot indicates the optimal number of clusters or states underlying the dataset. The β and γ band have a knee at three across all sets of runs.

optimal number of synchrostates in the α and θ bands may once again be attributed to the fact that they represent different background cognitive processes, executed during the cognitive task which are not directly related to the present task and therefore may vary between the trials.

3.3.1.2 Analysis for scrambled face

A similar analysis has been carried out for the scrambled face case. Figure 3.8 shows the optimal k for the scrambled face run in the β band which is once again obtained at $k = 3$. The normalised average phase difference head plots were also plotted in a similar way to those for normal face perception in β band to get a better idea of the topographical structures of the synchrostates which are shown in Figure 3.9. Interestingly, the maps appear very similar to the plots resulting from the normal face (Figure 3.6) stimuli showing that the actual phase topographies remain same for both of the tasks. In one sense this is expected as both of the tasks fall into the generic category of visual perception and are plots from the same subject. The optimal number of synchrostates in the other EEG bands (θ, α, γ) once again varies from 3 to 5 in this case as shown in Figure 3.10, as it did during a normal face perception task. Once again this phenomenon is attributed to the existence of background cognitive processes, independent of the present task and inter-trial variability.

The existence of consistent number of synchrostates in β band for both the cases conforms to the theory that β rhythm is more related to visual perception tasks (Gross et al.

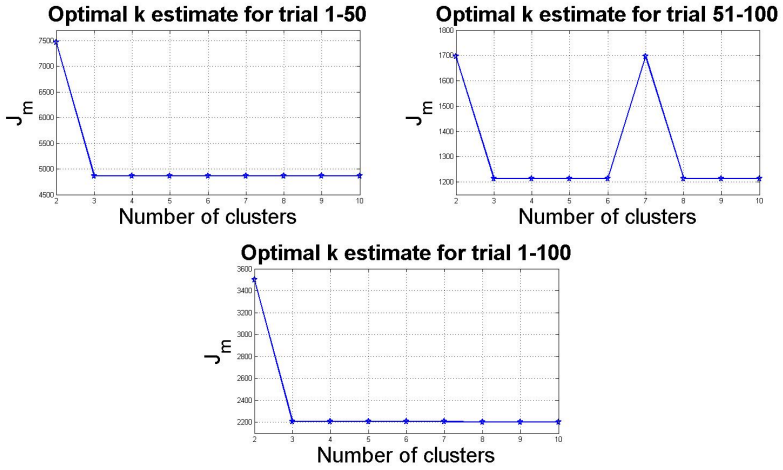

Figure 3.8: Determination of the optimum number of underlying clusters (k) for different group of EEG trials during scrambled face perception. All the plots show that the first significant knee is three, i.e. the optimal number of synchrostates is three.

(2004), Wróbel (2000)) and therefore one may expect dominant and stable information exchange patterns in the β band. On the other hand, the very small variability of the number of optimal synchrostates in the other EEG bands (3 - 5 in both the cases) also indicates towards consistency of the existence of synchrostates in these bands.

Table 3.2 shows the number of times each state has occurred for each run during the presentation of scrambled face stimulus in the β band. The important point to note is that in this case although the topographic maps of the synchrostates are similar to those of the normal face perception stimulus, the number of occurrence of each of them is markedly different. State 3 although shows a similar number of occurrence to that of the normal face perception, the number of occurrence of state 1 and state 2 differ significantly between the two cases. A close observation reveals that the state 1 occurs more frequently during normal face processing whereas state 2 occurs more often during the scrambled face processing indicating towards different types of processing which is dependent on the type of stimulus. This supports the claim that the stability and occurence of the synchrostates is depended on the stimulus given to the subject.

3.3.1.3 Switching characteristics of synchrostates for normal and scrambled face

In order to distinguish between the time-course of each synchrostate specific to a stimulus that may be indicative to the processing time required for a task, their switching time-course were plotted over 400 samples (approximately 195 ms) after the onset of the stimulus for both normal and scrambled face. Each subplot in Figure 3.11 shows the switching transition between the 3 states obtained from the average EEG signals using

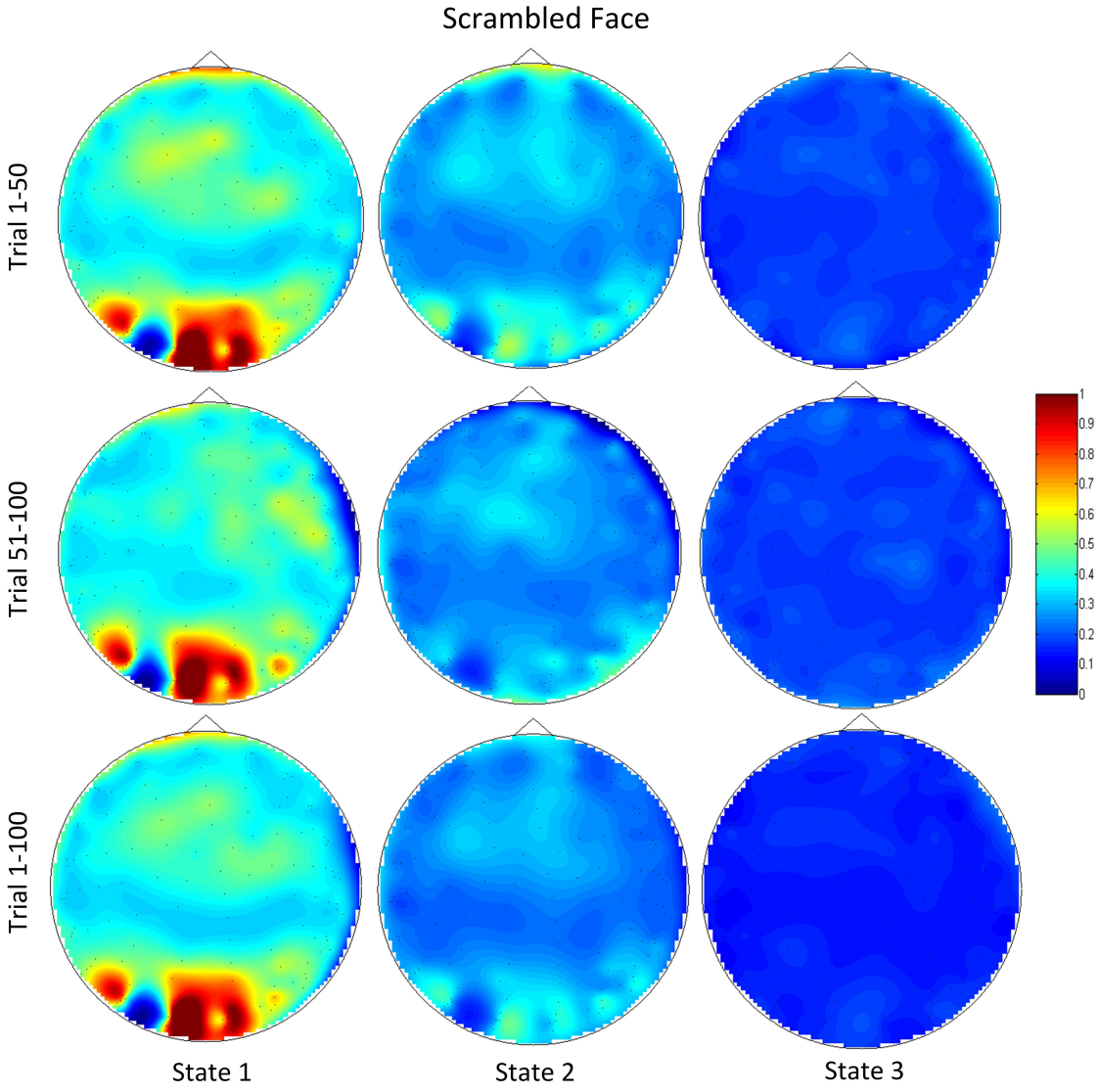

Figure 3.9: Clustered synchrostate headplots showing the gross phase difference between different electrodes over the scalp during the occurrence of the state for trials 1-50, 51-100 and 1-100 of scrambled face perception in the β band.

the 1-50 trials, 51-100 trials and 1-100 trials for normal and scrambled face stimuli. As can be seen from Figure 3.11, the switching time-course of the synchrostates for different trials for each of the considered cases follow a consistent pattern, whereas they are markedly different between the normal and scrambled face perception, indicating toward the stimulus-specific nature of it.

Also it can be noted that the inter-synchrostate transition in Figure 3.11 occurs abruptly which is again similar to the transitional nature of the microstates (Pascual-Marqui et al. (1995)). Assuming that each task can be broken down into a sequence of subtasks, the time duration of each synchrostate in the time-course sequence may be indicative to the processing time required by the underlying brain circuitry for a subtask. In addition, the sequence and duration in which the synchrostates occur may reflect the sequence

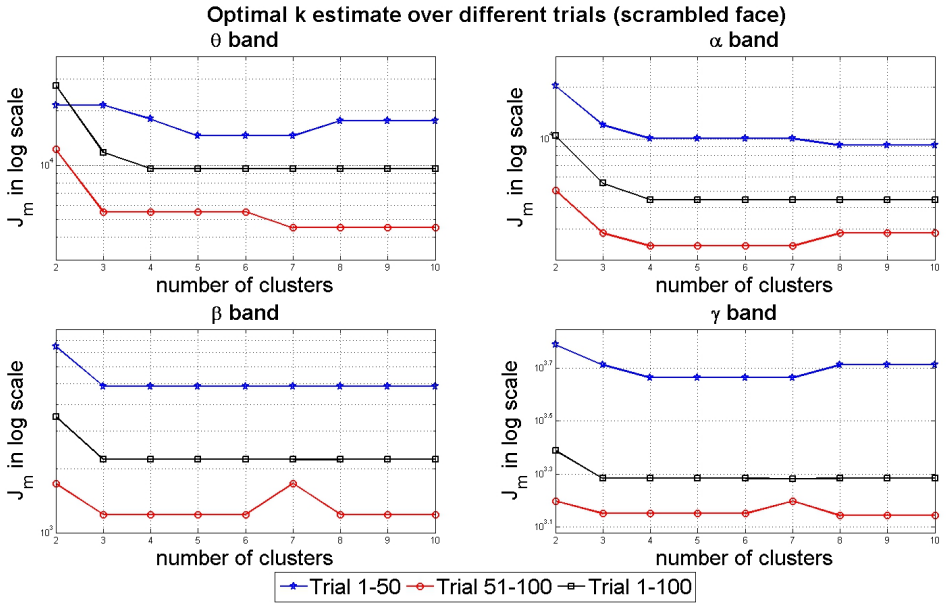

Figure 3.10: Cost functions for clustering in different EEG bands with increasing k during scrambled face perception across different trial groups.

Table 3.2: Number of Occurrence (time instants) for Three States in β Band with Scrambled Face Stimulus

EEG segments	State 1	State 2	State 3
trial 1-50	29	123	248
trial 51-100	31	155	214
trial 1-100	29	137	234
Mean	29.67	138.33	232

and time of information exchange that is characteristic to a particular task. Therefore analysis of synchrostates could be an effective tool for quantitatively characterising information processing ability of brain in different neurophysiological disorders where information integration and processing speed are the biggest issues, by comparing the sequence and duration of the synchrostates with those in a control population.

3.3.1.4 Consistency of the synchrostates in different ensembles of EEG trials during normal and scrambled face perception

So far the clustering results over large number of trials (50s and 100s) have been reported. It may be argued that this may have possibly averaged out small inter-trial variability of the new physical phenomenon i.e. the existence of synchrostates during normal and scrambled face perception. This is fundamental and worth looking at, in two different contexts of face perception task, to understand the basic physical nature of processing of these stimuli within the brain. It is verified that the patterns obtained in larger ensembles of EEG trials are consistent, even in smaller groups as well. The clustering results that produce the optimal k estimates under normal and scrambled face stimuli

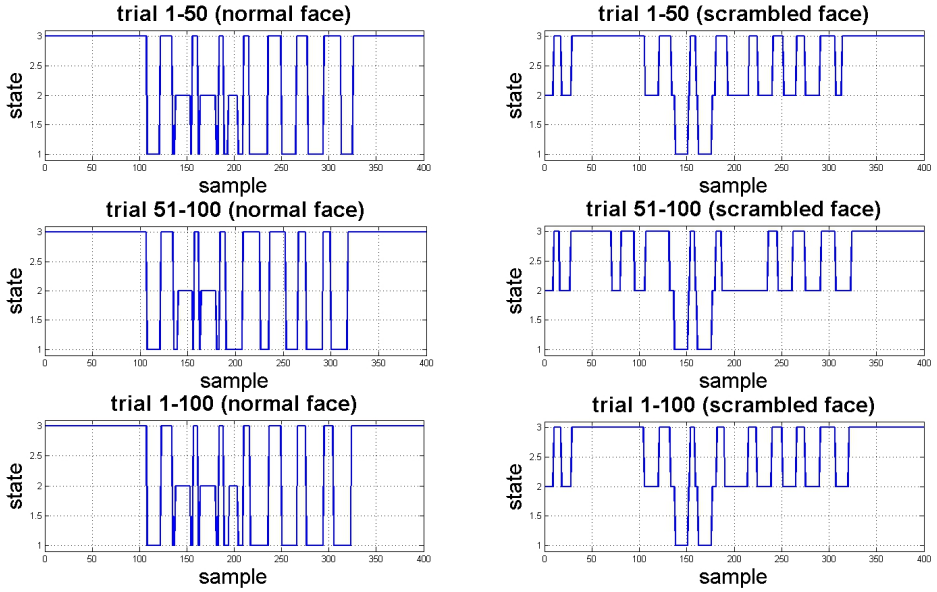

Figure 3.11: β band temporal evolution of synchrostates for different trials of EEG during normal and scrambled face perception. The temporal switching patterns amongst these states during the same face stimuli are similar across different ensemble of trials however they are very different between the two stimuli (normal and scrambled face)

have been reported here. The 100 trials of the 128 channel EEGs are grouped into different ensembles as groups of 10s and 20s and then the clustering algorithm was run on each ensemble. Figure 3.12 shows that in each group of normal and scrambled face processing, the optimal unique phase synchronised patterns or synchrostates is three. These three unique states have been shown to be the same with larger ensembles as well (50s and all) as in Figure 3.5 and Figure 3.8. As discussed in Section 3.2.2, in different trials the characteristic knee can be found by the first significant fall in the cost function J_m. In some cases, there is an increase in the cost function indicating that the total sum of Euclidean distances of all data points from the respective mean of clusters has increased due to splitting of large compact clusters into several smaller ones.

The fact of consistently obtaining three optimal states also confirms that the number of states obtained in the synchrostate analysis does not depend on how the data was divided in groups and on the choice of the number of trials used. Any stochastic process, such as EEGs are expected to have some inter-trial variability but the statistical measures, capturing the common underlying characteristics of different ensembles have been found to be the same. The results show that irrespective of the starting point, i.e. the number of trials the user selects at the beginning, a consistent number of synchrostates is still obtained.

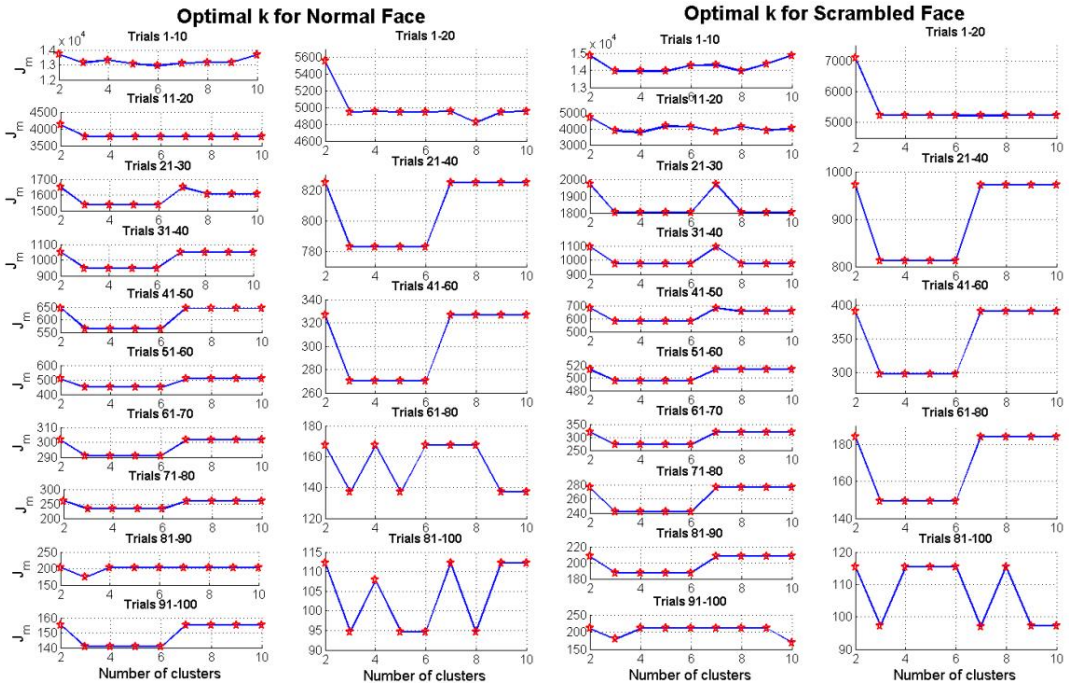

Figure 3.12: Determination of the optimum number of underlying synchrostates for different ensemble of EEGs during normal and scrambled face perception. All ensembles show a significant knee at cluster 3 hence the optimal number of synchrostates is consistent across different ensembles of the data.

3.3.2 Synchrostate analysis of multiple subjects involving multiple trials during face perception

The results shown in the foregoing section are only based on a single subject. In order to explore whether the result holds true for a number of different subjects, a similar exploration was run on EEG recorded from 10 subjects, when they were presented with three types of face perception stimuli i.e. famous face, scrambled face and unfamiliar face. An example of these stimuli and the presentation protocol is shown in Figure 3.13. Data available in Henson et al. (Henson et al. (2011)) was used, where EEG was recorded simultaneously from 70 electrodes at 1.1 kHz, with the recording reference set at the nose electrode. The data was epoched from -200 ms to 600 ms to produce 100 trails for each subject and subsequently was pre-processed, filtered and artifact rejected, using the same algorithms and criteria used in the previous single subject study (Section 3.3.1). The results presented in this section show the average synchrostate response of the 10 subjects which were obtained by taking the mean of the phase response of the 100 trials of each stimulus of each of the 10 individuals. The EEG phase difference of each 10 adults were averaged to generate the mean phase response of the cohort.

Using this mean phase response and following the steps (described in detail in Section 3.2) to generate the optimal states using k-means clustering from the wavelet based time-frequency domain decomposition of the EEG signals, the obtained the results are

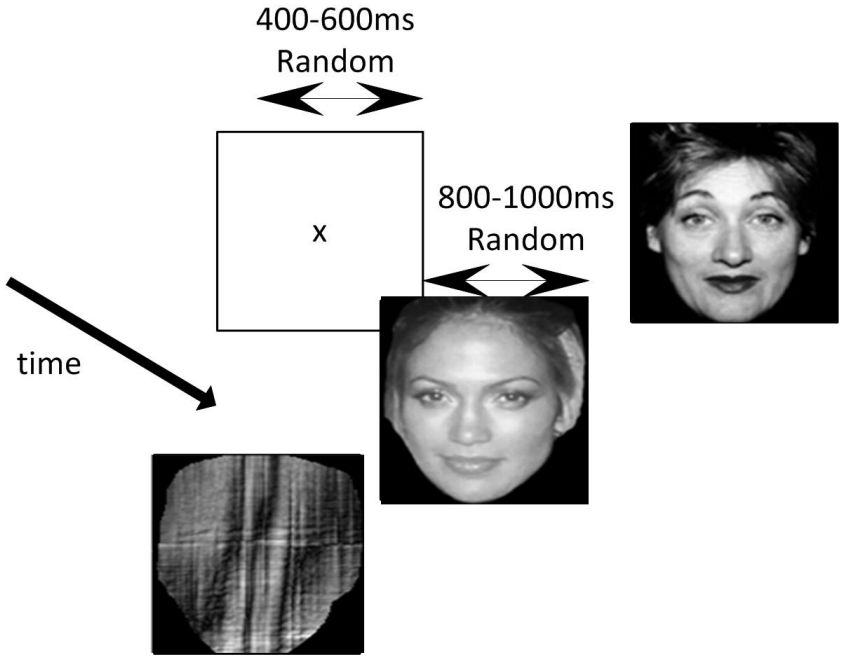

Figure 3.13: Stimulus presentation scheme for the multiple subject adult face perception dataset.

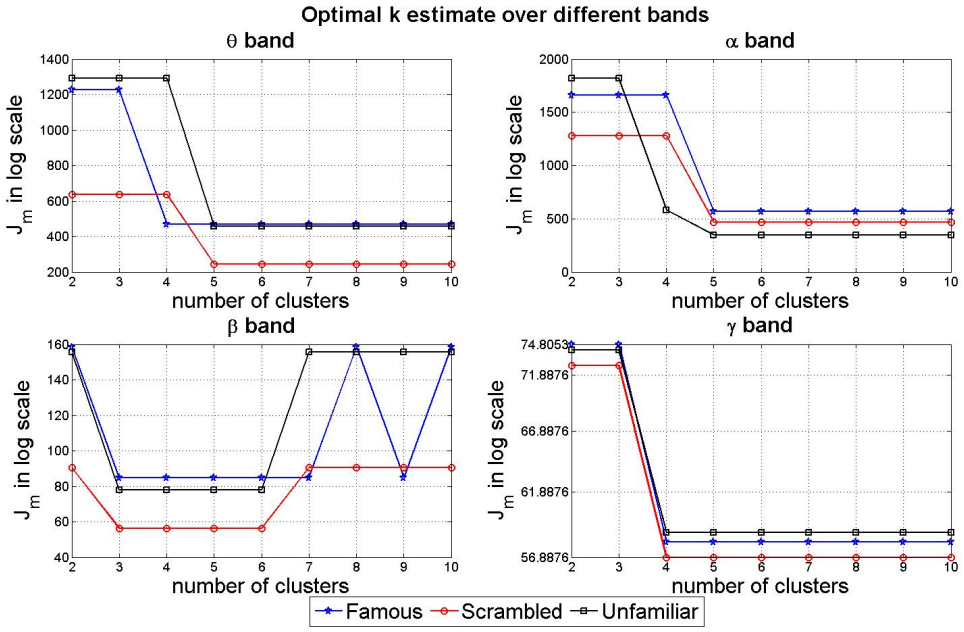

Figure 3.14: Determination of the optimum number of underlying clusters for different EEG bands during famous, scrambled and unfamiliar face perception for 10 subject group analysis. The number of states for all three stimuli in the β band is three.

shown in Figure 3.14. For all the three stimuli (famous, scrambled and unfamiliar), the α, β and γ-band - all cluster at 5, 3 and 4 respectively, as the first significant knee is observed at these values. In the θ band however, the famous face stimulus yields four optimal states whereas the other two (scrambled and unfamiliar) stimuli have five optimal synchrostates. To corroborate the results from the single subject study reported in previous section, the results of the β-band synchrostate analysis for multiple subject group analysis are detailed here.

The head-plots for the synchrostates for all the three stimuli (in the β band) have been reported in Figure 3.15. As confirmed from Figure 3.14 the optimal number of synchrostates for all three stimuli is 3 in β band. The corresponding unique phase topographies or head-plots (Figure 3.15) show that for the general task of perceiving a face, be that famous or unfamiliar, the synchrostate topographies for both the famous face and the unfamiliar face are comparable. However, when perceiving the scrambled face, the state topography is different. The difference between the face (famous and unfamiliar) and the scrambled topographies in this experiment could be an indication that every individual perceives the scrambled face in a different form to each other, hence scrambled face does not yield a topography that is similar to the face (famous and unfamiliar) topography of the cohort. One may conclude that the every individual perceives the face category in a similar way hence both of the famous and unfamiliar headplots are similar. Another point to be noted here is that in this experiment the no. of electrodes were less than that of the study with single subject described earlier. This leads to loss of resolution in the computation process itself. Hence the result is expected to be less consistent and have more variability with fewer electrode EEG systems.

The transition plots in Figure 3.16 show the 363 ms post stimulus response. The state labels between both experiments are arbitrarily labelled, so state 1 in analysis 1 (single subject analysis) is not analogous to state 1 in the second (group analysis). It is evident from Figure 3.16 that both famous and unfamiliar faces have similar transient synchrostate switching dynamics and response. However, similar to the conclusion from the face perception study, discussed earlier, it appears that for this pool of subjects as well, the state transitions are different for the general category of normal face (famous and unfamiliar faces) and scrambled face. These observations obtained from the results of 10 subjects, during a different experiment, affirm the phenomenon of the existence of the synchrostates and the consistency in the results. The number of occurrence of each of the three states in the β band for all three stimuli has been reported in Table 3.3.

Figure 3.17 shows the number of states for each of the 10 individual in the θ, α and γ band across the three different stimuli in a box plot. The red cross marks the outliers, the blue box shows inter-quartile range and the solid red line shows the median. From the figure it is evident that the number of synchrostates lie between a 3 to 6 for this cohort of subjects. The number of states in the γ band is three for all subjects, same number as β (as seen from results above). The other bands have slight variations in

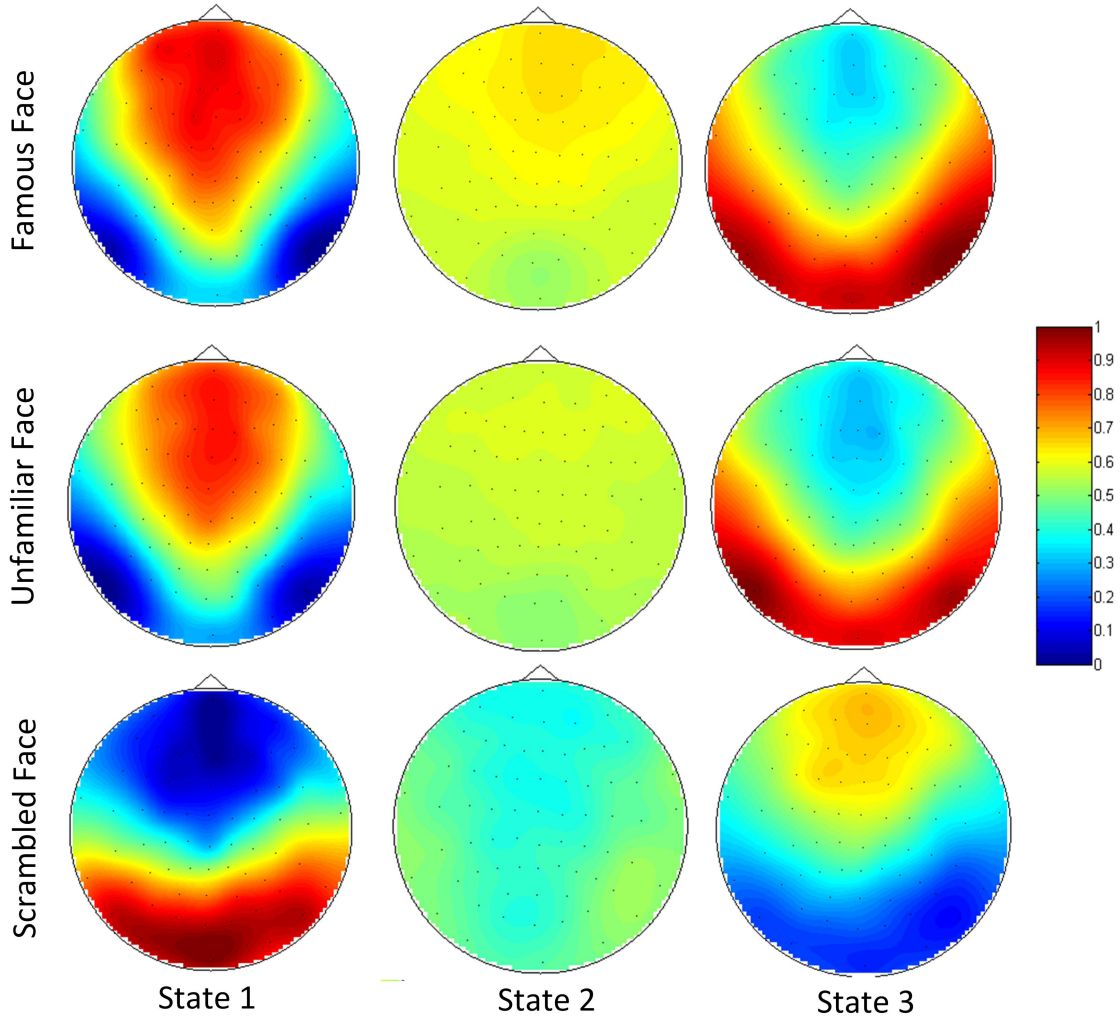

Figure 3.15: Multiple-subject average synchrostates during famous, unfamiliar and scrambled face perception in the β.

Table 3.3: Number of occurrence of the three synchrostates in β band with three different face stimulus in the multiple-subject averaged EEG

Stimuli	State 1	State 2	State 3
Famous	58	239	104
Scrambled	69	176	156
Unfamiliar	59	251	91

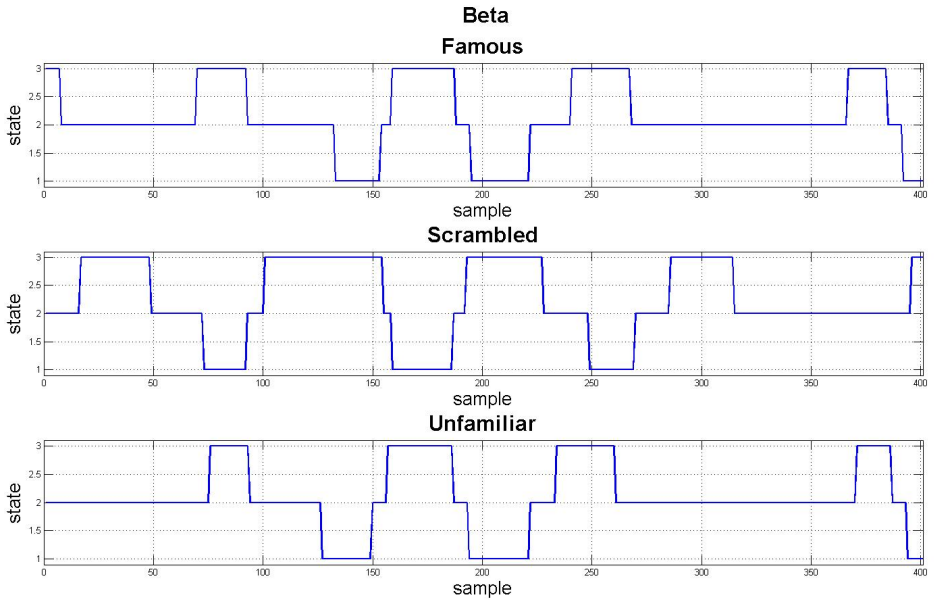

Figure 3.16: Multiple-subject averaged temporal evolution of β band synchrostates in 363ms for three different face stimuli. The famous and unfamiliar face show similar responses compared to scrambled.

the number of synchrostates across individuals which is very likely due to interperson variability in the processing each stimuli.

From these results, one can conclude that there exist a small number of states which might have different topography in a face perception task. The results from the individual study show that the synchrostate properties are almost consistent across different trials from the same individual. The similarity between the group analysis and the individual analysis shows that the number of states is consistently three in the β band for both the cases. The topographies and the transitions between the two experiments are very likely to be different as the data collection paradigms are not the same. The number of electrodes, electrode layout as well as the sampling rate of EEG acquisition for both these studies are also not equivalent.

3.3.3 Possible artifact and volume conduction effect

Before continuing discussion about the implications of these results one needs to eliminate possible artifact effect that may bias the observation. It is worth mentioning once again the head plots shown here are fundamentally different from those obtained from qEEG analysis where the average power spectrum is plotted over the scalp. Any possible artifact in such cases is manifested as strong correlation at the scalp edges. On the contrary, the head plots shown here are more like the visualisation of the phase difference patterns distributed over the scalp. The bluish hues imply nearly zero phase difference whereas the reddish hue implies large phase difference.

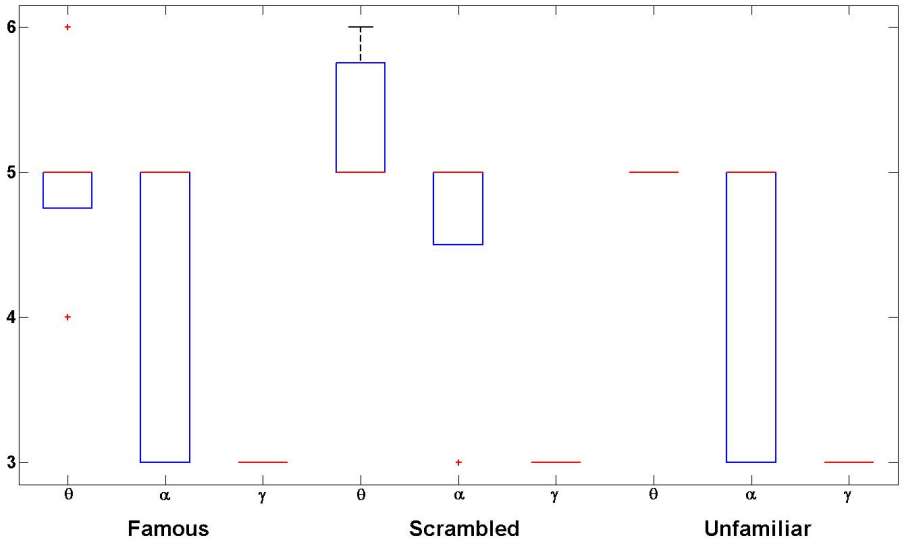

Figure 3.17: The no. of synchrostates for each subject during famous, scrambled and unfamiliar face perception for 10 subject group analysis in the θ, α and γ band shown in a boxplots.

Furthermore, in the side edges of the headplots, like that in Figure 3.6, concentration of large phase difference should not be confused with the presence of artifacts. This is because the synchrostates change at the time resolution of milliseconds (ms) and the artifacts generally occur in the time interval of seconds. Here, each of the head plots show phase difference topographies existing of the order of ms. Since the synchrostate topographies are constructed in the ms order and as the transition diagrams show that the topographies switch from one configuration to another and back, in the ms order time interval, in the presence of possible artifacts all of the states should exhibit similar phase relation at the scalp edge for all the states which is not the case. Because artifacts could not appear in millisecond level time resolution, then disappear and again reappear within this small time window, they do not account for the observation of the synchrostates, as all states are following a switching sequence in a small window of time. While processing the data, as mentioned in Section 3.3, the epochs above 200μV were eliminated as possible artifacts. Therefore the data used in the analysis is likely to be artifact free in the first place.

Secondly, eye artifacts are generally concentrated in the forehead and are constrained mainly in the low frequency ranging from 1-5 Hz (McFarland et al. (1997a)). Muscle activity is reported to be maximal at frequencies higher than 30 Hz (Fatourechi et al. (2007),Anderer et al. (1999), McFarland et al. (1997b)). It is also well known that prominent broad-band signal power above 30 Hz can be attributed to micro-saccadic artifacts (Yuval-Greenberg and Deouell (2009)). The plots in Figure 3.6 are the results in the β band (13-30 Hz) synchronisation, so are likely to be minimally affected by eye

or muscle artifacts. Therefore while interpreting the results one may eliminate the effect of possible artifacts.

The validity of phase synchrony, derived from EEG signals recorded over the scalp has been doubted in past literatures, as it is considered as the effect of spurious synchronisation that occur due to volume conduction (Nunez et al. (1997)). As studied in Section 2.2.2, zero phase lag is characteristic of volume conduction and interactions reported from them are not reliable, whereas the network properties are measured through phase differences (Thatcher et al. (2008)). Volume conduction involves zero phase delays between any two points within the electrical field as collections of dipoles oscillate in time (Nunez and Srinivasan (1981)). Zero phase delay is an important property of volume conduction based on which measures such as imaginary spectrum, bi-coherence, phase reset and coherence of long phase delays are considered critical in measuring brain connectivity, independent of volume conduction (Nolte et al. (2004), Pascual-Marqui (2007), Peraza et al. (2012)). According to the assumptions in pioneering paper regarding identifying true brain interaction by Nolte et al. (Nolte et al. (2004)), phase shifts (phase differences) cannot be explained by volume conduction. In this study from the very beginning the same premise is used and only non-zero phase differences between EEG is investigated. The synchrony reported in this study does not report zero phase lag synchronisation as can be seen from the experiment shown in Figure 3.18. The figure shows individual cross electrode phase differences for all channel-pairs along time (continuous blue lines) for the adult EEG over 1-100 trail run as an example. The plot of red circles shows the average cross channel phase difference. From Figure 3.18 it is observed that the cross electrode phase difference is consistently non-zero in time. Also, as per the study of Stam et al. (Stam et al. (2007)), the existence of a consistent non-zero phase lag cannot be explained by volume conduction. The non-zero value of pair-wise phase differences along time in the study, suggests that the synchronies are not artifactual hence is a reflection of brain interactions and is not a result of volume conduction.

Thatcher et al. (Thatcher (2012)), also pointed out that if phase difference in the space between two electrodes uniformly equals to zero then this is volume conduction. On the other hand, if a point intermediate between two sources is not at phase zero, then it cannot be explained by volume conduction. Hence this means in high density EEG space, if at a single time instant the phase difference between intermediate electrodes is zero, the data can be labeled as corrupted with volume conduction. However if the relative phase difference between an electrode and its neighbouring electrodes are non zero then there is no effect of volume conduction. To investigate if the phase information in this study is affected by volume conduction the phase difference of a single electrode with respect to all others was observed. Figure 3.19 shows the phase difference from the single subject EEG in Section 3.3.1 (in degrees) between electrode A1 and other 127 electrode at $t = 19$ms and then at $t = 24$ms. From both the plots it can been seen, that the phase difference between A1 and the other electrodes in the scalp are never zero

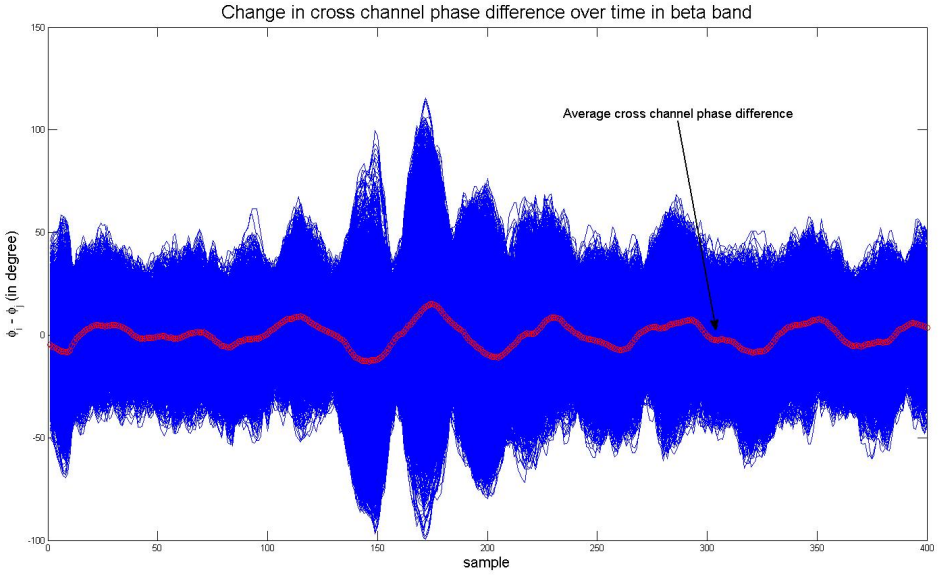

Figure 3.18: Cross channel phase difference evolution over time and of their average across all possible pairs.

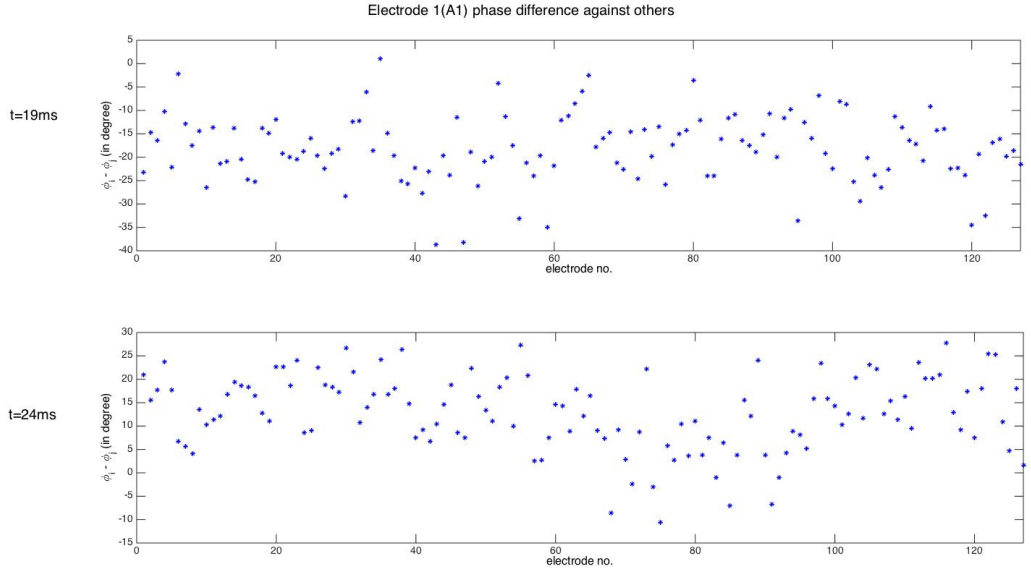

Figure 3.19: Absence of volume conduction revealed from consistent non-zero phase difference across EEG channel pairs.

and $\Delta\varphi_{ij}$ (where i = A1 and j are channel numbers) is not uniformly zero between any intermediate electrodes in space. Therefore it can be concluded that the phase locking observed in synchrostates cannot be explained by volume conduction.

Another property of the new phenomena in this study - 'synchrostates' that cannot be explained by volume conduction is the desynchronisation and resynchronisation (Rodriguez et al. (1999)) of different electrode signals over time i.e. the transition between

the states in ms order. If the synchrony captured was in fact the effect of volume conduction it does not account for the change in the synchronisation pattern in both strength and between relative electrodes over time (in ms) during state changes. Synchrony resulting from volume conduction would result in constant synchronisation configuration prevailing over the scalp throughout the recording time for all the synchrostates. Even the signals from a single intermittent source will simultaneously affect all the electrode recordings. Thus time delays between electrodes cannot be accounted for by a single intermittent source (Koenig et al. (2005), Studer et al. (2006)). If the single source activity was conducted through a distributed lead field its intermittent activation patterns would also be volume conducted to several of scalp electrodes. Such a scenario would entail there would be no change in the effective phase difference between two electrode signals during these intermittently active sources (Rodriguez et al. (1999)). Stam et al. (Stam et al. (2007)), states that the asymmetric distribution of instantaneous phase differences between two signals cannot be explained by volume conduction from a single source. The time varying desynchronising and resynchronising nature of the synchrostates is due to the asymmetric nature of the reported phase differences which causes to be sometimes positive or negative and larger or smaller indicating towards a phase lag and a phase lead and hence changes the synchronisation pattern between electrodes as a result. The phase difference between a pair of electrodes abruptly change and then can reconfigure into new topographies which confirms that the synchrostates are not affected by volume conduction.

Techniques such as mutual information (Gysels and Celka (2004)), cross covariance (Kramer (1980), Urbano et al. (1998)) PDC (Baccalá and Sameshima (2001)), DTF (Kamiński et al. (2001), Babiloni et al. (2005)), Granger causality methods, Phase lag index - PLI (Stam et al. (2007)) and PLV (Lachaux et al. (1999)) are some popular synchrony measures in EEG that are widely used in current brain research. All of the above mentioned literature devise methods or report EEG coherence or synchronisation that are not manifested through volume conduction based on the theory of zero phase lag and the asymmetric distribution of phase difference. This research in phase synchrony is an extension of these concepts of functional connectivity analysis using EEG signals. The same premise and arguments are used to validate that the observed phenomenon is not an effect of volume conduction.

3.4 Conclusion

The most important finding in this study is that over all the subject groups and individual subject a small set of unique phase difference patterns - synchrostates - each being stable of the order of ms have been found to exist. These synchrostates switch from one to another abruptly and thereby constructing a characteristic time-course to the applied stimulus. This is qualitatively similar to the results obtained with microstates (Koenig

et al. (2005)) albeit the microstate topographies are constructed in the EEG amplitude domain where the number of states may go up to 10. From these experiments, it is observed that the number of synchrostates is bounded between 3 and 6 depending on individual subjects, stimuli and also the number of EEG electrodes for recording. From the time-course plots it is evident that different synchrostates show different duration of stability at different time points depending on the applied stimulus and thereby possibly capturing the dynamics of phase synchronisation at a finer temporal granularity level. The results from the individual subject study show that the synchrostate properties are almost consistent across different trials from the same individual. Without loss of generality the same synchrostate analysis approach can be applied to an average subject group with multiple trials and also a single subject from EEG recorded over multiple trials. The similarity between the group analysis and the individual analysis shows that the number of states is consistently ranged between 3-6 in both the cases, although the synchrostate topographies seem to be different due to difference in number of electrodes, electrode layout as well as the sampling rate of EEG acquisition.

Physically it means that during an information processing task, in this case, a face perception task a well defined information exchange process is initiated between different regions of brain and the state transition characteristics resulted indicates the dynamics of such a process. Assuming that each task can be broken down into a sequence of subtasks, this may mean that the time duration of each synchrostate in the time course sequence is indicative to the processing time required for the underlying brain circuitry for processing a subtask. Therefore this could be an effective tool for quantitatively characterising information processing ability of brain in neurophysiological disorders like Autism and ADHD where information integration and processing speed are the big concerns.

Chapter 4

Synchrostates in pathological populations

The results and discussion from the previous chapter established that synchrostates exist during face perception in normal adults. However, whether the same phenomenon exists in a pathological subjects, needs to be explored. Given the stimulus specific nature of synchrostate and its inherent ability to describe temporal evolution of phase relationship at different sites of the brain, it could offer new possibility for understanding pathological brain function if such a phenomenon is found to exist. In this chapter the method discussed in the previous chapter was applied on EEG from two groups of children - typically growing and autistic and high and low anxiety children in two separate experiments.

As discussed earlier β band modulations have been correlated to face processing and cognition. It has also been argued that γ band synchronisation is a fundamental process that follows any elemental operation of cortical computation (Fries (2009)). Since these two band have been revered as bands of interest in face processing and cognition (Table 2.1) from here on the work concentrates on the synchrostate analysis on these bands only.

4.1 Experimental results and analysis of Typical and ASD population

Data from a high-density EEG study was used for this experiment. The experimental sample of the dataset contains EEG data from 24 participants; 12 children with ASD and 12 typical controls. The ASD group had subjects with an age range of 6-13 years with a mean age of 10.2 years. The control population was aged between 6-13 years as well with an average age of 9.7 years. The subjects for group with ASD were diagnosed according

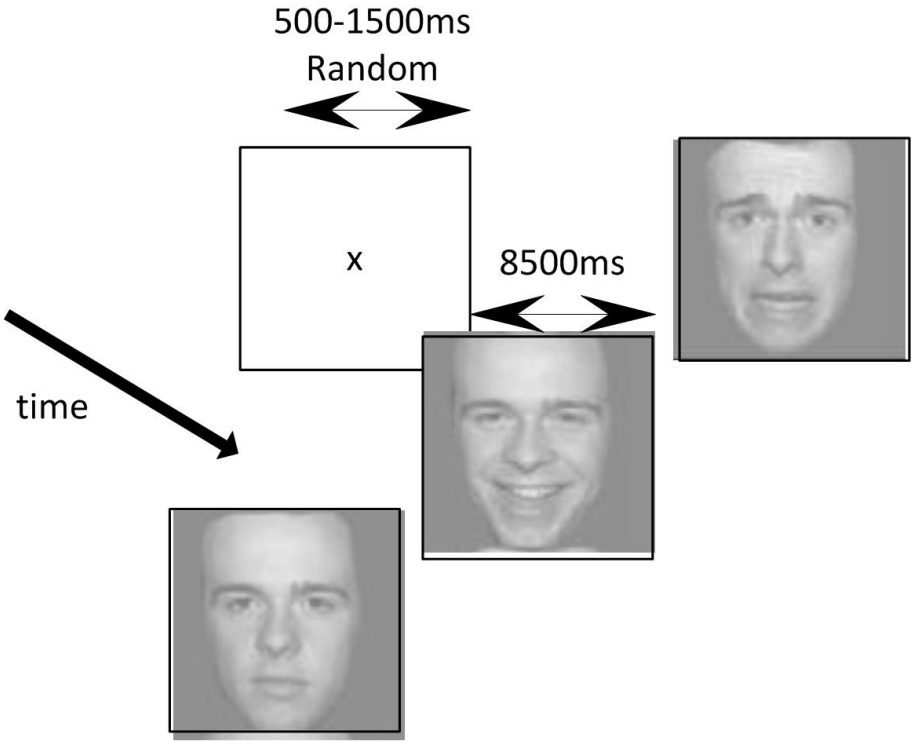

Figure 4.1: The face stimuli shown to the children during the experiment

to the Diagnostic and Statistical Manual of Mental Disorders (DSM-IV-TP) criteria (Association (2000)). The diagnosis was confirmed by Autism Diagnostic Observation Schedule-Generic (ADOS-G) and Autism Diagnostic Interview-Revised (ADI-R). The stimuli for the experiment run with these groups were taken from a database of widely used standardised facial expressions (Tottenham et al. (2009)). 30 faces from 5 male and 5 female subjects were taken, each exhibiting fearful, happy and neutral expressions. The Figure 4.1 shows the stimulus presentation protocol adopted during the data acquisition. The experiment was conducted in 4 blocks and in each block 10 fearful, 10 neutral and 10 happy faces were presented at random. Data was acquired at 250 Hz using a 128-channel HydroCel Geodesic Sensor net (Apicella et al. (2012)). The continuous EEG data was segmented into 1000ms epochs and segments with signals over a threshold of 200μV were rejected. Data was band-pass filtered from 0.5 Hz to 50 Hz and baseline corrected.

The results for this experiment are presented in two steps: first as a population average and then for individual subjects belonging to a population. To study the population average, first the average phase difference matrix for each subject is formulated by averaging the phase difference matrices across all trails. Then again, an average of the phase matrices of each subject belonging to that population is taken at every time instant and then k-means clustering is invoked on that set of average matrices as described in Section 3.2.1 and 3.2.2. In essence this gives a general picture of temporal evolution of phase relationship between different electrode sites for a specific population. The

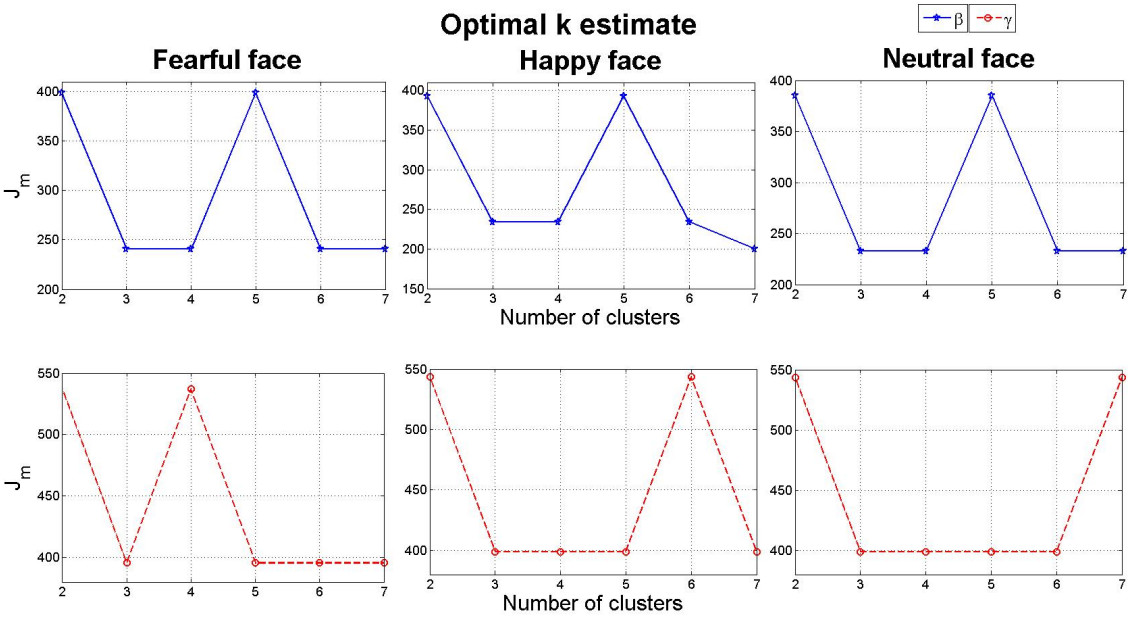

Figure 4.2: k-means clustering result of β and γ band for the typical group. In both bands the optimal number of states is three as the plot shows a significant knee at three.

exploration shows that the cost function for clustering does not fall arbitrarily with the increase in the number of clusters confirming the existence of a finite number of compact underlying clusters or states during the whole time-course of the EEG data. The detailed results for the individual groups are furnished in the following subsections.

4.1.1 Typically developing children

Figure 4.2 shows the results of the incremental k-means clustering algorithm in both the bands (β and γ) for all the given stimuli from the population average of 12 children with typical development (group I). It is clear that the dominant knee of cost function for all the three stimuli appears at $k = 3$ although in some cases after the knee the cost function increases and then again decreases. These are the typical situations already discussed in Section 3.2.2 and accordingly where the earliest knee appeared needs to be considered only. This means that in the dataset considered, there exist three unique phase difference matrix configurations - synchrostates - from the onset of stimulus till the end of an action.

In Figure 4.3, from the corresponding head-plots it is evident that the topographies of all the three synchrostates are very similar for all the different stimuli in the β band. A similar result is observed for the γ band in Figure 4.4 where the synchrostate topographic plots are similar and more importantly closely resembles to those obtained in the β band although differing slightly in the numerical values, in particular in the reddish hue regions. However, an interesting difference is observed in the state transition plots shown

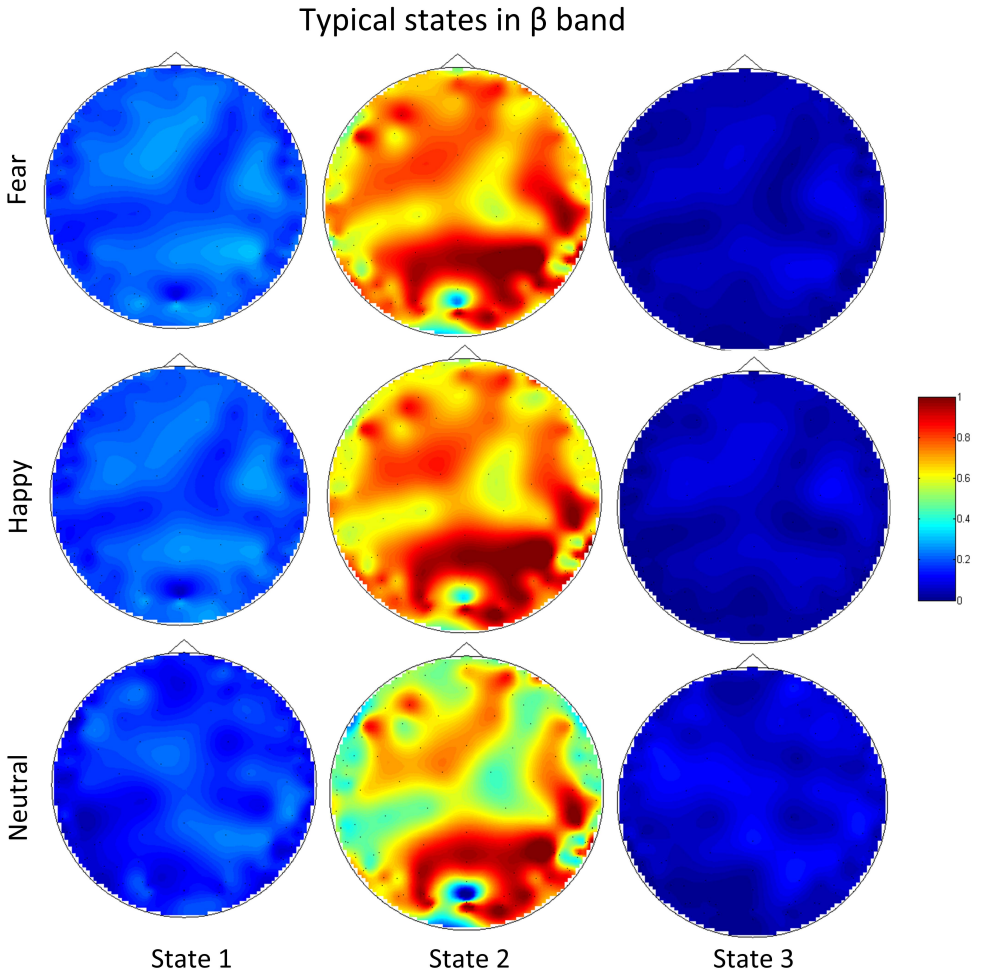

Figure 4.3: The topographic map for all the three stimuli in β band for the typical group. The plots show similar topography across the stimuli,

in Figure 4.5. Although in both the bands the transitions start from state 2, the overall transition patterns are markedly different not only between the β and γ band but also between different stimuli within a band. This demonstrates the stimulus specific nature of the synchrostates. It is evident from this experimental study that the β and γ bands characteristics are significantly different for the two bands.

From the headplots one can infer that in state 1 and state 3 for both the β and the γ band the average phase difference distribution across the scalp is almost uniform across all electrodes. This could be due to uniform information exchange in the brain during the existence of these states. Looking at the state transition plots (Figure 4.5) for this cohort of subjects it is observed that, the typical population spends most of the task execution time in state 1 and state 2 and hence one may say that they reside at a state of phase homogeneity for longer. This supports the theory that the face recognition is a multiscale integration system (Goudail et al. (1996)) and is in agreement with current literature suggesting that re-entrant integration of the occipito-temporal face-sensitive is necessary for face processing (Rossion et al. (2003)).

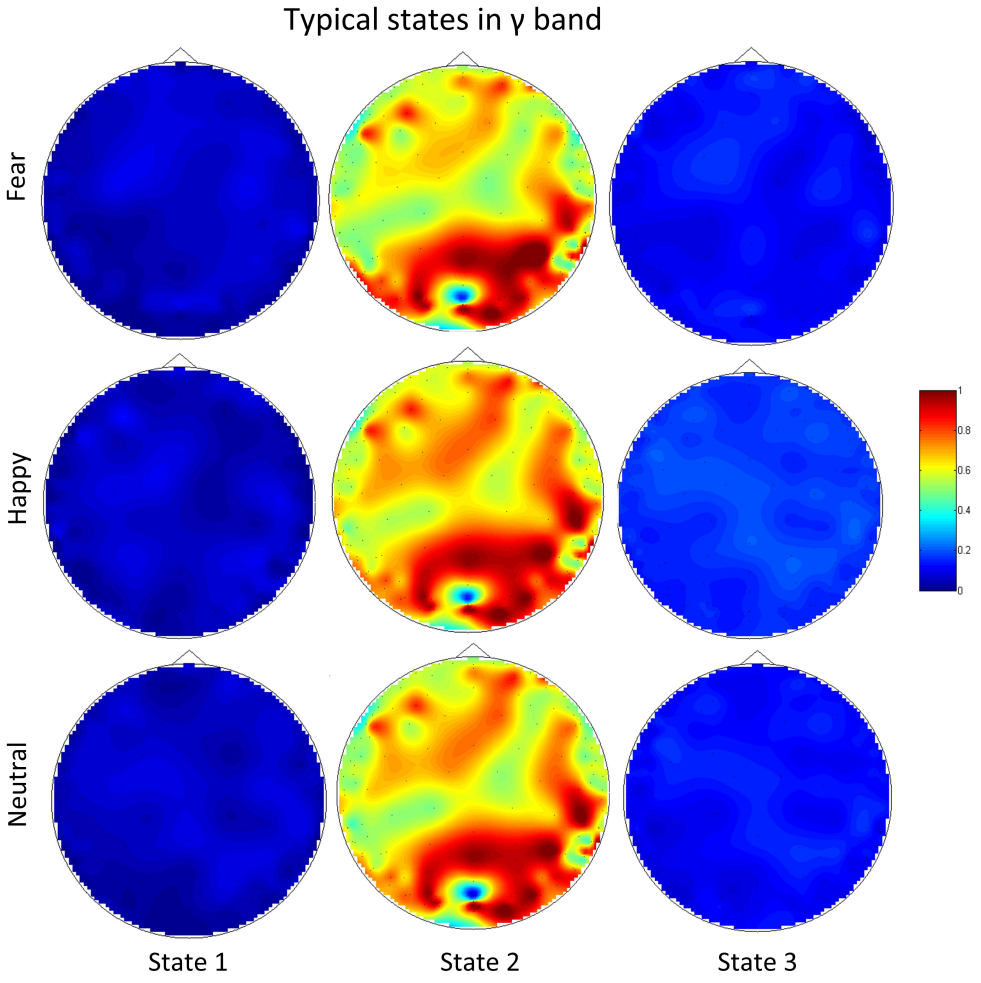

Figure 4.4: The topographic map for all the three stimuli in γ band for the typical group. The states share similar topography across all the stimuli.

4.1.2 ASD

The k-means clustering results for ASD population is shown in Figure 4.6 for the β and γ bands for all the three applied stimuli i.e. fearful, happy and neutral faces. Once again the significant knee appears at $k = 3$ implying existence of three synchrostates similar to the typical case. The corresponding phase difference topographies over the scalp are shown in Figure 4.7- Figure 4.8 as head plots with each of the colours signifying a particular range of phase differences as shown in the legend (in a normalised scale with respect to the maximum and minimum phase difference). It appears that although the stimuli are different the topographies are nearly similar in the β bands (in Figure 4.7) in particular for state 1 and state 3. However topographies corresponding to state 2 are slightly different. On the other hand, in γ band the state 1 for happy and neutral stimuli are similar while it differs significantly for fear stimulus (Figure 4.8). State 3 shows close similarity under all the three stimuli. As a further investigation, the time-course plots of the synchrostate transition are shown in Figure 4.9. In the both the bands the time

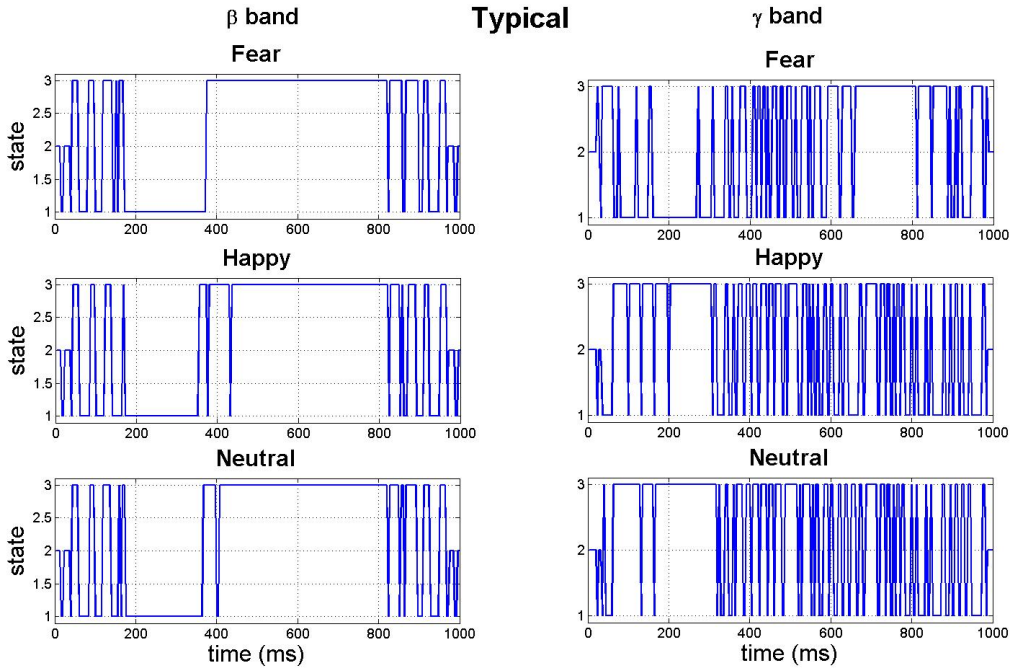

Figure 4.5: The time-course plot of synchrostate transitions in β and γ band for the typical group for fearful, happy and neutral face stimuli for 1 second.

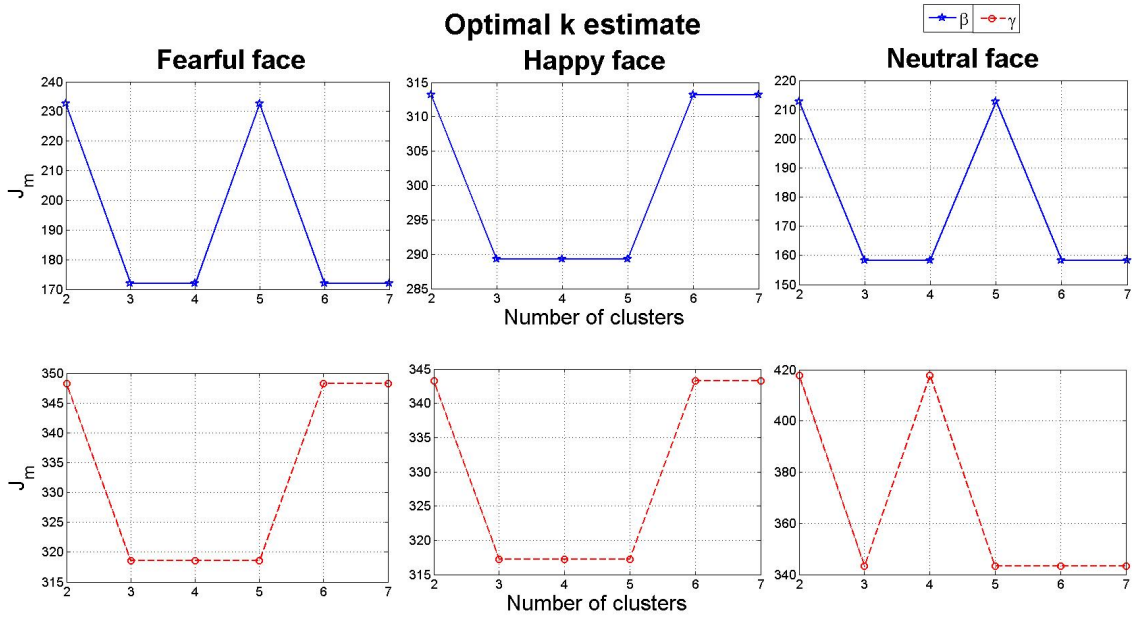

Figure 4.6: k-means clustering result of β and γ band for the ASD group. The optimal number of states for both the bands is three.

course plots are markedly different depending upon the stimulus and thereby indicating different temporal stability period of the synchrostates at different points in time.

Observing the transition plots closely shows that some states in the transition plot are existing for a very small time and move quickly to another. It must taken into consideration that the sampling rate for EEG in these experiments were 250Hz. Hence there is a loss in the temporal granularity of the transition plots of these experiments compared to those conducted in the previous chapter. Another interesting observation from the β band state transition plot is that in the ASD group spend significantly more time in state 2 during fearful and happy face stimuli compared to the typical. The headplot of state two shows a more heterogenous distribution of the phase difference across the electrodes. Current literature stresses on the need for integration in face processing. The state 2 characteristic of this ASD cohort is that of sparsely distributed phase distribution which is not uniform. Compared to the typical subjects it is observed that the ASD population spend more time in sporadic phase distribution states.

These visual anomalies observed from the typical and ASD headplots and transition diagrams need to be investigated in quantifiable measures. In order to do so one must first determine if these differences manifest themselves into phase synchronisation features, which may allow us to use them as biomakers for the disease.

4.2 Experimental results and analysis of Low and High Anxiety population

For the next set of experiments standard EEG acquisition protocol was followed for acquiring the data at 250 samples/s. The subjects in this group are children with behaviour disorder with anxiety problems and were assessed using the DOMINIC (Valla et al. (2000)) which is a DSM-IV based pictorial interview for children aged 6-11 years. Children in this group met the recommended cut-off points for generalised anxiety (Valla et al. (2000)). The stimuli presented to the children is shown in Figure 4.10. The experiment had 180 trials (60 trials per emotion type) with stimuli presented in random order in two blocks of 90 trials. A 30 channel EEG system was used for data acquisition and data was epoched at 100 ms pre-stimulus to 1000 ms post-stimulus. Collected data was band-pass filtered in the range 0.1 - 70 Hz for eliminating the drift and noise as done in the former cases.

4.2.1 Low Anxiety

The k-means clustering when run on the population average of the children with low anxiety for the β band resulted with four states for all the three stimuli i.e. angry,

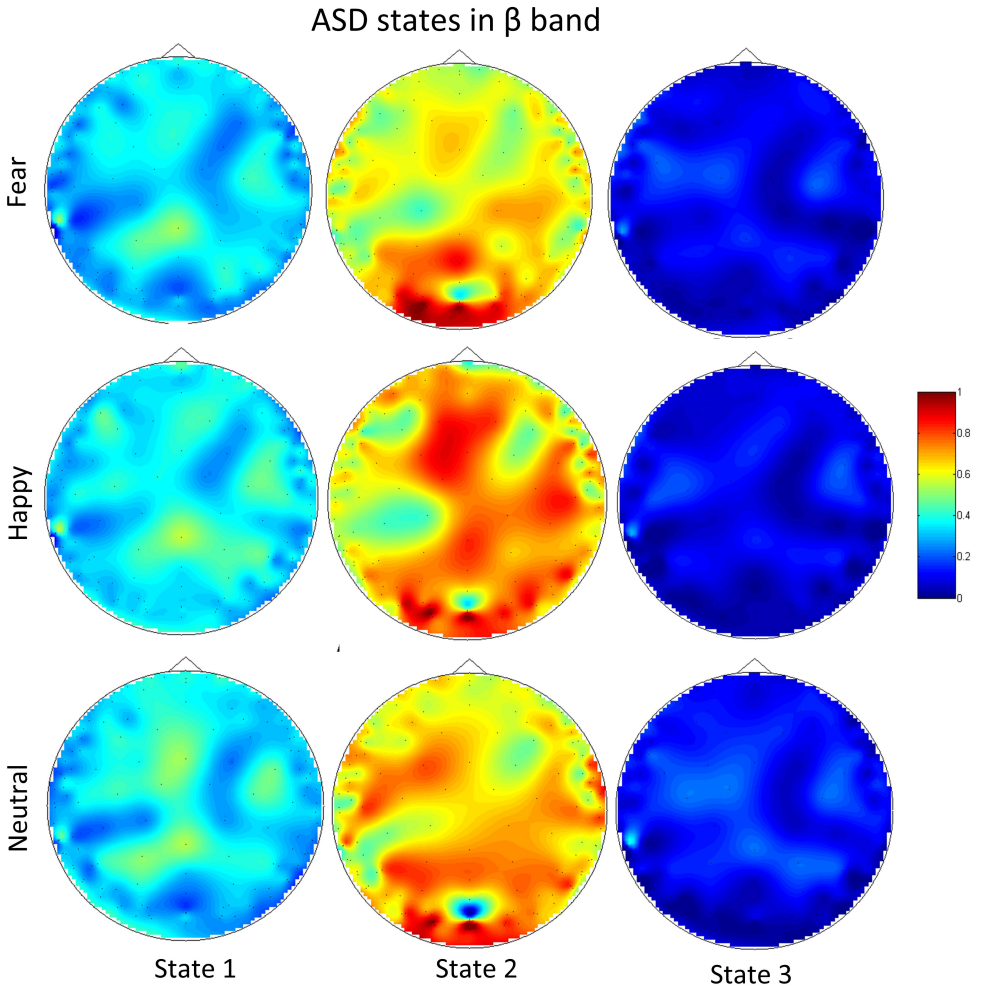

Figure 4.7: The topographic map for all the three stimuli in β band for the ASD group.

happy and neutral face. This is shown in Figure 4.11 as all three plots have the earliest significant "knee" in the cost function plot at $k = 4$. However in the γ band the number of states is different for the neutral face perception case. The number of states in the γ band for angry and happy face remain unchanged at $k = 4$ whereas for neutral face it is 6. In the head topographies for the β band, (Figure 4.12) although the number of synchrostate is consistently four, their characteristics for each different task are quite different. From the γ band head plots in Figure 4.13 it can be seen that the states 1, 4, 5 and 6 head plots are almost similar and common for all the three stimuli. However the neutral stimulus has two extra states which did not exist in the other two stimuli of angry and happy as can be seen from Figure 4.13. The transition of the states in β band is shown for each specific stimulus in Figure 4.14. It can be observed that during the execution of the angry face stimuli the inter-state transition is not as frequent as compared to the other two stimuli viz. happy and neutral. The β band state transition shows that except for angry stimuli for both the other stimuli the sequence start with state 4, whereas for the angry visual stimuli it starts from state 2. In the γ band, the

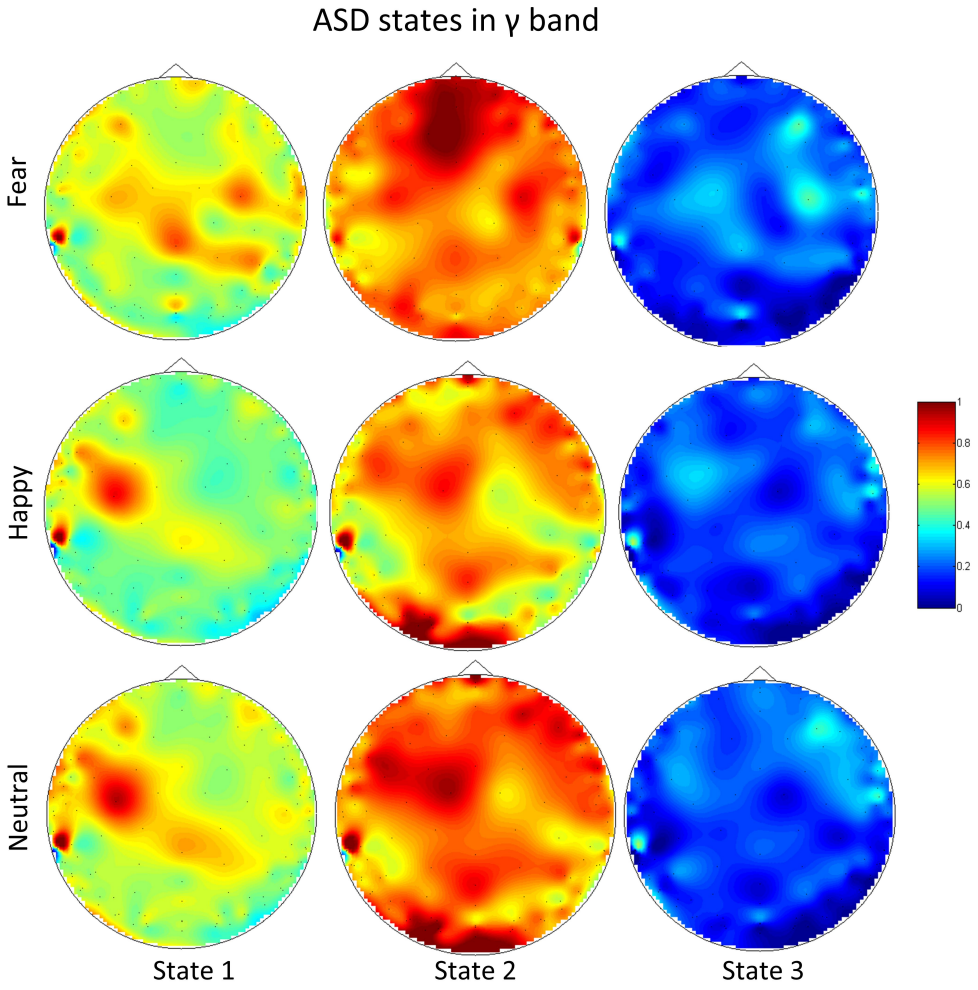

Figure 4.8: The topographic map for all the three stimuli in γ band for the ASD group.

state transitions are much faster in neutral face perception compared to the other two stimuli as shown in Figure 4.14.

Again in this stimulation short lived states are observed and these can be attributed to the sampling frequency of the data which is low at 250Hz. The fast dynamic brain response to these stimuli may be too fast to be captured with good temporal granularity at this sampling rate.

4.2.2 High Anxiety

For the group of high anxiety subjects, as shown in Figure 4.15, for both the bands the number of synchrostates is consistently four for different stimuli. The head plots for the average β responses of the children as can be seen from Figure 4.16 are to some extent similar across all the stimuli. This close similarity is even more prominent in the γ band head plots depicted in Figure 4.17. The transitions of the states in β, shown in Figure

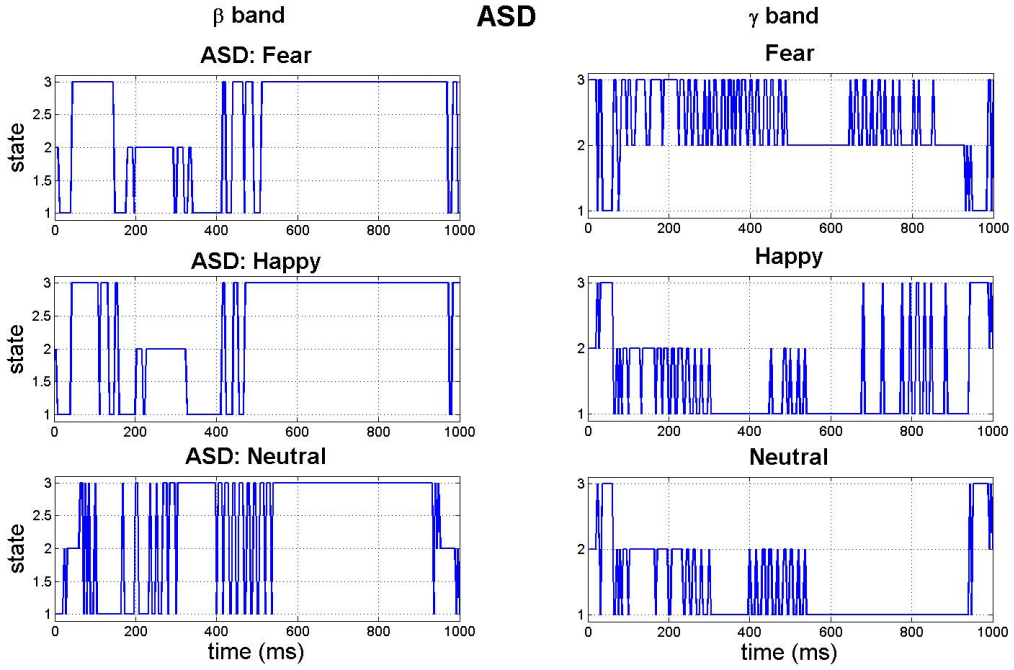

Figure 4.9: The time-course plot of synchrostate transitions in β and γ band for the ASD group for fearful, happy and neutral face stimuli for 1 second.

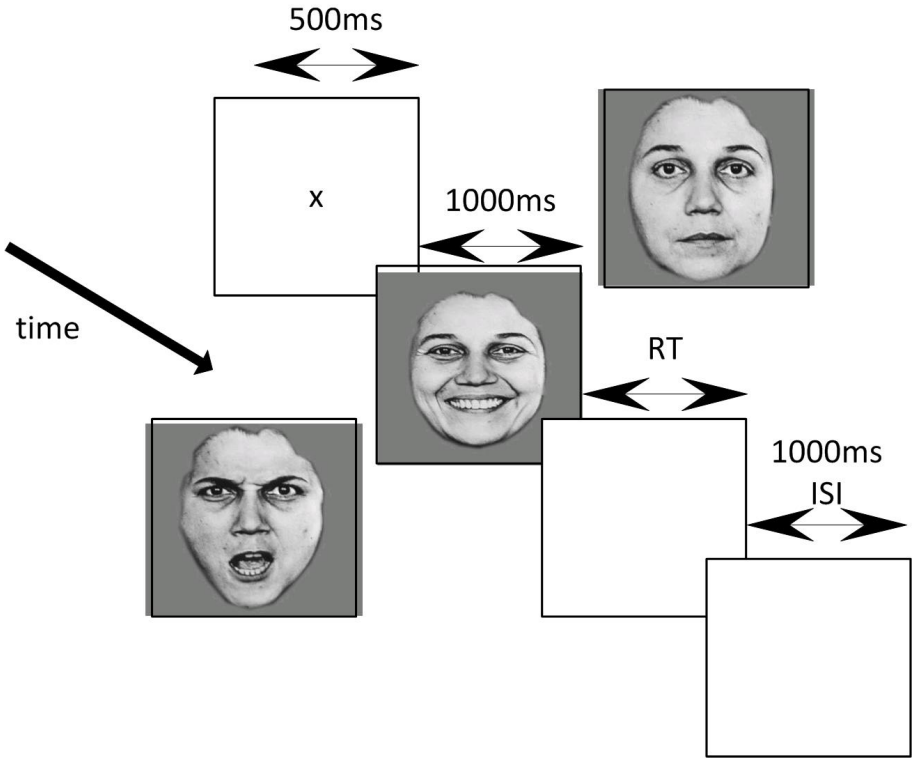

Figure 4.10: The stimulus presentation protocol administered during the data acquisition on children

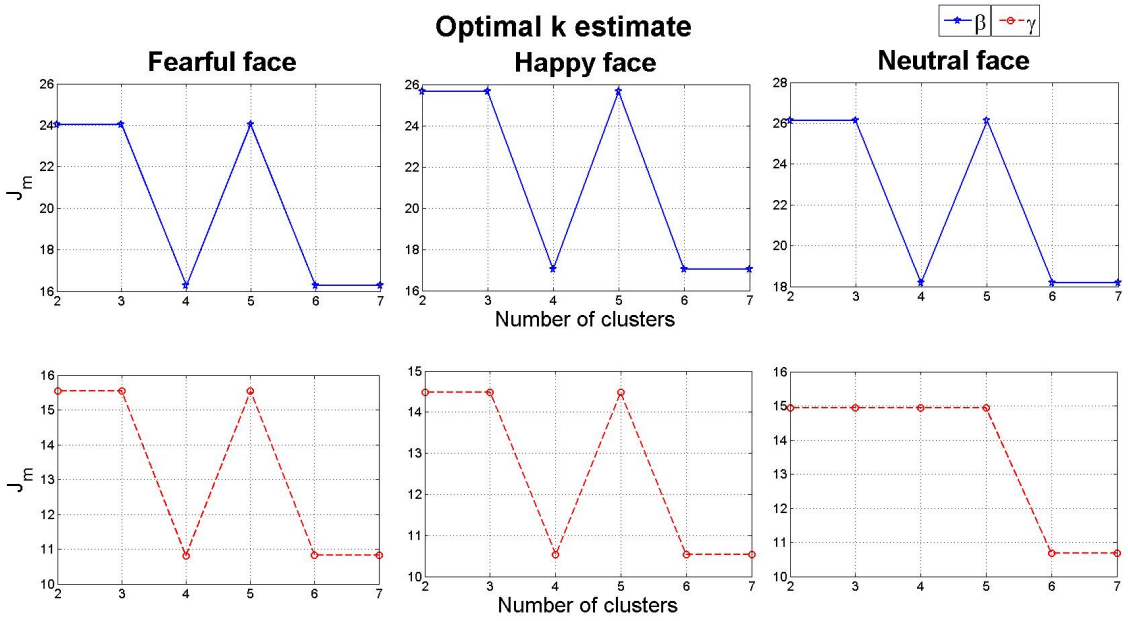

Figure 4.11: k-means clustering result of β and γ band for the low anxiety group. β has fours optimal states for all three stimuli. γ has four states for angry and happy face and six states for neutral face stimuli.

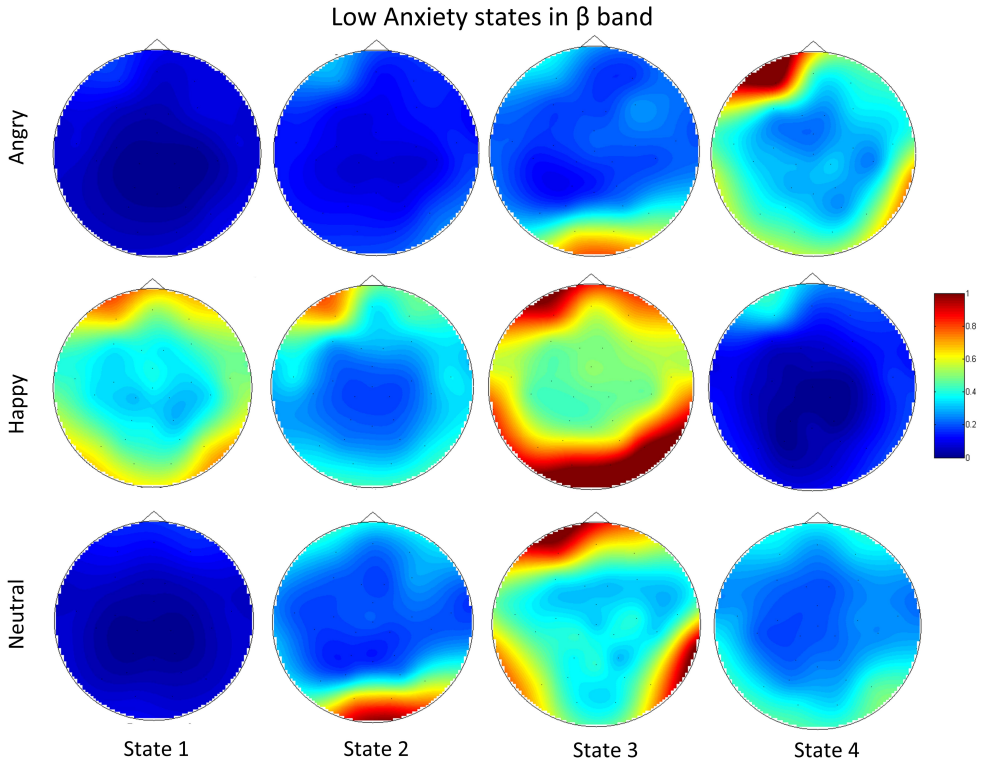

Figure 4.12: The topographic map for all the three stimuli in β band for the low anxiety group.

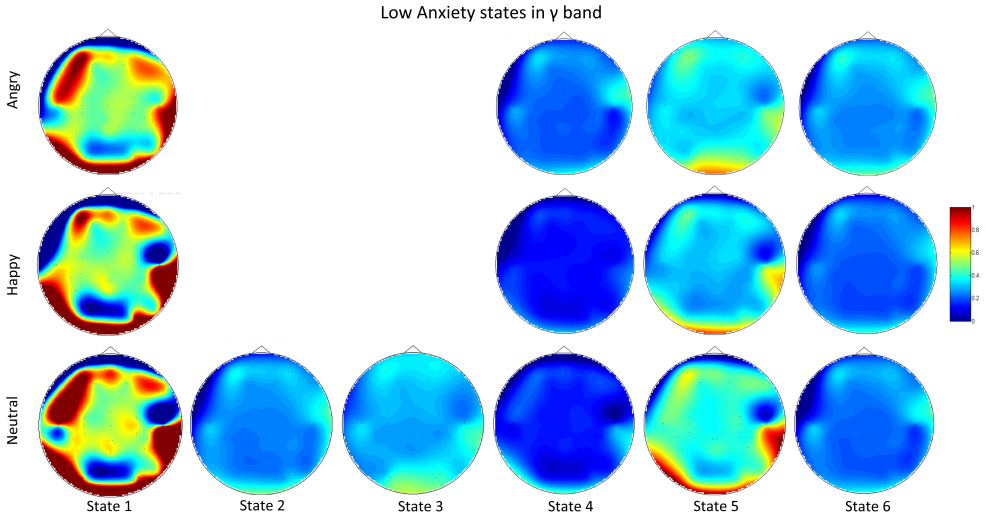

Figure 4.13: The topographic map for all the three stimuli in γ band for the low anxiety group

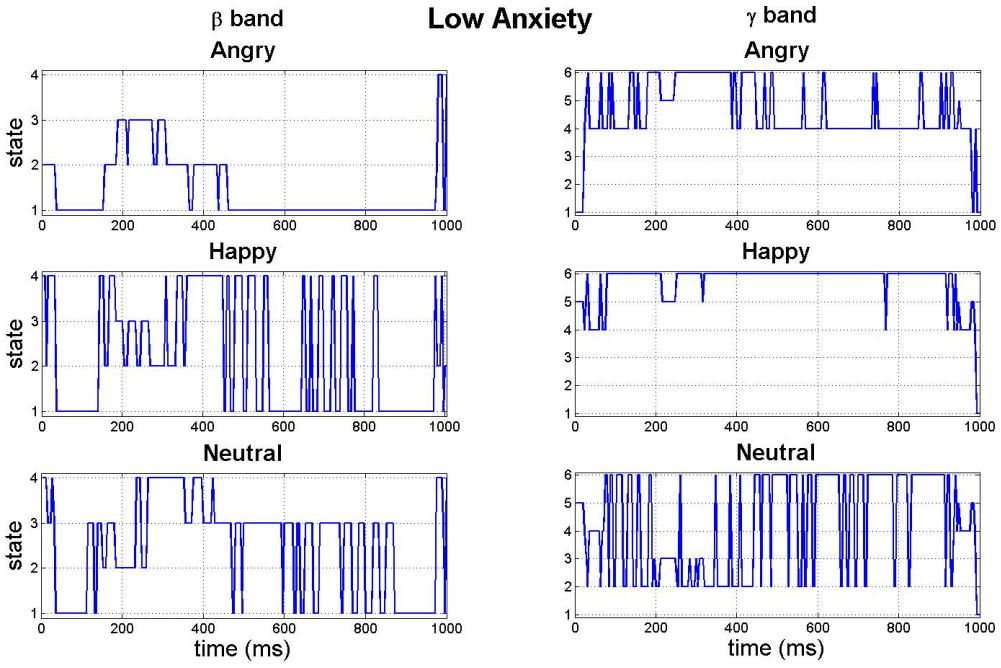

Figure 4.14: The time-course plot of synchrostate transitions in β and γ band for the low anxiety group during angry, happy and neutral face stimuli for 1 second.

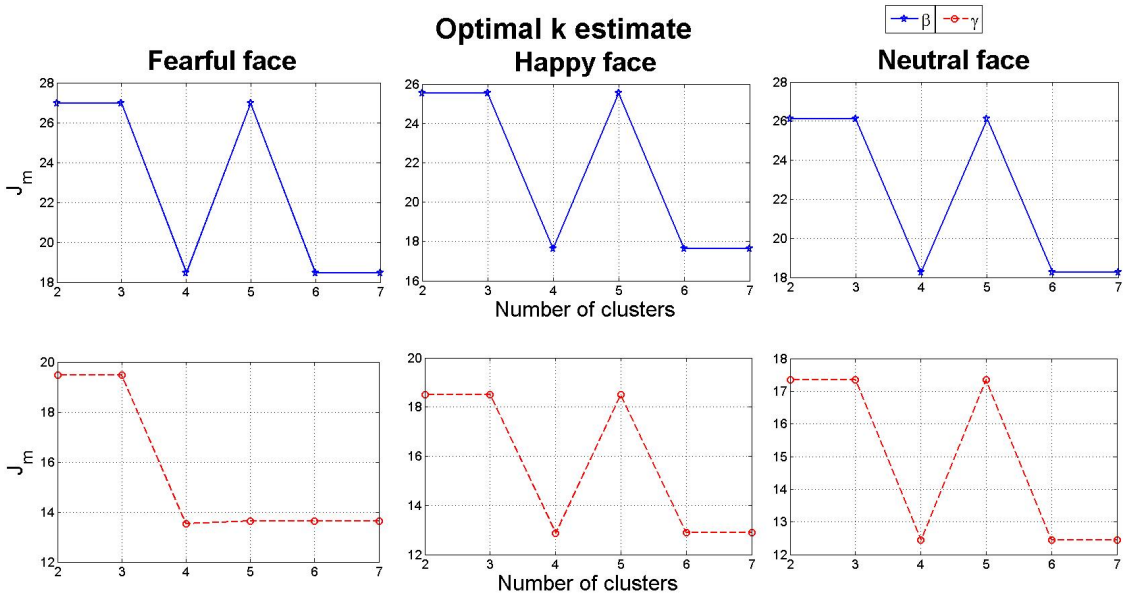

Figure 4.15: k-means clustering result of β and γ band for the high anxiety group. Both bands have four synchrostates for all stimuli.

4.18 end in state 1 for all the three stimuli. Also state 3 is the most occurring state over the duration shown for happy and neutral face. This is also the case for γ band state transitions for all stimuli as shown in the Figure 4.18.

Comparing visual observations it can been seen that in the γ the low anxious children have state 1 as the most stable (longest occurring) state and the high anxiety subjects have state 3 as there most stable state. Referring back to their subsequent headplots a significant difference among these two topographies it observed and hence it could be worth investigating the implications of these differences in a more quantitative form.

4.3 Variability analysis for individual subjects

So far the reported figures for the group-wise analysis highlight subtle changes in the average phase difference topographies over the scalp and state transition plots for different stimuli. Now the statistical measures like the median, inter-quartile ranges of the inter-person variability for the optimal number of synchrostates in both β and γ band are shown in the box-plots given in Figure 4.19. The red line in the plot indicates the median and the crosses show the outliers. The blue boxes denote the inter quartile range for the data. This is obtained by applying incremental k-means clustering on the phase-difference matrices obtained from individual subjects at different time instants under different stimuli. The variability in the number of synchrostates observed when results from the individual subjects are compared to the respective population average is not significant. For the pool of typical children there are consistently three states for every child in the γ band but in the β band the number of states for the children varies from

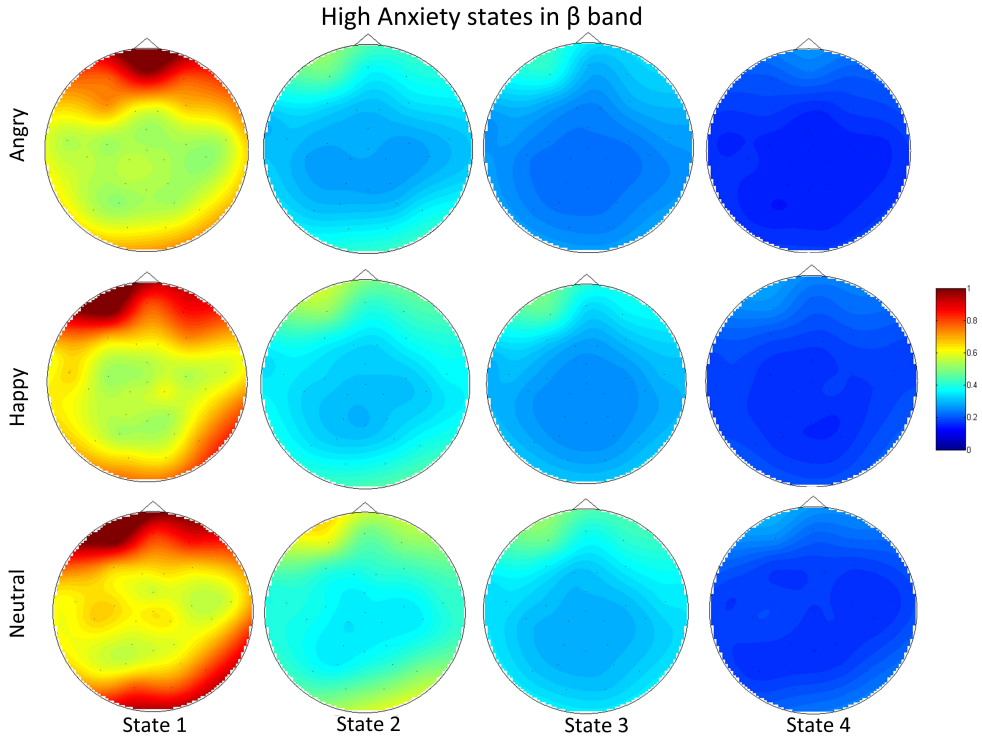

Figure 4.16: The topographic map for all the three stimuli in β band for the high anxiety group.

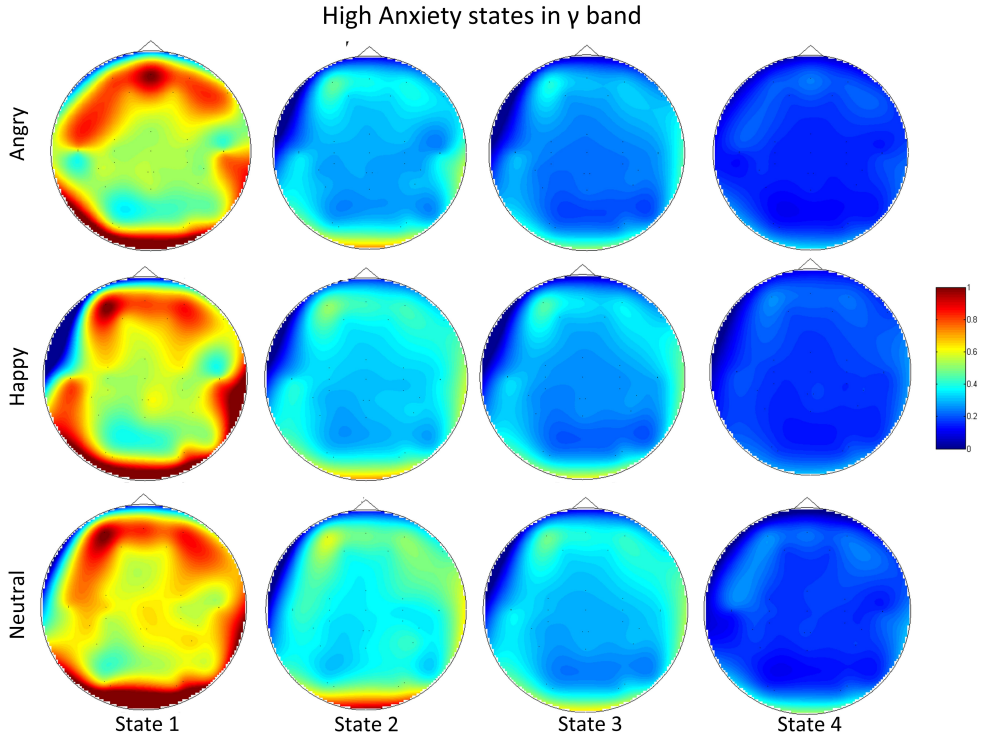

Figure 4.17: The topographic map for all the three stimuli in γ band for the high anxiety group.

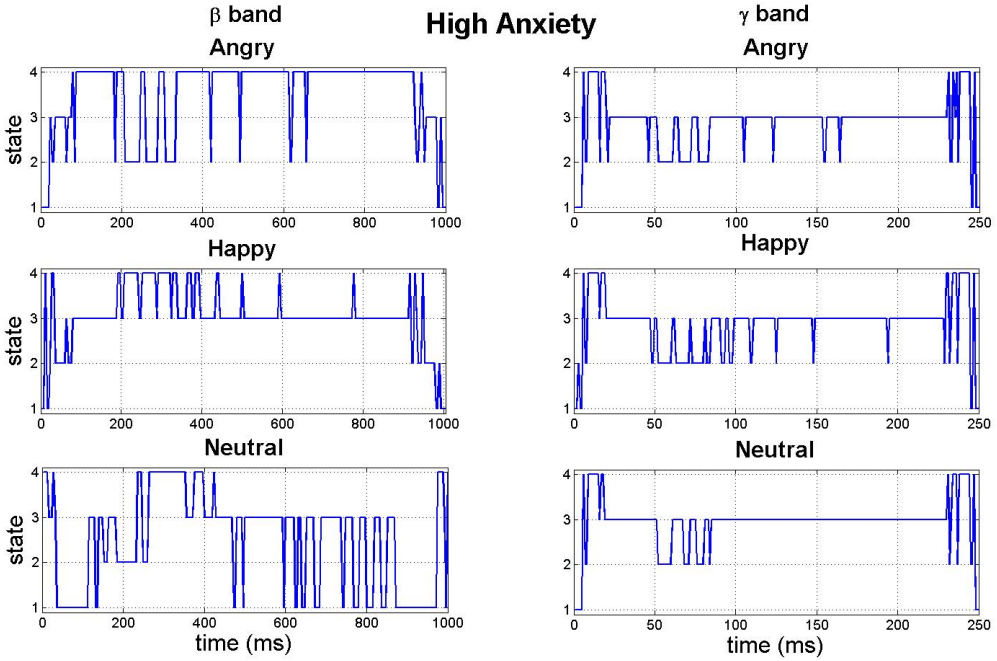

Figure 4.18: The time-course plot of synchrostate transitions in β and γ band for the high anxiety group during angry, happy and neutral face stimuli for 1 second.

3-7. This observation leads us to believe that the number of synchrostates is person-specific although this number is bounded within a small range only. Also in Figure 4.19, for ASD group in the β and γ band only 4 subjects show 5 synchrostates whereas the population average result as well as for the other subjects, the number of synchrostates is consistently 3. For the low anxiety and high anxiety groups (low-density EEG) it is interesting to note that the median of the number of synchrostates varies between 5 and 6 whereas the median is consistently 3 for the ASD and typical children (high-density EEG).

4.4 Variability in results due to electrode numbers

It has been seen in Chapter 3 that variation in the headplots are likely to occur due to less number of electrodes. The important factor to note here that only 30 electrodes were used for EEG acquisition for the anxiety groups and 128 electrodes for the ASD and typical groups. This reduced number of electrodes inherently introduced less resolution in computing the phase difference matrix and as a consequence may introduce a larger variability in the synchrostate formulation. Therefore it is evident that the optimal number of synchrostates largely depends on the number of electrodes and high-density EEGs (as in the first two groups, Typical and ASD) are more likely to give consistent result. Apart from that, the small variability observed in all the four cases is also

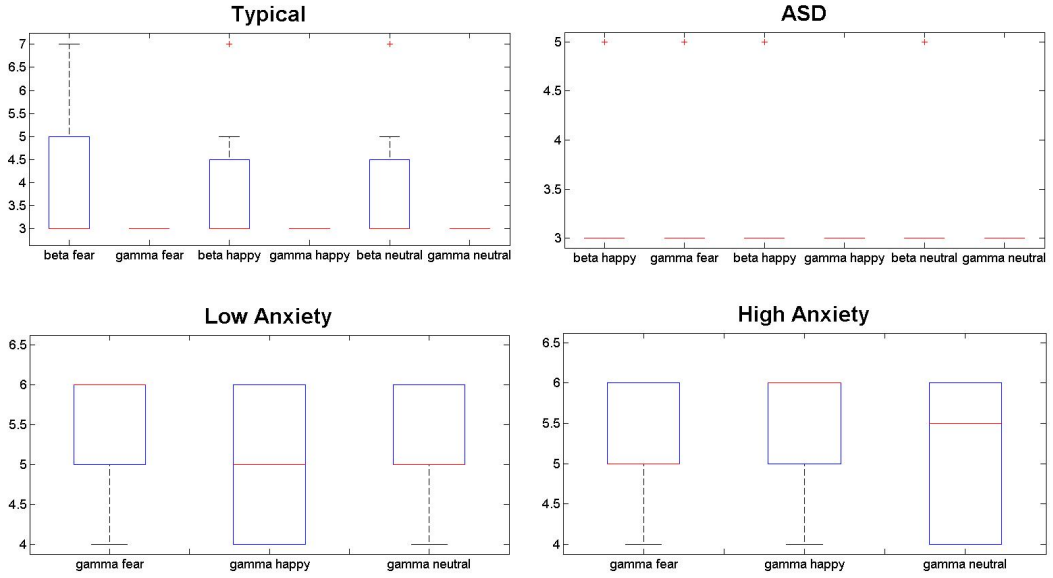

Figure 4.19: Box-plot of the variation in the optimal number of synchrostates in each group of subjects.

expected because of inter-person and inter-trial variability and possible existence of parallel background processes not related to the cognitive task given.

Another conclusion one can draw is that the synchrostate transitions are better projected in data with high sampling frequency as it allows the algorithm to trace the dynamics of the phase evolution of the EEG signals at a coarser time scale. This results to a more detailed time series for the state transition of the synchrostates. This is the case as the instantaneous phase differences are estimated from discrete sampling points of the EEG signal hence a higher sampling rate would yield a more detailed stream of phase time information.

An interesting observation for the case of typical development population is that the topographies of population average synchrostates (Figure 4.3 and Figure 4.4) are almost similar for all the applied stimuli in both the bands. This is similar to the observation in Section 3.3.1 where initial exploration was carried out with single normal adult subject with 128 electrodes. Intuitively this implies that although different stimuli have been applied, since all of them belong to the general class of face perception task, the fundamental phase relationship over the scalp remains nearly the same indicating a specific type of information integration phenomenon pertaining to the general face perception scenario. However the effect of different stimuli within the general class of face perception is reflected in the respective time-course plot (Figure 4.5) which showed marked difference and hence different synchronisation dynamics characteristic to the applied stimulus. On the other hand, although the topographies (Figure 4.7 and Figure 4.8) in the case of ASD population showed certain similarities they are more variable compared to the typical case along with their time-course. This may be due to the difference in

information processing in the brain between the two subject groups. In addition, it is apparent that generally for the ASD group the gross phase difference of each electrode across the scalp is higher than that compared to the typical group as there is more presence of red and yellow hues in the ASD states in the γ band (Figure 4.8) compared to the more blue hues in the states for the typical (Figure 4.4) group. Similar considerations apply to the children with anxiety. However as discussed earlier in this section it seems that determination of the optimal number of synchrostates depends on the electrode systems used for EEG recording and more consistent result could be obtained using high-density system.

4.5 Conclusion

From the results presented here one can conclude that the synchrostate phenomenon also exists in pathological patient data during a face perception task. The data from a group can be studied in a holistic way by analysing their synchrostates on the response of the cohort or they can be investigated individually. For the group analysis, the synchrostate properties and transition plots amongst different individuals could be slightly different within one experimental paradigm. There is some variation in the number of synchrostates, headplots between the EEG bands and across different stimuli. These variations have been attributed to the difference in the electrode number during acquisition as well the inter-person variability. The transition plots are also affected by the sampling frequency of the EEG as they lose both time and frequency domain granularity. There are some very evident differences between the headplots and stable states between the populations and this observation warrants a more in-depth analysis on how these differences translate into more quantifiable measures that can be used for detection and therapy of these disorders.

Chapter 5

Modelling Synchrostate Transitions

In Chapter 3 and 4, the basic principles of synchrostate analysis is discussed in details and the concept is validated on face perception EEG. Results from six set of different experiments were presented and synchrostates were shown to exist across all groups. The multi-step processing in EEG synchrostate analysis reduces the EEG signals to a simplistic process of stable phase difference maps which are assigned to synchrostates using clustering. The synchrostate analysis as a theoretical model helps grasp the phase evolution properties and hence provide insights into the underlying cognitive process. This is especially interesting since the analysis is reduced to the observed synchrostates and their transitions rather than the complex EEG time series.

This chapter proposes a stochastic model using the concept of Markov chains for the inter-state transitions of the millisecond order quasi-stable phase synchronized patterns or synchrostates. First and second order transition probability matrices are estimated for Markov chain modelling from 100 trials of 128-channel EEG signals during two different face perception tasks. Prediction accuracies with such finite Markov chain models for synchrostate transition are also compared, under a data-partitioning based cross-validation scheme. Later on the temporal switching sequence of the synchrostates were modelled in a probabilistic framework for the typical, ASD, high and low anxiety group of children studied earlier.

5.1 Predicting Synchrostate Transitions in single subject EEG over multiple trials using First and Second Order Markov Chain Models

In Chapter 3 the temporal evolution of the frequency band-specific phase difference topographies was investigated to find periods of phase locking in multichannel EEG signals. It has been found that the phase difference topographies do not change continuosly and microstate-like (Koenig et al. (2002)) quasi-stable phase locked patterns are observed in a temporal resolution of the order of milliseconds. These synchrostates switches from one to the other within the time interval of a cognitive task. The existence of synchrostates during face perception tasks was observed in the (β) band with different ensembles of EEG signals in Section 3.3.1. For similar visual stimuli, the inter-state switching patterns only slightly change among different ensembles or trials (as evident from Figure 3.11), however it is different for different stimuli and also across different pathological groups of people. Hence, statistical modelling of the pseudo-random and abrupt temporal switching characteristics of synchrostates can be helpful in understanding the dynamic evolution of the stimulus induced brain response particularly in different pathological population. Such a model could be effective in predicting the future behaviour of the state transitions in a probabilistic way using a Bayesian like framework, once the initial state is known.

Previously, the microstate transitions have also been shown to follow the Markovian property in (Schack et al. (2001)). In addition, the Markov Chain Monte Carlo (MCMC) approach has been applied to fit neural mass model with EEG signals (Hettiarachchi et al. (2012)) and for the necessary cortical sources (Kincses et al. (2003)). Studies have shown that in order to mathematically model microstate transitions a higher order or n-step Markov model may be needed due to the inherent long range temporal correlations in such sequences (Van de Ville et al. (2010)). There has been also few attempts to simulate epileptic seizure spikes in EEG using the Markov model and HMM (Shayegh et al. (2014), Shayegh et al. (2009)). Automated evaluation of stages of sleep from EEG has been modelled using Hidden Markov Model (HMM) in (Flexerand et al. (2002)). Recently, phase synchronization dynamics have been modelled using the HMM and Semi-Markov Model (SMM) in (Daly et al. (2013)) however their work does not consider the presence of synchrostates. The process of deriving synchrostates allows us to represent a multivariate stochastic process (EEG) as a collection of few univariate quasi-static subsystems (unique states) which randomly switches amongst themselves. The unique phase synchronized patterns or synchrostates can be considered as the discrete cognitive states underlying the information exchange and integration within the brain. In contrast to the above mentioned literatures, here a probabilistic model of the EEG synchrostate switching sequences is first constructed using the first and second order Markov chains

in order to predict their occurrences and validate the predictions with multiple EEG trials during normal and scrambled face perception tasks.

The present work in this section is aimed to model the switching sequence of synchrostates as a stochastic process over multiple trials, considering that the switching time courses have the Markovian property and hence the source of these switching can be modeled as a finite Markov chain. 100 independent trials of EEG signals during scrambled and normal face perception tasks were used. The details of the dataset, synchrostate derivation and subsequent discussion has been provided earlier in Section 3.3.1. First order and second order transition probability matrix of Markov chain models were developed using 90% of the data (EEG trials) in order to predict the state transitions from the knowledge of the state at the first time step and the subsequent predictions were verified and compared using the remaining 10% data under a 10-fold cross validation scheme. Markovian property of first and second order inter-synchrostate transition essentially implies that the value of each state at any time instant depends only on the state in the last one/two previous step(s) respectively.

5.1.1 Markov Chain Modeling for Synchrostate Transitions

The probabilistic evolution of many dynamic systems have been modeled by Markov chains (Luenberger (1979)). The Markov chain can jump from one state or condition to another, provided the transition is probabilistic and not deterministic. Due to the probabilistic nature of the model it cannot predict the future states from the present with certainty, however it can assign probabilities to the possible states that can occur. Thus in a Markov process the future states are assessed by a vector of probabilities (Grinstead and Snell (1998)). The evolution of these vectors essentially describes the underlying dynamical nature of a system. In a first order Markov chain, the state at any time instant depends only on the state immediately preceding it, and hence is defined as a single-dependence chain. However, in Markov chains with higher order dependency relationships like second or higher order chains, the subsequent state depends on two or more preceding ones.

In an n^{th} order discrete Markov chain, the process can be in any one of the finite number (m) of possible states S_1,S_2,...,S_m at any time instant. As the chain progresses, the states may change from one to another. This process is determined by transition probabilities between discrete states in the observed system which is estimated using the maximum likelihood approach (Shamshad et al. (2005)), where $p_{ij} = N_{ij} \Big/ \sum_j N_{ij}$, $i = 1, 2, .., m$, $j = 1, 2, , m$. Here, N_{ij} is the number of transitions from state i to j. Given an initial condition (state), if the process is in S_i at time n, then at time $(n+1)$ it will be at state S_j with probability p_{ij}. This study only considers stationary Markov chains i.e. p_{ij} does not vary with time or space (Shamshad et al. (2005)). The transition

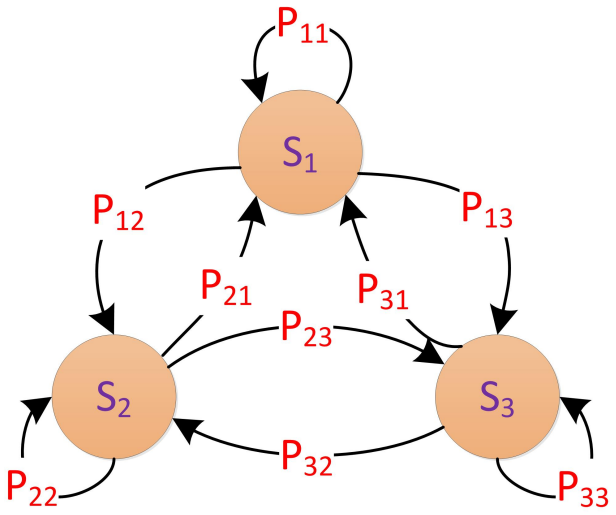

Figure 5.1: The state transition diagram for three synchrostates along with the transition probabilities p_{ij}

probabilities, p_{ij} of Markov chain are considered as the elements of the $m \times m$ non-negative stochastic matrix P, commonly known as the state transition matrix. The sum of the transition probabilities along each row of the transition matrix P equals one. If one looks at the Markov process after two steps given an initial state S_i, the transition is governed by applying the underlying transition matrix, P twice. In other words if $p_{ij}^{(2)}$ is the transition probability of reaching state S_j from initial state S_i in two steps, then $p_{ij}^{(2)} = \sum_{k}^{n=2} p_{ik}p_{kj} = \left[P^2\right]_{ij}$. Therefore, the two-step transition matrix is given by P^2, the three step transition matrix is given by P^3 and n-step transition matrix is P^n, such that the ij^{th} entry of P^n is the probability of the system reaching state i to state j in n steps.

The basic limit theorem (Luenberger (1979)) states that for certain types of Markov chains there exists a unique limiting probability vector p^T. In other words, in n-steps for any initial state i the transition matrix tends toward a limit $m \times m$ matrix, $\overline{P}$, known as the steady state transition matrix, each of whose rows equals p^T i.e. $\lim_{n\to\infty} P^n = \overline{P}$, where each row of P^n converges to p^T, as $n \to \infty$. This type of chains are called regular Markov chains. A Markov chain can be considered as a linear dynamic system with a positive system matrix (Luenberger (1979)).

A schematic representation of the transition amongst three synchrostates as an example case is shown in Figure 5.1 where S_i represents state i and p_{ij}, i,j=1,2,3 indicates the probabilities of switching from state i to j which needs to be estimated from the observed synchrostate sequence dataset. Once the transition probability matrix is obtained, the future steps of the synchrostate transition can be predicted given an initial state using the first and second order Markov chain models (Shamshad et al. (2005), Ataharul Islam and Chowdhury (2006)).

5.1.2 Results

The synchrostates analysis was carried out on the SPM multimodal face-evoked dataset (Ashburner et al. (2008)). The dataset consisted of 128-channel EEG signals acquired from an adult during the execution of face perception tasks when presented with multiple normal and scrambled face stimuli (details of the dataset, synchrostate derivation and discussion in Section 3.3.1). The 100 trials of EEG signals were epoched and pre-processed and then different ensembles of the data was segmented into 10 equal partitions, each of them containing 10 trials of the EEG. The phase response of each individual 10 segments of EEG for both scrambled and normal face stimulus, were clustered using incremental k-means clustering algorithm following the technique proposed and described in section 3.2 to obtain the synchrostates. Here, the optimal number of synchrostates in β band of EEG signals during face perception task from the incremental k-means clustering algorithm is found to be three for both the face stimuli for all the ten segments (Please refer to Figure 3.12 for the results of the clustering algorithm). The clustering also generated associated inter-synchrostate switching sequence patterns which may be described as probabilistic switching between the three discrete and unique synchrostates in a configuration of Figure 5.1, over the task completion time of 400 time steps. The temporal switching patterns amongst these states during normal face stimuli were found to be similar across different ensemble of trials, however they differ between two stimuli (normal and scrambled face) and thus could be considered as a unique signature of the visual stimuli provided. This allows us to generate two probabilistic models of first and second order Markov chain to fit the state transition dynamics for each of the two stimuli.

The state transition sequences for the whole 100 trials without data-partitioning have been shown in Figure 5.2 for both the normal and scrambled face stimuli. The associated optimal three synchrostate topographies have also been depicted in Figure 5.2 for all 100 trials of EEG taken together. It is evident from Figure 5.2 that the state topographies are almost similar for both the stimuli but their transition sequences differ significantly. For example during normal face perception the sequence starts from state 3 whereas for scrambled face perception it starts from state 2. In addition, for the normal face perception state 2 occurs minimum times whereas for scrambled face perception state 1 occurs the least times, indicating the cognitive task-specific nature of the synchrostate switching patterns. The principle diagonal elements of the transition probability matrix p_{ii}, i=1,2,3 can now easily be estimated from the state sequences shown in Figure 5.2 with prevalence of the same state and so as for the rest of the terms p_{ij}, $i \neq j$ by counting the number of transitions. From the switching sequences obtained for each of the $k = 10$ folds of the partitioned EEG trials, synchrostate switching patterns are derived next yielding a similar characteristics like in Figure 5.2.

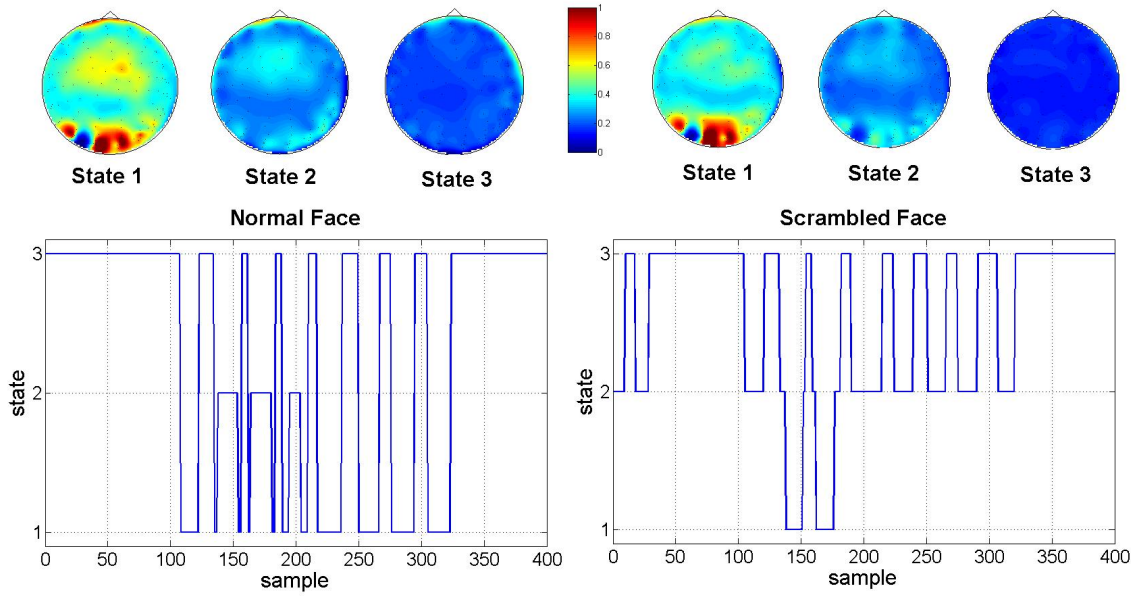

Figure 5.2: Synchrostate topographies for normal and scrambled face perception for 100 EEG trials.

The aim is to model and simulate the switching sequences of synchrostates as a finite Markov process for each of the $k = 10$ folds of synchrostate switching diagrams based on the characteristics of 90 EEG signals. Starting from the ten group (or fold) of EEG synchrostate observations, a cross-validation scheme has been adopted to generalize the model across different ensembles (or group of trials) and generate the probabilistic model which can give best use of limited data with less chance of introducing bias from the validation data-set (Rogers and Girolami (2011)). During the experiment, each of the single folds containing 10 EEG trials was held out as the validation dataset and then the rest 9 folds containing 90 EEG signals were used to train the probabilistic model.

The Markov models introduced here may provide interesting information about the evolution process of the synchrostates and their long term behaviour. The limit theorem is used to consider the long term performance of the estimated model. Figure 5.3 shows that the synchrostate transition is a regular Markov chain process when estimated on the whole 100 trials of the data. This has been verified by obtaining the state transition matrix P and then raising the power as P^n as $n \to \infty$. Figure 5.3 shows that all the 9 elements of the transition matrix obtained from the three synchrostate switching sequences converge to the steady state transition probability or eigen-vectors of the state transition matrix as the number of time steps are increased (Luenberger (1979), Grinstead and Snell (1998)). The steady state probabilities of the three synchrostates are found to be $p^T_{normal} = \{0.6763, 0.13, 0.1937\}$ for normal face stimulus and $p^T_{scrambled}$ $= \{0.6301, 0.2504, 0.1195\}$ for the scrambled face stimulus respectively, no matter at which state the sequence or the chain has started.

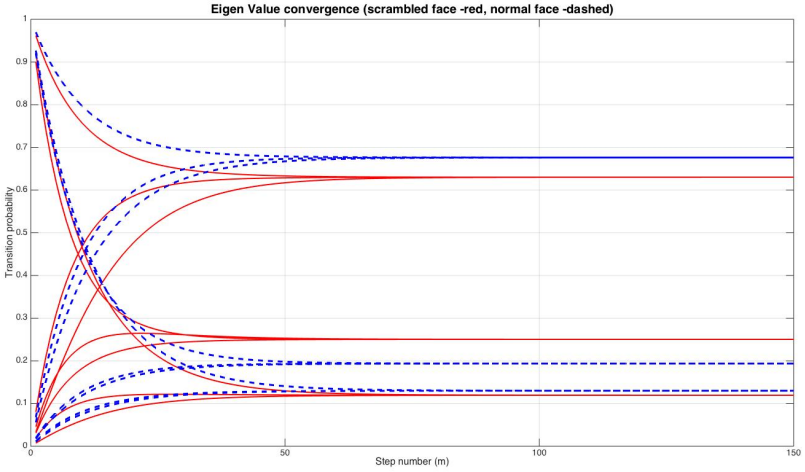

Figure 5.3: Steady state transition probability for normal and scrambled face stimuli (continuous line(red) scrambled, dashed line(blue) normal face)

For the validation of the Markov model, the synthetic generation of state sequences is simple and straightforward once the model is built from the 9-folds of the whole dataset. From the estimated Markov model representing a stochastic dynamical system, the outcome as the synchrostate switching sequences will vary in different realizations of the underlying random process, due to the probabilistic nature of the problem. Therefore, during the validation phase, the synthetic data from the same Markov chain model will be different considering multiple independent realizations of the same Markov chain given the initial synchrostate condition at the beginning of the cognitive task. Also, it is mathematically incorrect to match a real data with a single outcome of a trained Markov process. To circumvent this problem, within each fold of data and at each time step, by referring to the estimated transition matrix and given initial state, the program makes 100 independent realizations for the prediction of which state the system moves to in subsequent time steps, using a discrete random sequence generator. Based on the estimated or trained Markov model using the past n number of samples, the expected value of 100 independent predictions of the possible state at step $(n+1)$ have been validated with the real observation of the held out state at time step $(n+1)$. The mis-predictions are tracked over all the 100 independent realizations and across the 400 time steps for all the $k = 10$ folds of data segments. The misprediction rate or error for each fold is then averaged to produce the average error rate of the model for a particular order (first or second) of Markov chain. For building the second order Markov chain model the $(n+2)^{th}$ sample has been predicted in a similar way given the synchrostate knowledge at time steps n and $(n+1)$. The Markov chain model training and validation algorithm for the synchrostate transition is illustrated in the following steps:

Step1: For each fold i, i={1,...,k}, calculate the transition probability matrix P by taking the average of all the P's over the 90% of the all training sequences.

Step2: Given the knowledge of the initial state from the test sequence generate the discrete events for the next time step for 100 independent realizations. This produces random states from the discrete probability values of the state transition matrix.

Step3: Compare the 100 predicted states with the observed state in the test sequence. If mispredicted, increase the error counter.

Step4: Increment iterations for the next time step and repeat steps 2 to 3.

Step5: Compute the expected error across the 100 independent realizations of the Markov model.

Applying the above proposed algorithm yields Figure 5.4 which shows that the error rates for each of the first and second order Markov models for normal and scrambled face stimuli across 10 folds. The median percentage errors for the first and second order Markov chains for normal and scrambled face are 8.49, 8.37, 10.68 and 10.7 respectively. The small median value and inter-quartile ranges of the error rates for the two first order Markov chain models indicates that the model is quite successful in predicting the synchrostate transitions. In the present study, the normal face perception related Markov model performs better than the scrambled face one, as evident from the smaller interquartile ranges as well as the medians in Figure 5.4.

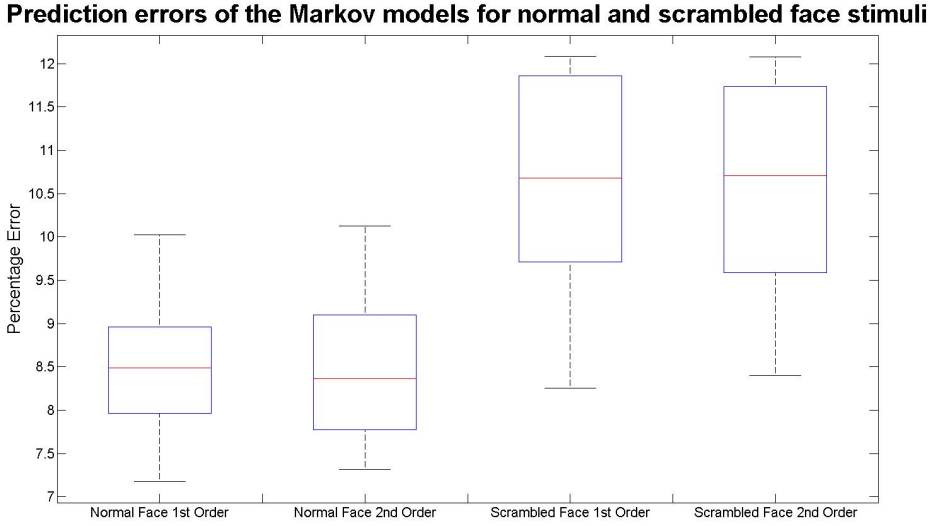

Figure 5.4: Average prediction errors using 1st and 2nd order Markov model. The normal face stimuli show lower errors compared to scrambled face.

Also, given the state transition matrix P^n, it is possible to compute the probability of getting state j starting from state i in n time steps i.e. $S_i(n) = S_i(0)P^n$. This allows us to check the Markovian property of the data using the estimated model for predicting the state at n^{th} time-step from the knowledge of the initial state. The experiments were run for n=400 subsequent time steps and the prediction errors were plotted for

100 different realizations over all the 10-folds as shown in Figure 5.5. It is evident that the long-term prediction from a given initial state becomes poorer as the error bounds diverges and becomes more prone to outliers as time evolves.

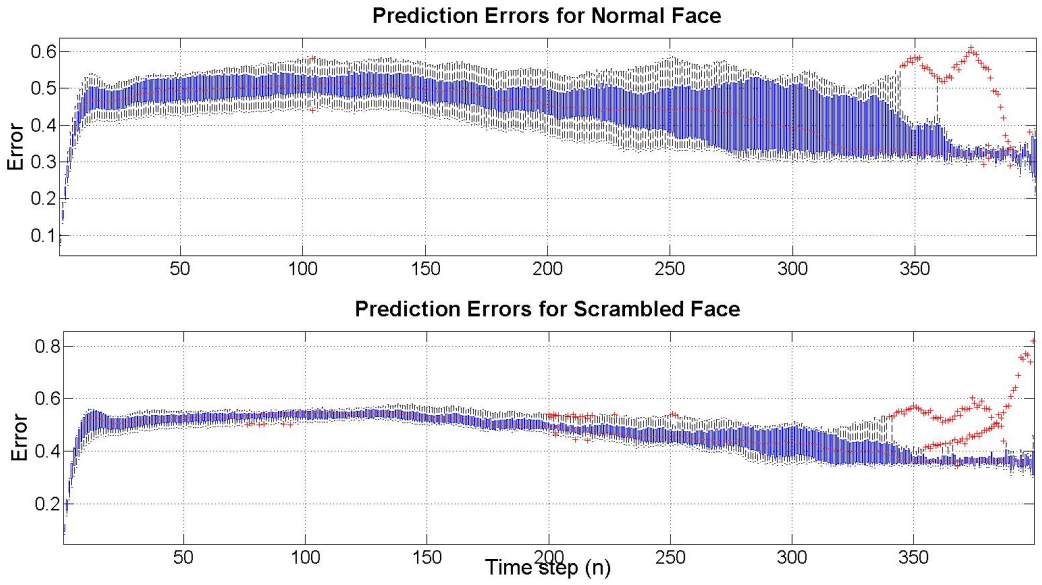

Figure 5.5: Box-plot of the error rates for 10 folds across the n steps.

From this study it is found that one can synthetically generate the EEG synchrostate switching sequences from a first and second order Markov model and then the predictions can be validated using a 10-fold cross validation scheme. Representing the synchrostate transitions as a Markov model provides interesting information about the temporal evolution process of these states characterising the underlying probabilistic brain dynamics. This model successfully predicts the inter-synchrostate transitions with average accuracy of 91.63% and 89.32% for normal and scrambled face respectively. These results allow us to conclude that synchrostate transitions may be modelled accurately as a Markov process.

5.2 Quantification of the synchrostate transition in typical, ASD, high and low anxiety group

The section above demonstrates that modelling the synchrostate sequence as Markov chains with a simple description of the transition probabilities is effective as one can apply statistical significance tests and validation schemes to generate models that are indicative of the probabilistic nature of the synchrostate dynamics. Here the temporal switching sequence of the synchrostates are modelled in a probabilistic framework for the case of typical, ASD, high and low anxiety groups. The study is limited to the transition probabilities and the degee of self transition and is not extended to the predictive model

as these datasets have limited number of trials in the experiments, not enough to do data partitioning and run a viable validation scheme which will not overfit the model.

The transition probability ($P_{ij} = n_{ij} \Big/ \sum_j n_{ij}$) of the synchrostate sequence is constructed which show the probabilistic nature of each of the state transitions. Here, n_{ij} is the number of transitions from state i to j. When the number of states is 3, the three probability values - P_{11}, P_{22}, and P_{33} show how long each state remain stable i.e. how stable each of the states (S_1, S_2, S_3) are in terms of the probability of staying in the same state, for different population groups. These probabilities in essence estimate the stability of phase difference configuration shown in the topoplots in Chapter 3 and 4 and thus potray a key factor of synchronisation.

Figure 5.6 shows the average state transition (across different stimuli) diagrams for the typical and ASD group in the β and γ bands. It is evident in from the typical transition probability diagrams that state three in both β and γ bands is most the stable one. From Figures 4.3 and 4.4 it can be observed that this state has a more uniform and low phase difference topography. The γ band probability P_{11} is the highest, indicating state 1 is likely to be the most synchronised state. The topoplot of this state (Figure 4.8) is very different to the most stable state of typical children (state 3). This difference in the highly stable synchrostates in the γ band of typical and autistic children is worth investigating and a more quantitative analysis in this band may provide more discriminating results.

The other probabilities i.e $P_{ij}, \{i, j\} \in [1, 2, 3]$ when $i \neq j$ show the probability of the interstate changes. The elements of the state transition matrix ($P_{ij}, \{i, j\} \in [1, 2, 3]$) for different population are more informative, although the phase difference topographies for two different population could be similar. Therefore, the average value of the self-transitions ($(1/N) \sum_{i=1}^{N} P_{ii}$, N being the optimal number of synchrostates) for a particular band, can be considered as one of the discriminating measure between two groups. Table 5.1 shows the self transition in both the β and γ bands for the typical and ASD group. It is evident from the Table 5.1 that for the β band with fear and happy stimuli the ASD group has got a higher probability of self-transition than the typical case. On contrary the γ band shows an decrease in self-transition for happy face stimulus in the ASD. The evident difference in the self transition between the cohort warrants a study to see which stimuli can quantitatively discriminate between the populations.

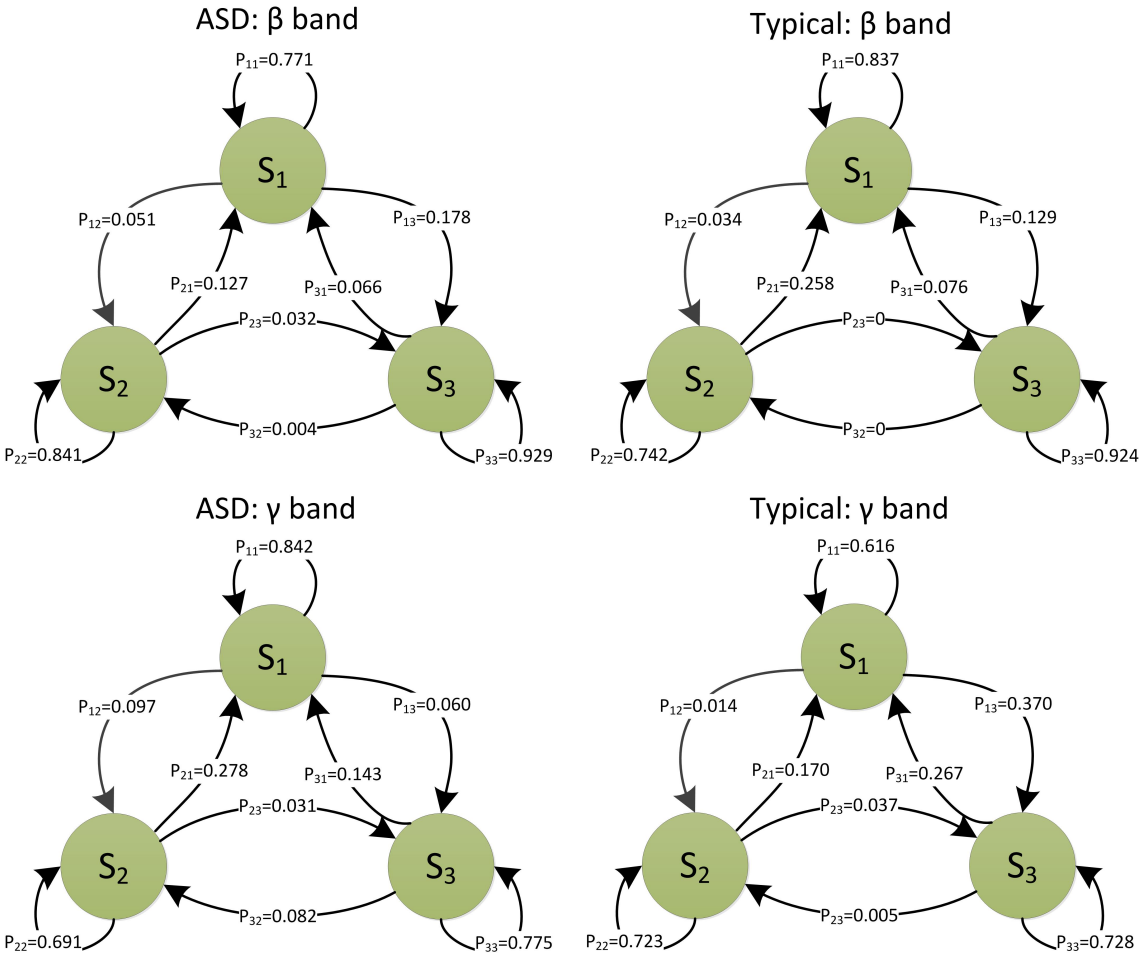

Figure 5.6: Average state transition (across different stimuli) diagrams for the typical and ASD group in the β and γ band

Table 5.1: Self-transitions in β and γ band for the typical and ASD group with different stimuli

Stimuli	**Typical**		**ASD**	
	β	γ	β	γ
Fear	0.84329	0.7562	0.88044	0.66087
Happy	0.83432	0.69536	0.90409	0.67486
Neutral	0.88044	0.68469	0.7577	0.7528

Table 5.2: Average state transition (across different stimuli) diagrams for the low anxiety group in the β band

		i			
	P_{ij}	1	2	3	4
j	1	0.892835	0.010685	0.051948	0.044532
	2	0.024242	0.815494	0.056354	0.10391
	3	0.042042	0.111134	0.837815	0.009009
	4	0.173333	0.030352	0.053225	0.743089

Without loss of generality the same method could be applied for analysing systems with more states and the anxiety groups as well. Table 5.2 and Table 5.3 tabulates the average state transition matrices for the the low anxiety group across all stimuli for the β and the γ band respectively. In the low anxiety group β has four synchrostates and γ has six synchrostates (Figure 4.11), consequently their transition matrices are 4x4 and 6x6 respectively. Figure 5.7 on the other hand shows the same properties but for the high anxiety group. The self transition values show that state 1 is the most stable and synchronised in the low anxiety group. State 1 has different topographies for the two frequency bands. The state 1 headplot for the γ band (Figure 4.13) has a heterogenous spread of phase difference across the scalp. On the contrary the state 1 topography in the β band (Figure 4.12) is more subdued and uniform across the scalp, except for the happy face state 1.

Table 5.4 shows the self transitions for the low and high anxiety group across all three stimuli. In the β band the low anxiety group has a higher probability of self transition compared to that of high anxiety. However for the γ band the self transitions are a lot higher in the high anxiety group. It seems from this table that the γ band synchronisation could potray the varied anxiety traits between the different subject best.

Table 5.3: Average state transition (across different stimuli) diagrams for the low anxiety group in the γ band

		i					
	P_{ij}	1	2	3	4	5	6
j	1	0.925926	0	0	0.074074	0	0
	2	0	0.210317	0.019841	0.011905	0	0.09127
	3	0	0.117647	0.215686	0	0	0
	4	0.035517	0.016667	0.016667	0.704968	0.081169	0.145013
	5	0	0	0	0.207935	0.678828	0.113238
	6	0	0.067797	0	0.095914	0.007638	0.828651

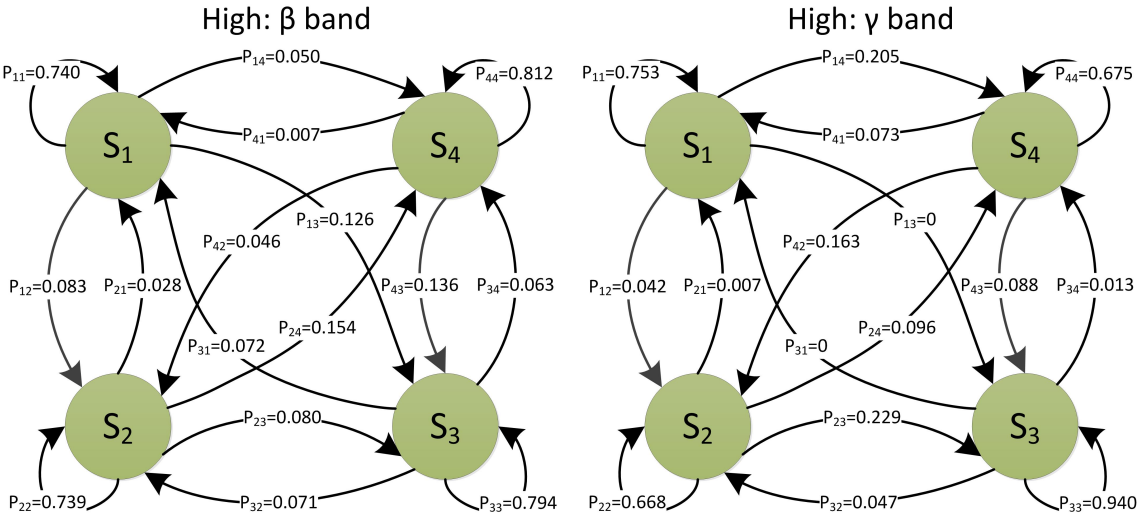

Figure 5.7: Average state transition (across different stimuli) diagrams for the high anxiety group in the β and γ band

Table 5.4: Self-transitions in β and γ band for the low and high anxiety group with different stimuli

Stimuli	**Low Anxiety**		**High Anxiety**	
	β	γ	β	γ
Angry	0.843881	0.51635	0.752731	0.752731
Happy	0.791473	0.542314	0.72929	0.72929
Neutral	0.83157	0.723524	0.81774	0.795766

5.3 Discussion

Deriving synchrostates allows us to represents a multivariate stochastic process, EEG as a few univariate quasi-static synchrostates which randomly switches amongst themselves. The evolution of these states essentially describes the underlying dynamical nature of a system.

It is observed that a particular simple structure in the empirical synchrostate transition sequence that can be described with a first order or second order Markov chain (Norris (1998)). A statistical synchrostate analysis is performed on the data set reported in the previous chapters. Temporal parameters eg. the rate or mean duration of intervals of each state can be inferred from the parameters of the Markov chain. By exploiting the relation between the observed Markov chain and the synchrostate process, one can get insights about temporal properties of the EEG process. Modelling of the pseudo-random and abrupt temporal switching characteristics of synchrostates may be useful to understand the dynamic nature of the stimulus induced brain response in different

pathological populations. Microstate duration is a central parameter for spontaneous EEG activity analysis (Gärtner et al. (2014)). Koenig et. al. reported a decrease in microstate durations with increasing age (Koenig et al. (2002)). Other studies have found correlates between the shortening of the duration of single microstate map with clinical symptoms in schizophrenic patients (Strelets et al. (2003) and Kindler et al. (2011)), as well as increase in microstate durations in slow wave deep sleep (Brodbeck et al. (2012)). Conducting a statistical analysis on the synchrostate transitions similar to the way microstates have been studied is necessary to investigate the correlates between this new observed phenomenon and other environmental, experimental, demographic and physical factors.

5.4 Conclusion

In this chapter, a probabilistic model is developed in order to synthetically generate the EEG synchrostate switching sequences as first and second order Markov process and then the predictions are validated using a 10-fold cross validation scheme. The Markov model provides interesting information about the temporal evolution process of the synchrostates characterising the underlying probabilistic brain dynamics. This probabilistic model successfully predicts the inter-synchrostate switching patterns with the best average accuracy of 91.63% (for normal face perception) and 89.32% (for scrambled face perception) on average. The proposed modeling approach may shed new light in understanding stochastic dynamical basis of cognition in humans. The average self transition probabilities for a particular band show some discriminating characteristics as well. The γ band self transitions have shown varied stability across different cohorts. It may well be worth investigating how the synchronisation in this band is reflective of the underlying connections and hence trace if there are parameters that can quantitatively express these differences.

It reports the simple transition structure that was observed from EEG synchrostate analysis. For all the experiments, a first order Markov chain was used to describe the transition frequencies between different states. The resulting transition matrix is consistent with the observations of the state transition and hence it is suggested that Markov chains can be used as a simple description of the transition probabilities from which one can apply statistical significance tests like the one done by Gartner et. al. on microstates (Gärtner et al. (2014)) to find deviations from a simple model of background EEG. Secondly, a simplified Markov chain model also provides a way to deal with the question of how the empirical observation of synchrostate transition sequence is related to the underlying process.

Chapter 6

Connectivity analysis using complex networks

Synchrostates and their transition have been shown to exist in different groups of subjects, both children and adult, healthy and pathological. Their stability when studied in a probabilistic perspective as self transitions showed varied values across cohorts as well stimuli. To study phase synchrony one needs to consider stability in the context of time. Interpretation of the synchrostate topographies and the state transitions should be done together by combining the stability duration and their respective numerical values of phase difference. When considered together one can formulate a synchronisation index corresponding to each of the synchrostates from which scalp-level functional connectivity network could be derived. These dynamic brain networks are governed by the nature of switching patterns of the synchrostates and, therefore, in essence capture the temporal evolution of functional connectivity in stimulus-specific way at fine temporal granularity level. Fundamental graph-theoretic measures could be used for characterising such networks for gaining quantitatively deeper insight into the temporal dynamics of the connectivity pattern prevailing after the onset of stimuli and therefore may provide a quantitative means for assessing cognitive functionalities, which is one of the objective of the work.

6.1 Functional Connectivity using Phase Synchronisation Index

Synchrostates have been previously defined as states within which the inter electrode relative phase difference remains approximately constant over time. Once such possible unique clusters or states are identified, their temporal stability needs to be analysed since the clustering technique only identifies possible unique stable phase difference

patterns, but it does not capture the length of time for which each of them are stable. Quantitatively, this can be described by the synchronisation index $\Gamma_{xy}(B)$ which is an inverse circular statistical analogue of variance given in (6.1) (Peng et al. (2010)).

$$\Gamma_{xy}(B) = \frac{1}{P_s}\sqrt{\left[\sum_t \cos\left(\Delta\varphi_B(t)\right)\right]^2 + \left[\sum_t \sin\left(\Delta\varphi_B(t)\right)\right]^2} \tag{6.1}$$

Here, P_s is the number of data-points in the clustered time series with $P_s < P$ or it can be viewed as the time points associated with a single state (s) and $\Gamma_{xy}(B) \in [0, 1]$. A high value of $\Gamma_{xy}(B)$ indicates that the phase difference between the two signals at a given frequency band B has low variation over time and therefore can be considered in synchrony. This in essence quantifies the average temporal stability of the clustered phase synchronisation states in that band. In contrast to the coherence based measures (Engel et al. (2001b)), this index is capable of capturing the band-specific temporal behaviour of the synchronisation phenomena. Once the values of $\Gamma_{xy}(B)$ are computed for each of the channel pairs (x,y), they can be plotted for all the electrodes resulting in a global synchronisation matrix, which is symmetric and square in nature describing the phase synchronisation in the entire EEG space.

6.2 Complex network measures of brain connectivity

After the global synchronisation matrix describing the stability of each of the clusters is formed, it can be translated into a complex network that may shed light on the temporal evolution of phase synchrony amongst different brain regions and hence describe the nature of the associated information coupling. Similar to the other connectivity networks in nature, brain connectivity can be analysed with the graph theoretic approach by considering the EEG electrodes as nodes and the $\Gamma_{xy}(B)$ values between them expressed as weighted edges signifying the connection strength between the $(x, y)^{th}$ node. The usefulness of complex network analysis was demonstrated in the study of anatomical as well as functional brain networks. Network measures have been used to quantify the brain connectivity (Fallani et al. (2008), Astolfi et al. (2008)) and have been useful to draw network topology comparisons between healthy subjects and patients with neurological injury or disorder (Cao and Slobounov (2010)). The topological properties and intrinsic meaning of the networks thus created can then be studied by interpreting the appropriate network measures. Two specific types of generic measures that are most relevant in understanding the brain's capability for information processing are segregation and integration.

Measures of segregation in a brain network quantify the ability for specialised processing within highly connected brain regions. Segregation is suggestive of the segregated neural processing and can be applied to evaluate local connectivity. Modularity of a

network is a sophisticated measure of network segregation where the degree to which a network can be subdivided to a group of nodes with small number of between group links (edges) and large number of within group links is measured (Rubinov and Sporns (2010)). Modularity (Q^w) of a network is expressed as (6.2).

$$Q^w = \frac{1}{l^w} \sum_{x,y \in N} \left[w_{xy} - \frac{k_x^w k_y^w}{l^w} \right] \delta_{m_x, m_y} \tag{6.2}$$

where, w_{xy} is the connection weights, ${k_x}^w = \sum_{y \in N} w_{xy}$ is the weighted degree, $l^w = \sum_{x,y \in N} w_{xy}$ is the sum of all weights in the network. Also, $\delta_{m_x, m_y} = 1$ if $m_x = m_y$, and 0 otherwise (m_x is the module containing node x). Here, the superscript w indicates the weighted nature of the graphs, as adopted in the present analyses, whereas binary and directed versions are also possible.

Transitivity (T^w), which is the ratio of the triangle to triplets of the network, is also a measure of segregation in complex network analysis and is a normalised variant of clustering coefficient (Strogatz (2001)), which is expressed in (6.3).

$$T^w = \frac{1}{\widetilde{N}} \frac{\sum_{i \in N} 2t_x^w}{\sum_{x \in N} k_x \left(k_x - 1 \right)} \tag{6.3}$$

where, $t_x^w = \frac{1}{2} \sum_{y,h \in N} \left(w_{xy}, w_{xh}, w_{yh} \right)^{1/3}$ is the weighted geometric mean of the triangles around x.

The neurobiological context and significance of modularity and transitivity is that they quantitatively describe the highly segregated communities with information passing within them (Fallani et al. (2008), Sporns (2011)). Nodes belonging to a cluster or module share significant information with each other, on the contrary units belonging to different clusters remain segregated from each other with little interactions. However, it is to be noted that measurement of phase synchrony represents only the information coupling strengths amongst different brain regions rather than giving a direction of information flow. Therefore, in this work is restricted to the analysis of weighted undirected brain networks only.

Characteristic path length (L^w) and global efficiency (E^w) are common measures of integration, which captures the capacity of global interaction in a network and may represent the ease of network wide communication (Sporns (2011)). Characteristic path length, given in (6.4), is the average of the shortest path length between a node and all other nodes (Watts and Strogatz (1998)). It is the global mean of the distance matrix. On the other hand, the global efficiency, given in (6.5), is computed by averaging the inverse of the distance matrix. Therefore, a fully connected network has the maximum

global efficiency (Sporns (2011)).

$$L^w = \frac{1}{\widetilde{N}} \sum_{x \in N} \frac{\sum\limits_{y \in N, j \neq x} d^w_{xy}}{\widetilde{N} - 1} \tag{6.4}$$

$$E^w = \frac{1}{\widetilde{N}} \sum_{x \in N} \frac{\sum\limits_{y \in N, y \neq x} \left(d^w_{xy}\right)^{-1}}{\widetilde{N} - 1} \tag{6.5}$$

where, d^w_{xy} is the shortest weighted path length between x and y.
The two important measures, i.e. radius and diameter of any complex network, can be derived from its eccentricity (e^w_i), which refers to the maximum value of each row of the Hadamard (dot) product of d^w_{xy}. Radius (r) and the diameter (D) are the minimum and the maximum values of eccentricity respectively and are mathematically expressed in (6.6).

$$e^w_x = \max\left(d^w_{xy} \circ d^w_{xy}\right),\ r^w = \min\left(e^w_x\right),\ D^w = \max\left(e^w_x\right) \tag{6.6}$$

Quantitative measures of the above mentioned metrics therefore are expected to characterise the ability of the brain network for information processing in terms of specialised processing (segregation) within local regions and global integration. In the above mentioned network parameters in (6.2)-(6.6), N is the set of all nodes in the network and $\widetilde{N}$ is the number of nodes.

6.3 Analysis and results

6.3.1 Connectivity analysis of single subject multiple trial EEG dataset

In order to gain a better insight into the implications of the synchrostates, the complex networks corresponding to each of them are constructed from the results following from section 3.3.1 for the single subject adult EEG. The analysis is restricted to β band as it is more relevant to the information processing in the present case. The brain connectivity graphs and other relevant network measures, reported in this section are computed using the clustering results over all the ensembles (1-100 trials). While the EEG electrodes have been used as nodes, the synchronisation indices $\Gamma_{xy}(B)$, calculated using (6.1) are used as the edges connecting the $(x, y)^{th}$ nodes. The cross-electrode plots of $\Gamma_{xy}(B)$ are shown in Figure 6.1 where the close to unity value of $\Gamma_{xy}(B)$(depicted as red color) indicates high degree of synchronisation. This yields the basic connectivity matrix for the complex network analysis. From Figure 6.1 it is evident that there exist two distinct groups indicating good modularity in state 1 and state 2 (the smaller square box electrodes (1-32) and the larger square box (33-128)) forming strongly connected groups amongst themselves with weak connections with the outside nodes.

In Figure 6.2 the plots of Figure 6.1 are translated into complex network structures. Owing to the property of $\Gamma_{xy}(B)$ the weight of the edges between the nodes describe the degree of synchronisation amongst them (how well connected they are) which also encompasses the temporal stability of each state. Figure 6.2 depicts the brain network structures for the normal face perception corresponding to each of the synchrostates 1, 2 and 3 respectively and also the same for the scrambled face scenario. All of the brain connectivity network plots have been made using the Gephi software (Bastian et al. (2009)). For the ease of visualisation only 7% amongst the highly connected edges are shown in Figure 6.2. The densely connected nodes are shown as the nodes with large diameters. As an example, the larger diameter of the node A6 in Figure 6.2 (state 1 of normal face) signifies higher connectivity than the relatively smaller diameter node A5. The connection strength to each node is based on the total connections to it before the 7% threshold was applied. Table 6.1 lists the results from the complex network analysis (without threshold) to obtain further insight into the functional organisation of human brain at each of these states. The complex network measures in Table 6.1 have been computed using the brain connectivity toolbox (Rubinov and Sporns (2010)) from the fully connected graph.

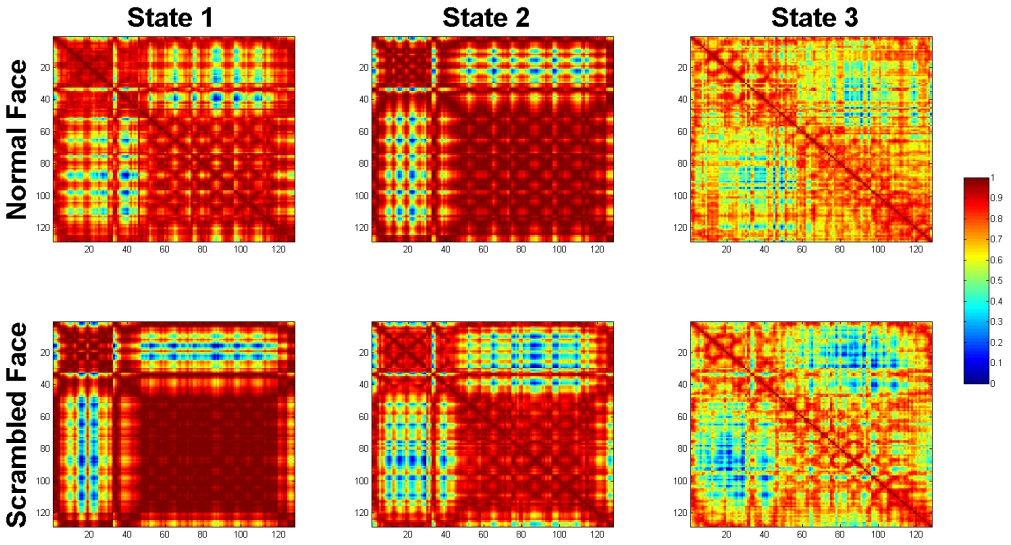

Figure 6.1: Synchronisation index ($\Gamma_{xy}(B)$) for different states with normal and scrambled face stimuli. This shows the adjacency matrix used to form the connectivity plots for the synchrostates

6.3.1.1 Comparison of the connectivity analysis for normal and scrambled face

The macroscopic phase change, a discernible transition from one state to the other from the statistical physics point of view, is clearly exhibited in these three state changes

(Figure 3.11) and is also reflected in the modularity and transitivity values. However, a close comparison of the modularity (or transitivity) values for each of the states in both the cases shows significant differences. The modularity value for normal face perception is the maximum for state 2 whereas for the scrambled face processing the maximum modularity is reflected in state 1. On the other hand the modularity values of state 3 for both of the cases are nearly same which is an order lower than the dominant modularity state in the two cases. One possible implication of this is that for normal and scrambled face processing, segregated specialised information processing within an area of highly-connected node assembly takes place in state 2 and state 1 respectively whereas in both of the cases, state 3 pertains to minimal specialised segregated processing. Visual observation of connectivity maps depicted in Figure 6.2 also confirms this observation where these highly connected nodal assemblies could be identified. As an example, a comparison of Figure 6.2 (a) and (b) clearly shows that state 1 for scrambled face processing (Figure 6.2 (b)) shows denser connections between the nodes in the frontal and parietal regions compared to state 1 for normal face processing (Figure 6.2 (a)) and also exhibits less connectivity between this region and other regions of the brain. The effect is exactly opposite for state 2 (Figure 6.2(c) and (d)) where normal face processing shows denser connections than the scrambled one. The connectivity between different brain regions is less but more uniformly distributed for state 3 in both the cases (Figure 6.2 (e) and (f)) than state 1 and state 2 confirming less value of modularity in Table 6.1.

Table 6.1: Network measures for the brain connectivity corresponding to each synchrostate during normal and scrambled face perception (for trials 1-100) in the β band

Network measures	Normal face			Scrambled face		
	State1	State2	State3	State1	State2	State3
transitivity	0.9371	0.9015	0.9917	0.8325	0.9506	0.9906
modularity	0.0083	0.0339	0.0016	0.0649	0.0172	0.0022
characteristic path length	0.9579	0.8836	0.9761	0.6325	0.9362	0.9751
global efficiency	1.0367	1.1502	1.0165	1.9377	1.0631	1.0176
radius	0.9919	0.9119	0.9918	0.7136	0.9916	0.9918
diameter	0.9986	0.9988	0.998	0.9993	0.9981	0.9985

From Table 6.1, observing the two major indices of information integration capability in a complex network global efficiency and characteristic path length once again a similar behaviour has been found. Here, state 2 and state 1 possess larger global efficiency and smaller characteristic path length for the normal and scrambled face perceptions respectively, compared to those for the two cases of state 3 which indicate towards maximum information integration ability in these two states. This affirms the study by Straaten and Stam (van Straaten and Stam (2013)). It is also apparent from Table 6.1 that for state 2 of the normal face and state 1 of the scrambled face, the radius is the minimum. This implies that the graph is strongly connected and more information can

flow very quickly from one region to the other due to lower radius and therefore resulting in more information integration ability in these states. The respective stability periods for each of these states may determine the time spent in global information exchange allowable by that state. During these periods the brain network is configured to share more information between distant nodes with ease. Combining these observations with the conclusions drawn from the values of modularity and transitivity, it is apparent that state 2 and state 1 represent dominant information processing states for normal and scrambled face processing respectively. These parameters can assess the efficiency or extent to which optimal partitioning occurs in the functional organisation of brain (Sporns (2012), Rubinov and Sporns (2011)).

However, although state 2 in normal face perception exhibits higher global efficiency and minimum characteristic path length, their values are still comparable with those in the other two states. Similar observation is true for the radius as well. This indicates that although state 2 is dominant for information integration, the other states also contribute to a comparable level for that process. However, modularity value of state 2 is significantly higher than that of the other states indicating the majority of segregated specialised processing taking place in this state. On the other hand, the above-mentioned parameter values for state 1 of scrambled face perception case are significantly different from those of the other two states indicating its dominance in both the processes of segregated information processing, (represented by high modularity) and information integration (small characteristic path length and high global efficiency). This supports the study by Stam (Stam (2010)) that modularity reflects segregation and characteristic path length indicates towards integration. Another interesting point to observe is that the information integration indices for the non-dominant states in the case of scrambled face processing show comparable values with even the dominant state (state 2) for normal face perception. This may mean that in general the information integration process required for scrambled face processing is more intense compared to that of the normal face processing. This is also evident from the significant difference of the network parameter values corresponding to state 1 of scrambled face processing among all 6 states (3 for normal face and 3 for scrambled face) in Table 6.1 viz. lowest transitivity, highest modularity, lowest characteristic path length, highest global efficiency and lowest radius. This argument also matches with the intuitive and practical understanding of the problem that a person will need greater attention or require more information integration to discern the scrambled face and therefore confirms the task-specific nature of information integration.

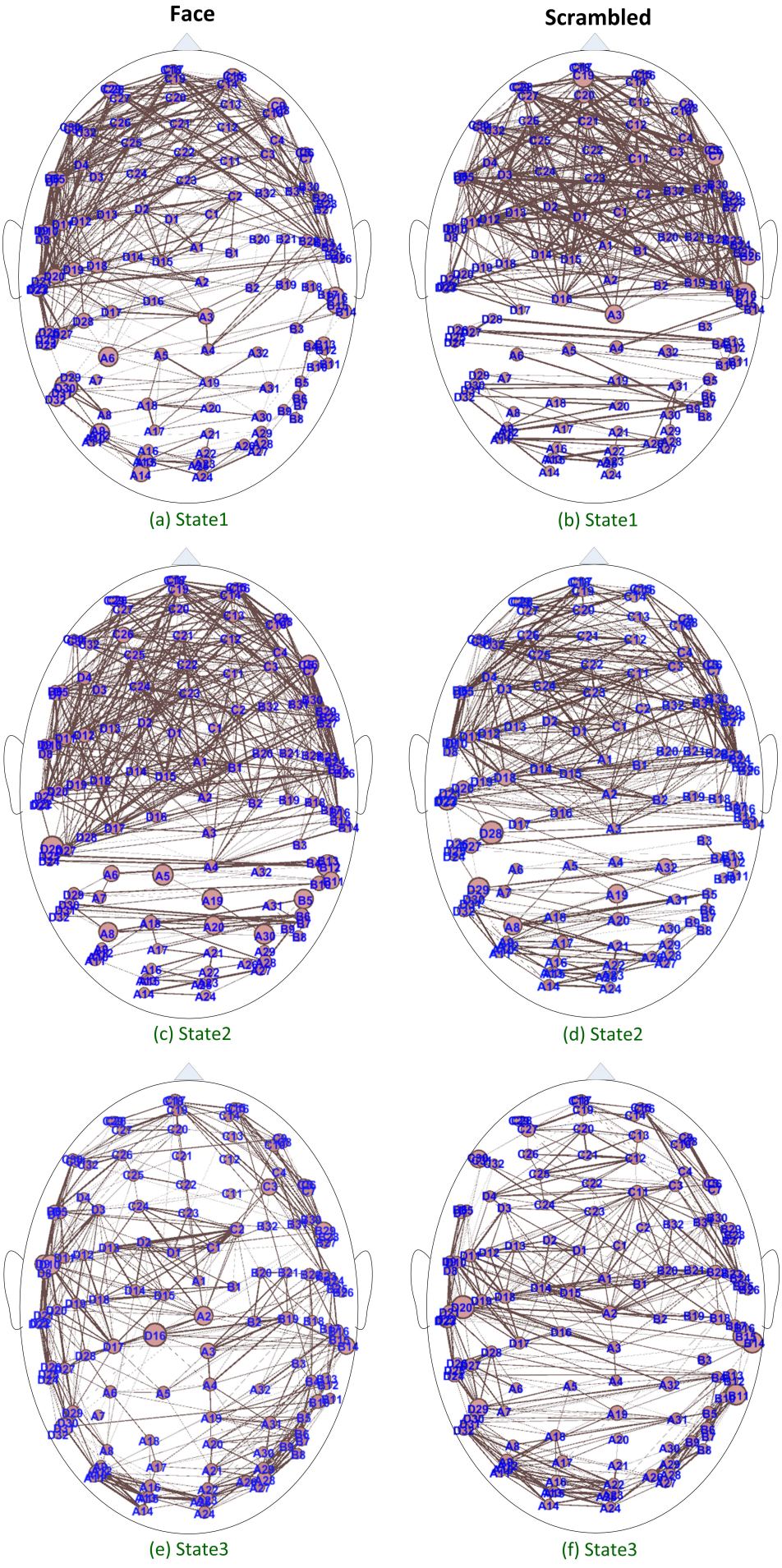

Figure 6.2: Brain connectivity plots of three synchrostates for normal face and scrambled face stimuli in the β band.

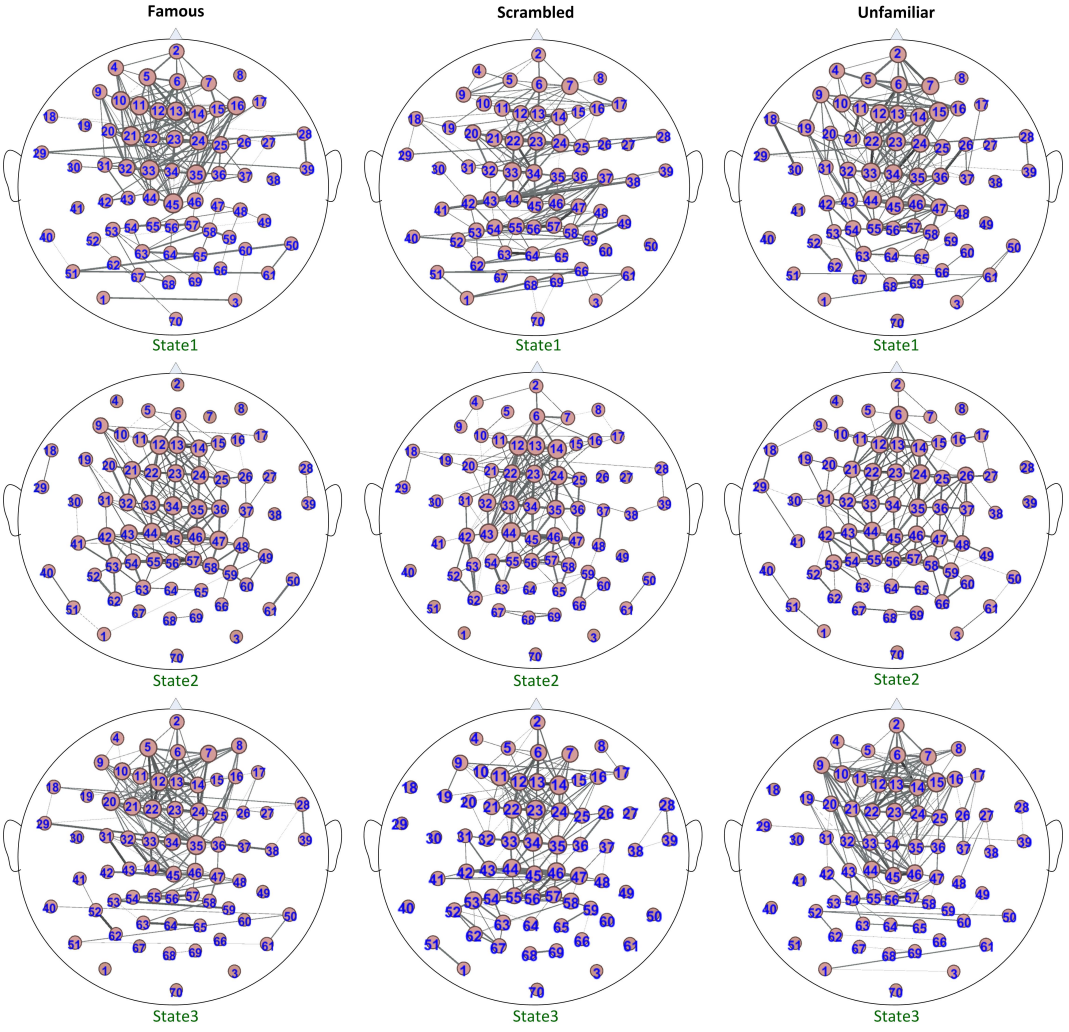

Figure 6.3: Brain connectivity plots of three synchrostates for famous, scrambled and unfamiliar face stimuli in the β band.

6.3.2 Connectivity Analysis of multiple subjects involving multiple trials EEG dataset

Following on from the previous study, the synchronisation index given in (6.1) is used to derive the connectivity diagram for the states (derived in section 3.3.2) of the multi-subject multiple trial EEG face perception data. These have been shown graphically in Figure 6.3 where only the strongest 7% amongst all the connections are shown. Figure 6.3 shows the network structures for the synchrostates over the three face perception stimuli corresponding to each of the synchrostates 1, 2 and 3 respectively. These results show that, without the loss of generality the same synchrostate analysis approach can be applied to an average subject group with multiple trials and also a single subject from EEG recorded over multiple trials. Highly connected nodes have a larger diameter than the sparsely connected ones.

Once again the discernable changes in the state connectivity plots for the different states is seen which is also reflected in the network parameters calculated in Table 6.2. For both the famous and unfamiliar face stimuli state 3 is the state with the highest modularity values. Following on from the previous assumptions about the interpretation of the network parameter one may say that state 3 is where the segregated information processing is happening for famous and unfamiliar face processing. This state for both the stimuli have minimal global interactions which is quantified with a low value of characteristic path length. For this case both famous and unfamiliar face stimuli can be categorised under the normal face stimulus group. It is evident that both of these stimuli although intrinsically different render similar brain responses when categorised as normal face. Incase of scrambled face, state 1, which is the minimum occurring state has the highest modularity and lowest value of characteristic path length i.e the high local connectivity and low global connectivity. Previously in the single subject analysis both stimuli (normal and scrambled face) had minimal specialised segregated processing occurring at the same state 3. Here the same phenomenon is observed, i.e state 2 has the minimum modularity (localised special processing) values for all the stimuli. From these observations one may conclude that adults perceive a scrambled face differently to the way they perceive a general category of normal face stimulus (either famous and unfamiliar). These differences in the encoding of the normal and scrambled faces (George et al. (1996)) are reflected in the network parameters of the synchrostate connectivity maps.

Table 6.2: Network measures for the brain connectivity corresponding to the multi subject synchrostates during famous, scrambled and unfamiliar face perception

Network measures	Famous face			Scrambled face			Unfamiliar face		
	State1	State2	State3	State1	State2	State3	State1	State2	State3
transitivity	1.0129	1.0139	1.0116	1.0129	1.0139	1.0135	1.0128	1.0139	1.0118
modularity	2.77E-4	7.46E-5	7.52E-4	3.44E-4	9.87E-5	1.93E-4	3.47E-4	7.40E-5	7.02E-4
characteristic path length	0.9842	0.9852	0.9829	0.9843	0.9851	0.9847	0.9840	0.9852	0.9831
global efficiency	1.0015	1.0006	1.0029	1.0015	1.0006	1.0010	1.0017	1.0050	1.0027
radius	0.9997	0.9997	0.9994	0.9998	0.9996	0.9997	0.9996	0.9998	0.999
diameter	1	0.9999	0.9999	1	1	1	0.9999	0.9999	1

6.3.3 Effect of Volume conduction on Connectivity analysis

The possible effects of volume conduction on phase synchrony analysis has been discussed in detail in earlier chapters and the results revealed that the synchrostate phenomenon is free from volume conduction. Here again through the connectivity analysis results it is verified that the brain networks extracted from the phase synchronisation reported is not due to volume conduction.

Studies which model the effect of distance between scalp electrodes suggest that the effects of volume conduction registered phase synchrony is significantly reduced at a distance of 4 cm (Nunez et al. (1997), Nunez et al. (1999)). Some papers state spurious coherence from volume conduction dropping to near zero when scalp electrodes were separated by 4 cm or more (Doesburg et al. (2008)). This can lead to difficulties in distinguishing between volume conduction and true synchrony in the short range (<4 cm) and limits the understanding of short range synchrony. The results in the brain connectivity diagram (Figure 6.2 and Figure 6.3) show that most of the strong synchrony or connections are between distant electrodes which cannot be accounted for due to volume conduction. Only 9.4% (with a standard deviation of 2.1) of the synchronies reported here were between recording sites that are <4 cm apart. The rest of the connections (approximately 90.6%) and interactions are between electrodes with a distance >4 cm. Such long range connections cannot be explained with volume conduction. This evidence adds to the previous comments about the effect of volume conduction and strongly supports the claim that results presented in all these experiments should not be perceived to be resulting from volume conduction.

6.3.4 Connectivity Analysis of Emotional face response in Typical and Autistic Children

Next the same principles of the multiple subject group connectivity analysis were applied to the typical and ASD group synchrostates. The synchronisation index of (6.1) is used for formulating the connectivity graphs for each of the synchrostates corresponding to each of the stimuli with the EEG electrodes representing the nodes and the synchronisation index value as the edges between them.

From the observations of the two experimental results earlier it was observed that the states which occur the most, i.e the most stable and frequent states hold crucial information about the underlying network dynamics. It was also concluded that it is worth investigating the least occurring state incase of finding stimulus specific signatures in the brain connectivity measures. Hence as an exploration, only those synchrostates which occur the most and the least frequently (termed max_state and min_state respectively) during the entire task were considered. The synchrostates of the groups were derived and then their transition sequence along with the phase relations were used to calculate the degree of synchronisation between each pair of electrodes for the duration of the synchrostate. The resulting connectivity graphs for the max_state and the min_state are shown in Figure 6.4 - 6.6 with only 4% of the strongest connections retained with the colors representing the degree of synchronisation. The max and min values of the colour bars in these figures represent the maximum and minimum values of the 4% highly connected edges respectively. An interesting observation from Figure 6.4 - 6.6 is that in general the min_states show more segmented and highly localised connectivity compared

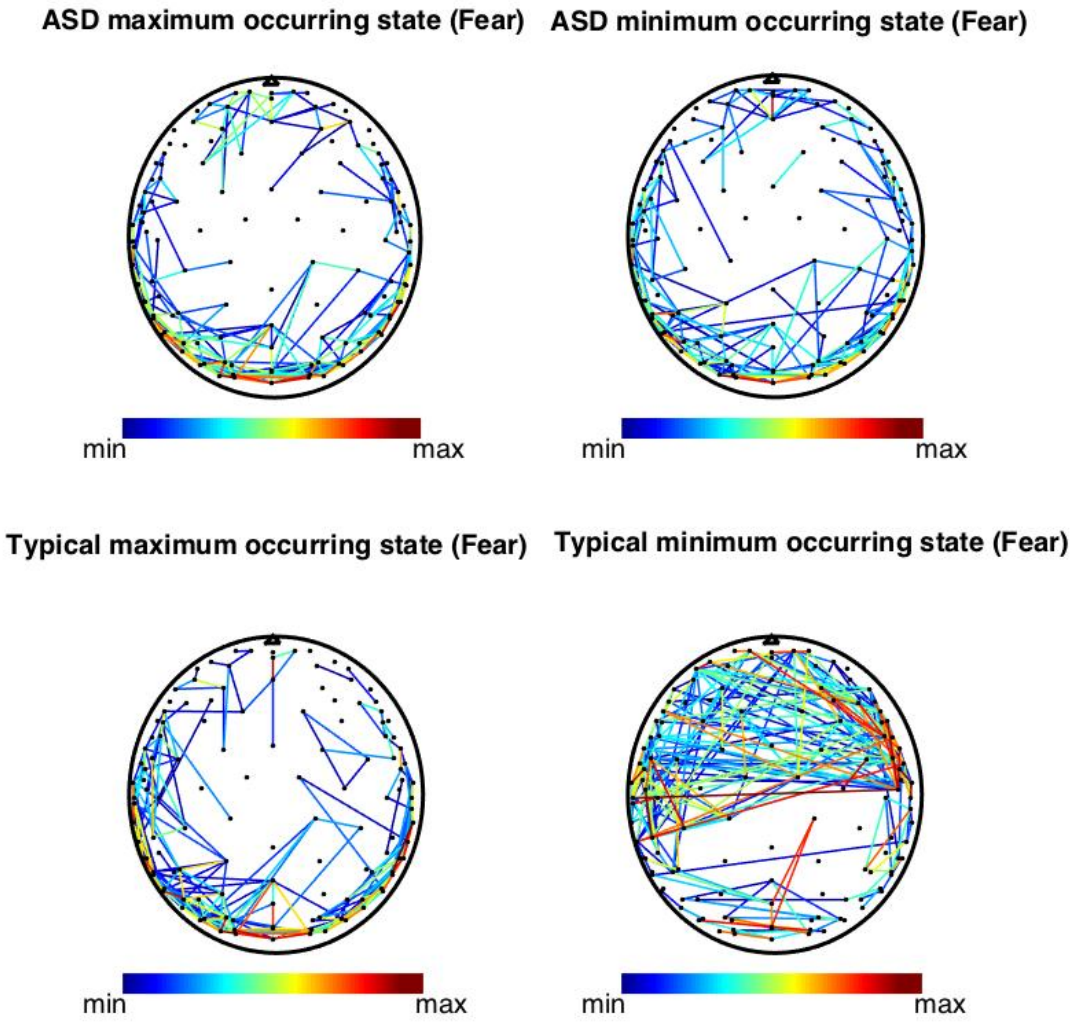

Figure 6.4: Brain connectivity of typical/ASD with fearful face stimuli, shows the different structures of connections being formed in the two cohorts

to those of the corresponding max_states for all the three stimuli in both the ASD and typical groups. This may mean that most of the specialised information integration operations occur during the min_state and therefore its quantitative characterisation may be indicative towards the ability of information integration in ASD and typical children.

Table 6.3 shows the results of modularity comparison for the two groups under consideration for their respective min_state and max_state. It is evident that for all the stimuli the modularity values of the max_state in both the groups are of the same order whereas the same for the min_state in typical group are consistently an order higher than those in the ASD group. Putting into the perspective of physical meaning of modularity of a network this difference implies that the ASD subjects are less able to do specialised

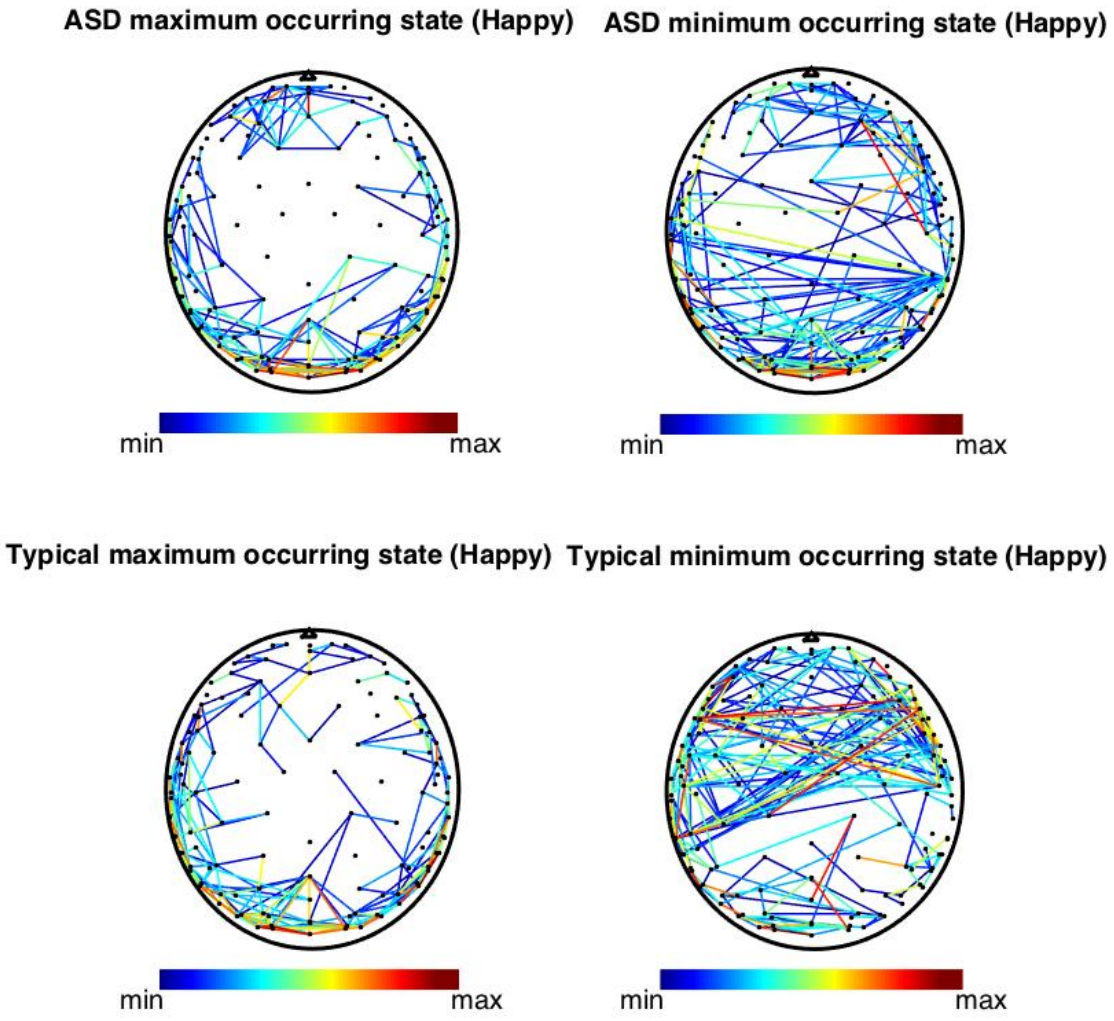

Figure 6.5: Brain connectivity of typical/ASD with happy face stimuli, shows the different structures of connections being formed in the two cohorts

processing during the min_states as their ability to form these localised networks is less than that of the typical. In one sense this conforms to the findings in the anatomical study of Tommerdahl et al. (Tommerdahl et al. (2008)). On the other hand this also shows that modularity could be used as a possible marker for distinguishing ASD from typically-growing children.

Since measure of segregation in a brain network quantifies its ability for specialised processing and therefore describes the organisational property of the local connectivity during information integration, it is deemed that modularity could be a useful index for characterising an Autistic brain.

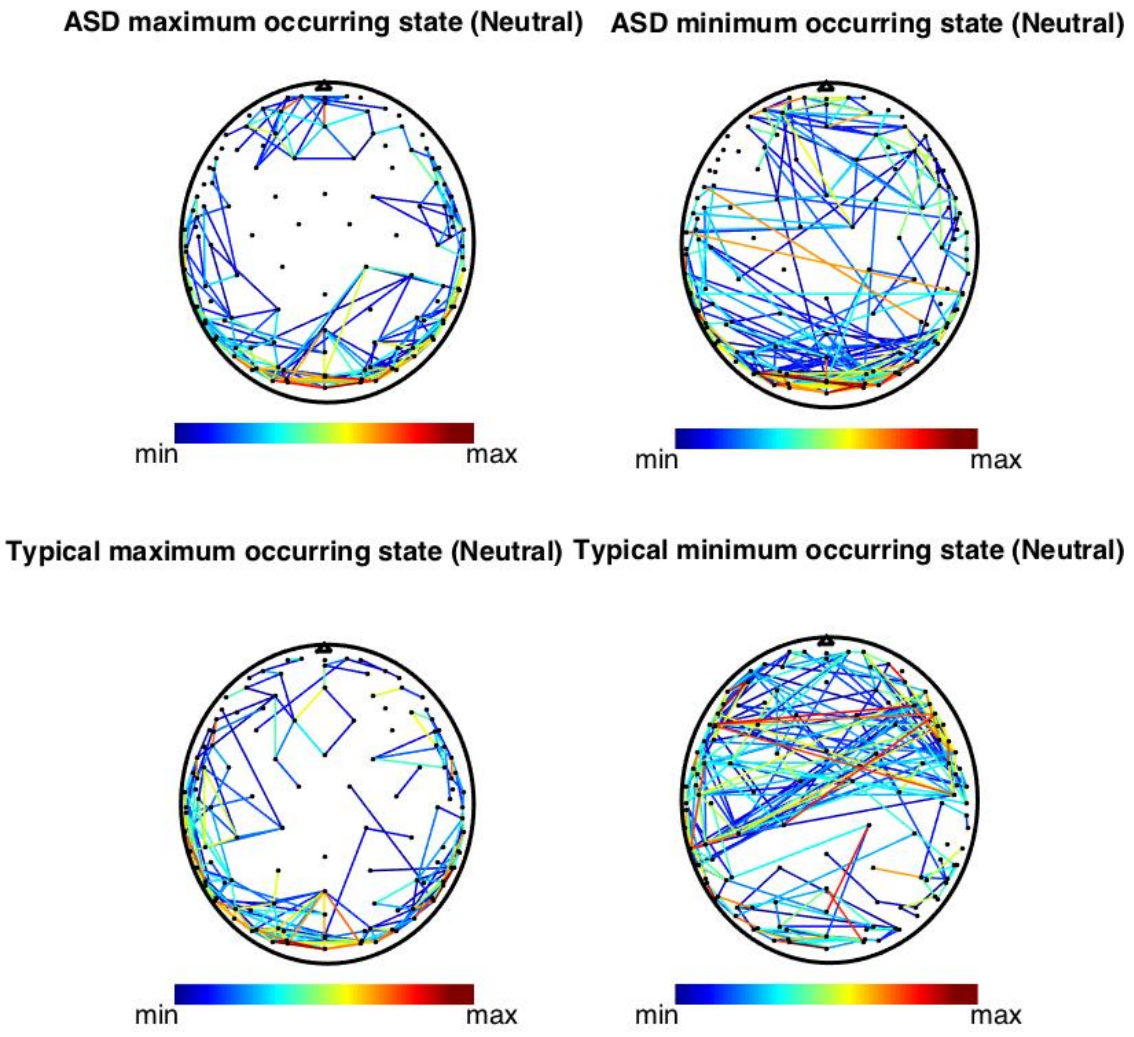

Figure 6.6: Brain connectivity of typical/ASD with neutral face stimuli, shows the different structures of connections being formed in the two cohorts

Table 6.3: Modularity values of the max/min synchrostates for ASD and typical children with different stimulus

Stimulus	**Modularity of max_state**		**Modularity of min_state**	
	ASD	***Typical***	***ASD***	***Typical***
fear	$1.85\text{x}10^{-06}$	$2.50\text{x}10^{-06}$	$3.72\text{x}10^{-06}$	$1.859\text{x}10^{-05}$
happy	$1.82\text{x}10^{-06}$	$2.01\text{x}10^{-06}$	$1.81\text{x}10^{-06}$	$1.862\text{x}10^{-05}$
neutral	$1.77\text{x}10^{-06}$	$1.97\text{x}10^{-06}$	$1.96\text{x}10^{-06}$	$1.8627\text{x}10^{-05}$

6.4 Conclusions

Complex network analysis for the temporal stability and the nature of the synchrostates could potentially be effective in objectively measuring their characteristic interactions in terms of specialised segmented processing and information integration. Therefore comparison of the resulting metrics between a normal and a neurologically impaired subject in a task specific manner is expected to identify the information processing impairments in the latter leading to a methodology for person-specific characterisation of neurological anomalies given the EEG data. There have been recent studies on time-frequency analysis based dynamic functional connectivity modelling (Lu et al. (2011), Chang et al. (2013), Mehrkanoon et al. (2013)) which are based on spectral power analysis. The fundamental difference between this study and (Lu et al. (2011), Chang et al. (2013), Mehrkanoon et al. (2013)) is that this study explores the evolution and organisation of cognitive states or synchrostates that switch amongst themselves during the execution of the task.

The possibility of finding a marker to distinguish between ASD and typical population using graph theoretic measure of brain connectivity network is also explored. It shows that modularity of the connectivity network formulated following synchrostate analysis of non-invasively recorded EEG data could be an effective identifier of ASD children from age-matched typically-growing ones. Further analysis can be conducted on individual subjects to explore the degree of distinction modularity values or the other complex network measures give between these groups.

Chapter 7

Application of Synchrostates in classifying and characterising pathological groups

Chapter 6 demonstrated how synchronisation index can be used to translate the synchrostates and their transition plots into brain connectivity maps. Complex network measures were then applied to the connectivity matrices of the synchrostates to derive metrics to quantify information flow in the brain connectivity plots. The different network measures were demonstrated to reflect the structure of the underlying connectivity as a quantitative value indicative of the degree of local and global functional connectivity. It was shown that the maximum and minimum occurring states have the potential to distinguish between population groups. Chapter 2 presented studies which reported anomalies and disruptions in the connectivity structure of pathological patients (Simmons et al. (2009), Kleinhans et al. (2008)). It also reports how brain networks are correlated to behavioural traits portrayed by humans (Sala-Llonch et al. (2012)). Based on these reports one can assume that the functional connectivity networks from specific populations or a general population would be embedded with distinctive information about their individual patterns of brain response to stimuli. With this assumption, in this chapter the network properties of the maximum and minimum occurring states is used and applied to solve two distinct problems. First, to distinguish subjects from two pathologically different population in a classification problem and next try use the graph theory measures to develop a generalised model which can characterise negative affectivity behavioural traits in children.

7.1 Classification of Autism Spectrum Disorder using Brain Connectivity Measures Extracted from Synchrostates

Data from the high-density EEG study conducted on 12 children with ASD and 12 healthy controls described in Section 4.1 was used for the current experiment. The purpose of the current experiment is to show that brain network parameters derived from the synchrostates of EEG acquired while the children were performing a face perception task can effectively classify ASD and typical children. The xperimental paradigm which yields the most distinguishable result in terms of the nature of face stimuli i.e. fear, happy and neutral is also explores. Additionally, the best obtained brain network measures or features and the role of minimum and maximum occurring synchrostates for discriminating ASD and healthy subjects with relatively less complex classifier and kernels have been investigated.

For obtaining the synchrostates and the subsequent brain connectivity metrics, the following steps are carried out: 1) apply CWT to produce the time varying phase information amongst the EEG electrodes, 2) cluster the characteristic phase difference patterns and use the synchronisation index to quantify the temporal stability of each synchrostate, and then 3) translate the unique clusters into a complex brain network using a graph theoretic approach and 4) derive quantitative measures for each connectivity map. Researchers have argued that gamma-band (30 Hz and above) synchronisation is the key process that reflects underlying cortical computations (Fries (2009)). Thus here the gamma band phase synchronisation is computed from synchrostates to characterise the underlying connections that are formed in the autistic and the typical brain during the execution of the face perception task.

7.1.1 Feature selection

The global synchronisation matrix derived from synchrostates (6.1) is translated into a complex network that is useful to shed light on the phase synchrony amongst different regions and hence describe the nature of the functional network configuration of the brain. The brain connectivity map is configured by considering the EEG electrodes as nodes and the synchronisation values between them as the weighted edges i.e. connection strength between the nodes. The appropriate graph metrics when studied can facilitate the interpretation of the topological properties and intrinsic meaning of the functional brain networks. The two types of generic measures that are most relevant in this particular study for understanding the autistic and typical brains capability for information processing are segregation and integration. Measures of segregation in a brain network account for the ability of segregated specialised neural processing within highly connected brain regions. It has been used as the means to evaluate the local connectivity (Rubinov and Sporns (2011)). The common measures of integration are

capable of capturing the capacity of global interaction in a network and estimate the ease of networkwide communication (Sporns (2011)). The chosen features have been listed in Table 7.1 along with the physical network attributes they portray.

Table 7.1: Different features of the brain connectivity graphs used for classification

Name	**Physical significance**
Modularity	Measure of segregation. Quantifies the degree to which a network can be subdivided into a group of nodes with small number of between group links (edges) and large number of within group links (Rubinov and Sporns (2011))
Transitivity	It is the ratio of the triangle to triplets of the network. Is a measure of segregation in complex network analysis (Strogatz (2001)).
Characteristic path length	It is essentially the global mean of the distance matrix i.e. the average of the shortest path length between a node and all other nodes (Watts and Strogatz (1998)). It is a measure of network integration.
Global efficiency	A measure of integration, that is the calculated by averaging the inverse of the distance matrix (Sporns (2012))
Radius	Radius is derived from a networks eccentricity (e_i^w) which refers to the minimum value of each row of the Hadamard (dot) product of d_{ij}^w
Diameter	Diameter is the maximum value of eccentricity (e_i^w)

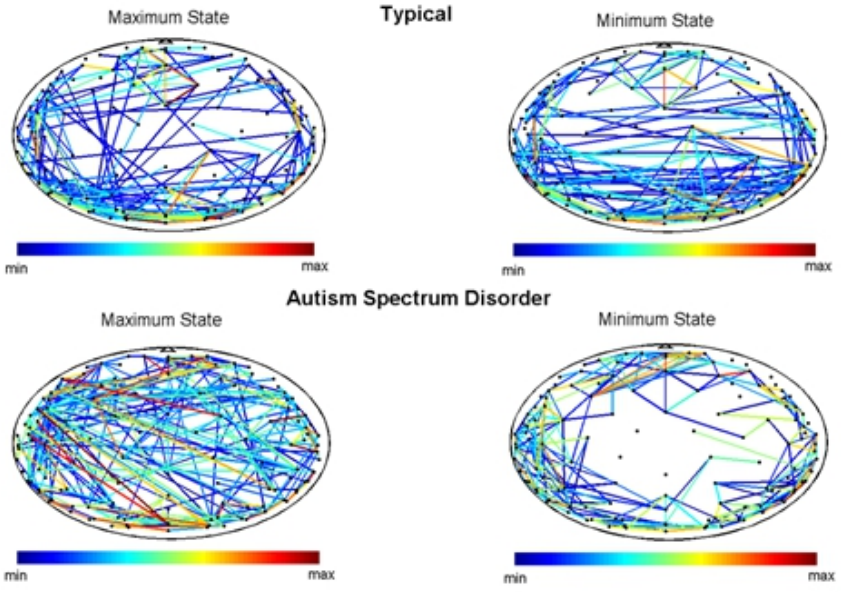

Figure 7.1: Brain connectivity for a typical and an ASD child. The max and min values of the colour bar represent the maximum and minimum values of the 7% highly connected edges respectively

These features were generated by averaging the phase response of the CWT across all channels for each individual over all trials corresponding to a single stimulus and carrying out the synchrostate analysis. From the resulting synchrostate sequence of each child the complex network parameters of the connectivity network are computed from the functional connectivity graphs of the maximum and minimum occurring states. The maximum and minimum states are utilised since previous study of synchrostates in autistic population in the results from Section 6.3.4 showed distinguishing properties in graph metrics derived from these states. The phase-locked matrices obtained from clustering, the maximum and minimum occurring synchrostates can be converted to analogous undirected graphs using the synchronisation index in (6.1). In the undirected brain network, each edge represents the value of the synchronisation index as the coupling strength between two electrodes and has been represented in Figure 7.1 for a typical and ASD child.

There is an observable difference between the maps for the typical and ASD child across both the maximum and minimum state. The max state of the autistic child shows a general spread of connections across all electrodes indicating higher global connectivity. Although the typical child's maximum map has long range connections they are restricted to certain regions (parietal) on the scalp. In contrast the minimum state for the autistic child has more modular connections with more small range connections compared to the typical child's map. These observable differences are quantified using the graph theoretic measures reported in Table 7.1. Figure 7.2 shows a flowchart for the whole process of deriving synchrostates from the EEG signals and subsequently obtaining the corresponding brain connectivity measures.

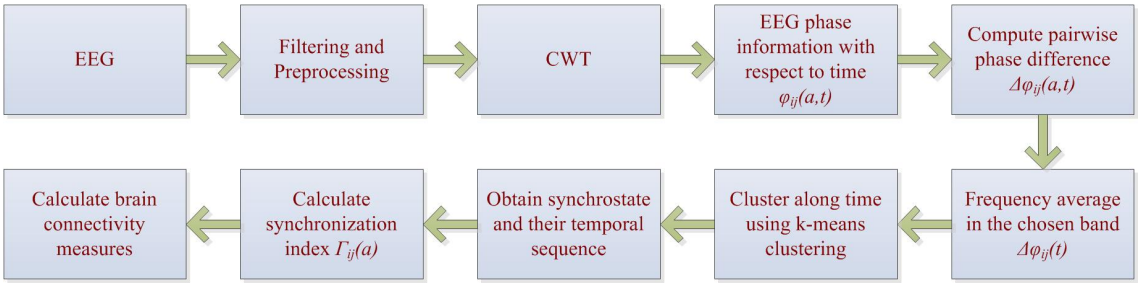

Figure 7.2: The processes involved in deriving synchrostates and brain connectivity measures.

7.1.2 Description of the classification techniques

Since the features have been extracted from a population of healthy and autistic children the problem is a binary classification task where the aim is to classify autism given the network measures of EEG phase synchronised states. The aim of this exploration is to find the optimal feature pool and classifier that can best distinguish between the two classes of subjects. Given this goal, the choice of the classifier is crucial for obtaining

consistent classification results. The use of probabilistic classification approaches in the present context is not suitable due to the limited number of subjects, as it is not reliable to construct multi-dimensional probability densities functions (pdfs) from the features for Bayesian classifier and even one dimensional pdf for each feature in Naïve Bayes classifier (Rogers and Girolami (2011)). Whereas, non-probabilistic classification techniques like discriminant analysis and SVM (Support Vector Machine) with polynomial kernels which map the feature vectors to a higher dimensional space in order to separate the classes using a linear separation boundary or hyper-plane can be used. However, their performance varies significantly depending on the assumption they make about utilising all the data-points or the marginal data-points from the two classes while adapting the classifiers weights in the training phase. Discriminant analysis gives emphasis to all the data points of the two classes to determine the weights of the classifier, thus is prone to get affected by outliers. In contrast SVM is based on the principle of maximizing the margin between the critical points (support vectors) of the classes.

7.1.3 Discriminant analysis based classifiers

The LDA classifier separates two classes using a linear decision boundary in the multi-dimensional feature space. The linear discriminant function is given by equation(7.1).

$$y = \sum_{i=1}^{N} x_i w_i + b = \sum_{i=1}^{N+1} x_i w_i = Xw \tag{7.1}$$

where, y is the predicted class label ($y \in [-1, 1]$), N is the number of features, x_i is the i^{th} feature, w_i are the weights and b is the bias. Given an N dimensional input, the corresponding decision boundary is given by a $(N-1)$ dimensional hyper-plane. If y is greater than zero the object is assigned to one class and if is less than zero the input is assigned to the other class. A least squared estimation (LSE) based approach is commonly used to train the classifiers weight w where the squared error of the predicted class and actual class is minimized. The classifier's optimum weight w_{opt} is obtained in the form of pseudo-inverse of the input features X, multiplied by the class information vector y.

$$w_{opt} = \left(X^T X\right)^{-1} X^T y \tag{7.2}$$

LDA (Linear Discriminant Analysis) classifier performs well in data that is linearly separable. In practice especially in biomedical applications, more complex decision boundaries may be necessary. The use of higher order kernels is one way to circumvent this problem. Polynomial kernels transform feature vectors to a higher dimensional feature space. According to Covers theorem any data-set can be made linearly separable in some higher dimensional space, if the order of the kernel is gradually increased (Semmlow (2009)).The higher dimensional feature space can be created by performing nonlinear transformation on the input feature using a kernel function $k(x_i)$. For an example a

polynomial kernel of order two (also known as Quadratic Discriminant analysis, in short QDA) produces a higher dimensional space with the original features plus their cross products. In the case of a two dimensional feature space with two-variable, x_1 and x_2, the quadratic kernel transforms the space into a 5-dimensional space with the variables $\left\{x_1, x_2, x_1x_2, x_1^2, x_2^2\right\}$. Although the higher order kernels effectively increases the number of features by taking their inner products and use their combinations to train the classifier, the same least square technique is employed for discriminant analysis. However this increases the computational complexity and is prone to over-fitting resulting in failure to generalise on a new data-set, unless a large number of data-points are used in the training phase.

7.1.4 Support vector machine (SVM)

Contrary to the least-square approach for training discriminant analysis based (LDA or QDA) classifiers which give emphasis to all the data-points in the training-set while constructing the decision boundary, the SVM give priority to the critical data points that lie closest to the decision boundary and data-points of the other class. These critical points are known as support vectors. The classifier that maximize the distance between these critical vectors or support vectors are known as SVM. This approach is more likely to give a better separation of data as the basis lies on maximizing the margin between the support vectors producing the optimum hyper-plane. When the data is linearly separable in the original feature space, standard SVM uses a linear decision boundary. However, it tries to find a boundary which maximizes the margin (M) which involves using an optimisation routine, with a constraint that all data points lie on the appropriate side of the hyper-plane. If the class labels are $y \in [-1, 1]$ the decision boundary can be defined in between i.e. y=0 following equation (7.3).

$$y = x_i w + b = 0 \tag{7.3}$$

Given the value of y at the support vectors must be ± 1, one gets $y_i\left(x_i w + b\right) \geq 1$, which means the optimisation algorithm should yield $\{w, b\}$ describing a hyper-plane in the feature space, such that the two classes fall on the appropriate side of the support vectors [42]. The margin can be derived as in (7.4).

$$M = \frac{(1-b)}{\|w\|} - \frac{(-1-b)}{\|w\|} = \frac{2}{\|w\|} \tag{7.4}$$

The margin M, i.e. the distance between the lines separating the two classes is maximized by minimizing $\|w\|$. The minimization is constrained by the equation to ensure the boundaries are on the accurate side and is done using sequential minimal optimisation (SMO), although the well-known quadratic programming (QP) can also be employed

for the same purpose. When the data is not linearly separable, linear SVM is not that effective. In such cases, the data can be transformed into a higher dimension space using the kernel methods described earlier in section 7.1.3. However this is computationally intensive and is prone to over-fitting similar to the use of kernels in discriminant analysis. Higher the order of the kernel, the more complicated the decision boundary becomes and the chance of over-fitting increases. Although these complex boundaries may perform well on the training data, most of the time they fail to generalise with increasing order of the kernel. This particular phenomenon is observed since the classifier becomes prone to capture small inconsistent patterns underlying the data-set.

7.1.5 Cross-validation scheme to avoid over-fitting of classifiers

A classifier should be able to generalise beyond the examples of the training set and the model should be able to make accurate predictions on unseen data. When the data available is small, in order to overcome the problem of over-fitting and reduce the sensitiveness to the choice of the training set a cross-validation technique allows more efficient use of the limited data. Given a data-set with N observations, in the Leave-One-Out Cross Validation (LOOCV), each observation of the data is held out in turn for validating the model which is trained on the remaining $(N-1)$ number of data-points. Averaging over the resulting accuracies of time independent runs of the classifier training, gives the final average classifier accuracy. This ensures that all the test labels are shuffled and results in the best average estimate of the classifier accuracy. The LOOCV does not suffer from the problem of labelling which all other N-fold cross validation schemes possess. Since the LOOCV is the most extreme case of N-fold cross validation with N set to the number of data-points available, the chance of introducing an undesired bias is minimum (Molinaro et al. (2005)). Although the LOOCV is known to be computationally heavier than the N-fold cross validation scheme, for relatively manageable length of data-set it is preferred over the others. The use of the commonly used 10-fold cross-validation was restricted in this exploration by the limited number of subjects.

7.1.6 Preprocessing of Features, Feature Ranking and Classification Performance Measures

In the machine learning literature (Theodoridis et al. (2010)), there are two different paradigms of feature selection viz. scalar feature selection and feature vector selection. The scalar feature selection is independent of the classifier where the features are ranked using a score like Fisher's Discriminant Ratio (FDR) etc. For feature vector selection there are several suboptimal search techniques e.g. sequential forward search (SFS) and sequential backward search (SBS). Using a class separability criterion (like FDR) the

poorly ranked features can be eliminated one by one or the best ranked features can be added to the feature subset to check a particular classifier's performance. Compared to the exhaustive search method, the suboptimal search techniques like FDR based feature ranking and grouping and adopting the SFS using these groups, is computationally less expensive. There could be several other possibilities of optimal feature selection considering dependency of the features, but the ultimate goal is to get a reliable and good classification. Normalising the features can remove bias from features having high value when training the classifier. Normalisation scales the feature vector so that they are within the maximum (x_{max}) and minimum (x_{min}) value.

$$x_{norm} = \frac{x - x_{\min}}{x_{\max} - x_{\min}} \tag{7.5}$$

The FDR is an efficient measure that allows finding the discriminating power of a feature and helps in dimension reduction. The larger the squared difference of the means of the features along with a small within-class variance, the better discriminating power the feature has. The features with higher FDR will have higher ranking implying they are compact and located distantly. The FDR of a feature is calculated using the mean and variance of individual classes i.e. $\{\mu_1, \mu_2\}$ and $\left\{\sigma_1^2, \sigma_2^2\right\}$ as (7.6).

$$FDR = \frac{\left(\mu_1 - \mu_2\right)^2}{\left(\sigma_1^2 + \sigma_2^2\right)} \tag{7.6}$$

The classifiers performance is assessed using the conventional measures sensitivity, specificity and accuracy. Typically the diseased class or abnormal condition is called, positive (P) and the typical or normal class as negative (N). The correct detection or true classification of abnormal conditions is known as true positive (TP). Likewise correct classification of typical population is true negative (TN). An incorrect classification can be of two types: classifying diseased as typical i.e. false negative (FN) and classifying typical as diseased i.e. false positive (FP).Sensitivity and specificity are also known as true positive rate (TPR) and true negative rate (TNR). These measures along with accuracy rate (ACC) are given by equation (7.7).

$$\begin{aligned}
&\text{Sensitivity or TPR} = \tfrac{\text{TP}}{\text{TP+FN}} \times 100\% = \tfrac{\text{TP}}{\text{P}} \times 100\% \\
&\text{Specificity or TNR} = \tfrac{\text{TN}}{\text{TN+FP}} \times 100\% = \tfrac{\text{TN}}{\text{N}} \times 100\% \\
&\text{Accuracy or ACC} = \tfrac{\text{TP+TN}}{\text{TP+TN+FP+FN}} \times 100\% = \tfrac{\text{TP+TN}}{\text{P+N}} \times 100\%
\end{aligned} \tag{7.7}$$

7.1.7 Results

One of the aims of this study is to find the optimal pool of features that can best distinguish the two classes of subjects. Collectively the data generates 36 features from the six network parameters ($N_{parameter} = 6$) i.e. corresponding to three stimuli (fear,

happy and neutral i.e. $N_{stimuli} = 3$) with maximum and minimum occurring state ($N_{state} = 2$). As a result, their combination has yielded $N_{parameter} \times N_{stimuli} \times N_{state} = 36$ possible set of features for classification of the ASD from typical. Therefore, it might be interesting to look at which network parameter (in Table 1) or state (among max or min) or their combination has the best discriminating capability. Also, from the better discrimination point of view of ASD, the preference of the nature of stimuli (happy, angry and fearful face) can be analysed from the FDR rankings.

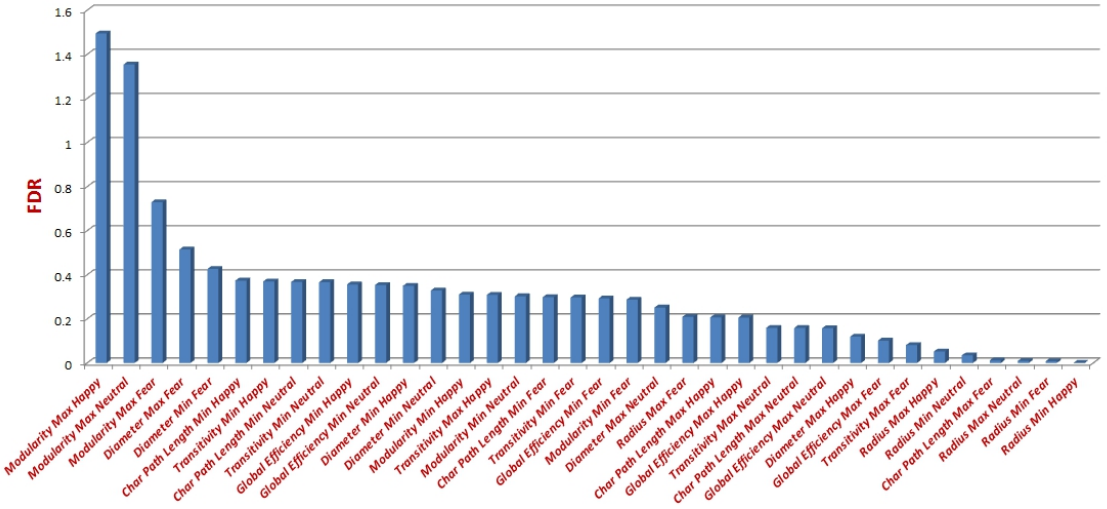

Figure 7.3: FDR ranking of different features for case-1 (all features).

Table 7.2: Different cases for classification considering max/min states, 6 network parameters and 3 stimuli

Case number	Feature Combinations	Number of features
Case1	All max and min state features for all 3 stimuli	36
Case2	All max state features for all 3 stimuli	18
Case3	All min state features for all 3 stimuli	18
Case4	Transitivity for all 3 stimuli	6
Case5	Modularity for all 3 stimuli	6
Case6	Characteristic path length for all 3 stimuli	6
Case7	Global efficiency for all 3 stimuli	6
Case8	Diameter for all 3 stimuli	6
Case9	Radius for all 3 stimuli	6

The whole 36 feature set was broken down into nine different cases as shown in Table 7.2 so as to determine the feature set that is most effective in classifying the data. In the first case (case-1) all the 36 features resulting from the combination of all the six network parameters corresponding to the maximum and minimum states for all the stimuli are used. This case allows us to find the best combination of network parameter, stimulus and max/min state which has the best discriminating power. For case-2 and case-3, only the features from the max states and min states were chosen respectively. From the

results of case-2 and case-3 one may conclude which of the max state features or min state features are more efficient and even which state among the max/min is most effective in the current classification problem among the available $N_{parameter} \times N_{stimuli} = 18$ features in each case. For exploring the discriminative nature of the features (in each of the three cases 1-3) to separate the typical and autistic subjects, FDR is used to assign a ranking according to their decreasing order of importance. The FDR ranking and the values are shown in Figure 7.3-Figure 7.5 for the three cases respectively where the x-axis denotes the considered features and the relative weightage (FDR) is plotted in the y-axis. The ranked features are plotted in Figure 7.6 with decreasing order of importance using the FDR criterion. From Figure 7.6 it is evident that there exist four feature groups for case-1 to case-2 and three feature groups for case-3 where the features contained in one group have closer class-discrimination capability i.e. projections on y-axis are closer for the features in a single group. In case-1, the first group consists of top two features and next groups with three, four and 36 features respectively. In case-2, the four groups have top 2, 4, 7 and 18 respectively. In the case of all minimum-state features (case-3) the three groups have the top 7, then top 15 and then all 18 features as evident from Figure 7.6. Classification performance using LOOCV and different classifiers with these groups of FDR based ranking are compared next.

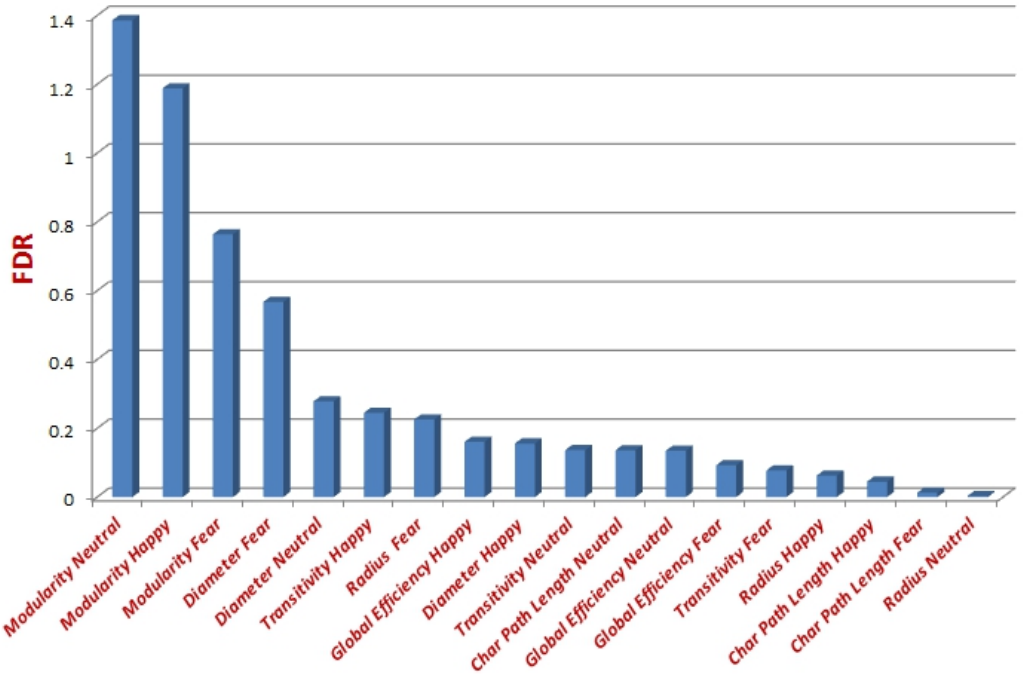

Figure 7.4: FDR ranking of different features for case-2 (max-state features).

The LOOCV classification performance for case-1 i.e. the entire feature set is shown in Figure 7.7. It shows that for the discriminant analysis increasing the number of features reduce the accuracy rate. This is in conjunction with the intuition that more features trained will cause over-fitting. When SVM was run on the data, it can be noticed

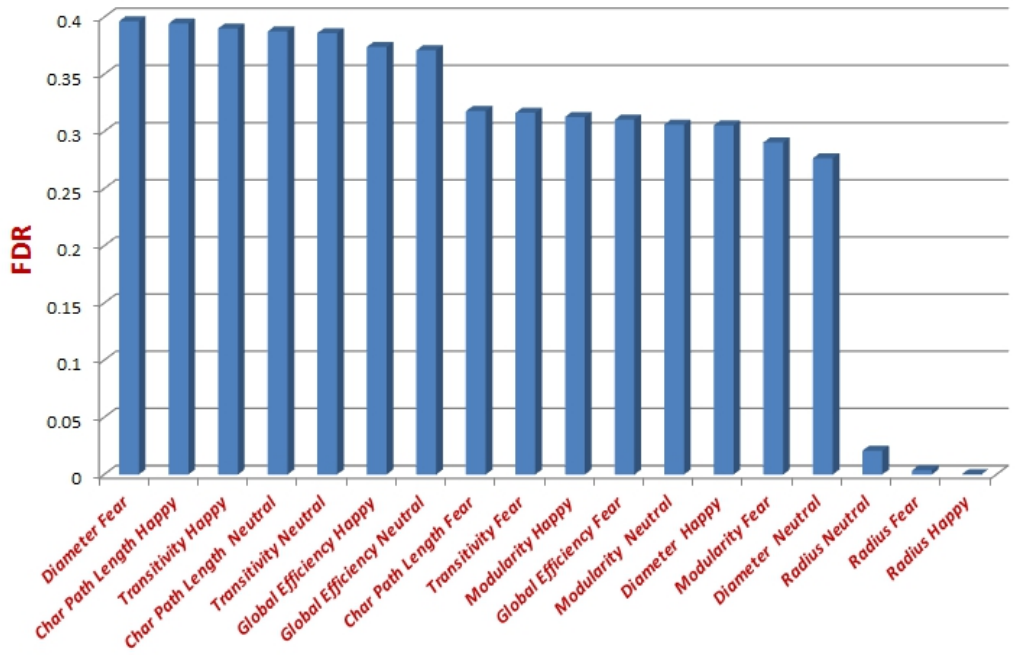

Figure 7.5: FDR ranking of different features for case-3 (min-state features).

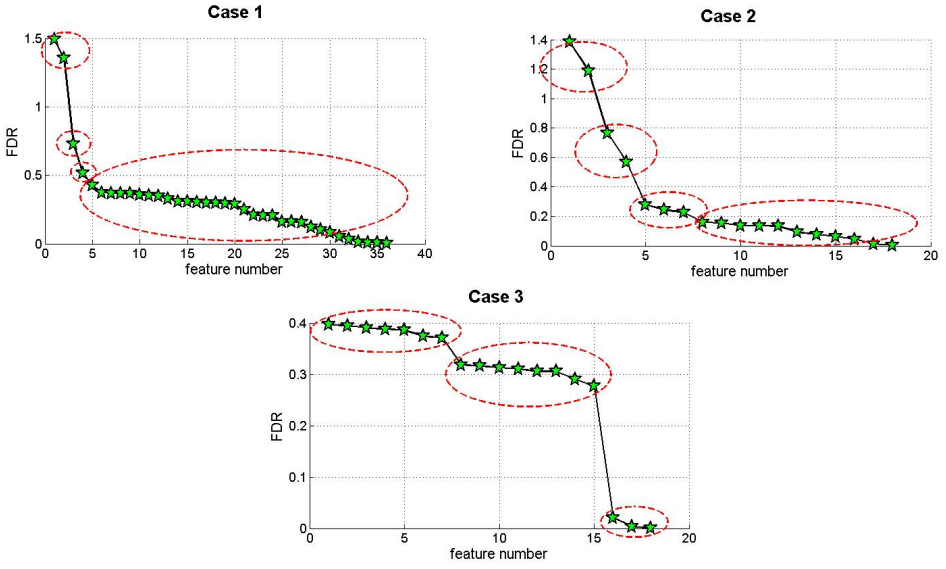

Figure 7.6: FDR based feature grouping for cases-1 to case-3. The dotted red lines indicate the grouping of features.

that beyond SVM kernel order-2, the performance and the generalising capability of the classifier reduces. The best accuracy for case-1 is 94.7% (with 85.7% sensitivity and 100% specificity) when the top 4 features are used to train an SVM classifier with a second order polynomial kernel. The top four features are the modularity values of the maximum states of all the three stimuli and the maximum state diameter for fearful face stimulus. This result is in agreement with the findings from section 6.3.4 where the modularity of synchrostates can distinguish between autistic and non-autistic classes.

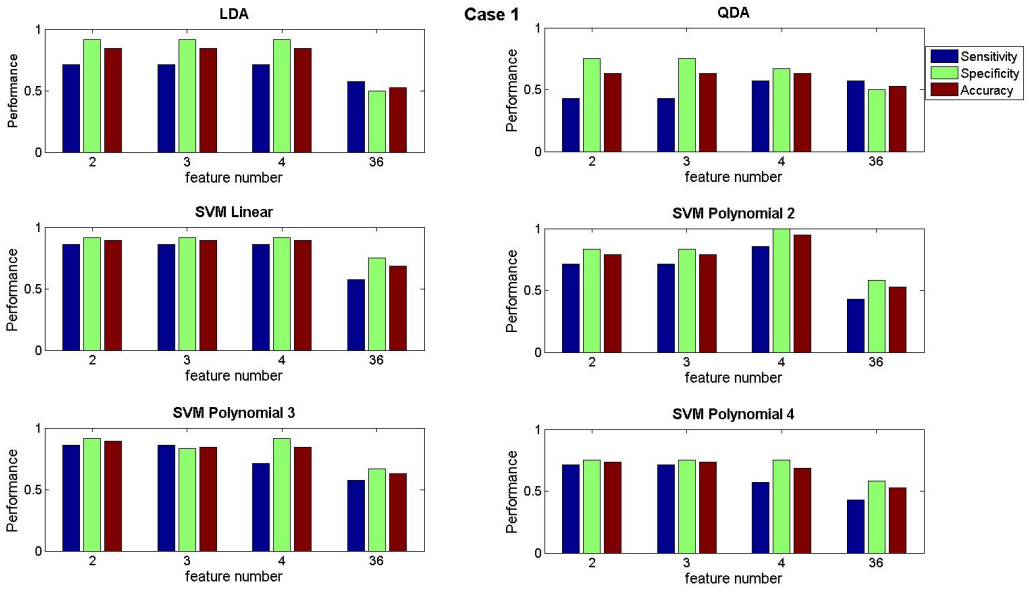

Figure 7.7: Performance of different classifiers with different group of features for case-1.

In case-2, only uses the maximum state features for all three stimuli for classification. As can be seen from Figure 7.8 the overall performance of QDA is poor compared to LDA. However when SVM is applied with a linear and 2nd order polynomial kernel the results are significantly better when compared to the discriminant analysis. Thus giving priority to the support vectors allows enhanced class separation. In this scenario, the highest accuracy value achieved is 94.7% (with 85.7% sensitivity and 100% specificity) which is the same for case-1 and so is the classifier configuration. The top four feature group contains the same features as of case-1.

In case-3 shown in Figure 7.9, the overall accuracy levels are lower than compared to case-1 and case-2. The highest accuracy value achieved is 84.2% (with 85.7% sensitivity and 83.3% specificity). This is accomplished by applying SVM on the dataset in three cases i.e. with a linear kernel with top 7 features, with 2nd order kernel on the top 7 features and a linear kernel with top 15 features. The configuration which has the least computational complexity is the linear SVM training with 7 features. Comparing this case with the previous two cases, one may conclude that the minimum state values are not as effective in differentiating between the two groups as the maximum state. There is also a disadvantage since more (seven) features need to be used to achieve this result in contrast to case-1 and case-2 where better accuracy can be achieved by using only 4 features.

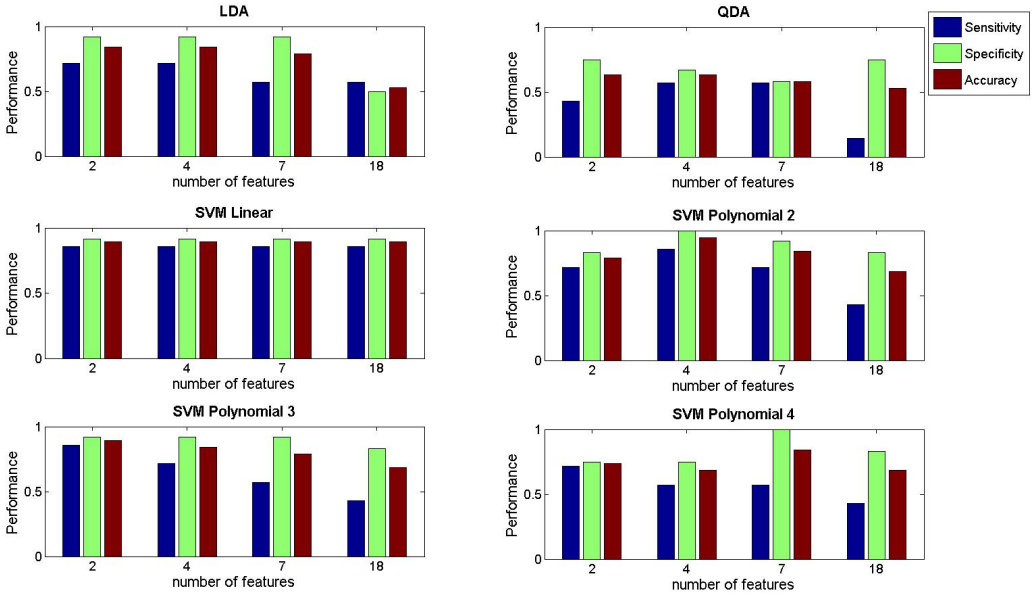

Figure 7.8: Performance of different classifiers with different group of features for case-2.

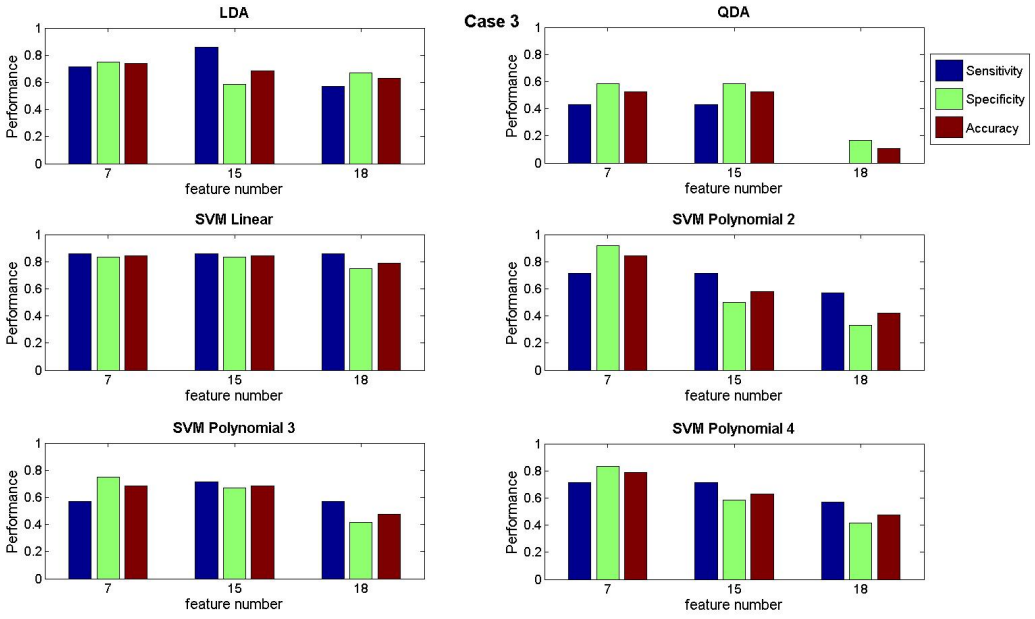

Figure 7.9: Performance of different classifiers with different group of features for case-3.

The above case scenarios allowed us to factor out which combinations from the pool of features perform the best. It also gives an idea about the best classifier-setting that learns the dataset most effectively. The same principle is applied again but this time, to find out which of the complex network parameters have the best discriminating power. Six cases are designed with the maximum and minimum state values of the individual brain-network measures in Table 7.1 for all of the three stimuli. Hence each case has six features i.e. max/min state features for three stimuli for each choice of network

Table 7.3: FDR based feature ranking for different network measures (case-4 to case-9)

Rank	Transitivity (case 4)		Modularity (case 5)		Characteristic Path Length (case 6)		Global Efficiency (case 7)		Diameter (case 8)		Radius (case 9)	
	FDR	Description	FDR	Description	FDR	Description	FDR	Description	FDR	Description	FDR	Description
1	0.390	Min Happy	1.386	Max Neutral	0.394	Max Happy	0.374	Min Happy	0.567	Max Fear	0.226	Max Fear
2	0.386	Min Neutral	1.188	Max Happy	0.388	Min Neutral	0.371	Min Neutral	0.396	Min Fear	0.062	Max Happy
3	0.316	Min Fear	0.764	Max Fear	0.318	Min Fear	0.310	Min Fear	0.305	Min Happy	0.021	Min Neutral
4	0.245	Max Happy	0.313	Man Happy	0.136	Max Neutral	0.160	Max Happy	0.278	Max Neutral	3.63×10^{-3}	Min Fear
5	0.136	Max Neutrxl	0.306	Min Neutral	0.045	Max Happy	0.135	Max Neural	0.277	Min Neutral	3.53×10^{-3}	Max Neutral
6	0.078	Max Fear	0.290	Min Fear	0.013	Max Fear	0.092	Max Fear	0.156	Max Happy	7.16×10^{-5}	Min Happy

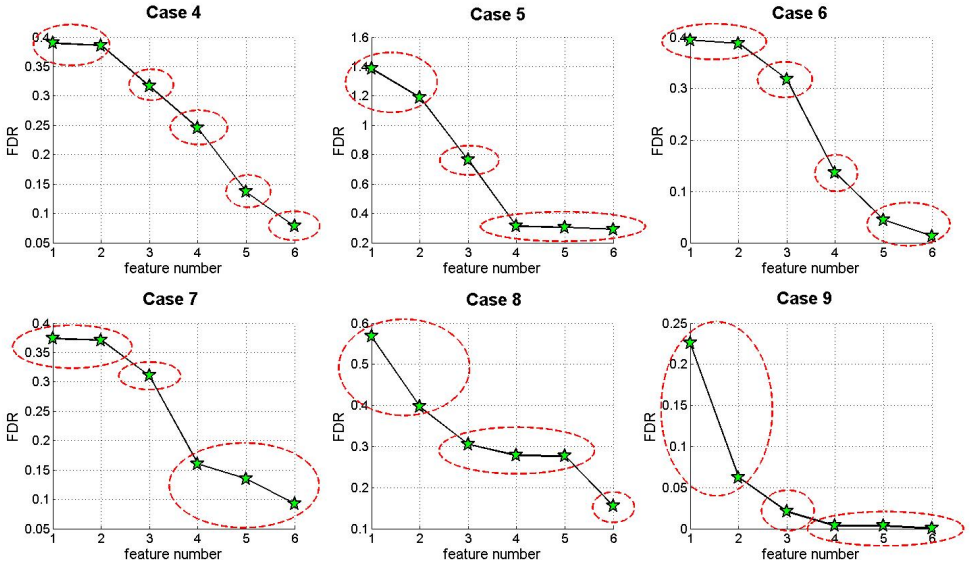

Figure 7.10: FDR based feature grouping for cases-4 to case-9. The dotted red lines indicate the grouping of features.

parameters like transitivity, modularity, characteristic path length, global efficiency, diameter and radius. This will reveal the discerning capability of each of the complex network measures for three different stimuli i.e. happy, angry and fearful face. Each of the cases (from case-4 to case-9) has a pool of six features (i.e. $N_{stimuli} \times N_{state} = 6$) which represent the network metrics. In every case the FDR value was used to designate a rank to the feature in decreasing order of importance. The FDR value projection on the y-axis against the ranking number was used to group the features with the most discriminating power into one and so on. The FDR based feature grouping for the case-4 to case-9 has been elucidated in Table 7.3 and Figure 7.10. Although there are several algorithms available in the machine learning community for effective selection of least correlated features like scalar feature selection, sequential forward and backward selection etc., this study is restricted to the FDR based feature grouping only, as it is a much simpler concept and easy to understand and implement. In fact, increasing the number of features using closely spaced FDR groups instead of individually adding them in the feature pool is quite similar to the concept of sequential forward feature selection method.

Case-4 used all the transitivity values for the maximum and minimum occurring states of all stimuli. Overall the discriminant analysis classifiers achieve poor results compared to SVM. When using SVMs it is noticeable that using more number of features is favorable in this case and yields better accuracy as evident in Figure 7.11. A top accuracy value of 89.5% (with 85.7% sensitivity and 91.7% specificity) is attained with a linear and 3rd order kernel of SVM using the top five features, without considering the maximum transitivity of fear (the lowest ranked feature). Training all six features with linear SVM

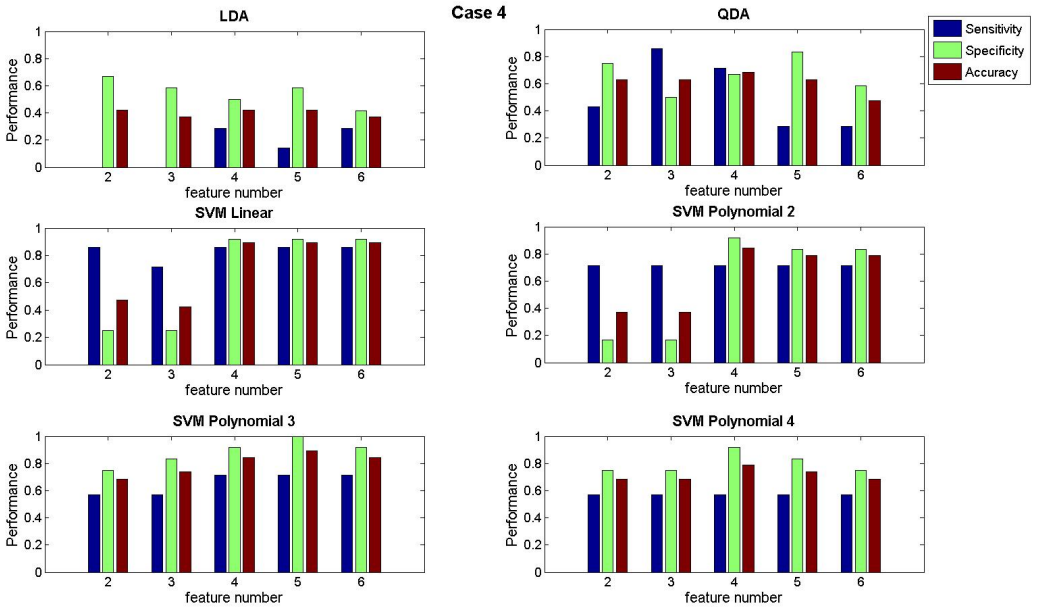

Figure 7.11: Performance of different classifiers with different group of features for case-4.

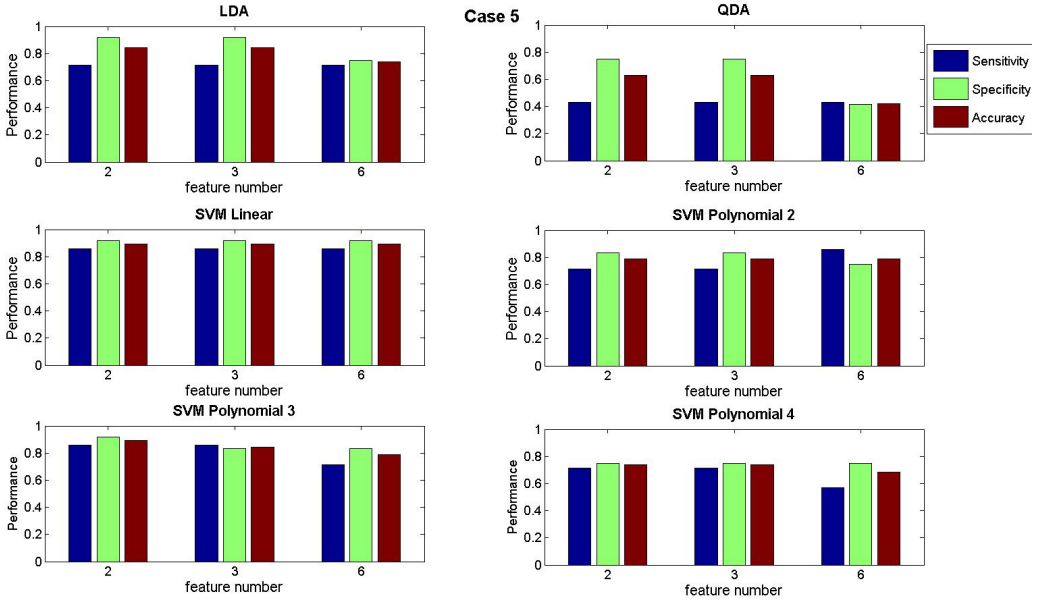

Figure 7.12: Performance of different classifiers with different group of features for case-5.

also gives an accuracy of 89.5%. However, training the SVM using five features and a linear kernel will be most efficient due to less number of features.

In case-5 where all the modularity values were considered, similar grouping results is observed with that of case-1 and case-2. The maximum modularity values are grouped as top 2 and top 3, whereas the modularity values for minimum state are grouped as least discriminant among all six features. The SVM classifiers have almost similar

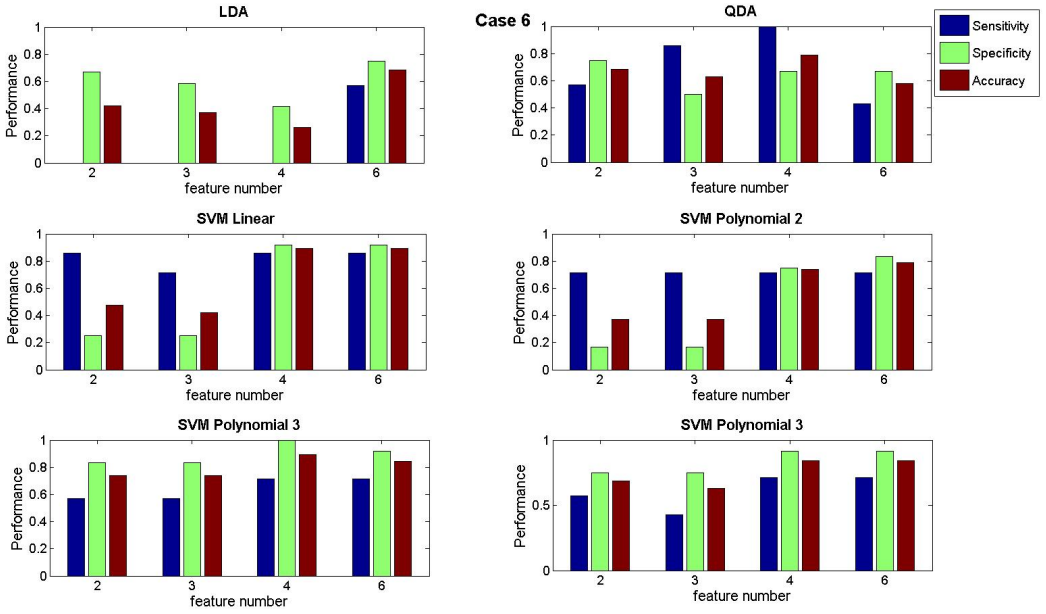

Figure 7.13: Performance of different classifiers with different group of features for case-6.

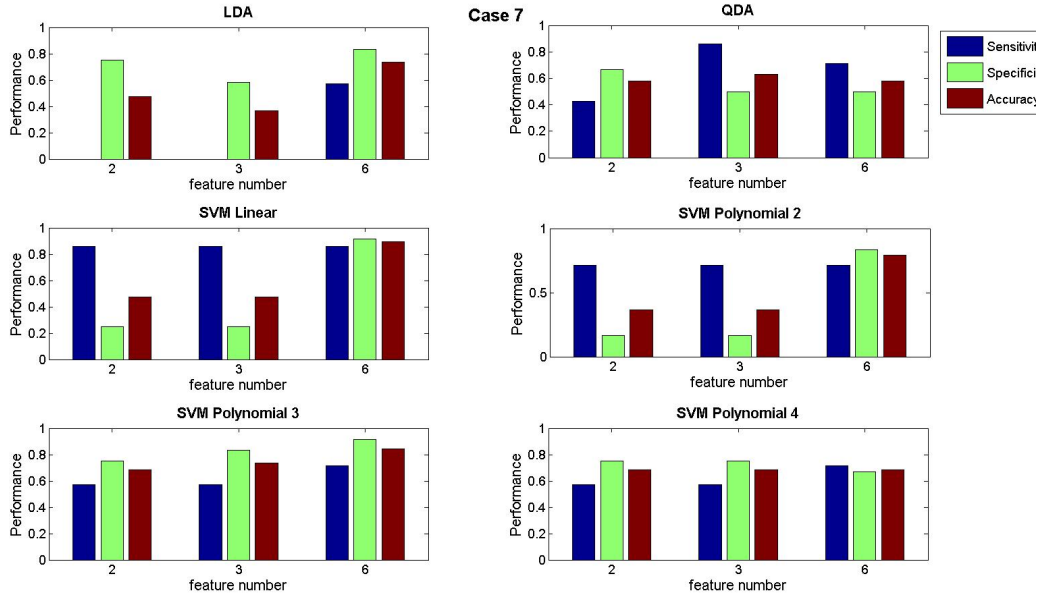

Figure 7.14: Performance of different classifiers with different group of features for case-7.

performance for different group of features while having the best accuracy for top two or top three features. Using all six features reduces the accuracy as it over-fits the data. Another interesting observation is increasing the SVM kernel order leads to poor performance as can be seen from Figure 7.12. From the SVM linear kernel plot, it is observed, that accuracy reaches its maximum value of 89.5% (with 85.7% sensitivity and 91.7% specificity) for all feature groups. Increasing the number of features in this case

is not improving the performance of the classifier. The maximum state modularity of the neutral and happy face stimuli when trained with a linear SVM is most effective in this scenario.

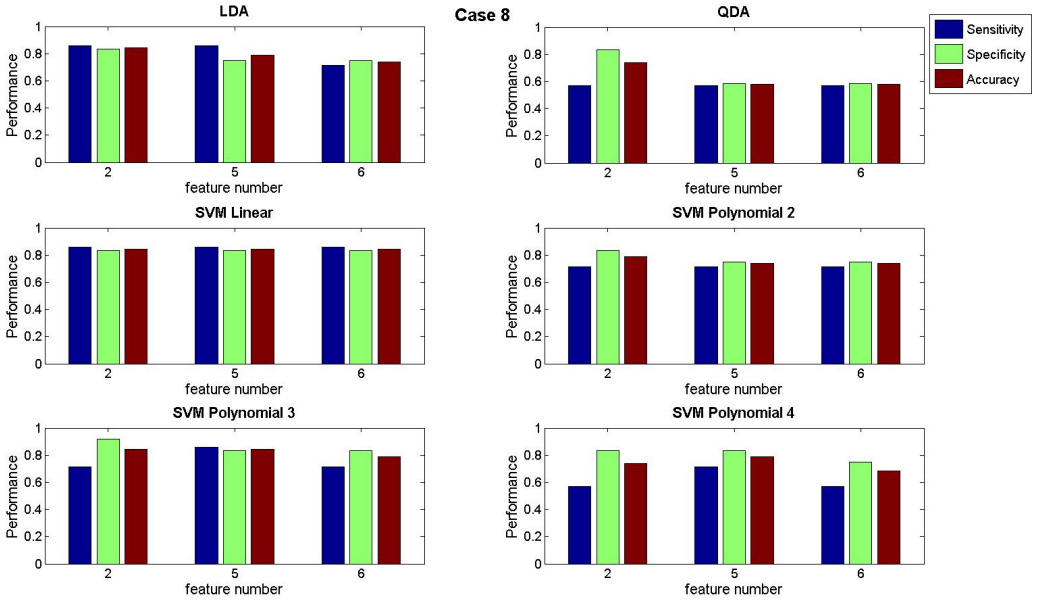

Figure 7.15: Performance of different classifiers with different group of features for case-8.

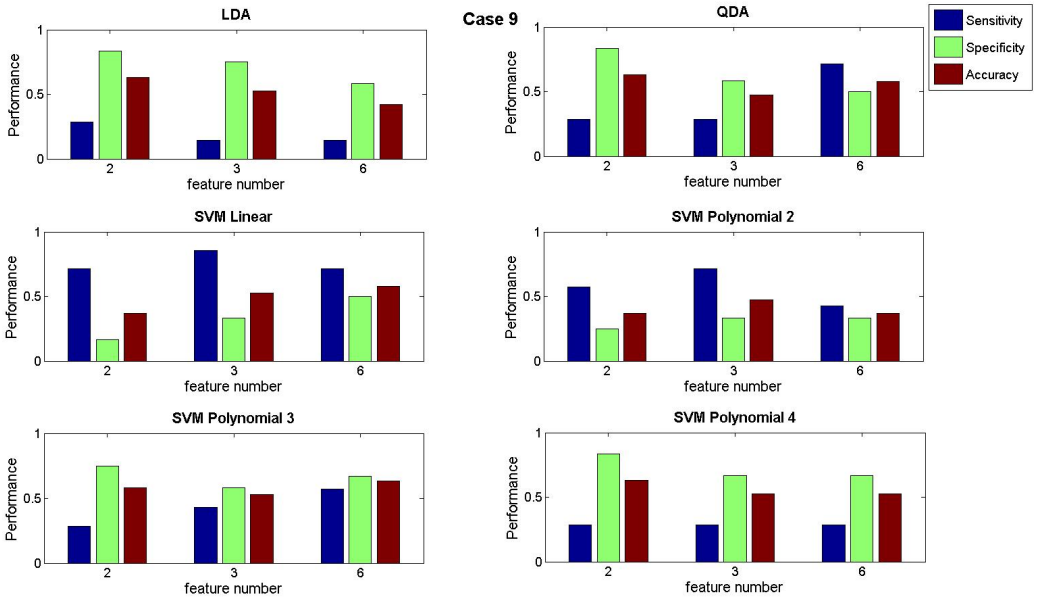

Figure 7.16: Performance of different classifiers with different group of features for case-9.

The classification results when considering only the characteristic path lengths (case-6) for all the three stimuli are given in Figure 7.13. The discriminant analysis techniques give poor performance for the characteristic path length features. In this case using

more features increases the accuracy and the overall performance. This could be due to the quality of the feature. The classifier that achieves the best result is the linear SVM when applied to learn all six or top four features; however the latter requires less computational power. The best accuracy obtained was 89.5% (with 85.7% sensitivity and 91.7% specificity). The overall performance of global efficiency features (case-7) is quite modest as shown in Figure 7.14. The accuracy levels with top 2 and 3 features are low for most of the classifiers. Using all features increases the accuracy with a maximum value of 89.5% (with 85.7% sensitivity and 91.7% specificity) when the linear SVM is trained using all the six features.

In case-8 all the diameter metrics are used as the features for classification. From the FDR plots the features are grouped as top 2, 5 and 6. Here the performance of LDA and linear SVM is comparable as shown in Figure 7.15. The best accuracy of 84.2% (with 85.7% sensitivity and 83.3% specificity) can be achieved by training the classifier with top 2 features with LDA and linear SVM. Using the top five features to train SVM with linear and 3rd order polynomial also yields the same results. However LDA is much less complex than SVM training.

The overall performance of the network metric radius (case-9) is the worst among all the other complex network measures which is depicted in Figure 7.16. It can be concluded that this has the least discerning power for the current classification problem. None of the classifiers accuracy in this case is satisfactory. The highest achievable accuracy of 63.2% (with 57.1% sensitivity and 66.6% specificity) is obtained using SVM with a 3rd order polynomial kernel and all the features. This summarises the exhaustive classification results of ASD vs. typical children with 6 network measures, two states and three stimuli while highlighting the best achievable accuracy with a particular classifier setting amongst the discriminant analysis and support vector family.

7.1.8 Summary and Discussion

The purpose of this study was to explore the possibility of using brain connectivity parameters derived from synchrostates to classify autistic and typical children. The aim was also extended to determine which facial stimuli and complex network parameters yielded the best classification results with the least complex classifier. The summary of the key findings of the present work for detection of ASD from graph theoretic measures from multi-channel EEG are as follow:

- The phase synchronisation patterns or synchrostates in multi-channel EEG has been investigated in autistic and typical children during a face perception task. The complex brain network parameters have been extracted from the functional connectivity graphs of maximum and minimum occurring synchrostates which have been further used to classify an autistic group from the typical with an accuracy

rate of 94.7% with corresponding sensitivity and specificity values of 85.7% and 100%.

- From the comprehensive study one can see that in most cases, considering more features during the training phase causes the gross accuracy to fall (Rapp et al. (2013)). Also, the increase in complexity of the kernel does not always enhance the performance of the classifier due to over-fitting of the underlying inconsistent patterns.
- As a whole the maximum occurring state metrics have better discriminating capability than the minimum occurring state metrics.
- The best features to use for the classification of autistic children from normal ones is the maximum state modularity values during fear, happy and neutral stimuli and maximum diameter during fear stimuli. These features when trained using a 2nd order polynomial kernel with SVM produces the best overall accuracy.
- The best graph metrics for classification are neutral and happy stimuli maximum state modularity.

It is well-known that Autism is a broad spectrum of disorders and a simple binary test may not be sufficient to make clinical decisions about the presence of autism. Although the classification results shown in the current work is promising it is to be noted that a more rigorous prospective study with a large cohort of patients may be required to unequivocally eliminate the possible effects of misclassification and to establish the clinical validity of the technique before the methodology is put into clinical practice. However, any EEG based evaluation method that can make a distinction between the two populations will be able to facilitate the clinicians in their behavioural assessment and prognosis. The synchrostates and the corresponding network measures effectively characterise the underlying functional brain connectivity of the subjects and hence may possess some signature of the particular characteristics of the ASD children. In order to obtain markers for the detection of ASD from the observation of EEG, the present work can be considered as the first step where small number of brain network measures can discriminate between the ASD and healthy subjects. The synchrostates might represent only a single biomarker of a very complex and heterogeneous spectrum of conditions such as ASD that require more complex clinical and neurobiological evaluation. The perspective of using synchrostates as one of the many tools used for the diagnosis of ASD is promising, but it needs further evidence obtained on larger and additional series. However, the severity or degree of ASD can further be classified in future using a similar procedure while deriving network measures from EEG synchrostates especially from different subclasses of ASD patients. Further extension of the present work can be directed towards further classification of the degree of ASD as a multi-class classification problem by using some psychological or behavioural assessment score as a threshold or decision boundary between the degrees of severity of ASD.

7.1.9 Comparison of results with other classification studies

Apart from this study there have been a few attempts to detect or classify autism from EEG/MEG using machine learning algorithms. Bosl et al. (Bosl et al. (2011)) classified infants with high risk of autism vs. control group using SVM, k-nearest neighbors (k-NN) and Naïve Bayes classifiers. The study was based on modified multiscale entropy (mMSE) as feature for different age groups which resulted in an overall accuracy of 80%. Pollonini et al. (Pollonini et al. (2010)) used Granger causality of MEG signals to discriminate autistic and healthy population using graph theoretic measures as features and SVM classifier which resulted in 87.5% accuracy. Discriminant analysis and SVM based classifiers were adopted in Stahl et al. (Stahl et al. (2012)) using event related potential (ERP) data resulting in an accuracy of 64% for discriminating between groups of high risk and low risk of autism. Compared to the approaches mentioned above here the maximum and minimum occurring synchrostates are first extracted and the associated brain network parameters are obtained which are then fed into the discriminant and SVM classifiers to differentiate ASD and healthy subjects. In this study, the overall classification accuracy (94.7% with SVM and four network measures) outperformed that reported in the previous mentioned literatures. It has been reported that individuals with ASD have long range functional under-connectivity and they compensate for this trait by forming more dense local connections in the frontal and posterior brain regions (Kana et al. (2011)). Complex network measures such as modularity, transitivity, global efficiency and characteristic path length which have been used as features here, can effectively capture the integration (global connectivity) and segregation (local connectivity) ability of brain functional networks (Sporns (2011)). That is why the impact of these brain network measures is extensively investigated for potential classification between the ASD and typical cases.

7.2 Brain connectivity to characterise negative affectivity in children

Current methods of assessing anxiety in children and adolescents encompass a wide range of interview formats and behavioural screening tests. Many of these methods rely on parent-rated symptoms of child anxiety and researchers have questioned the extent to which adults are able to detect and accurately report internalising symptoms in children and adolescents (Choudhury et al. (2003)). Diagnostic accuracy and reliability of self-reported measures is also questioned and clinician administered formats are limited by difference in opinion and potential bias (Antony (2001)). More objective, psychophysiological measures, have the potential to supplement the existing conventional methods in providing a more accurate evaluation of anxiety symptoms in the general population. This approach, if further developed in clinical samples, can aid diagnostic accuracy of

anxiety disorders. The purpose of the current study is to develop a generalised model which can fit behaviour scores so as to facilitate the prediction of child's emotional traits directly from the brain connectivity measures extracted from EEG. A model such as the one proposed here may help supplement diagnostic decisions based on scores obtained from conventional methods of assessment of behaviour disorders including anxiety.

Recent research using structural and resting-state fMRI techniques has shown that childhood internalising symptoms (anxiety) are associated with increased connectivity between the amygdala and distributed brain systems involved in attention, emotion perception and regulation (Qin et al. (2014)). In addition, in the same study machine learning algorithms have shown that levels of childhood anxiety could be reliably predicted by amygdala morphometry and intrinsic functional connectivity at a surprisingly young age (Qin et al. (2014)). Similar research has shown that temperamental precursors of anxiety (shyness) were associated with structural and functional connectivity changes in cortical and limbic regions involved with processing socio-emotional stimuli in healthy adult individuals (Yang et al. (2013)). These findings have important implications for the development of predictive biomarkers to identify children at risk of anxiety related disorders. This study is based on the hypothesis that temperamental traits of internalising symptoms (i.e. sadness, anger, shyness, etc.) can be predicted by the functional brain network hence the connections made in the brain. Consequently here the aim is to model traits of negative affectivity in children based on the connectivity parameters in order to provide a more objective, less differential measure of child negative affectivity (sadness and anger) based on EEG signals.

Studies have shown correlation between functional connectivity and behavioural performance like reading ability in MRI signals of adults (Hampson et al. (2006)). Research has been conducted to show the role of EEG asymmetry on moderating temperamental negative reactivity in children (Henderson et al. (2001)). In healthy adults, fMRI findings suggest that the default mode network can predict inter-individual behavioural differences (Sala-Llonch et al. (2012)). It is suggested that the connectivity-behaviour relationship is rendered due to the employment of attentional and motivational links to a behavioural outcome. Research on externalising adolescent boys showed reduced effective connectivity (Shannon et al. (2009)). Recently behaviour has been positively linked to functional connectivity in aging adults in a DTI and fMRI study (Davis et al. (2011)). All these findings suggest that functional connectivity in the brain guides the internalising symptoms in human.

The aim was to develop a regression model and find a relationship between the EEG guided brain connectivity metrics with the standardised self-reported behavioural measures. The aim was to generate a model with low complexity, to avoid over-fitting of the data, but still equipped enough to predict the behavioural scores accurately. For this, generalised self-reported measures such as trait anxiety, depression, state anxiety,

anger, attention focusing, sadness, fear, temperamental shyness and emotionality scores from 20 children from the general population were used.

7.2.1 Behavioural measures

20 children aged between 6 -12 years were interviewed and asked to complete questionnaires to gauge their behavioural scores for the purpose of this study. Trait Anxiety and Depression scores were assigned by adding up the individual item scores of the self-reported anxiety and depression measures from the DOMINIC, a DSM- IV based pictorial interview (Valla et al. (2000)). State anxiety scores were derived by summing the scores of the individual items using the State Trait Anxiety Inventory for Children (STAIC) (Spielberger et al. (1970)). Trait anxiety refers to an individual's usual level of anxiety while state anxiety refers to an individual's current level of anxiety. State anxiety was measured twice, once before the experiment (state anxiety before) and once after the experiment (state anxiety after). A 'Children's Behavior Questionnaire' (Putnam and Rothbart (2006)) was used to measure temperamental traits including sadness, attention focusing, anger and fear. The 'Temperament Survey' questionnaire which assesses the temperamental shyness and emotionality was also completed by the subjects (Buss and Plomin (1984)). Parent-report measures were utilised which do not reflect clinical symptoms but dimensions of problem behaviour in the general population. The main focus was to examine dimensional accounts of internalising symptoms (i.e. high compared to low levels of symptoms) rather than diagnostic categories as this offers a more accurate representation of problem behaviour in the general population.

The distribution of the behavioural scores is shown in the boxplot shown in Figure 7.17. Each value lies within a specific range. In the box plot the mean is indicated by the cross ($\times$) and the outliers are represented as circles (o). The distribution of some of the scores like attention focussing, temperamental shyness and emotionality are skewed hence these scores are unlikely to be effectively modelled by simple linear models. The sadness and state anxiety before task have three outliers in total. The scores for temperamental shyness, temperamental emotionality, sadness, attention focussing, anger and fear lie between 1 and 5. State anxiety after the task and state anxiety before the task vary from 19 to 57 and anger problems from -1 to 1. The range for trait anxiety and depression are 0-14 and 0-18 respectively.

7.2.2 EEG processing and connectivity measures

EEG data from each of 20 children interviewed were used for the current analysis. The standard EEG acquisition protocol was followed for acquiring the data from 30 channels at 250 Hz. EEG was recorded while the children were shown face stimuli. The stimuli were standardised angry, happy and neutral facial expressions taken from the FEEST

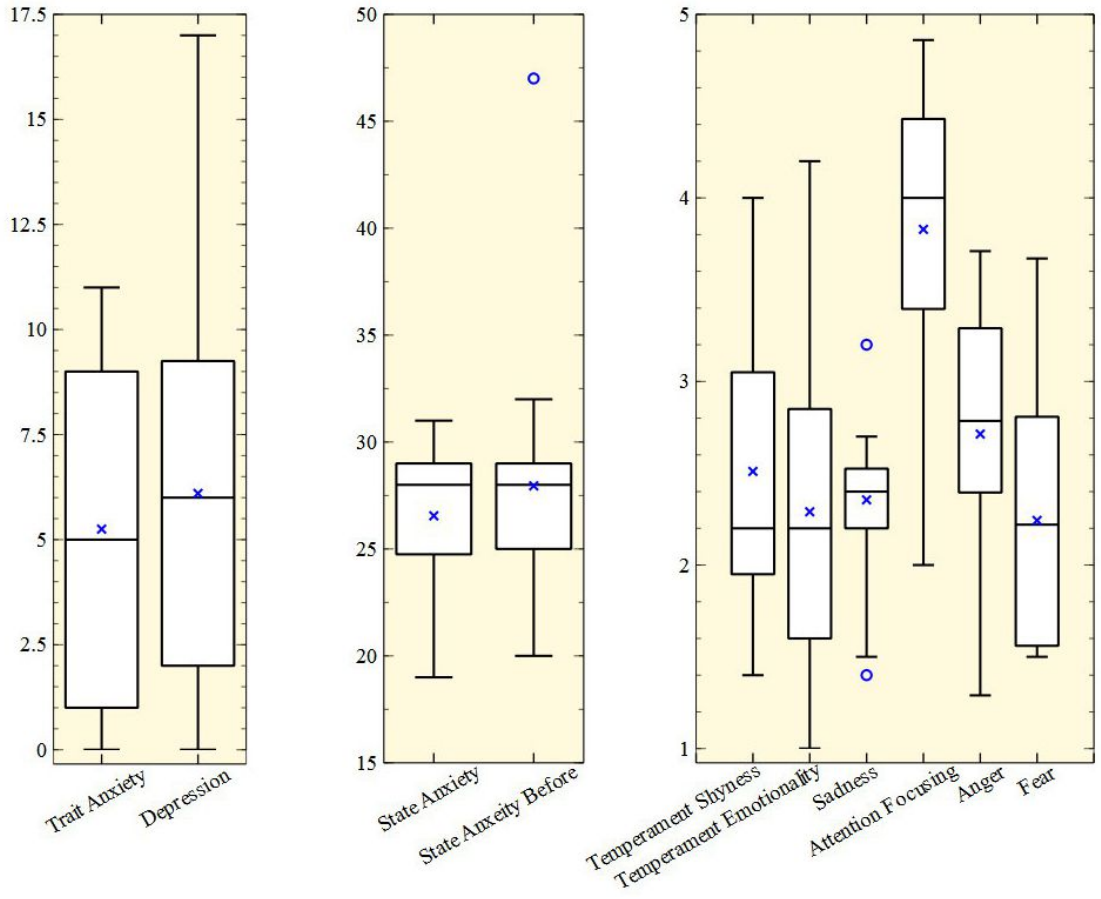

Figure 7.17: Distribution of the emotional and behavioural scores.

database (Chronaki (2011), Young et al. (2002)). The experiment included a total of 180 trials with 60 trials per emotion type presented to participants in random order.

Synchrostates were extracted from EEG signals and their subsequent connectivity patterns were derived from phase synchronisation representing the state of the functional connectivity of a person through EEG following the method described in section 3.2. The incremental k-means algorithm for this set of subjects revealed varied number of optimal synchrostates across each child (Figure 4.19). The variability in the number of synchrostates is due to the smaller number of electrodes used while acquiring the EEG. In order to draw equivalent measures from these subjects with different number of optimal states, the network parameters were calculated only from their maximum and minimum occurring states. Earlier experiments have shown that max and min states are essential in the understanding of face evoked brain response in adult subjects (Section 6.3.1.1). In addition these states have distinguished characteristics which were successfully used to classify autistic from typically developing children. The significance of the role of γ band synchronisation in perception, attention and emotion processing is a widely established concept (Luo et al. (2007), Bichot et al. (2005), Tallon-Baudry et al. (2005)). Only the maximum (max) and minimum (min) states of the γ band response were used to obtain

the connectivity maps and then estimate the network parameters. The complex network measures obtained from the connectivity maps where the transitivity, modularity, characteristic path length and global efficiency. The objective of this modelling process is to examine whether these parameters extracted from EEG recorded under different stimuli can correctly predict the behavioural state of the child by matching their psychological scores. The classical way to model such problems is the univariate correlation analysis, however if the model depends on more than one parameter, one has to go for a bi- or multivariate regression. The approach taken in this study is to match the scores with minimum complexity with the network parameters from both max and min states and henceforth a bivariate regression model is developed. Hence for developing the regression model, both the max and min state network measures were used from every sample for each stimulus to predict the clinical scores listed above in Section 7.2.1. The boxplot for all the network measures of both the maximum and minimum state is given in Figure 7.18. The parameters for the maximum state have outliers as opposed to the minimum state parameters. Each individual child's connectivity features for the maximum and minimum occurring states for every stimuli are then used to model the childs behavioural or emotional scores. The scores are modelled with both linear and polynomial regression with an order going up to three.

7.2.3 Fitness measures

A number of goodness of fit statistics were computed, including root mean squared error ($RMSE$), co-efficient of determination (R^2) and adjusted r-square (Adj R^2), to encapsulate the discrepancy between the expected values from the model and the observed values of the behavioural scores. The sum of squared error (SSE) measures the sum of the total deviation of the predicted values from the fit to the observed value.

$$SSE = \sum_{i=1}^{n} w_i (y_i - \widehat{y}_i)^2 \tag{7.8}$$

where y_i is the observed value and $\widehat{y}_i$ is the predicted value from the model. w_i is usually set to 1 and is the weight applied to each data point. Values closer to one indicate that the model is more likely to predict the outcome variable accurately. SSE is criticised for heavily weighting the outliers as squaring each error term effectively prioritises large errors to small ones.

The RMSE, also known as root mean square deviation, estimates the standard deviation of the random component of the data. It represents the standard deviation differences between the predicted and the observed values. Lower values indicate better fits. RMSE is an absolute measure and hence is not always ideal for making comparisons across methods as it is influenced by extreme values. It is influenced by the variability of the

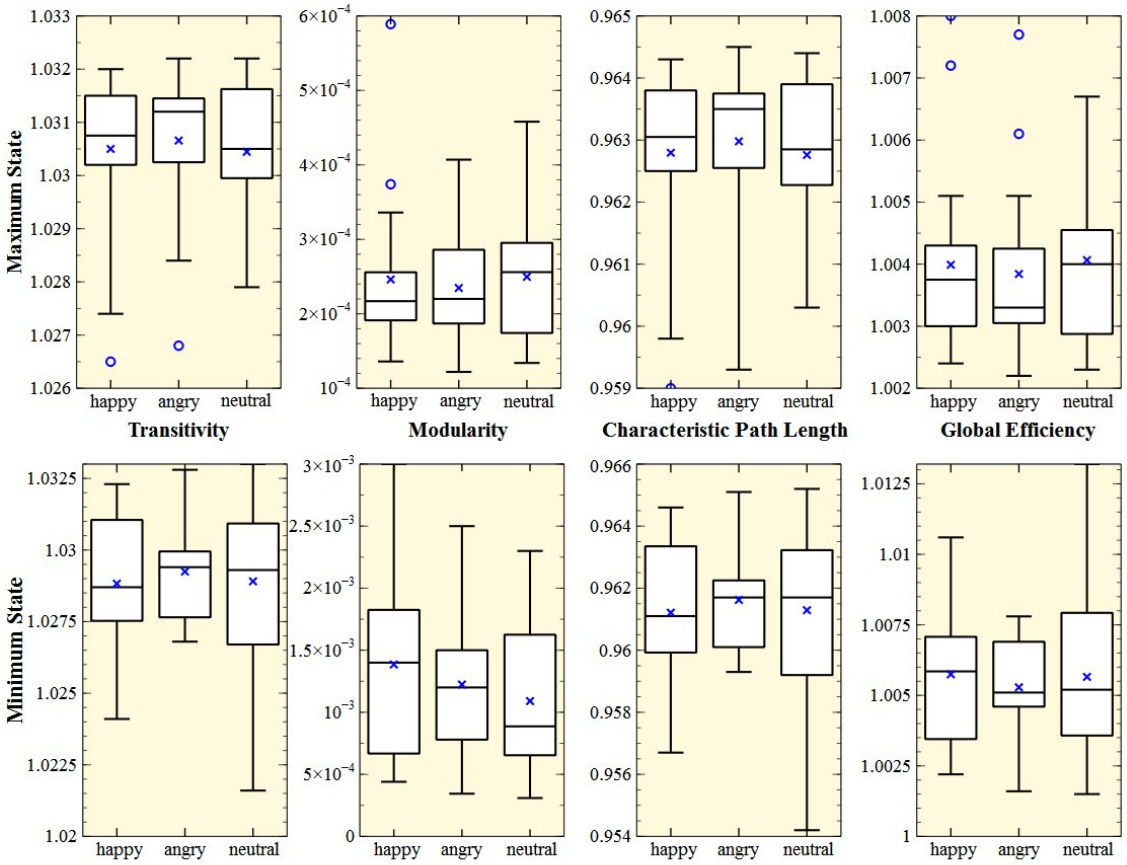

Figure 7.18: The box plots of the complex network connectivity measures for the maximum and minimum occurring synchrostates (γ band) for all the subjects across all three face stimuli (angry, happy, neutral).

error magnitudes and the total error (Willmott and Matsuura (2005)).

$$RMSE = \sqrt{MSE}; \qquad MSE = \frac{SSE}{v} \tag{7.9}$$

here $v = n - m$, where n and m are the number of response values and the fitted coefficients respectively.

R^2, or coefficient of determination is the statistical measure which is the square of the correlation between the observed values and the predicted values. $R^2 \in [0, 1]$ and values near 1 mean that the model accounts for a greater proportion of the variance. It is the ratio of the sum of squares of the regression (SSR) to the total sum of squares (SST) where $SSR = \sum_{i=1}^{n} w_i(\widehat{y}_i - \overline{y})^2$ and $SST = \sum_{i=1}^{n} w_i(y_i - \overline{y})^2$ and $\overline{y}$ is the mean of the observed values. R^2 may yield negative values when it is applied on nonlinear models.

$$R^2 = \frac{SSR}{SST} = 1 - \frac{SSE}{SST} \tag{7.10}$$

Adj R^2 is the R^2 measure adjusted on the residual degrees of freedom where, p is the

number of regressors in the model excluding the constant term. It is used to compensate for the addition of independent variables to a model. Unlike R^2 it penalises the model if the addition of the variable does not improve the model. For both R^2 and adjusted R^2 values closer to one is indicative of a better fit.

$$\text{Adjusted}R^2 = 1 - \left(1 - R^2\right)\frac{n-1}{n-p-1} = R^2 - \left(1 - R^2\right)\frac{p}{n-p-1} \tag{7.11}$$

Although RMSE, R^2 and adjusted R^2 - all represent the goodness of fit, each of them individually characterise different aspects of the data driven model. As such none of the three measures are adequate alone to judge the quality of the model and hence should assist each other to choose the best combination in a regression problem. One has to investigate each of the criteria to judge the robustness of the model.

7.2.4 Results

Using a population sample of 20 a model was developed and validated which can act as a template to predict internalising traits in children using EEG signals. Recorded EEG signals were used to calculate computer generated parameters which was fed into the model to provide us with an estimate of the behavioural score of an individual. Systems which can identify emotional or behavioural characteristics using EEG signals can be used to guide applications in computer science and robotics to inform human computer interaction models.

Results shown in Table 7.4 reports the top fifteen models for predicting behavioural measures (z) as a polynomial function of the brain connectivity measures, x and y representing the complex network metrics for the max and min state respectively. Therefore the parametric models reported in Table 7.4 can be viewed as a mapping $f(.)$ that projects EEG brain connectivity parameters (x, y) to the space of behavioural measures i.e.

$$z = f(x, y), \quad \{x, y\} \in \mathbb{R}_+, z \in \mathbb{R}$$
$$z \sim p_{00} + p_{10}x + p_{01}y + p_{20}x^2 + p_{11}xy + p_{02}y^2 + p_{30}x^3 + p_{21}x^2y + p_{12}xy^2 + p_{03}y^3$$

Up to third order polynomial was used in both x and y to keep the complexity within a limit and trained the model using the least square technique.

Results showed that using the minimum RMSE criteria (see the top 5 models of Table 7.4), the brain network measures could accurately predict sadness in children using characteristic path length (CPL), global efficiency (GE) and transitivity (Tran). Whereas using the maximum R^2 criteria, the best explained behavioural measures were the state anxiety before the task (individual's level of anxiety before the EEG task), state anxiety

(individual's current level of anxiety) and anger using the modularity (Mod) connectivity metric. Also, with the adjusted R^2 criteria, sadness, state anxiety before and anger can be characterised reliably with CPL, Mod and GE as brain network measures. The fitting performance of the top five models have been shown graphically in Figure 7.19, for all the three measures of fitness RMSE (top), R^2 (middle) and Adjusted R^2 (bottom). It must be noted that here only the best models for the behavioural measures which could be obtained with simple calculation with EEG based connectivity metrics were reported.

A total of 1080 parametric models were formed with the 1080 number of possible combinations (4 network parameters $\times$ 9 regressors for third order polynomial $\times$ 10 psychological parameter $\times$ 3 stimuli). The parametric models which predict other behavioural measures with moderately good accuracy (top 15 models) are reported in Table 7.4. Among the four behavioural measures (mentioned above) the top fifteen models also included conduct anger problems.

Both RMSE and R^2 have disadvantages as mentioned before in Section 7.2.3. Adjusted R^2 is perceived to be the most robust fitness measure against the influence from outliers as well as fitting complex models. Hence the results from the adjusted R^2 ranking could be used to determine the best model. The top five models from both RMSE and R^2 are the top 10 models of the adjusted R^2, however ranked in a different order. This reenforces the comment on the robustness of the fitness measure as well as the effectiveness of these models.

Sadness appears five times in the top ten adj R^2 models and was predicted using CPL, GE, Tran and Mod. All these network parameters are indicative of local and global connectivity in the brain. One may say that the emotion of sadness is best encoded in the EEG connectivity derived during emotion face perception. The other best models of state anxiety, anger and state anxiety before (task) scores are predicted by max and min state modularity values. Modularity is a signature of local connectivity hence these emotions may be best reflected by local network formation.

More importantly, it was found that in the top 15 reported models, the happy and neutral face stimuli gave the best fit compared to the angry face stimulus. A possible explanation for this is that neutral faces can be considered an ambiguous stimuli and, consistent with previous research (Eubank et al. (2002)), individuals with internalising symptoms may present some difficulty coping with ambiguity. Associations with happy stimuli are also consistent with previous research showing that sadness is associated with lower responsiveness to happy stimuli (Clark and Watson (1991)).

Table 7.4: Top fifteen models [EEG parameter (max order, min order)] depending on different goodness of fit measures. The table illustrates prediction of behavioural measures from the different characteristics of the EEG.

Rank	RMSE				R^2				Adjusted R^2			
	value	z	x,y (max order, min order)	Stimuli	value	z	x, y (max order, min order)	Stimuli	value	z	x, y (max order, min order)	Stimuli
1	0.2536	sadness	CPL_{max}, CPL_{min} (1,3)	happy	0.8062	anger	Mod_{max}, Mod_{min} (3,3)	happy	0.6324	sadness	CPLmax, CPL_{min} (1,3)	happy
2	0.2555	sadness	GE_{max}, GE_{min} (1,3)	happy	0.7899	anger	Mod_{max}, Mod_{min} (3,2)	happy	0.6274	state anxiety before	Mod_{max}, Mod_{min} (3,2)	neutral
3	0.2626	sadness	$Tran_{max}$, $Tran_{min}$ (1,3)	happy	0.7849	state anxiety before	Mod_{max}, Mod_{min} (3,3)	neutral	0.6269	sadness	GE_{max}, GE_{min} (1,3)	happy
4	0.2766	sadness	CPL_{max}, CPL_{min} (2,3)	happy	0.7843	state anxiety before	Mod_{max}, Mod_{min} (3,2)	neutral	0.6218	anger	Mod_{max}, Mod_{min} (3,2)	happy
5	0.2777	sadness	GE_{max}, GE_{min} (2,3)	happy	0.7775	state anxiety	Mod_{max}, Mod_{min} (3,3)	neutral	0.6124	anger	Mod_{max}, Mod_{min} (3,3)	happy
6	0.28	sadness	GE_{max}, GE_{min} (3,3)	happy	0.776	sadness	GE_{max}, GE_{min} (3,3)	happy	0.6059	sadness	$Tran_{max}$, $Tran_{min}$ (1,3)	happy
7	0.2863	sadness	$Tran_{max}$, $Tran_{min}$ (2,3)	happy	0.7583	sadness	CPL_{max}, CPL_{min} (3,3)	happy	0.5912	state anxiety before	Mod_{max}, Mod_{min} (3,3)	neutral
8	0.2908	sadness	CPL_{max}, CPL_{min} (3,3)	happy	0.7571	sadness	CPL_{max}, CPL_{min} (2,3)	happy	0.5773	state anxiety	Mod_{max}, Mod_{min} (3,3)	neutral
9	0.3004	sadness	$Tran_{max}$, $Tran_{min}$ (3,3)	happy	0.7551	sadness	GE_{max}, GE_{min} (2,3)	happy	0.5627	sadness	CPL_{max}, CPL_{min} (2,3)	happy
10	0.3508	sadness	Mod_{max}, Mod_{min} (1,3)	happy	0.7549	sadness	CPL_{max}, CPL_{min} (1,3)	happy	0.5592	sadness	GE_{max}, GE_{min} (2,3)	happy
11	0.3705	conduct anger problems	Mod_{max}, Mod_{min} (3, 2)	happy	0.7513	sadness	GE_{max}, GE_{min} (1,3)	happy	0.5589	state anxiety	Mod_{max}, Mod_{min} (3,1)	neutral
12	0.3737	sadness	Mod_{max}, Mod_{min}(1, 2)	happy	0.7506	conduct anger problems	Mod_{max}, Mod_{min} (3,3)	happy	0.552	sadness	GE_{max}, GE_{min} (3,3)	happy
13	0.3739	sadness	Mod_{max}, Mod_{min} (2, 1)	happy	0.7446	state anxiety	Mod_{max}, Mod_{min} (2,3)	neutral	0.5425	state anxiety	Mod_{max}, Mod_{min} (3,1)	neutral
14	0.3819	sadness	Mod_{max}, Mod_{min} (3, 2)	happy	0.7432	conduct anger problems	Mod_{max}, Mod_{min} (3,2)	happy	0.5378	conduct anger problems	Mod_{max}, Mod_{min} (3,2)	happy
15	0.3838	sadness	Mod_{max}, Mod_{min} (2, 2)	happy	0.7261	state anxiety	Mod_{max}, Mod_{min} (3,2)	neutral	0.5317	sadness	$Tran_{max}$, $Tran_{min}$ (2,3)	happy

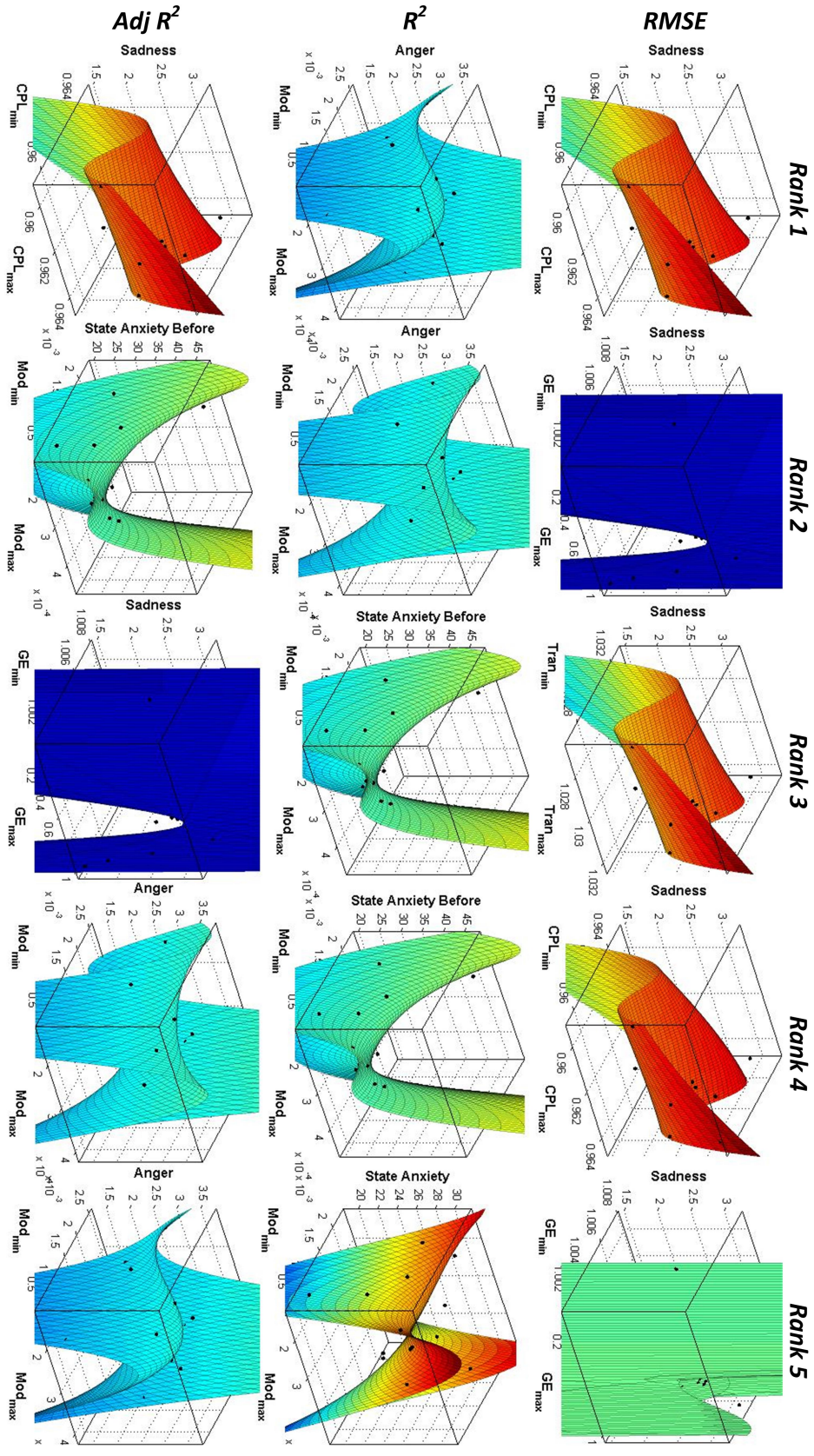

Figure 7.19: Surface plots of the top five bivariate regression models, depending on each choice of the goodness of fit, (top: RMSE, middle: R^2, bottom: Adjusted R^2) showing prediction of behavioural measures from characteristics of the EEG signals

7.2.5 Discussion

Here a generic framework for parametric modelling of behavioural measures of negative affectivity in children as a polynomial function of the brain connectivity measures has been reported. The study was conducted to explore the possibility of mapping a qualitative parameter (behaviour and emotions) with quantitative metrics (network measure from EEG).

Three measures of goodness of fit were used in order to identify the best model to predict the behavioural scores accurately. All three measures of regression analysis verify that it is sadness which can be best modelled using two dimensional curve fitting with the brain connectivity derived from maximum and minimum occurring synchrostates. With rigorous exploration of 1080 combinations of connectivity measures and behavioural measures, it was observed that the sadness, anger and state anxiety could be predicted most consistently using the EEG synchrostate connectivity. The proposed modelling paradigm, if further developed in future research and validated with larger samples and clinical populations, has the potential to ultimately be utilised for automated unbiased measurement of behavioural traits of negative affectivity (sadness) in children directly from the EEG signal and pave the path in conceptualising new applications in the clinical and commercial brain computer interface domain. This study sets a foundation for a more exhaustive study that may be carried out for building a more rigourous model for the predication of emotion and behavioural scores in children and also likewise adults. A EEG based evaluation method that can predict the emotional state will be able to facilitate the clinicians in their behavioural assessment and prognosis of various disorders.

A limitation of the current study includes the low number of subjects involved. Although the model is based on 20 children with three types of stimuli, the generated model needs to be validated in larger samples in future research. In addition, although this study focused on dimensions of problem behaviour, findings should be replicated in clinical samples of children with internalising behaviour problems. Finally, although the present study offers valuable new knowledge that has the potential to inform diagnostic practices, it does not address the question of which mechanisms underlie the development of anxiety traits in children, an essential step for targeted intervention efforts. Future research should explore this important question.

Using a large population one can create a model which after it has been validated can act as a template to predict the internalising traits in children using EEG signals. Recorded EEG signals can be easily used to calculate computer generated parameters which when fed into the model can provide us with an estimate of the behavioural score of a subject. Systems which can identify the emotional or behavioural characteristics of a child using EEG can be used to guide applications in computer science and robotics to inform human computer interaction models.

7.3 Conclusion

This chapter proposes the use of the network metrics derived from synchrostates to be applied for two separate applications. The exploration aimed to use the brain connectivity parameters for the least and most occurring states for the purpose of classification and parametric modelling in pathological populations. Complex network features extracted from synchrostate connectivity maps were firstly used to classify two populations, typical and autistic. The classifier gives state of the art results with a high accuracy of 94.7% with corresponding sensitivity and specificity values of 85.7% and 100%. Maximum state modularity values during happy, angry and neutral face was shown to be the best features to use for classification. The second study used the same network parameters derived from synchrostate from another population of children to develop a generalised model to predict the scores about the behavioural or emotional state of the child. The results show that sadness, anger and state anxiety are the best predicted behavioural traits. These are new validated and simulated applications of synchrostates. From the results one can say that these metrics are capable of quantifying the underlying functional networks during perception and capture the signature characteristics of perception of a subject. These applications can have a big impact if they are escalated and applied to a larger clinical population to validate the finding presented in this section.

Chapter 8

Conclusions and Future Directions

Research on neurobiological disorders has shown patients suffering from such disorders have shown atypical connectivity patterns and have reduced information exchange ability. These observations have lead to researchers to theorise that these disorders stem from disrupted neural circuitry which in hand affect their ability to integrate information from segregated regions of the brain.

This work has shown how EEG data can be effectively used to find time varying dynamic phase synchronisation in order to determine the connectivity in the brain in a stimulus specific way. The degree of phase synchronisation between different EEG channels has been identified as the manifestation of the underlying mechanism of information coupling between different brain regions. The time-frequency preservation property of wavelet transform is adopted here and applied on EEG data to explore the temporal dynamics and evolution of synchronisation amongst different areas of the brain from the onset of a stimulus. The EEG phase difference matrices were clustered to group synchronised patterns, called synchrostates, which are quasi-stable over the period of millisecond, similar to the concept of EEG microstates. During processing of the stimulus, the switching between these states occurs abruptly but the switching characteristic follows a well-behaved and repeatable sequence. Synchrostates and their transitions preserve the information regarding the temporal evolution of phase synchrony and hence allow deeper understanding into the dynamics of information exchange in the brain. This property of the synchrostates is crucial and can be applied for understanding disorders where subjects have inferior dynamic information integration abilities. The synchrostate phenomenon was ratified to be free from the effect of volume conduction by showing that the phase locking reported here does not show zero phase lag coherence. The desynchonisation and resynchronisation property of synchrostates at ms order cannot be accounted for by volume conduction as well.

This is the first time such a phenomenon has been reported from EEG signals and has been found to exist in the β and γ band in single subject and multiple subjects during face perception. It was also shown that although in normal population these patterns remain topographically similar for the general category of face perception task, the sequence of their occurrence and their temporal stability varies markedly between different face perception scenarios (stimuli) indicating towards different dynamics for information processing that is stimulus-specific in nature. Their existence has also been shown in groups of typical, autistic and behavioural disorder children. The new observation of quasi-static phase synchronised patterns in EEG or the synchrostates can be considered a step forward over the existing state of the art techniques reported in literature. It is believed the reported synchrostate in multichannel EEG is a generic phenomenon and may also be observed in various multivariate stochastic time series data.

In essence, it shows that it would be possible to quantify the stochastic EEG response for such cognitive activities in terms of a few discrete states with switching amongst them. This reductionist approach of mapping stochastic time domain signals in terms of probabilistic switching between a small number of discrete states may have long term implication towards mathematical modeling and quantitative understanding of the human brain.

Then the switching sequence of synchrostates is modeled as a stochastic process over multiple trials, considering that the switching time courses have the Markovian property and hence the source of these switching can be modeled as a finite Markov chain. A stochastic model is proposed using the Markov chains for the synchrostate transition. The model was built and tested under a data partitioning based cross validation scheme. Both first and second order Markov chain models were used to predicted the future synchrostates. Using a 10-fold cross validation scheme, the prediction the model successfully predicts the inter-synchrostate switching patterns with the best average accuracy of 91.63% (for normal face perception) and 89.32% (for scrambled face perception). It was also shown that such synchrostates shows different transition characteristics and self transition probabilities depending on the nature of the stimuli and hence may characterise the brain dynamics in a task specific way.

Therefore combining these two aspects of synchrostates and their stability in time a new possible method of formulating connectivity is proposed from which a set of parameters could be extracted for quantifying cognitive functionality.

The translation of the new observation i.e. synchrostates to produce brain connectivity and using connectivity or complex-network measures to characterise the stimulus are systematically presented in this thesis. The usefulness of complex network measures to quantify the underlying brain connectivity maps were shown in Chapter 6. The network measures help characterise the degree of segregated processing and information

integration in the synchrostates which lead to a new methodology for characterising information processing in human brain.

The concept of synchrostates over the scalp derived from EEG recording was utilised for formulating brain connectivity network in Autism Spectrum Disorder (ASD) and typically-growing children. The minimal and maximally occurring synchrostates for each subject are chosen for extraction of brain connectivity features, which are used for classification between these two groups of subjects. Among different supervised learning techniques, the discriminant analysis and support vector machine was explored both with polynomial kernels for the classification task. The leave one out cross-validation of the classification algorithm gives 94.7% accuracy as the best performance with corresponding sensitivity and specificity values as 85.7% and 100% respectively. The proposed method gives high classification accuracies and outperforms other contemporary research results. The effectiveness of the proposed method for classification of autistic and typical children suggests the possibility of using it on a larger population to validate it for clinical practice. The study also revealed that the maximum occurring synchrostate holds the best discerning information and its modularity index can be considered as a unique biomarker for the detection of autism. These results may be used as a foundation to drive a pilot study on a larger autistic population to investigate these differences across more subjects and different age groups as well.

The use of the proposed new methodology for characterising information processing in the brain was extended to a regression analysis. EEG from children with behaviour disorder was analysed and their synchrostates were computed. The graph metrics of the the minimal and maximal occurring states were used to fit a model with the clinically provided scores for the child's emotional state. A rigourous study was carried out to match each network parameter to all the clinical scores. The sadness, anger and state anxiety of a child was successfully predicted by the model fit between these scores and the functional network parameters. These results open up the possibility for using the new proposed method to do more extensive studies in order to establish the relationships that were found between the clinical scores and the graph measures computed from EEG signals.

It is believed that the concept of reported semi-deterministic phenomenon (which is call as synchrostates) in a stochastic multivariate time series data (in multi-channel EEG) and translating these states to complex networks to characterise the stimulus would attract the attention of other sub-branches of statistical physics. The work presented here highlights, a new way of characterising brain dynamics by using a methodology that investigates the temporal evolution of phase coupling. This may in turn lay the foundation of a methodology that will allow one to reliably supplement the diagnostic process or characterise different atypical neuro-pathological conditions more accurately.

8.1 Future Work and Direction

The research done in this thesis provides a foundation for further exploration and use of advance techniques to study functional brain dynamics. This work was the first attempt to propose a new methodology capable of quantitatively representing the functional brain during the execution of a task. The future prospects and other interesting avenues of research are outlined as follows:

Clinical studies and other applications of connectivity analysis using synchrostates

In the results reported in Chapter 7 only show two routes the application of the synchrostates can take. The ability to the quantify dynamic brain functional network opens the door to many such application which may be explored in the future. Following on from the classification study future work may be directed towards acquiring the brain connectivity measures for large populations of ASD and typical children in order to effectively bring it in to regular clinical practices. A larger, more clinically driven study with an extensive EEG data collection is required for the dissemination of the concept of using synchrostate connectivity as a diagnostic aid to clinical evaluation of autism. It is also well known that autism encapsulates a broad spectrum of disorders hence a binary classification test may not suffice as an effective and useful tool in the clinics. Hence the data from such a study can be further used to classify the severity or degree of ASD in future using a similar procedure while deriving network measures from EEG synchrostates especially from different subclasses of ASD patients.

The implication of the second application study conducted in this thesis is vast. A rigorous and more thorough study may yield more accurate models to predict emotional and behavioural state of children. A similar study may also be carried out with adults. Having such models will enable one to apply it for the rehabilitation purposes of anxiety, ADHD, depression and dementia patients. The knowledge about the trait of the patient's emotional state can help trigger medication alerts, send automated warning messages to doctors, actuate environmental changes such as turn on music or dim the lights following computer generated instructions. The use of such models also extends to brain computer interface scenarios that can open up many doors and change the way computers or robots can react to human emotion or behaviour.

Neurofeedback

The quantification of functional brain networks, which provide a deeper understanding of the underlying dynamics, into computer recognisable features

will enable the use of connectivity guided neurofeedback to provide therapy. The network features may be used as the regulating score in the feedback loop for deep brain stimulation, transcranial magnetic stimulation as well as biofeedback systems. Such a protocol would mean better and more patient centric individualised therapy may be provided. In order to get the best use out of the metrics a pilot study can be carried out to find out which graph parameter is most effective for regulating in accordance to the therapy suggest by the clinicians.

In the case of autism, a study conducted on the atypical connections may be followed by customised neurofeedback routines that may be designed with the help of the neuro- physiologist, psychologists and clinicians. The coupling parameters and the connection can be regularly monitored and a study can be conducted on patients to check for improvements and adjust the neurofeedback routine accordingly.

Source space and EEG network fusion

fMRI data has very accurate spacial resolution but lacks in the temporal resolution that is inherent in EEG signals. fMRI provides source information that will help in identifying the cortical regions of interest in a particular experiment. The use of fMRI will allow various networks to be set at the source level using existing literature to model connections between these regions. Once such anatomical networks are formed the synchrostate network and their networks parameters can be mapped to the structural model and metrics to formulate an effective model that maps the sensor level connectivity onto the structural one. This will allow for synchrostate sensor level connectivity maps to be adequately mapped to anatomical regions for better and more meaningful interpretation about the synchrostates.

Clustering

In a temporal resolution of millisecond, it is assumed that the brain stays only in one state. Hence hard clustering is used to assign each data-point corresponding to each time instant to only one of the classes or states. This means that a single data-point should belong to one of the clusters as dictated by the adopted unsupervised learning technique. The assignment of the data-points in different clusters or states by the k-means clustering algorithm is ensured by the final value of the cost-function as the clustering minimises the sum of the Euclidean distances for all the data-points where the phase difference matrix at each sample is considered as a new data point. Other paradigms of soft clustering like fuzzy c-means or similar methods (Dimitriadis et al. (2013)) where a single data-point can be associated with more than one cluster according to its degree of associativity with different classes,

can also be applied in the present problem and may be explored as future research.

Here the clustering of the phase difference matrices were done on the Euclidean space, based on the premise that the data is linearly distributed in that space. The knowledge of the data distribution in a given space is essential before the application of clustering techniques however since the EEG phase difference have a very high dimension it is not possible to visualise the data in order to determine if this assumption holds in the Euclidean space. The scope of the problem is such that the methodology can be changed and future research can be directed to studying the effects of applying linear clustering methods in different spaces. If need be, non-linear kernels like RBF can be applied to transform the data into a space where one can show that the data is linearly distributed. Hence applying clustering in that space would yield more accurate grouping results.

Appendix A

Electrode layout for Datasets

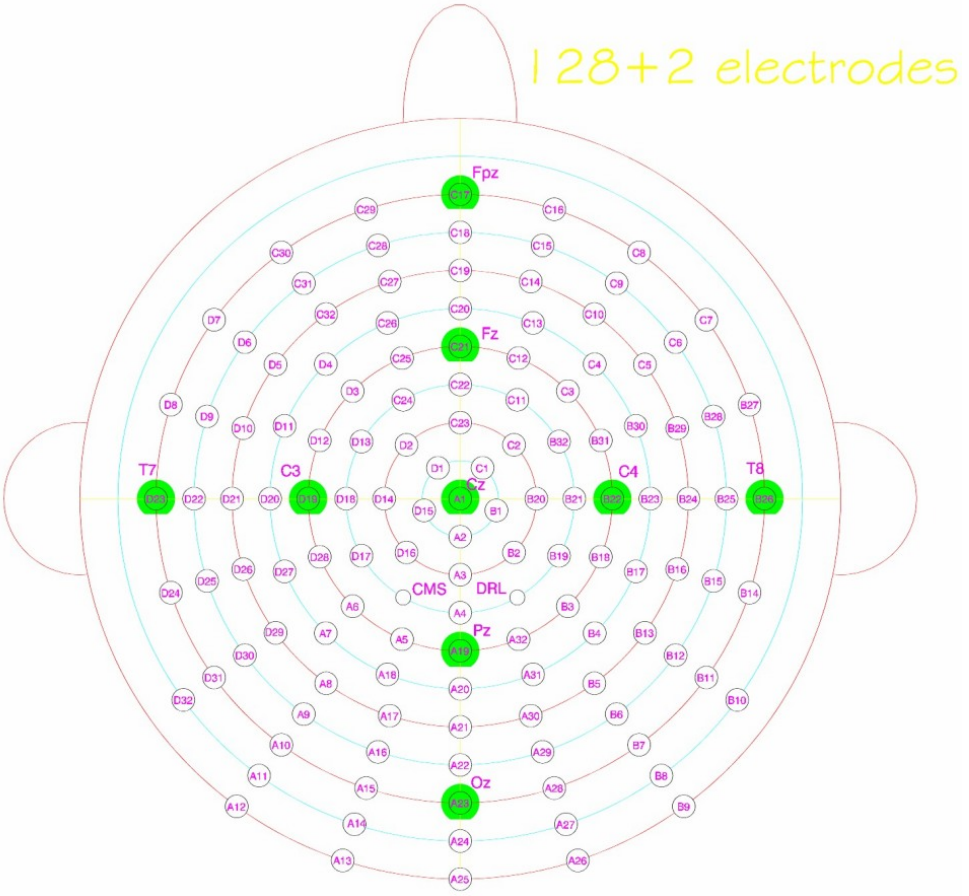

Figure A.1: The sensor layout, nose up.

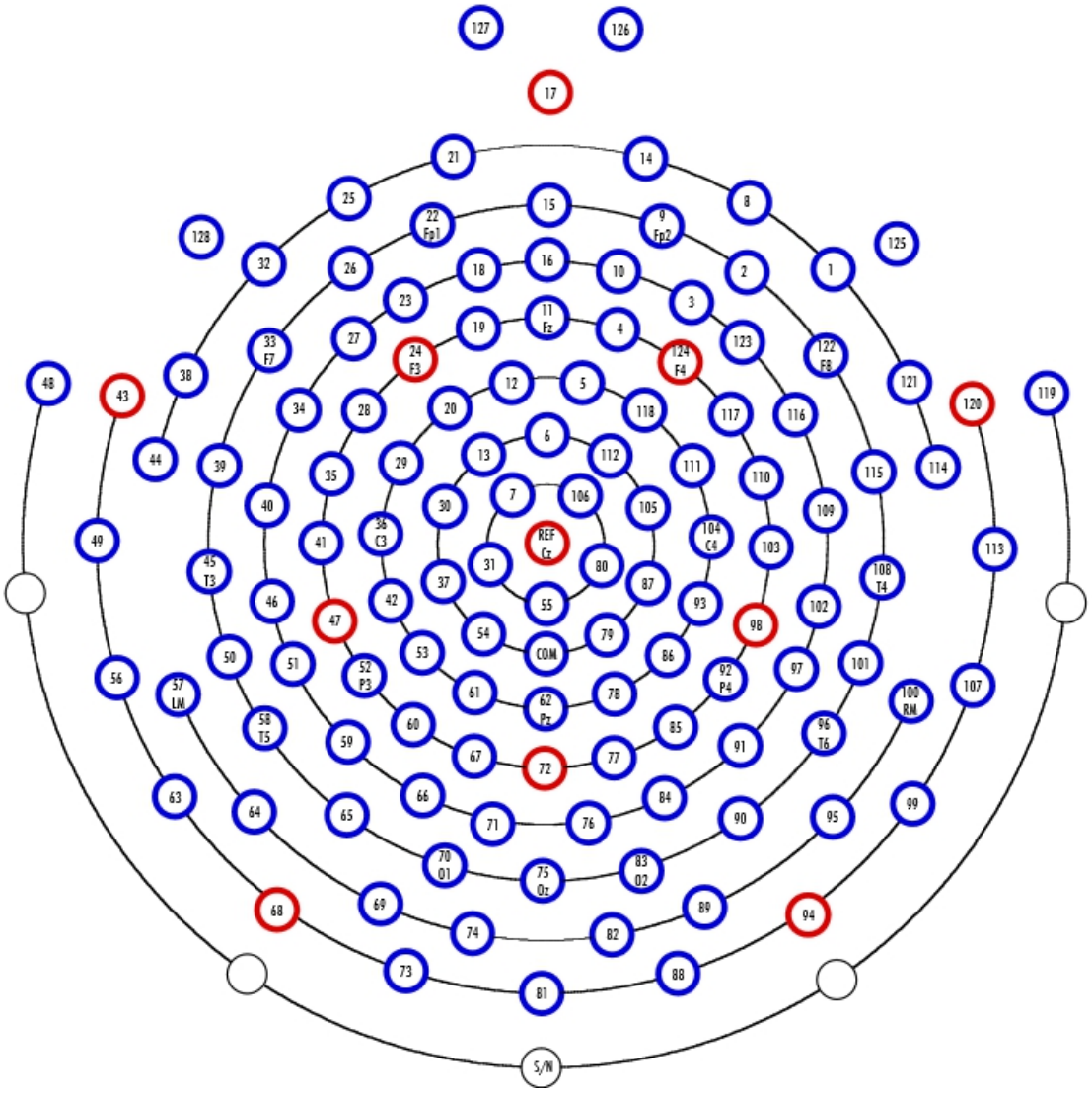

Figure A.2: HGSN sensor layout, nose up.

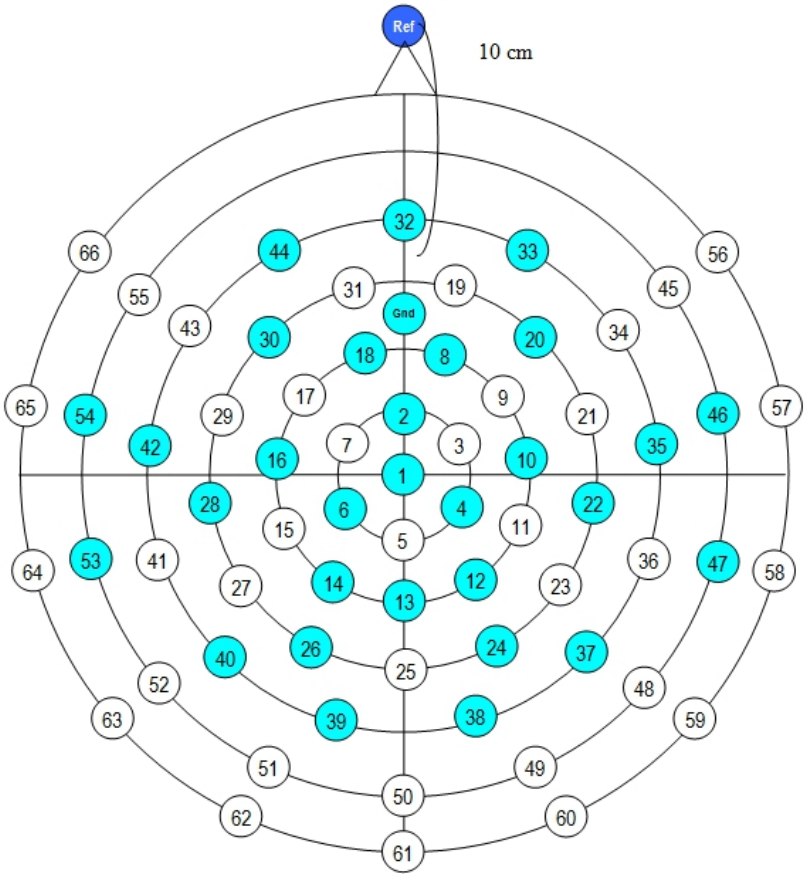

Figure A.3: EasyCap sensor layout, nose up. Sensors used are colored in blue

Appendix B

Different Layers in the Human Head

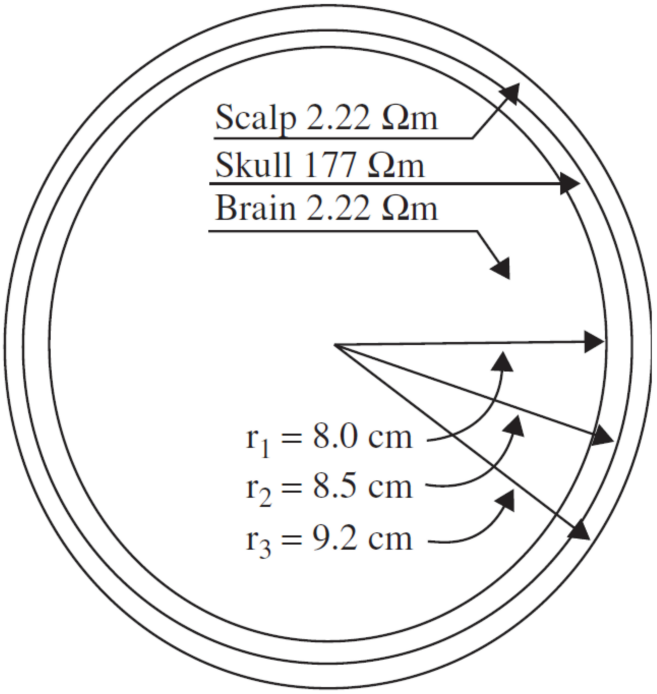

Figure B.1: Figure showing the three main layers of the head, with their approximate thickness and resistivity. Image taken from Sanei and Chambers (2007)

References

Multimodal face-evoked dataset.

Zeynep Akalin Acar and Scott Makeig. Effects of forward model errors on eeg source localization. *Brain topography*, 26(3):378–396, 2013.

Paul S Addison. *The illustrated wavelet transform handbook: introductory theory and applications in science, engineering, medicine and finance*. CRC Press, 2010.

Hojjat Adeli, Ziqin Zhou, and Nahid Dadmehr. Analysis of eeg records in an epileptic patient using wavelet transform. *Journal of neuroscience methods*, 123(1):69–87, 2003.

Ralph Adolphs. Recognizing emotion from facial expressions: Psychological and neurological mechanisms. *Behavioral and cognitive neuroscience reviews*, 1(1):21–62, 2002.

W.A. Altemeier and L.E. Altemeier. How can early, intensive training help a genetic disorder? *Pediatric Annals*, 38:167–170, 2009.

David G Amaral, Cynthia Mills Schumann, and Christine Wu Nordahl. Neuroanatomy of autism. *Trends in neurosciences*, 31(3):137–145, 2008.

Peter Anderer, Stephen Roberts, A Schlögl, Georg Gruber, G Klösch, Werner Herrmann, Peter Rappelsberger, Oliver Filz, Manel J Barbanoj, Georg Dorffner, et al. Artifact processing in computerized analysis of sleep eeg–a review. *Neuropsychobiology*, 40(3): 150–157, 1999.

MartinM. Antony. Practitioners guide to empirically based measures of anxiety, 2001.

Fabio Apicella, Federico Sicca, Rosario R Federico, Giulia Campatelli, and Filippo Muratori. Fusiform gyrus responses to neutral and emotional faces in children with autism spectrum disorders: a high density erp study. *Behavioural Brain Research*, 2012.

J Arnhold, P Grassberger, K Lehnertz, and CE Elger. A robust method for detecting interdependences: application to intracranially recorded eeg. *Physica D: Nonlinear Phenomena*, 134(4):419–430, 1999.

John Ashburner, Gareth Barnes, C Chen, Jean Daunizeau, Guillaume Flandin, Karl Friston, D Gitelman, S Kiebel, J Kilner, V Litvak, et al. Spm8 manual. *Functional Imaging Laboratory, Institute of Neurology*, 2008.

American Psychiatric Association. *Diagnostic and statistical manual of mental disorders: DSM-IV-TR*. American Psychiatric Pub, 2000.

American Psychiatric Association et al. *The Diagnostic and Statistical Manual of Mental Disorders: DSM 5*. bookpointUS, 2013.

Laura Astolfi, F De Vico Fallani, F Cincotti, D Mattia, L Bianchi, MG Marciani, S Salinari, A Colosimo, A Tocci, R Soranzo, et al. Neural basis for brain responses to tv commercials: a high-resolution eeg study. *Neural Systems and Rehabilitation Engineering, IEEE Transactions on*, 16(6):522–531, 2008.

M Ataharul Islam and Rafiqul Islam Chowdhury. A higher order markov model for analyzing covariate dependence. *Applied Mathematical Modelling*, 30(6):477–488, 2006.

H. L. Attwood and W. A. MacKay. *Essentials of Nerophysiology*. Hamilton, Canada, 1989.

A Aukahi Austin and Bruce F Chorpita. Temperament, anxiety, and depression: Comparisons across five ethnic groups of children. *Journal of Clinical Child and Adolescent Psychology*, 33(2):216–226, 2004.

Selin Aviyente, Edward M Bernat, Westley S Evans, and Scott R Sponheim. A phase synchrony measure for quantifying dynamic functional integration in the brain. *Human Brain Mapping*, 32(1):80–93, 2011.

F Babiloni, F Cincotti, C Babiloni, F Carducci, D Mattia, L Astolfi, A Basilisco, PM Rossini, L Ding, Y Ni, et al. Estimation of the cortical functional connectivity with the multimodal integration of high-resolution eeg and fmri data by directed transfer function. *Neuroimage*, 24(1):118–131, 2005.

Luiz A Baccalá and Koichi Sameshima. Partial directed coherence: a new concept in neural structure determination. *Biological Cybernetics*, 84(6):463–474, 2001.

Erol Bacsar, Christina Schmiedt-Fehr, Adile Öniz, and Canan Bacsar-Erouglu. Brain oscillations evoked by the face of a loved person. *Brain research*, 1214:105–115, 2008.

Alain Barrat, Marc Barthelemy, Romualdo Pastor-Satorras, and Alessandro Vespignani. The architecture of complex weighted networks. *Proceedings of the National Academy of Sciences of the United States of America*, 101(11):3747–3752, 2004.

Danielle S Bassett, Andreas Meyer-Lindenberg, Sophie Achard, Thomas Duke, and Edward Bullmore. Adaptive reconfiguration of fractal small-world human brain functional networks. *Proceedings of the National Academy of Sciences*, 103(51):19518–19523, 2006.

Mathieu Bastian, Sebastien Heymann, and Mathieu Jacomy. Gephi: an open source software for exploring and manipulating networks. In *ICWSM*, pages 361–362, 2009.

M.K. Belmonte, E.H. Cook, G.M. Anderson, J.L.R. Rubenstein, W.T. Greenhough, A. Beckel-Mitchener, E. Courchesne, L.M. Boulanger, S.B. Powell, P.R. Levitt, E.K. Perry, Y.H. Jiang, T.M. DeLoey, and E. Tierney. Autism as a disorder of neural information processing: directions for research and targets for therapy.molecular psychiatry. *Molecular Psychiatry*, 9:646–663, 2004.

Narcisse P Bichot, Andrew F Rossi, and Robert Desimone. Parallel and serial neural mechanisms for visual search in macaque area v4. *Science*, 308(5721):529–534, 2005.

Benjamin Blankertz, Steven Lemm, Matthias Treder, Stefan Haufe, and Klaus-Robert Müller. Single-trial analysis and classification of erp componentsa tutorial. *NeuroImage*, 56(2):814–825, 2011.

Frans Boiten, Joseph Sergeant, and Reint Geuze. Event-related desynchronization: the effects of energetic and computational demands. *Electroencephalography and Clinical Neurophysiology*, 82(4):302–309, 1992.

William Bosl, Adrienne Tierney, Helen Tager-Flusberg, and Charles Nelson. Eeg complexity as a biomarker for autism spectrum disorder risk. *BMC Medicine*, 9(1):18, 2011.

Matthew Brett, Ingrid S Johnsrude, and Adrian M Owen. The problem of functional localization in the human brain. *Nature Reviews Neuroscience*, 3(3):243–249, 2002.

Juliane Britz, Dimitri Van De Ville, and Christoph M Michel. Bold correlates of eeg topography reveal rapid resting-state network dynamics. *Neuroimage*, 52(4):1162–1170, 2010.

J. Brock, C.C. Brown, J. Boucher, and G. Rippon. The temporal binding deficit hypothesis of autism. *Development and Psychopathology*, 14:209–224, 2002.

Verena Brodbeck, Alena Kuhn, Frederic von Wegner, Astrid Morzelewski, Enzo Tagliazucchi, Sergey Borisov, Christoph M Michel, and Helmut Laufs. Eeg microstates of wakefulness and nrem sleep. *Neuroimage*, 62(3):2129–2139, 2012.

Thomas E Brown. *Attention-deficit disorders and comorbidities in children, adolescents, and adults.* American Psychiatric Publishing, Inc., 2000.

Thomas E Brown. *ADHD comorbidities: Handbook for ADHD complications in children and adults.* American Psychiatric Pub, 2009.

Arnold H Buss and Robert Plomin. Temperament: Early developing personality traits. 1984.

C Cao and S Slobounov. Alteration of cortical functional connectivity as a result of traumatic brain injury revealed by graph theory, ica, and sloreta analyses of eeg signals. *Neural Systems and Rehabilitation Engineering, IEEE Transactions on*, 18 (1):11–19, 2010.

LJ Carver and G Dawson. Development and neural bases of face recognition in autism. *Molecular Psychiatry*, 7:S18, 2002.

S.R. Chandana, M.E. Behen, C. Juhsz, O. Muzik, R.D. Rothermel, T.J. Mangner, P.K. Chakraborty, H.T. Chugani, and D.C. Chigani. Significance of abnormalities in developmental trajectory and asymmetry of cortical serotonin synthesis in autism. *International Journal of Developmental Neuroscience*, 23:171–182, 2005.

Catie Chang, Zhongming Liu, Michael C Chen, Xiao Liu, and Jeff H Duyn. Eeg correlates of time-varying bold functional connectivity. *NeuroImage*, 72:227–236, 2013.

Muniya S Choudhury, Sandra S Pimentel, and Philip C Kendall. Childhood anxiety disorders: Parent–child (dis) agreement using a structured interview for the dsm-iv. *Journal of the American Academy of Child & Adolescent Psychiatry*, 42(8):957–964, 2003.

Georgia Chronaki. *A behavioural and electrophysiological exploration into facial and vocal emotion processing in children with behaviour problems*. PhD thesis, University of Southampton, 2011.

Lee A Clark and David Watson. Tripartite model of anxiety and depression: psychometric evidence and taxonomic implications. *Journal of abnormal psychology*, 100(3): 316, 1991.

Robert Coben. Connectivity-guided neurofeedback for autistic spectrum disorder. *Biofeedback*, 35(4):131–135, 2007.

Robert Coben, Adam R Clarke, William Hudspeth, and Robert J Barry. Eeg power and coherence in autistic spectrum disorder. *Clinical Neurophysiology*, 119(5):1002–1009, 2008.

Robert Coben, Michael Linden, and Thomas E Myers. Neurofeedback for autistic spectrum disorder: a review of the literature. *Applied psychophysiology and biofeedback*, 35(1):83–105, 2010.

Alexander L Cohen, Damien A Fair, Nico UF Dosenbach, Francis M Miezin, Donna Dierker, David C Van Essen, Bradley L Schlaggar, and Steven E Petersen. Defining functional areas in individual human brains using resting functional connectivity mri. *Neuroimage*, 41(1):45–57, 2008.

Cold Spring Harbor Partha Mitra Cold, Cold Spring Harbor Hemant Bokil Cold, et al. *Observed brain dynamics*. Oxford University Press, 2007.

Eric Courchesne, CM Karns, HR Davis, R Ziccardi, RA Carper, ZD Tigue, HJ Chisum, P Moses, K Pierce, C Lord, et al. Unusual brain growth patterns in early life in patients with autistic disorder an mri study. *Neurology*, 57(2):245–254, 2001.

Ian Daly, Catherine M Sweeney-Reed, and Slawomir J Nasuto. Testing for significance of phase synchronisation dynamics in the eeg. *Journal of computational neuroscience*, 34(3):411–432, 2013.

Simon W Davis, James E Kragel, David J Madden, and Roberto Cabeza. The architecture of cross-hemispheric communication in the aging brain: linking behavior to functional and structural connectivity. *Cerebral Cortex*, page bhr123, 2011.

G. Dawson. Early behavioral intervention, brain plasticity, and the prevention of autism spectrum disorder. *Development and Psychopathology*, 20:775–804, 2008.

G. Dawson, S. Rogers, J. Munson, M. Smith, J. Winter, J. Greenson, A. Donaldson, and J. Varley. Randomized, controlled trial of an intervention for toddlers with autism: the early start denver model. *Pediatrics*, 125:17–23, 2010.

Jennifer M DeCicco, Beylul Solomon, and Tracy A Dennis. Neural correlates of cognitive reappraisal in children: an erp study. *Developmental cognitive neuroscience*, 2(1):70–80, 2012.

Claudine Dietz, Sophie Swinkels, Emma van Daalen, Herman van Engeland, and Jan K Buitelaar. Screening for autistic spectrum disorder in children aged 14–15 months. ii: population screening with the early screening of autistic traits questionnaire (esat). design and general findings. *Journal of autism and developmental disorders*, 36(6): 713–722, 2006.

SI Dimitriadis, NA Laskaris, and A Tzelepi. On the quantization of time-varying phase synchrony patterns into distinct functional connectivity microstates (fcstates) in a multi-trial visual erp paradigm. *Brain Topography*, 26(3):397–409, 2013.

Sam M Doesburg, Alexa B Roggeveen, Keiichi Kitajo, and Lawrence M Ward. Large-scale gamma-band phase synchronization and selective attention. *Cerebral Cortex*, 18 (2):386–396, 2008.

Alysa E Doyle. Executive functions in attention-deficit/hyperactivity disorder. *The Journal of clinical psychiatry*, 67:21–26, 2005.

Nancy Eisenberg, Amanda Cumberland, Tracy L Spinrad, Richard A Fabes, Stephanie A Shepard, Mark Reiser, Bridget C Murphy, Sandra H Losoya, and Ivanna K Guthrie. The relations of regulation and emotionality to children's externalizing and internalizing problem behavior. *Child development*, 72(4):1112–1134, 2001.

Paul Ekman. Strong evidence for universals in facial expressions: a reply to russell's mistaken critique. 1994.

Sharon Eldar, Roni Yankelevitch, Dominique Lamy, and Yair Bar-Haim. Enhanced neural reactivity and selective attention to threat in anxiety. *Biological psychology*, 85 (2):252–257, 2010.

M Elsabbagha, A Voleina, G Csibra, K Holmboea, H Garwood, L Tucker, S Krljes, S Baron-Cohen, P Bolton, T Charman, and et al. Neural correlates of eye gaze processing in the infant broader autism phenotype. *Biological Psychiatry*, 65(1):31–38, 2009.

A. K. Engel, P. Fries, and W. Singer. Dynamic predictions: oscillations and synchrony in top-down processing. *Nature Reviews Neuroscience*, 2(10):704–716, October 2001a.

Andreas K Engel, Pascal Fries, and Wolf Singer. Dynamic predictions: oscillations and synchrony in top–down processing. *Nature Reviews Neuroscience*, 2(10):704–716, 2001b.

Steve K Esser, Sean L Hill, and Giulio Tononi. Sleep homeostasis and cortical synchronization: I. modeling the effects of synaptic strength on sleep slow waves. *Sleep*, 30 (12):1617, 2007.

Amit Etkin, Katherine E Prater, Alan F Schatzberg, Vinod Menon, and Michael D Greicius. Disrupted amygdalar subregion functional connectivity and evidence of a compensatory network in generalized anxiety disorder. *Archives of general psychiatry*, 66(12):1361–1372, 2009.

Martin Eubank, Dave Collins, Nick Smith, et al. Anxiety and ambiguity: it's all open to interpretation. *Journal of Sport & Exercise Psychology*, 24(3):239–253, 2002.

F De Vico Fallani, Vito Latora, Laura Astolfi, Febo Cincotti, Donatella Mattia, Maria Grazia Marciani, Serenella Salinari, Alfredo Colosimo, and Fabrizio Babiloni. Persistent patterns of interconnection in time-varying cortical networks estimated from high-resolution eeg recordings in humans during a simple motor act. *Journal of Physics A: Mathematical and Theoretical*, 41(22):224014, 2008.

Mehrdad Fatourechi, Ali Bashashati, Rabab K Ward, and Gary E Birch. Emg and eog artifacts in brain computer interface systems: A survey. *Clinical Neurophysiology*, 118 (3):480–494, 2007.

J. Fell and N. Axmacher. The role of phase synchronization in memory processes. *Nature Reviews Neuroscience*, 12(2):105–118, February 2011a.

Juergen Fell and Nikolai Axmacher. The role of phase synchronization in memory processes. *Nature Reviews Neuroscience*, 12(2):105–118, 2011b.

A Flexerand, Georg Dorffner, P Sykacekand, and Iead Rezek. An automatic, continuous and probabilistic sleep stager based on a hidden markov model. *Applied Artificial Intelligence*, 16(3):199–207, 2002.

Pascal Fries. Neuronal gamma-band synchronization as a fundamental process in cortical computation. *Annual Review of Neuroscience*, 32:209–224, 2009.

Pascal Fries, John H Reynolds, Alan E Rorie, and Robert Desimone. Modulation of oscillatory neuronal synchronization by selective visual attention. *Science*, 291(5508): 1560–1563, 2001.

Karl Friston. Causal modelling and brain connectivity in functional magnetic resonance imaging. *PLoS biology*, 7(2):e1000033, 2009.

Karl J Friston. Functional and effective connectivity: a review. *Brain connectivity*, 1 (1):13–36, 2011.

K.J. Friston, C.D. Frith, and R.S.J. Frackowiak. Time-dependent changes in effective connectivity measured with pet. *Human Brain Mapping*, 1:69–80, 1993a.

K.J. Friston, C.D. Frith, P.F. Liddle, and R.S.J. Frackowiak. Functional connectivity: the principal component analysis of large (pet) data sets. *Journal of Cerebral Blood Flow and Metabolism*, 13:5–14, 1993b.

Deon Garrett, David A Peterson, Charles W Anderson, and Michael H Thaut. Comparison of linear, nonlinear, and feature selection methods for eeg signal classification. *Neural Systems and Rehabilitation Engineering, IEEE Transactions on*, 11(2):141–144, 2003.

Matthias Gärtner, Verena Brodbeck, Helmut Laufs, and Gaby Schneider. A stochastic model for eeg microstate sequence analysis. *NeuroImage*, 2014.

Nathalie George, Julie Evans, Nicole Fiori, Jules Davidoff, and Bernard Renault. Brain events related to normal and moderately scrambled faces. *Cognitive Brain Research*, 4(2):65–76, 1996.

Lorena RR Gianotti, Pascal L Faber, Matthias Schuler, Roberto D Pascual-Marqui, Kieko Kochi, and Dietrich Lehmann. First valence, then arousal: the temporal dynamics of brain electric activity evoked by emotional stimuli. *Brain Topography*, 20 (3):143–156, 2008.

H Hill Goldsmith and Kathryn S Lemery. Linking temperamental fearfulness and anxiety symptoms: A behavior–genetic perspective. *Biological Psychiatry*, 48(12):1199–1209, 2000.

Pierre Gosselin and Janik Simard. Children's knowledge of facial expressions of emotions: Distinguishing fear and surprise. *The Journal of genetic psychology*, 160(2):181–193, 1999.

Francois Goudail, Eberhard Lange, Takashi Iwamoto, Kazuo Kyuma, and Nobuyuki Otsu. Face recognition system using local autocorrelations and multiscale integration. *Pattern Analysis and Machine Intelligence, IEEE Transactions on*, 18(10):1024–1028, 1996.

C. M. Gray, P. Konig, A. K. Engel, and W. Singer. Oscillatory responses in cat visual cortex exhibit inter-columnar synchronization which reflects global stimulus properties. *Nature*, 338(6213):334–337, March 1989.

Roberta Grech, Tracey Cassar, Joseph Muscat, Kenneth P Camilleri, Simon G Fabri, Michalis Zervakis, Petros Xanthopoulos, Vangelis Sakkalis, and Bart Vanrumste. Review on solving the inverse problem in eeg source analysis. *Journal of neuroengineering and rehabilitation*, 5(1):25, 2008.

Michael D Greicius, Benjamin H Flores, Vinod Menon, Gary H Glover, Hugh B Solvason, Heather Kenna, Allan L Reiss, and Alan F Schatzberg. Resting-state functional connectivity in major depression: abnormally increased contributions from subgenual cingulate cortex and thalamus. *Biological psychiatry*, 62(5):429–437, 2007.

Charles Miller Grinstead and James Laurie Snell. *Introduction to probability*. American Mathematical Soc., 1998.

Joachim Gross, Frank Schmitz, Irmtraud Schnitzler, Klaus Kessler, Kimron Shapiro, Bernhard Hommel, and Alfons Schnitzler. Modulation of long-range neural synchrony reflects temporal limitations of visual attention in humans. *Proceedings of the National Academy of Sciences of the United States of America*, 101(35):13050–13055, 2004.

Bahar Güntekin and Erol Basar. Emotional face expressions are differentiated with brain oscillations. *International Journal of Psychophysiology*, 64(1):91–100, 2007.

D Gupta, CJ James, and W Gray. De-noising epileptic eeg using ica and phase synchrony. 2006.

Elly Gysels and Patrick Celka. Phase synchronization for the recognition of mental tasks in a brain-computer interface. *Neural Systems and Rehabilitation Engineering, IEEE Transactions on*, 12(4):406–415, 2004.

T. Isotani P.L. Faber K. Sasada T. Kinoshita H. Katayama, L.R.R. Gianotti and D. Lehmann. Classes of multichannel eeg microstates in light and deep hypnotic conditions. *Brain Topography*, 20(1):7–14, Sep 2007.

Julie A Hadwin, Nick Donnelly, Christopher C French, Anne Richards, Antonia Watts, and Dave Daley. The influence of children's self-report trait anxiety and depression on visual search for emotional faces. *Journal of Child Psychology and Psychiatry*, 44 (3):432–444, 2003.

Yuko Hakamata, Shmuel Lissek, Yair Bar-Haim, Jennifer C Britton, Nathan A Fox, Ellen Leibenluft, Monique Ernst, and Daniel S Pine. Attention bias modification treatment: a meta-analysis toward the establishment of novel treatment for anxiety. *Biological psychiatry*, 68(11):982–990, 2010.

Michelle Hampson, Fuyuze Tokoglu, Zhongdong Sun, Robin J Schafer, Pawel Skudlarski, John C Gore, and R Todd Constable. Connectivity–behavior analysis reveals that functional connectivity between left ba39 and broca's area varies with reading ability. *Neuroimage*, 31(2):513–519, 2006.

Heather Cody Hazlett, Michele Poe, Guido Gerig, Rachel Gimpel Smith, James Provenzale, Allison Ross, John Gilmore, and Joseph Piven. Magnetic resonance imaging and head circumference study of brain size in autism: birth through age 2 years. *Archives of General Psychiatry*, 62(12):1366, 2005.

Bin He, Lin Yang, Christopher Wilke, and Han Yuan. Electrophysiological imaging of brain activity and connectivitychallenges and opportunities. *Biomedical Engineering, IEEE Transactions on*, 58(7):1918–1931, 2011.

Heather A Henderson, Nathan A Fox, and Kenneth H Rubin. Temperamental contributions to social behavior: The moderating roles of frontal eeg asymmetry and gender. *Journal of the American Academy of Child & Adolescent Psychiatry*, 40(1):68–74, 2001.

Richard N Henson, Daniel G Wakeman, Vladimir Litvak, and Karl J Friston. A parametric empirical bayesian framework for the eeg/meg inverse problem: generative models for multi-subject and multi-modal integration. *Frontiers in Human Neuroscience*, 5, 2011.

Imali Hettiarachchi, Shady Mohamed, and Saeid Nahavandi. A marginalised markov chain monte carlo approach for model based analysis of eeg data. In *Biomedical Imaging (ISBI), 2012 9th IEEE International Symposium on*, pages 1539–1542. IEEE, 2012.

B. Horwitz. The elusive concept of brain connectivity. *NeuroImage*, 19(2 Pt 1):466–470, 2003.

B. Horwitz, J. M. Rumsey, C. L. Grady, and S. I. Rapoport. The cerebral metabolic landscape in autism. intercorrelations of regional glucose utilization. *Archives of Neurology*, 45(7):749–755, 1988.

Carroll Izard, Sarah Fine, David Schultz, Allison Mostow, Brian Ackerman, and Eric Youngstrom. Emotion knowledge as a predictor of social behavior and academic competence in children at risk. *Psychological science*, 12(1):18–23, 2001.

Wasifa Jamal, Saptarshi Das, and Koushik Maharatna. Existence of millisecond-order stable states in time-varying phase synchronization measure in eeg signals. In *Engineering in Medicine and Biology Society (EMBC), 2013 35th Annual International Conference of the IEEE*, pages 2539–2542, 2013a.

Wasifa Jamal, Saptarshi Das, Koushik Maharatna, Doga Kuyucu, Federico Sicca, Lucia Billeci, Fabio Apicella, and Filippo Muratori. Using brain connectivity measure of eeg synchrostates for discriminating typical and autism spectrum disorder. In *Neural Engineering (NER), 2013 6th International IEEE/EMBS Conference on*, pages 1402–1405. IEEE, 2013b.

Wasifa Jamal, Saptarshi Das, I-A Oprescu, and Koushik Maharatna. Prediction of synchrostate transitions in eeg signals using markov chain models. *Signal Processing Letters, IEEE*, 22(2):149–152, 2015.

Wasifa Jamal, Saptarshi Das, Ioana-Anastasia Oprescu, Koushik Maharatna, Fabio Apicella, and Federico Sicca. Classification of autism spectrum disorder using supervised learning of brain connectivity measures extracted from synchrostates. *Journal of Neural Engineering*, June 2014.

Peter S Jensen, Stephen P Hinshaw, Helena C Kraemer, Nilantha Lenora, Jeffrey H Newcorn, Howard B Abikoff, John S March, L Eugene Arnold, Dennis P Cantwell, C Keith Conners, et al. Adhd comorbidity findings from the mta study: comparing comorbid subgroups. *Journal of the American Academy of Child & Adolescent Psychiatry*, 40(2):147–158, 2001.

M. Atienza J.L. Cantero and R.M. Salas. Human alpha oscillations in wakefulness, drowsiness period, and rem sleep: different electroencephalographic phenomena within the alpha band. *Neurophysiologie Clinique/Clinical Neurophysiology*, 32(1):54–71, Jan 2002.

M.H. Johnson, H. Halit, S.J. Grice, and A. Karmiloff-Smith. Neuroimaging of typical and atypical development: a perspective from multiple levels of analysis. *Development and Psychopathology*, 14:521–536, 2002.

Nisrine Jrad, Marco Congedo, Ronald Phlypo, Sandra Rousseau, Rémi Flamary, Florian Yger, and Alain Rakotomamonjy. sw-svm: sensor weighting support vector machines for eeg-based brain–computer interfaces. *Journal of Neural Engineering*, 8(5):056004, 2011.

Marcel Adam Just, Vladimir L Cherkassky, Timothy A Keller, Rajesh K Kana, and Nancy J Minshew. Functional and anatomical cortical underconnectivity in autism: evidence from an fmri study of an executive function task and corpus callosum morphometry. *Cerebral Cortex*, 17(4):951–961, 2007.

Marcel Adam Just, Vladimir L Cherkassky, Timothy A Keller, and Nancy J Minshew. Cortical activation and synchronization during sentence comprehension in high-functioning autism: evidence of underconnectivity. *Brain*, 127(8):1811–1821, 2004.

Maciej Kamiński, Mingzhou Ding, Wilson A Truccolo, and Steven L Bressler. Evaluating causal relations in neural systems: Granger causality, directed transfer function and statistical assessment of significance. *Biological Cybernetics*, 85(2):145–157, 2001.

Rajesh K Kana, Timothy A Keller, Nancy J Minshew, and Marcel Adam Just. Inhibitory control in high-functioning autism: decreased activation and underconnectivity in inhibition networks. *Biological Psychiatry*, 62(3):198–206, 2007.

Rajesh K Kana, Lauren E Libero, and Marie S Moore. Disrupted cortical connectivity theory as an explanatory model for autism spectrum disorders. *Physics of Life Reviews*, 8(4):410–437, 2011.

Stefan J Kiebel, Olivier David, and Karl J Friston. Dynamic causal modelling of evoked responses in eeg/meg with lead field parameterization. *NeuroImage*, 30(4):1273–1284, 2006.

Wilhelm Emil Kincses, Christoph Braun, Stefan Kaiser, Wolfgang Grodd, Hermann Ackermann, and Klaus Mathiak. Reconstruction of extended cortical sources for eeg and meg based on a monte-carlo-markov-chain estimator. *Human brain mapping*, 18 (2):100–110, 2003.

Jochen Kindler, D Hubl, WK Strik, T Dierks, and T Koenig. Resting-state eeg in schizophrenia: auditory verbal hallucinations are related to shortening of specific microstates. *Clinical Neurophysiology*, 122(6):1179–1182, 2011.

E. Kirmizi-Alsan, Z. Bayraktaroglu, H. Gurvit, Y.H. Keskin, M. Emre, and T. Demiralp. Comparative analysis of event-related potentials during go/nogo and cpt: Decomposition of electrophysiological markers of response inhibition and sustained attention. *Brain Research*, 1104:114–128, 2006.

M. A. Kisley and Z. M. Cornwell. Gamma and beta neural activity evoked during a sensory gating paradigm: Effects of auditory, somatosensory and cross-modal stimulation. *Clinical Neurophysiology*, 117:2549–2563, 2006.

Natalia M Kleinhans, Todd Richards, Lindsey Sterling, Keith C Stegbauer, Roderick Mahurin, L Clark Johnson, Jessica Greenson, Geraldine Dawson, and Elizabeth Aylward. Abnormal functional connectivity in autism spectrum disorders during face processing. *Brain*, 131(4):1000–1012, 2008.

Thomas Koenig, L Prichep, D Lehmann, PV Sosa, E Braeker, H Kleinlogel, R Isenhart, and ER John. Millisecond by millisecond, year by year: normative eeg microstates and developmental stages. *Neuroimage*, 16(1):41–48, 2002.

Thomas Koenig, Maria Stein, Matthias Grieder, and Mara Kottlow. A tutorial on data-driven methods for statistically assessing erp topographies. *Brain Topography*, 27(1): 72–83, 2014.

Thomas Koenig, D Studer, D Hubl, L Melie, and WK Strik. Brain connectivity at different time-scales measured with eeg. *Philosophical Transactions of the Royal Society B: Biological Sciences*, 360(1457):1015–1024, 2005.

Kerstin Konrad and Simon B Eickhoff. Is the adhd brain wired differently? a review on structural and functional connectivity in attention deficit hyperactivity disorder. *Human brain mapping*, 31(6):904–916, 2010.

Mara Kottlow, Kay Jann, Thomas Dierks, and Thomas Koenig. Increased phase synchronization during continuous face integration measured simultaneously with eeg and fmri. *Clinical Neurophysiology*, 123(8):1536–1548, 2012.

Yury Koush, Maria Joao Rosa, Fabien Robineau, Klaartje Heinen, Sebastian W Rieger, Nikolaus Weiskopf, Patrik Vuilleumier, Dimitri Van De Ville, and Frank Scharnowski. Connectivity-based neurofeedback: dynamic causal modeling for real-time fmri. *NeuroImage*, 81:422–430, 2013.

Morton Kramer. The rising pandemic of mental disorders and associated chronic diseases and disabilities. *Acta Psychiatrica Scandinavica*, 62(S285):382–397, 1980.

Jean-Philippe Lachaux, Eugenio Rodriguez, Jacques Martinerie, Francisco J Varela, et al. Measuring phase synchrony in brain signals. *Human Brain Mapping*, 8(4): 194–208, 1999.

Janet E Lainhart. Advances in autism neuroimaging research for the clinician and geneticist. In *American Journal of Medical Genetics Part C: Seminars in Medical Genetics*, volume 142, pages 33–39, 2006.

Janet E Lainhart, Erin D Bigler, Maureen Bocian, Hilary Coon, Elena Dinh, Geraldine Dawson, Curtis K Deutsch, Michelle Dunn, Annette Estes, Helen Tager-Flusberg, et al. Head circumference and height in autism: a study by the collaborative program of excellence in autism. *American Journal of Medical Genetics Part A*, 140(21):2257–2274, 2006.

R.J. Landa. Diagnosis of autism spectrum disorders in the first 3 years of life. *Nature Clinical Practice Neurology*, 4:138–147, 2008.

Russell Lang, Mark OReilly, Olive Healy, Mandy Rispoli, Helena Lydon, William Streusand, Tonya Davis, Soyeon Kang, Jeff Sigafoos, Giulio Lancioni, et al. Sensory integration therapy for autism spectrum disorders: A systematic review. *Research in Autism Spectrum Disorders*, 6(3):1004–1018, 2012.

Kwang-Hyuk Lee, Leanne M Williams, Michael Breakspear, and Evian Gordon. Synchronous gamma activity: a review and contribution to an integrative neuroscience model of schizophrenia. *Brain Research Reviews*, 41(1):57–78, 2003.

D Lehmann, H Ozaki, and I Pal. Eeg alpha map series: brain micro-states by space-oriented adaptive segmentation. *Electroencephalography and Clinical Neurophysiology*, 67(3):271–288, 1987.

D Lehmann, WK Strik, B Henggeler, T Koenig, and M Koukkou. Brain electric microstates and momentary conscious mind states as building blocks of spontaneous thinking: I. visual imagery and abstract thoughts. *International Journal of Psychophysiology*, 29(1):1–11, 1998.

Klaus Lehnertz, Florian Mormann, Thomas Kreuz, Ralph G Andrzejak, Christoph Rieke, Peter David, and Christian E Elger. Seizure prediction by nonlinear eeg analysis. *Engineering in Medicine and Biology Magazine, IEEE*, 22(1):57–63, 2003.

L Leocani, C Toro, P Manganotti, P Zhuang, and M Hallett. Event-related coherence and event-related desynchronization/synchronization in the 10 hz and 20 hz eeg during self-paced movements. *Electroencephalography and Clinical Neurophysiology/Evoked Potentials Section*, 104(3):199–206, 1997.

Xiang Liao, Dezhong Yao, and Chaoyi Li. Transductive svm for reducing the training effort in bci. *Journal of Neural Engineering*, 4(3):246, 2007.

Yong Liu, Meng Liang, Yuan Zhou, Yong He, Yihui Hao, Ming Song, Chunshui Yu, Haihong Liu, Zhening Liu, and Tianzi Jiang. Disrupted small-world networks in schizophrenia. *Brain*, 131(4):945–961, 2008.

Sidath Ravindra Liyanage, Cuntai Guan, Haihong Zhang, Kai Keng Ang, JianXin Xu, and Tong Heng Lee. Dynamically weighted ensemble classification for non-stationary eeg processing. *Journal of Neural Engineering*, 10(3):036007, 2013.

Rolf Loeber, Jeffrey D Burke, Benjamin B Lahey, Alaina Winters, and Marcie Zera. Oppositional defiant and conduct disorder: a review of the past 10 years, part i. *Journal of the American Academy of Child & Adolescent Psychiatry*, 39(12):1468–1484, 2000.

Nikos K Logothetis and Brian A Wandell. Interpreting the bold signal. *Annu. Rev. Physiol.*, 66:735–769, 2004.

Fabien Lotte, Marco Congedo, Anatole Lécuyer, Fabrice Lamarche, Bruno Arnaldi, et al. A review of classification algorithms for eeg-based brain–computer interfaces. *Journal of Neural Engineering*, 4(2):R1, 2007.

Chia-Feng Lu, Shin Teng, Chih-I Hung, Po-Jung Tseng, Liang-Ta Lin, Po-Lei Lee, and Yu-Te Wu. Reorganization of functional connectivity during the motor task using eeg time–frequency cross mutual information analysis. *Clinical Neurophysiology*, 122(8): 1569–1579, 2011.

David Luenberger. Introduction to dynamic systems: theory, models, and applications. 1979.

Qian Luo, Tom Holroyd, Matthew Jones, Talma Hendler, and James Blair. Neural dynamics for facial threat processing as revealed by gamma band synchronization using meg. *Neuroimage*, 34(2):839–847, 2007.

T. A. Keller N. J. Minshew M. A. Just, V. L. Cherkassky. Cortical activation and synchronization during sentence comprehension in high-functioning autism: Evidence of underconnectivity. *Brain*, 127(8):1811–1821, 2004.

Keeran Maharajh, Peter Teale, Donald C Rojas, and Martin L Reite. Fluctuation of gamma-band phase synchronization within the auditory cortex in schizophrenia. *Clinical Neurophysiology*, 121(4):542–548, 2010.

Vladimir Makarenko and Rodolfo Llins. Experimentally determined chaotic phase synchronization in a neuronal system. *Proceedings of the National Academy of Sciences*, 95(26):15747–15752, December 1998.

Kanti V Mardia and Peter E Jupp. *Directional statistics*, volume 494. John Wiley & Sons, 2009.

Barbara Maughan, Richard Rowe, Julie Messer, Robert Goodman, and Howard Meltzer. Conduct disorder and oppositional defiant disorder in a national sample: developmental epidemiology. *Journal of Child Psychology and Psychiatry*, 45(3):609–621, 2004.

Erin B McClure, Kayla Pope, Andrea J Hoberman, Daniel S Pine, and Ellen Leibenluft. Facial expression recognition in adolescents with mood and anxiety disorders. *American Journal of Psychiatry*, 160(6):1172–1174, 2003.

Dennis J McFarland, A Todd Lefkowicz, and Jonathan R Wolpaw. Design and operation of an eeg-based brain-computer interface with digital signal processing technology. *Behavior Research Methods, Instruments & Computers*, 29(3):337–345, 1997a.

Dennis J McFarland, Lynn M McCane, Stephen V David, and Jonathan R Wolpaw. Spatial filter selection for eeg-based communication. *Electroencephalography and Clinical Neurophysiology*, 103(3):386–394, 1997b.

Saeid Mehrkanoon, Michael Breakspear, and Tjeerd W Boonstra. Low-dimensional dynamics of resting-state cortical activity. *Brain Topography*, pages 1–15, 2013.

Christoph M Michel and Micah M Murray. Towards the utilization of eeg as a brain imaging tool. *Neuroimage*, 61(2):371–385, 2012.

Nancy J Minshew and Diane L Williams. The new neurobiology of autism: cortex, connectivity, and neuronal organization. *Archives of Neurology*, 64(7):945, 2007a.

N.J. Minshew and D.L. Williams. The new neurobiology of austism. *Archieve of Neurology*, 64:945–950, 2007b.

Annette M Molinaro, Richard Simon, and Ruth M Pfeiffer. Prediction error estimation: a comparison of resampling methods. *Bioinformatics*, 21(15):3301–3307, 2005.

Florian Mormann, Klaus Lehnertz, Peter David, and Christian E Elger. Mean phase coherence as a measure for phase synchronization and its application to the eeg of epilepsy patients. *Physica D: Nonlinear Phenomena*, 144(3):358–369, 2000.

Tracy L Morris and John S March. *Anxiety disorders in children and adolescents*. Guilford Press, 2004.

AP Morrison, RP Bentall, P French, L Walford, A Kilcommons, A Knight, M Kreutz, and SW Lewis. Randomised controlled trial of early detection and cognitive therapy for preventing transition to psychosis in high-risk individuals study design and interim analysis of transition rate and psychological risk factors. *The British Journal of Psychiatry*, 181(43):s78–s84, 2002.

Allison J Mostow, Carroll E Izard, Sarah Fine, and Christopher J Trentacosta. Modeling emotional, cognitive, and behavioral predictors of peer acceptance. *Child Development*, 73(6):1775–1787, 2002.

C Mulert, V Kirsch, Roberto Pascual-Marqui, Robert W McCarley, and Kevin M Spencer. Long-range synchrony of gamma oscillations and auditory hallucination symptoms in schizophrenia. *International Journal of Psychophysiology*, 79(1):55–63, 2011.

Peter Muris, Cor Meesters, and Pim Blijlevens. Self-reported reactive and regulative temperament in early adolescence: Relations to internalizing and externalizing problem behavior and big three personality factors. *Journal of Adolescence*, 30(6):1035–1049, 2007.

Francesco Musso, Jürgen Brinkmeyer, Arian Mobascher, Tracy Warbrick, and Georg Winterer. Spontaneous brain activity and eeg microstates. a novel eeg/fmri analysis approach to explore resting-state networks. *NeuroImage*, 52(4):1149–1161, 2010.

Ali Yener Mutlu, Edward Bernat, and Selin Aviyente. A signal-processing-based approach to time-varying graph analysis for dynamic brain network identification. *Computational and mathematical methods in medicine*, 2012, 2012.

Committee on Interventions for Children With Autism. National Research Council. Educating children with autism., 2001.

Mark EJ Newman. Analysis of weighted networks. *Physical Review E*, 70(5):056131, 2004.

Guido Nolte. The magnetic lead field theorem in the quasi-static approximation and its use for magnetoencephalography forward calculation in realistic volume conductors. *Physics in medicine and biology*, 48(22):3637, 2003.

Guido Nolte, Ou Bai, Lewis Wheaton, Zoltan Mari, Sherry Vorbach, and Mark Hallett. Identifying true brain interaction from eeg data using the imaginary part of coherency. *Clinical Neurophysiology*, 115(10):2292–2307, 2004.

James R Norris. *Markov chains*. Number 2008. Cambridge university press, 1998.

P Nunez and R Srinivasan. Electrical fields of the brain. *New York: Oxford*, 1981.

Paul L Nunez. *Neocortical dynamics and human EEG rhythms*. Oxford University Press, USA, 1995.

Paul L Nunez, Richard B Silberstein, Zhiping Shi, Matthew R Carpenter, Ramesh Srinivasan, Don M Tucker, Scott M Doran, Peter J Cadusch, and Ranjith S Wijesinghe. Eeg coherency ii: experimental comparisons of multiple measures. *Clinical Neurophysiology*, 110(3):469–486, 1999.

Paul L Nunez, Ramesh Srinivasan, Andrew F Westdorp, Ranjith S Wijesinghe, Don M Tucker, Richard B Silberstein, and Peter J Cadusch. Eeg coherency: I: statistics, reference electrode, volume conduction, laplacians, cortical imaging, and interpretation at multiple scales. *Electroencephalography and Clinical Neurophysiology*, 103(5): 499–515, 1997.

LM. Oberman and Pascual-Leone. Cortical plasticity: A proposed mechanism by which genomic factors lead to the behavioral and neurological phenotype of autism spectrum and psychotic-spectrum disorders. *Behavioral Brain Sciences*, 31:276–277, 2008.

Office of the Surgeon General (US, Center for Mental Health Services (US, et al. Mental health: culture, race, and ethnicity: a supplement to mental health: a report of the surgeon general. 2001.

P. Knig P. R. Roelfsema, A. K. Engel and W. Singer. Visuomotor integration is associated with zero time-lag synchronization among cortical areas. *Nature*, 385:157161, January 1997.

Satu Palva and J Matias Palva. Discovering oscillatory interaction networks with m/eeg: challenges and breakthroughs. *Trends in cognitive sciences*, 16(4):219–230, 2012.

Roberto D Pascual-Marqui. Coherence and phase synchronization: generalization to pairs of multivariate time series, and removal of zero-lag contributions. *arXiv preprint arXiv:0706.1776*, 2007.

Roberto D Pascual-Marqui, Christoph M Michel, and Dietrich Lehmann. Segmentation of brain electrical activity into microstates: model estimation and validation. *Biomedical Engineering, IEEE Transactions on*, 42(7):658–665, 1995.

Tingying Peng, Alexander B Rowley, Philip N Ainslie, Marc J Poulin, and Stephen J Payne. Wavelet phase synchronization analysis of cerebral blood flow autoregulation. *Biomedical Engineering, IEEE Transactions on*, 57(4):960–968, 2010.

Luis R Peraza, Aziz UR Asghar, Gary Green, and David M Halliday. Volume conduction effects in brain network inference from electroencephalographic recordings using phase lag index. *Journal of Neuroscience Methods*, 207(2):189–199, 2012.

Christophe Phillips, Jeremie Mattout, Michael D Rugg, Pierre Maquet, and Karl J Friston. An empirical bayesian solution to the source reconstruction problem in eeg. *NeuroImage*, 24(4):997–1011, 2005.

Steven Phillips and Yuji Takeda. Frontal–parietal synchrony in elderly eeg for visual search. *International Journal of Psychophysiology*, 75(1):39–43, 2010.

Daniel S Pine, Patricia Cohen, Diana Gurley, Judith Brook, and Yuju Ma. The risk for early-adulthood anxiety and depressive disorders in adolescents with anxiety and depressive disorders. *Archives of general psychiatry*, 55(1):56–64, 1998.

F. Polleux and J.M. Lauder. Towards a developmental neurobiology of autism. *Mental Retardation and Developmental Disabilities Research Reviews*, 10:303–317, 2004.

Luca Pollonini, Udit Patidar, Ning Situ, Roozbeh Rezaie, Andrew C Papanicolaou, and George Zouridakis. Functional connectivity networks in the autistic and healthy brain assessed using granger causality. In *Engineering in Medicine and Biology Society (EMBC), 2010 Annual International Conference of the IEEE*, pages 1730–1733, 2010.

Samuel P Putnam and Mary K Rothbart. Development of short and very short forms of the children's behavior questionnaire. *Journal of personality assessment*, 87(1): 102–112, 2006.

Shaozheng Qin, Christina B Young, Xujun Duan, Tianwen Chen, Kaustubh Supekar, and Vinod Menon. Amygdala subregional structure and intrinsic functional connectivity predicts individual differences in anxiety during early childhood. *Biological psychiatry*, 75(11):892–900, 2014.

Lena C Quilty, Michael Van Ameringen, Catherine Mancini, Jonathan Oakman, and Peter Farvolden. Quality of life and the anxiety disorders. *Journal of anxiety disorders*, 17(4):405–426, 2003.

R. Q. Quiroga, A. Kraskov, T. Kreuz, and P. Grassberger. Performance of different synchronization measures in real data: a case study on electroencephalographic signals. *Physical Review E*, 65(4), 2002a.

R Quian Quiroga, A Kraskov, T Kreuz, and Peter Grassberger. Performance of different synchronization measures in real data: a case study on electroencephalographic signals. *Physical Review E*, 65(4):041903, 2002b.

M. L. V. Quyen, J. Foucher, J. Lachaux, E. Rodgriguez, A. Lutz, J. Martinerie, and F.J. Varela. Comparision of hilbert transform and wavelet methods for the analysis of neuronal synchrony. *Journal of Neuroscience Methods*, 111:83–98, 2001.

Herbert Ramoser, Johannes Muller-Gerking, and Gert Pfurtscheller. Optimal spatial filtering of single trial eeg during imagined hand movement. *Rehabilitation Engineering, IEEE Transactions on*, 8(4):441–446, 2000.

Paul E Rapp, Christopher J Cellucci, David O Keyser, Adele MK Gilpin, and David M Darmon. Statistical issues in tbi clinical studies. *Frontiers in Neurology*, 4(Article 177), 2013.

Nadja Razavi, Kay Jann, Thomas Koenig, Mara Kottlow, Martinus Hauf, Werner Strik, and Thomas Dierks. Shifted coupling of eeg driving frequencies and fmri resting state networks in schizophrenia spectrum disorders. *PloS One*, 8(10):e76604, 2013.

B. Reichow and M. Wolery. Comprehensive synthesis of early intensive behavioral interventions for young children with autism based on the ucla young autism project model. *Journal of Autism and Developmental Disorders*, 39:23–41, 2009.

Anne Richards, Christopher C French, Gilly Nash, Julie A Hadwin, and Nick Donnelly. A comparison of selective attention and facial processing biases in typically developing children who are high and low in self-reported trait anxiety. *Development and Psychopathology*, 19(02):481–495, 2007.

G. Rippon, Jon Brock, Caroline C Brown, and Jill Boucher. Disordered connectivity in the autistic brain: challenges for the "new psychophysiology". *International Journal of Psychophysiology*, 63(2):164–72, 2007a.

Gina Rippon, Jon Brock, Caroline Brown, and Jill Boucher. Disordered connectivity in the autistic brain: Challenges for the new psychophysiology. *International Journal of Psychophysiology*, 63(2):164–172, 2007b.

Brian J Roach and Daniel H Mathalon. Event-related eeg time-frequency analysis: an overview of measures and an analysis of early gamma band phase locking in schizophrenia. *Schizophrenia bulletin*, 34(5):907–926, 2008.

Eugenio Rodriguez, Nathalie George, Jean-Philippe Lachaux, Jacques Martinerie, Bernard Renault, and Francisco J Varela. Perception's shadow: long-distance synchronization of human brain activity. *Nature*, 397(6718):430–433, 1999.

Alard Roebroeck, Elia Formisano, and Rainer Goebel. Mapping directed influence over the brain using granger causality and fmri. *Neuroimage*, 25(1):230–242, 2005.

Simon Rogers and Mark Girolami. *A first course in machine learning.* 2011.

S.J. Rogers and L.A. Vismara. Evidence-based comprehensive treatments for early autism. *Journal of Clinical Child and Adolescent Psychology*, 37:8–38, 2008.

Rebeca Romo Vázquez, Hugo Vélez-Pérez, Radu Ranta, Valérie Louis Dorr, Didier Maquin, and Louis Maillard. Blind source separation, wavelet denoising and discriminant analysis for eeg artefacts and noise cancelling. *Biomedical Signal Processing and Control*, 7(4):389–400, 2012.

Michael G Rosenblum, Arkady S Pikovsky, and Jürgen Kurths. Phase synchronization of chaotic oscillators. *Physical Review Letters*, 76(11):1804, 1996.

Bruno Rossion, Roberto Caldara, Mohamed Seghier, Anne-Marie Schuller, Francois Lazeyras, and Eugene Mayer. A network of occipito-temporal face-sensitive areas besides the right middle fusiform gyrus is necessary for normal face processing. *Brain*, 126(11):2381–2395, 2003.

Amy Krain Roy, Roma A Vasa, Maggie Bruck, Karin Mogg, Brendan P Bradley, Michael Sweeney, R Lindsey Bergman, Erin B McClure-Tone, and Daniel S Pine. Attention bias toward threat in pediatric anxiety disorders. *Journal of the American Academy of Child & Adolescent Psychiatry*, 47(10):1189–1196, 2008.

Mikail Rubinov and Olaf Sporns. Complex network measures of brain connectivity: uses and interpretations. *NeuroImage*, 52(3):1059–1069, 2010.

Mikail Rubinov and Olaf Sporns. Weight-conserving characterization of complex functional brain networks. *NeuroImage*, 56(4):2068–2079, 2011.

T. Yagyu S. Morita K. Nishida K. Yamada M. Yoshimura G. Okugawa K. Nobuhara S. Irisawa, T. Isotani and T. Kinoshita. Increased omega complexity and decreased microstate duration in nonmedicated schizophrenic patients. *Neuropsychobiology*, 54 (2):134–139, 2006.

V. Sakkalis. Review of advanced techniques for the estimation of brain connectivity measures in eeeg/meg. *Computers in Biology and Medicine*, 41:1110–1117, 2011.

Roser Sala-Llonch, Cleofe Pena-Gomez, Eider M Arenaza-Urquijo, Dídac Vidal-Piñeiro, Nuria Bargallo, Carme Junque, and David Bartres-Faz. Brain connectivity during resting state and subsequent working memory task predicts behavioural performance. *Cortex*, 48(9):1187–1196, 2012.

S. Sanei and J.A. Chambers. *EEG Signal Processing*. John Wiley and Sons, 2007.

Saeid Sanei and Jonathon A Chambers. *EEG signal processing*. John Wiley & Sons, 2008.

B Schack, G Seidel, W Krause, F Heinrich, and U Krause. Coherence analysis of the ongoing eeg by means of microstates of synchronous oscillations. In *Engineering in Medicine and Biology Society, 2001. Proceedings of the 23rd Annual International Conference of the IEEE*, volume 2, pages 1792–1795. IEEE, 2001.

P Thomas Schoenemann. Evolution of the size and functional areas of the human brain. *Annu. Rev. Anthropol.*, 35:379–406, 2006.

John L Semmlow. *Biosignal and medical image processing*. CRC Press, 2009.

A Shamshad, MA Bawadi, WMA Wan Hussin, TA Majid, and SAM Sanusi. First and second order markov chain models for synthetic generation of wind speed time series. *Energy*, 30(5):693–708, 2005.

Katherine E Shannon, Colin Sauder, Theodore P Beauchaine, and Lisa M Gatzke-Kopp. Disrupted effective connectivity between the medial frontal cortex and the caudate in adolescent boys with externalizing behavior disorders. *Criminal justice and behavior*, 36(11):1141–1157, 2009.

F Shayegh, Saeed Sadri, Rassoul Amirfattahi, and K Ansari-Asl. Proposing a two-level stochastic model for epileptic seizure genesis. *Journal of computational neuroscience*, 36(1):39–53, 2014.

Farzaneh Shayegh, Saeed Sadri, and Rasoul Amirfattahi. A theoretical model for spontaneous seizure generation based on markov chain process. In *Neural Engineering, 2009. NER'09. 4th International IEEE/EMBS Conference on*, pages 637–640. IEEE, 2009.

David R Simmons, Ashley E Robertson, Lawrie S McKay, Erin Toal, Phil McAleer, and Frank E Pollick. Vision in autism spectrum disorders. *Vision Research*, 49(22): 2705–2739, 2009.

Marjorie Solomon, Sally J Ozonoff, Stefan Ursu, Susan Ravizza, Neil Cummings, Stanford Ly, and Cameron S Carter. The neural substrates of cognitive control deficits in autism spectrum disorders. *Neuropsychologia*, 47(12):2515–26, 2009.

Charles Donald Spielberger, Richard L Gorsuch, and Robert E Lushene. Manual for the state-trait anxiety inventory. 1970.

Olaf Sporns. *Networks of the Brain*. The MIT Press, 2011.

Olaf Sporns. From simple graphs to the connectome: networks in neuroimaging. *NeuroImage*, 62(2):881–886, 2012.

Ramesh Srinivasan. Methods to improve the spatial resolution of eeg. *International Journal of Bioelectromagnetism*, 1(1):102–111, 1999.

Daniel Stahl, Andrew Pickles, Mayada Elsabbagh, Mark H Johnson, BASIS Team, et al. Novel machine learning methods for erp analysis: A validation from research on infants at risk for autism. *Developmental Neuropsychology*, 37(3):274–298, 2012.

CJ Stam. Characterization of anatomical and functional connectivity in the brain: a complex networks perspective. *International Journal of Psychophysiology*, 77(3):186–194, 2010.

Cornelis J Stam, Guido Nolte, and Andreas Daffertshofer. Phase lag index: assessment of functional connectivity from multi channel eeg and meg with diminished bias from common sources. *Human Brain Mapping*, 28(11):1178–1193, 2007.

W.L. Stone and P.J. Yoder. Predicting spoken language level in children with autism spectrum disorders. *Autism*, bf 5:341–361, 2001.

V Strelets, PL Faber, J Golikova, V Novototsky-Vlasov, T Koenig, LRR Gianotti, JH Gruzelier, and Dietrich Lehmann. Chronic schizophrenics with positive symptomatology have shortened eeg microstate durations. *Clinical Neurophysiology*, 114 (11):2043–2051, 2003.

Steven H Strogatz. Exploring complex networks. *Nature*, 410(6825):268–276, 2001.

Daniel Studer, Ulrich Hoffmann, and Thomas Koenig. From eeg dependency multichannel matching pursuit to sparse topographic eeg decomposition. *Journal of Neuroscience Methods*, 153(2):261–275, 2006.

Yoichi Sugita. Innate face processing. *Current opinion in neurobiology*, 19(1):39–44, 2009.

Kaustubh Supekar, Vinod Menon, Daniel Rubin, Mark Musen, and Michael D Greicius. Network analysis of intrinsic functional brain connectivity in alzheimer's disease. *PLoS Computational Biology*, 4(6):e1000100, 2008.

Kaustubh Supekar, Mark Musen, and Vinod Menon. Development of large-scale functional brain networks in children. *PLoS Biology*, 7(7):e1000157, 2009.

P. Szatmari, S.E. Bryson, M.H. Boyle, D.L. Streiner, and E. Duku. Predictors of outcome among high functioning children with autism and asperger syndrome. *The Journal of Child Psychology and Psychiatry*, 44:520–528, 2003.

Catherine Tallon-Baudry, Olivier Bertrand, Marie-Anne Hénaff, Jean Isnard, and Catherine Fischer. Attention modulates gamma-band oscillations differently in the human lateral occipital cortex and fusiform gyrus. *Cerebral Cortex*, 15(5):654–662, 2005.

Steven Taylor. *Anxiety sensitivity: Theory, research, and treatment of the fear of anxiety.* Routledge, 2014.

Alvin V Terry and Sahebarao P Mahadik. Time-dependent cognitive deficits associated with first and second generation antipsychotics: cholinergic dysregulation as a potential mechanism. *Journal of Pharmacology and Experimental Therapeutics*, 320(3): 961–968, 2007.

Robert W Thatcher. Coherence, phase differences, phase shift, and phase lock in eeg/erp analyses. *Developmental Neuropsychology*, 37(6):476–496, 2012.

Robert W Thatcher, Duane M North, and Carl J Biver. Development of cortical connections as measured by eeg coherence and phase delays. *Human brain mapping*, 29 (12):1400–1415, 2008.

Sergios Theodoridis, Aggelos Pikrakis, Konstantinos Koutroumbas, and Dionisis Cavouras. *Introduction to Pattern Recognition: A Matlab Approach: A Matlab Approach.* Academic Press, 2010.

Simon Thorpe, Denis Fize, Catherine Marlot, et al. Speed of processing in the human visual system. *nature*, 381(6582):520–522, 1996.

Dardo Tomasi and Nora D Volkow. Abnormal functional connectivity in children with attention-deficit/hyperactivity disorder. *Biological psychiatry*, 71(5):443–450, 2012.

Mark Tommerdahl, Vinay Tannan, Jameson K Holden, and Grace T Baranek. Absence of stimulus-driven synchronization effects on sensory perception in autism: evidence for local underconnectivity. *Behavioral and Brain Functions*, 4(19):1–9, 2008.

Nim Tottenham, James W Tanaka, Andrew C Leon, Thomas McCarry, Marcella Nurse, Todd A Hare, David J Marcus, Alissa Westerlund, BJ Casey, and Charles Nelson. The nimstim set of facial expressions: judgments from untrained research participants. *Psychiatry Research*, 168(3):242–249, 2009.

Vernon L Towle, Ibrahim Syed, Catherine Berger, Robert Grzesczcuk, John Milton, Robert K Erickson, Philip Cogen, Eric Berkson, and Jean-Paul Spire. Identification of the sensory/motor area and pathologic regions using ecog coherence. *Electroencephalography and clinical neurophysiology*, 106(1):30–39, 1998.

Christopher J Trentacosta and Sarah E Fine. Emotion knowledge, social competence, and behavior problems in childhood and adolescence: A meta-analytic review. *Social Development*, 19(1):1–29, 2010.

Wilson A Truccolo, Mingzhou Ding, Kevin H Knuth, Richard Nakamura, and Steven L Bressler. Trial-to-trial variability of cortical evoked responses: implications for the analysis of functional connectivity. *Clinical Neurophysiology*, 113(2):206–226, 2002.

Peter J Uhlhaas, Corinna Haenschel, Danko Nikolić, and Wolf Singer. The role of oscillations and synchrony in cortical networks and their putative relevance for the pathophysiology of schizophrenia. *Schizophrenia bulletin*, 34(5):927–943, 2008.

A Urbano, C Babiloni, P Onorati, and F Babiloni. Dynamic functional coupling of high resolution eeg potentials related to unilateral internally triggered one-digit movements. *Electroencephalography and Clinical Neurophysiology*, 106(6):477–487, 1998.

Jean-Pierre Valla, Lise Bergeron, and Nicole Smolla. The dominic-r: A pictorial interview for 6-to 11-year-old children. *Journal of the American Academy of Child & Adolescent Psychiatry*, 39(1):85–93, 2000.

Dimitri Van de Ville, Juliane Britz, and Christoph M Michel. Eeg microstate sequences in healthy humans at rest reveal scale-free dynamics. *Proceedings of the National Academy of Sciences*, 107(42):18179–18184, 2010.

Elisabeth CW van Straaten and Cornelis J Stam. Structure out of chaos: Functional brain network analysis with eeg, meg, and functional mri. *European Neuropsychopharmacology*, 23(1):7–18, 2013.

F. Varela, J. P. Lachaux, E. Rodriguez, and J. Martinerie. The brainweb: phase synchronization and large-scale integration. *Nature Reviews Neuroscience*, 2(4):229–239, April 2001a.

Francisco Varela, Jean-Philippe Lachaux, Eugenio Rodriguez, and Jacques Martinerie. The brainweb: phase synchronization and large-scale integration. *Nature reviews Neuroscience*, 2(4):229–239, 2001b.

Frank C Verhulst, Jan van der Ende, Robert F Ferdinand, and Marianne C Kasius. The prevalence of dsm-iii-r diagnoses in a national sample of dutch adolescents. *Archives of General Psychiatry*, 54(4):329–336, 1997.

Michele E Villalobos, Akiko Mizuno, Branelle C Dahl, Nobuko Kemmotsu, and Ralph-Axel Mller. Reduced functional connectivity between v1 and inferior frontal cortex associated with visuomotor performance in autism. *NeuroImage*, 25(3):916–925, 2005.

Martin Vinck, Robert Oostenveld, Marijn van Wingerden, Franscesco Battaglia, and Cyriel Pennartz. An improved index of phase-synchronization for electrophysiological data in the presence of volume-conduction, noise and sample-size bias. *Neuroimage*, 55(4):1548–1565, 2011.

A. Arain P. Modur V.L. Morgan, R.R. Price and B. Abou-Khalil. Resting functional mri with temporal clustering analysis for localization of epileptic activity without eeg. *NeuroImage*, 21(1):473–481, Jan 2007.

Michele M Volbrecht and H Hill Goldsmith. Early temperamental and family predictors of shyness and anxiety. *Developmental psychology*, 46(5):1192, 2010.

Daniel A Waschbusch, William E Pelham Jr, J Richard Jennings, Andrew R Greiner, Ralph E Tarter, and Howard B Moss. Reactive aggression in boys with disruptive behavior disorders: behavior, physiology, and affect. *Journal of Abnormal Child Psychology*, 30(6):641–656, 2002.

S. Wass. Distortions and disconnections: Disrupted brain connectivity in autism. *Brain and Congnition*, 75:18–28, 2011.

Allison M Waters, Liza L Kokkoris, Karin Mogg, Brendan P Bradley, and Daniel S Pine. The time course of attentional bias for emotional faces in anxious children. *Cognition and Emotion*, 24(7):1173–1181, 2010.

Duncan J Watts and Steven H Strogatz. Collective dynamics of small-worldnetworks. *Nature*, 393(6684):440–442, 1998.

Sabine Weiss and Peter Rappelsberger. Long-range eeg synchronization during word encoding correlates with successful memory performance. *Cognitive Brain Research*, 9(3):299–312, 2000.

David E Welchew, Chris Ashwin, Karim Berkouk, Raymond Salvador, John Suckling, Simon Baron-Cohen, and Ed Bullmore. Functional disconnectivity of the medial temporal lobe in asperger's syndrome. *Biological Psychiatry*, 57(9):991–998, 2005.

Eiledh McGarry Jim White, Ray Jones. Cognitive behavioural computer therapy for the anxiety disorders: A pilot study. *Journal of Mental Health*, 9(5):505–516, 2000.

Kevin Whittingstall, Gerhard Stroink, Larry Gates, JF Connolly, and Allen Finley. Effects of dipole position, orientation and noise on the accuracy of eeg source localization. *Biomedical Engineering Online*, 2(1):14, 2003.

Sherri C Widen and James A Russell. Children acquire emotion categories gradually. *Cognitive development*, 23(2):291–312, 2008.

Cort J Willmott and Kenji Matsuura. Advantages of the mean absolute error (mae) over the root mean square error (rmse) in assessing average model performance. *Climate Research*, 30(1):79, 2005.

Tony W Wilson, Donald C Rojas, Martin L Reite, Peter D Teale, and Sally J Rogers. Children and adolescents with autism exhibit reduced meg steady-state gamma responses. *Biological Psychiatry*, 62(3):192–197, 2007.

Andrzej Wróbel. Beta activity: a carrier for visual attention. *Acta Neurobiologiae Experimentalis*, 60(2):247–260, 2000.

Xun Yang, Keith Maurice Kendrick, Qizhu Wu, Taolin Chen, Sunima Lama, Bochao Cheng, Shiguang Li, Xiaoqi Huang, and Qiyong Gong. Structural and functional connectivity changes in the brain associated with shyness but not with social anxiety. *PloS one*, 8(5):e63151, 2013.

AW Young, DI Perrett, AJ Calder, R Sprengelmeyer, and P Ekman. Facial expressions of emotion: Stimuli and tests (feest) thames valley test company, bury st. *Edmunds, UK*, 2002.

Shlomit Yuval-Greenberg and Leon Y Deouell. The broadband-transient induced gamma-band response in scalp eeg reflects the execution of saccades. *Brain Topography*, 22(1):3–6, 2009.